



## **University of Bradford eThesis**

This thesis is hosted in [Bradford Scholars](#) – The University of Bradford Open Access repository. Visit the repository for full metadata or to contact the repository team



© University of Bradford. This work is licenced for reuse under a [Creative Commons Licence](#).

**MSF PROCESS MODELLING, SIMULATION AND  
OPTIMISATION: IMPACT OF NON-CONDENSABLE GASES  
AND FOULING FACTOR ON DESIGN AND OPERATION**

Optimal Design and Operation of MSF Desalination Process with  
Non-condensable Gases and Calcium Carbonate Fouling, Flexible Design  
Operation and Scheduling under Variable Demand and Seawater Temperature  
using gPROMS

**Said Alforjani R. Said**

*BSc. Chem. Eng and MSc.*

Submitted for the Degree of

Doctor of Philosophy

School of Engineering Design and Technology

University of Bradford

United Kingdom

2012

# Abstract

Keyword: MSF, Modelling, Non-condensable gases, Simulation, Calcium Carbonate Fouling, Optimisation, gPROMS

Desalination is a technique of producing fresh water from the saline water. Industrial desalination of sea water is becoming an essential part in providing sustainable source of fresh water for a large number of countries around the world. Thermal process being the oldest and most dominating for large scale production of freshwater in today's world. Multi-Stage Flash (MSF) distillation process has been used for many years and is now the largest sector in the desalination industry.

In this work, a steady state mathematical model of Multistage Flash (MSF) desalination process is developed and validated against the results reported in the literature using gPROMS software. The model is then used for further investigation.

First, a steady state calcium carbonate fouling resistance model has been developed and implemented in the full MSF mathematical model developed above using gPROMS modeling tool. This model takes into consideration the effect of stage temperature on the calcium carbonate fouling resistance in the flashing chambers in the heat recovery section, heat rejection section, and brine heaters of MSF desalination plants. The effect of seasonal variation of seawater temperature and top brine temperature on the calcium carbonate fouling resistance has been studied throughout the flashing stage. In addition, the total annual operating cost of the MSF process is selected to minimise, while optimising the operating parameters such as seawater rejected flow rate, brine recycle flow rate and steam temperature at different seawater temperature and fouling resistance.

Secondly, an intermediate storage between the plant and the client is considered to provide additional flexibility in design and operation of the MSF process throughout the day. A simple polynomial based dynamic seawater temperature and different freshwater demand correlations are developed based on actual data. For different number of flash stages, operating parameters such as seawater rejected flow rate and brine recycle flow rate are optimised, while the total annual operating cost of the MSF process is selected to minimise. The results clearly show that the advantage of using the intermediate storage tank adds flexible scheduling in the MSF plant design and operation parameters to meet the variation in freshwater demand with varying seawater temperatures without interrupting or fully shutting down the plant at any time during the day by adjusting the number of stages.

Furthermore, the effect of non-condensable gases (NCG) on the steady state mathematical model of MSF process is developed and implemented in the MSF model developed earlier. Then the model is used to study effect of NCG on the overall heat transfer coefficient. The simulation results showed a decrease in the overall heat transfer coefficient values as NCG concentrations increased. The model is then used to study the effect of NCG on the design and operation parameters of MSF process for fixed water demand. For a given plant configuration (fixed design) and at different seawater and steam temperatures, a 0.015 wt. % of NCG results in significantly different plant operations when compared with those obtained without the presence of NCG. Finally, for fixed water demand and in the presence of 0.015 wt. % NCGs, the performance is evaluated for different plant configurations and seawater temperature and compared with those obtained without the presence of NCG.

Finally, three Neural Network (NN) based correlations for predicting the first dissociation constant ( $K_1$ ) and the second dissociation constant ( $K_2$ ) of carbonic acid in seawater as function of temperature and salinity are developed. These correlations are developed from different sources of the experimental from the literature. It found that the NN based correlation can predict  $K_1$  and  $K_2$  very accurately and for temperature less than 50 °C. Therefore, the NN correlations need to be extrapolated to adequate the MSF conditions where the operating temperature is more than 90 °C.

## **Acknowledgement**

I would like to express my sincere gratitude to my supervisor Professor I. M. Mujtaba for his invaluable guidance and advice, encouragement and support throughout this work.

I would also want to extend my sincere gratitude to Dr. M. Emtir of N.O.C for his wonderful guidance, encouragement and support from the beginning of my study.

I wish to express my sincere thanks to my parents, my wife and my children, Abdulrahman, Sara and Raghd for their invaluable encouragement and patience during my study.

Above all, I am very much grateful to almighty Allah for giving me courage and good health for completing the venture.

# Table of Contents

<b>Abstract</b> .....	i
<b>Acknowledgement</b> .....	iii
<b>List of Tables</b> .....	xii
<b>List of Figures</b> .....	xvi
<b>Nomenclature</b> .....	xxii
<b>Abbreviation</b> .....	xxix
<b>Chapter 1: Introduction</b> .....	1
1.1 Water Crisis and Need for Desalination.....	1
1.2 History of Desalination .....	2
1.3 Types of Desalination Process .....	3
1.3.1 Thermal Process.....	4
1.3.2 Membrane Process.....	7
1.4 Scale Formation and Non-condensable Gases in MSF Desalination Plant.....	10
1.4.1 Fouling Due to Scale Formation.....	10
1.4.2 Non-condensable Gases.....	11
1.5 State of the Art .....	12
1.6 Scope of this Research .....	16
1.7 Aims and Objectives of This Work.....	17

1.8 Thesis Layout .....	19
<b>Chapter 2: Literature Review .....</b>	<b>22</b>
2.1 Description of the MSF .....	22
2.2 Operation Variables in MSF Process .....	25
2.2.1 Top Brine Temperature (TBT) .....	25
2.2.2 Make-Up Flowrate (F) .....	25
2.2.3 Recirculating Brine Flowrate (R) .....	25
2.2.4 Steam Flowrate ( $W_{\text{steam}}$ ) and Steam Temperature ( $T_{\text{steam}}$ ) .....	26
2.2.5 Seawater Feed Temperature ( $T_{\text{seawater}}$ ) .....	26
2.2.6 Rejected Seawater Flowrate ( $C_w$ ) .....	26
2.2.7 Concentration Ratio .....	27
2.3 Venting System in the MSF Desalination Plant .....	27
2.4 The Carbonate System in Seawater .....	27
2.4.1 Thermodynamics of the Carbonate System .....	30
2.4.2 Equilibrium Constants in Seawater .....	31
2.5 Scale Formation Process in MSF Desalination Plants .....	34
2.5.1 Alkaline Scale Deposition Process .....	34
2.5.2 Factors Affecting $\text{CaCO}_3$ Scale Deposition Process .....	35
2.6 Prediction of $\text{CaCO}_3$ Scale Deposition Tendency .....	36
2.7 Scale Deposition Control Methods .....	38

2.7.1 Addition of Acid .....	38
2.7.2 Scale Inhibitor .....	39
2.7.3 Mechanical Cleaning .....	39
2.8 Process Modelling, Simulation and Optimisation of MSF Desalination Plant .....	40
2.8.1 Process Modelling of MSF Desalination Process .....	40
2.8.2 Simulation of MSF Desalination Process .....	48
2.8.3 Optimisation of MSF Desalination Process .....	53
2.9 Previous Work on the Modelling, Simulation of MSF Process: Impact of Non- condensable Gases and Scale Deposition Fouling .....	61
2.9.1 Effect of Scale Deposition Fouling.....	61
2.9.2 Effect of NCG.....	65
2.10 Conclusions .....	68
<b>Chapter 3: Modelling, Simulation and Optimisation using gPROMS .....</b>	<b>71</b>
3.1 Introduction .....	71
3.2 Features of gPROMS.....	72
3.3 Model Development using gPROMS.....	73
3.4 Defining a Model.....	75
3.5 Composite Models.....	77
3.6 Defining a Process.....	79
3.6.1 UNIT Section.....	80



3.6.2 SET Section .....	80
3.6.3 ASSIGN Section .....	80
3.6.4 INITIAL Section.....	81
3.6.5 SOLUTION PARAMETERS .....	81
3.6.6 SCHEDULE Section.....	82
3.7 Optimisation in gPROMS .....	83
3.8 Connecting to MS Excel Software .....	83
3.9 Comparison of gPROMS with other Commercial Software .....	84
3.10 Conclusions .....	85
<b>Chapter 4: Modelling and Simulation of the MSF Process using gPROMS .....</b>	<b>87</b>
4.1 Introduction .....	87
4.2 MSF Process Description .....	88
4.3 Steady State MSF Process Model .....	89
4.3.1 Model Equations .....	89
4.3.2 Degree of Freedom Analysis .....	97
4.4 Model Implementation in gPROMS.....	98
4.5 Model Validation.....	99
4.6 Conclusions .....	103
<b>Chapter 5: Effect of Fouling Factors on the Optimisation of MSF Desalination Process for Fixed Water Demand using gPROMS .....</b>	<b>104</b>

5.1 Introduction .....	104
5.2 Calcium Carbonate Fouling Process .....	105
5.3 Modelling of Calcium Carbonate Fouling deposition .....	106
5.4 Effect of MSF Operation Parameters on CaCO <sub>3</sub> Fouling Resistance .....	109
5.4.1 Effect of Seawater Feed Temperature on the CaCO <sub>3</sub> Fouling Resistance....	109
5.4.2 Effect of Top Brine Temperature on the CaCO <sub>3</sub> Fouling Resistance.....	110
5.5 Optimisation of MSF Process: impact of CaCO <sub>3</sub> Fouling Resistance for Fixed Water Demand.....	113
5.5.1 Optimisation Problem Formulation .....	114
5.5.2 Case Studies.....	116
5.6 Conclusions .....	123
 <b>Chapter 6: Flexible Design and Operation of MSF Desalination Process:</b>	
<b>Coping with Different Freshwater Demand .....</b>	<b>124</b>
6.1 Introduction .....	124
6.2 Dynamic Freshwater Demand .....	126
6.2.1 Dynamic Freshwater Demand during Weekends .....	126
6.2.2 Dynamic Freshwater Demand during Working Days.....	127
6.3 Seawater Temperature Dynamic Profile .....	128
6.4 Storage Tank and Level Control Models .....	129
6.4.1 Storage Tank Model.....	129

6.4.2 Storage Tank Level Control Model .....	130
6.5 Optimisation of MSF parameters .....	132
6.5.1 Optimisation Problem Formulation .....	132
6.6 Case Studies .....	133
6.6.1 Case Study 1 .....	134
6.6.2 Case Study 2 .....	138
6.7 Conclusion.....	142
<b>Chapter 7: Modelling and Simulation the Effect of Non-condensable Gases</b>	
<b>on the MSF Process.....</b>	<b>144</b>
7.1 Introduction .....	144
7.2 Modelling of MSF Process Model: Impact of NCG .....	144
7.2.1 Developing MSF Process Model with Effect of NCG .....	145
7.2.2 Effect of NCG on Overall Heat Transfer Coefficient and Plant Performance.....	147
7.3 Sensitivity of Design and Operation Parameters in the presence of NCG.....	150
7.3.1 Effect of Seawater and Steam Temperature on Freshwater Production (Fixed Design) .....	150
7.3.2 Effect NCG on MSF Operation Parameters at Different Number of Stages and Seawater Temperature for Fixed Water Demand .....	152
7.4 Conclusions .....	155

<b>Chapter 8: Neural Network Based Correlations for Estimating Dissociation Constants of Carbonic Acid in Seawater</b> .....	157
8.1 Introduction .....	157
8.2 Application of Neural Networks .....	157
8.3 Introduction to Neural Network Architecture .....	159
8.3.1 Back Propagation Training Algorithm .....	162
8.4 Dissociation Constants of Carbonic Acid in Seawater.....	165
8.4.1 Chemistry of Dissociation Constant of Carbonic Acid in Seawater.....	165
8.4.2 Empirical Correlations for Dissociation Constants of Carbonic Acid in Seawater.....	167
8.5 Neural Network and Development of Correlations for $K_1$ and $K_2$ .....	168
8.5.1 NN Architecture and Training .....	169
8.5.2 Development of the Correlations.....	170
8.6 Experimental Data and Correlations .....	173
8.6.1 Experimental Data .....	173
8.6.2 NN Based Correlations for Different Data Sets.....	181
8.7 Results and Discussions .....	187
8.8 Conclusions .....	191
<b>Chapter 9: Conclusions and Future Work</b> .....	204
9.1 Conclusions .....	204

9.2 Future Work .....	208
<b>References</b> .....	<b>210</b>
<b>List of Publications</b> .....	<b>226</b>

## List of Tables

Table 2.1 The composition of standard seawater (Al-Anezi and Hilal, 2007) .....	29
Table 2.2 Interpretation of the Langelier Saturation Index (Carrier 1965).....	37
Table 2.3 Interpretation of the Ryznar Stability Index (Carrier 1965) .....	38
Table 2.4 Summary of past work on steady state modelling of MSF process .....	41
Table 2.5 Summary of past work on simulation of MSF process.....	50
Table 2.6 Summary of past work on optimisation of MSF process.....	59
Table 4.1 Constant Parameters and Input Data (Rosso et al., 1996).....	100
Table 4.2 Summary of the simulation Results by (Rosso et al., 1996) and this work ..	101
Table 5. 1Constant Parameters and Input Data (Rosso et al., 1996).....	110
Table 5. 2 Summary of the optimisation results (Case 1).....	117
Table 5. 3 Summary of optimisation results (Case 2).....	121
Table 6.1 Constant parameters and input data .....	134
Table 6.2 Summary of optimization results (case 1).....	135
Table 6.3 Summary of optimisation results (case 2).....	139
Table 7.1 Constant Parameters and Input Data.....	147
Table 7.2 Simulation results of gPROMS model with effect of 0.015 % of NCGs.....	148
Table 7.3 Effect of NCGs on MSF Plant Performance .....	150

Table 7.4 Effect of Tseawater and Tsteam on DNS, GOR, TBT, and BBT at 0.015 % wt of NCG .....	151
Table 8.1 Commonly used transfer function (Hagan et al., 1996).....	164
Table 8.2 The salinity (S) and temperature (T) data range for different NN based correlations .....	174
Table 8.3 ( $K1 \times 107$ ) from Millero data (Millero et al., 1997) used in NN1_K1 .....	175
Table 8.4 ( $K2 \times 1010$ ) from Millero data (Millero et al., 1997) used in NN1_K2.....	176
Table 8.5 ( $K1 \times 106$ ) from Mehrbach data (Mehrbach et al., 1973) used in NN2_K1 ..	177
Table 8.6 ( $K2 \times 1010$ ) from Mehrbach data (Mehrbach et al., 1973) used in NN2_K2	178
Table 8.7 Sample of ( $K1 \times 107$ ) from Millero data (Millero et al., 2006) used in NN3_K1.....	179
Table 8.8 Sample of ( $K2 \times 1010$ ) from Millero data (Millero et al., 2006) used in NN3_K2.....	180
Table 8.9 Scaled up parameters for NN based correlations .....	183
Table 8.10 Weights and Biases of the NN1_K1 .....	184
Table 8.11 Weights and Biases of the NN1_K2 .....	184
Table 8.12 Weights and Biases of the NN2_K1 .....	185
Table 8.13 Weights and Biases of the NN2_K2 .....	185
Table 8.14 Weights and Biases of the NN3_K1 .....	186

Table 8.15 Weights and Biases of the NN3_K2 .....	186
Table 8.16 Comparison of $K1 \times 10^7$ values prediction by NN1_K1 and experiment data from Mehrbach et al. (1973) Range : T=<0-35 °C>, S=<19-43wt%>.....	192
Table 8.17 Comparison of $K2 \times 10^{10}$ values prediction by NN1_K2 and experiment data from Mehrbach et al. (1973) Range: T=<0-35 °C >, S=<19-43wt %>.....	193
Table 8.18 Comparison of $K1 \times 10^7$ values prediction by NN1_K1 and experiment data from Millero et al. (2006) Range: T=<1.1-50.5 °C>, S=<3.47-46.29wt %> .	194
Table 8.19 Comparison of $K2 \times 10^{10}$ values prediction by NN1_K2 and experiment data from Millero et al. (2006.) Range: T=<1.1-50.5 °C>, S=<3.47-46.29 wt%>	195
Table 8.20 Comparison of $K1 \times 10^7$ values prediction by NN2_K1 and experiment data from Millero et al. (1997) Range: T=<1-40 °C>, S=<5-35wt %> .....	196
Table 8.21 Comparison of $K2 \times 10^{10}$ values prediction by NN2_K2 and experiment data from Millero et al. (1997) Range: T=<1-40 °C>, S=<5-35wt %> .....	197
Table 8.22 Comparison of $K1 \times 10^7$ values prediction by NN2_K1 and experiment data from Millero et al. (2006) Range: T=<1.1-50.4 °C >, S=<3.47-36 wt %>.....	198
Table 8.23 Comparison of $K2 \times 10^{10}$ values prediction by NN2_K2 and experiment data from Millero et al. (2006) Range: T=<1.1-50.4 °C >, S=<3.47-36 wt %> ....	199
Table 8.24 Comparison of $K1 \times 10^7$ values prediction by NN3_K1 and experiment data from Millero et al. (1997) Range: T=<1-40 °C >, S=<5-35 wt %> .....	200
Table 8.25 Comparison of $K2 \times 10^{10}$ values prediction by NN3_K2 and experiment data from Millero et al. (1997) Range: T=<1-40 °C >, S=<5-35 wt. %> .....	201



Table 8.26 Comparison of  $K1 \times 10^7$  values prediction by NN3\_K1 and experiment  
data from Mehrbach et al. (1973) Range: T=<0-35 °C>, S=<19-43wt %>.....202

Table 8. 27 Comparison of  $K2 \times 10^{10}$  values prediction by NN3\_K2 and experiment  
data from Mehrbach et al. (1973) Range: T=<0-35 °C>, S=<19-43 wt%>.....203

## List of Figures

Figure 1.1 Types of desalination (Tanvir, 2007).....	3
Figure 1.2 MSF-once through process type (El-Dessouky and Ettouney, 2002).....	5
Figure 1.3 MSF-brine recycle process type (Rosso et al., 1996).....	6
Figure 1.4 MEE desalination plant (El-Dessouky and Ettouney, 1999).....	7
Figure 1.5 Representation of Reverse Osmosis (Sourirajan and Agrawal, 1996).....	8
Figure 1.6 Representation of Electrodialysis (Fritzmman et al., 2007).....	9
Figure 1.7 Scale formation regions in MSF plant (Shams EL Din et al., 2002).....	11
Figure 2.1 Typical MSF Process (Rosso et al., 1996).....	23
Figure 2.2 MSF flashing stage (El-Dessouky and Ettouney, 2002).....	23
Figure 2.3 Schematic represent of the carbonate system in gas, liquid and solid phase (Al-Rawajfeh, 2004).....	28
Figure 2.4 The first dissociation constant of carbonic acid in fresh and seawater as function of water temperature at salinities of 0, 5, 15, 25, and 35 % (Al-Anezi and Hilal, 2007).....	33
Figure 2.5 The second dissociation constant of carbonic acid in fresh and seawater as function of water temperature at salinities of 0, 5, 15, 25, and 35% (Al-Anezi and Hilal, 2007).....	33
Figure 2.6 Typical Simulations and Optimisation Architecture (Tanvir, 2007).....	49
Figure 3.1 Model builder in gPROMS.....	74

Figure 3.2 VARIABLES TYPES for gPROMS MODEL .....	77
Figure 3.3 Hierarchical sub-model decomposition .....	78
Figure 3.4 Composite model features in gPROMS software .....	79
Figure 3.5 Part of the process file for the MSF process model.....	82
Figure 3.6 Part of the optimisation file for tank model in MSF process model.....	84
Figure 4.1 Typical MSF Process (Rosso et al., 1996).....	88
Figure 4.2 MSF flashing stage .....	90
Figure 4.3 Brine heater and stage (1) .....	92
Figure 4.4 MSF Splitter and stage (N) .....	93
Figure 4.5 MSF Mixers .....	94
Figure 4.6 MSF simulation plants using gPROMS.....	99
Figure 4.7 Comparison of this work results with Rosso et al., (1996) results of flashing stage temperature (TBj) .....	100
Figure 4.8 Comparison of this work results with Rosso et al., (1996) results of distillate stage temperature (TDj).....	102
Figure 4.9 Comparison of this work results with Rosso et al., (1996) results of distillate stage temperature (TFj).....	102
Figure 4.10 Comparison of this work results with Rosso et al., (1996) results of brine rejected salinity CBj .....	103

Figure 5. 1 Removal of deposit from the metal surface (Bott, 1995) .....	107
Figure 5. 2 Effect of seawater temperature on fouling resistance in stage (1) of MSF recycle distiller .....	111
Figure 5. 3 Effect of seawater temperature on fouling resistance in stage (1) of MSF recycle distiller .....	111
Figure 5. 4 Effect of TBT on fouling resistance in stage (1) of MSF recycle distiller .	112
Figure 5. 5 Effect of TBT on fouling resistance in stages of MSF recycle distiller .....	113
Figure 5. 6 Effect of % increasing in fouling factor on TOC at different seawater temperature .....	118
Figure 5. 7 Effect of % increasing in fouling factor on steam cost at different seawater temperature .....	119
Figure 5. 8 Effect of % increasing in fouling factor on Q steam at different seawater temperature .....	119
Figure 5. 9 Effect of % decreasing in fouling factor on TOC at different seawater temperature .....	120
Figure 5. 10 Effect of % decreasing in fouling factor on steam cost at different seawater temperature .....	122
Figure 5. 11 Effect of % decreasing in fouling factor on Q steam at different seawater temperature .....	122
Figure 6.1 MSF desalination process with storage tank .....	126

Figure 6.2 Fresh water consumption profile on weekend (Saturday) (Herrera et al 2010).....	127
Figure 6.3 Fresh water consumption profile on working day (Monday) (Herrera et al 2010).....	128
Figure 6.4 Seawater temperature profile during the day and night (Yasunaga et al 2008) .....	129
Figure 6.5 Storage tank .....	130
Figure 6.6 (a) Tank level profile and (b) tank level violations during the MSF operation .....	131
Figure 6.7 Optimum rejected seawater flow rate throughout profile (case 1) .....	136
Figure 6.8 Optimum brine recycle flow rate throughout profile (case 1) .....	136
Figure 6.9 Fresh water plant production flow rate profile (case 1).....	137
Figure 6.10 Fresh water demand profile (case 1).....	137
Figure 6.11 Storage tank level profiles (case 1).....	138
Figure 6.12 Optimum rejected seawater ( $C_w$ ) flow rate throughout profile (case 2)...	140
Figure 6.13 Optimum brine recycle ( $R$ ) flow rate throughout profile (case 2).....	140
Figure 6.14 Fresh water production profile (case 2) .....	141
Figure 6. 15 Storage tank level profiles (case 2).....	141
Figure 6.16 Fresh water demand profile (case 2).....	142

Figure 7.1 Overall heat transfer coefficient through recovery stages at different NCGs wt % .....	149
Figure 7.2 Overall heat transfer coefficient through rejection stages .....	149
Figure 7.3 Effect of seawater temperature on steam flowrate for different number of stages at 0.015 % wt of NCG.....	153
Figure 7.4 Effect of seawater temperature on steam temperature for different number of stages at 0.015 NCG.....	154
Figure 7.5 Effect of seawater temperature on recycle brine flowrate for different number of stages at 0.015 % wt of NCG .....	154
Figure 7.6 Effect of seawater temperature on blow down temperature for different number of stages at 0.015 % wt of NCG .....	155
Figure 8.1 A single neuron.....	160
Figure 8.2 An artificial neuron.....	160
Figure 8.3 Structure of a typical multilayer neural network. ....	162
Figure 8.4 Neural network backpropagation training Scheme .....	170
Figure 8.5 Determination of optimum network Structure.....	171
Figure 8.6 A four layer neural network.....	173
Figure 8.7 Regression of NN1_K1 Predicted Data with Experiment K1 .....	183
Figure 8.8 Experimental K1 by Millero et al. (1997) and Prediction by NN1_K1.....	187
Figure 8.9 Experimental K2 by Millero et al. (1997) and Prediction by NN1_K2.....	188

Figure 8.10 Experimental K1 by Mehrbach et al. (1973) and Prediction by NN2\_K1 188

Figure 8.11 Experimental K2 by Mehrbach et al. (1973) and Prediction by NN2\_K2 189

Figure 8.12 Experimental K1 by Millero et al. (2006) and Prediction by NN3\_K1..... 189

Figure 8.13 Experimental K2 by Millero et al. (1997) and Prediction by NN3\_K2..... 190

## Nomenclature

$A_H$	Heat transfer area of brine heater ( $m^2$ )
$A_j$	Heat transfer area of stage $j$ ( $m^2$ )
$A_S$	Cross sectional area of storage tank ( $m^2$ )
$B_0$	Flashing brine mass flow rate leaving brine heater (kg/s)
BBT	Bottom brine temperature ( $^{\circ}C$ )
$B_D$	Blow-down mass flow rate (kg/s)
$B_j$	Flashing brine mass flow rate leaving stage $j$ (kg/s)
$B_N$	Flashing brine mass flow rate leaving stage $N$ (kg/s)
$C_{B0}$	Salt concentration in flashing brine leaving brine heater (wt. %)
$C_{Bj}$	Salt concentration in flashing brine leaving stage $j$ (wt. %)
$C_{BNS}$	Salt concentration in brine recycle (R) (wt. %)
$C_R$	Salt concentration in feed seawater (WR) (wt. %)
$C_S$	Salt concentration in makeup seawater (F) (wt. %)
$C_W$	Rejected seawater mass flow rate (kg/s)
$C_1$	Factor for the influence of tube turbulences
$C_2$	Factor for the influence of non-condensable gases
$C_{11}$	Constant



$C_{22}$	Constant
$D_j^i$	Internal diameter of cooling brine tubes, m
$D_j^o$	External diameter of cooling brine tubes, m
$D_j$	Distillate flow rate leaving stage j (kg/s)
$D_N$	Distillate flow rate leaving stage N (kg/s)
$E$	Activation energy
$EX_j$	Non-equilibrium allowance at stage j
$F$	Make-up seawater mass flow rate (kg/s)
$f_{CO_2}$	Fugacity of carbon dioxide (atm)
$f_j^H$	Brine heater fouling factor ( h m <sup>2</sup> °C/kcal)
$f_j^i$	Fouling factor at stage j ( h m <sup>2</sup> °C/kcal)
$GOR$	Gained output ratio
$h$	freshwater level in the storage tank (m)
$h_{Bj}$	Specific enthalpy of flashing brine at stage j (kcal/kg)
$h_{Dj}$	Specific enthalpy of saturated water at stage j (kcal/kg)
$h_F$	Specific enthalpy of make up stream (kcal/kg)
$h_R$	Specific enthalpy of recycle brine stream (kcal/kg)
$h_R$	Specific enthalpy of flashing brine at $T_F$ (kcal/kg)

$h_{vj}$	Specific enthalpy of flashing vapor at stage $j$ (kcal/kg)
$h_w$	Specific enthalpy of brine at $T_F$ (kcal/kg)
$K$	Thermal conductivity ( $w/m^2 K$ )
$K_1^{sw}$	First dissociation constant of carbonic acid in seawater (mol/kg)
$K_2^{sw}$	Second dissociation constant of carbonic acid in seawater (mol/kg)
$K_W^{sw}$	The dissociation constant of water in seawater (mol/kg)
$L$	Length of storage tank (m)
$L_H$	Length of brine heater tubes (m)
$L_j$	length of tubes at stage $j$ (m)
$LMTD_H$	The logarithmic mean temperature difference in brine heater
$LMTD_j$	The logarithmic mean temperature difference in stage $j$
$M$	Storage tank holdup
$n$	Number of tubes in vertical row
$N$	Total number of stages
$NJ$	Total number of stages in the rejection section
$NR$	Total number of stages in the recovery section
$N_t$	Total numbers of tubes in the condenser
$P_d$	Deposition of factor related to velocity and stickiness of deposit

R	Recycle stream mass flow rate (kg/s)
$R_{fi}$	Thermal resistance of scale on the inside of the tubes ( $m^2 K/w$ )
$R_{fo}$	Thermal resistance of scale on the outer of the tubes ( $m^2 K/w$ )
$R_g$	Gas constant
$r_t$	Thermal resistance of tubes material ( $m^2 K/w$ )
S	Seawater salinity (g/kg)
$SB_j$	Heat capacity of flashing brine leaving stage j (kcal/kg/°C)
$SD_j$	Heat capacity of distillate leaving stage j (kcal/kg/°C)
$SR_H$	Heat capacity of brine in brine heater (kcal/kg/°C)
$SR_j$	Heat capacity of cooling brine leaving stage j (kcal/kg/°C)
$SB_j$	Heat capacity of flashing brine leaving stage j (kcal/kg/°C)
T	Temperature (°C)
TA	Total alkalinity (mol/kg)
TBT	Top brine temperature (°C)
$T_{Bj}$	Temperature of flashing brine leaving stage j (°C)
$T_{BNS}$	Temperature of the brine in the recycle flowrate (°C)
$T_{B0}$	Temperature of flashing brine leaving brine heater (°C)
$T_{CO_2}$	Total carbon dioxide content (mol/kg)

- $T_{Dj}$  Temperature of distillate leaving stage  $j$  ( $^{\circ}\text{C}$ )
- $TE_j$  Boiling point elevation at stage  $j$  ( $^{\circ}\text{C}$ )
- $T_{Fj+1}$  Temperature of cooling brine leaving stage  $j$  ( $^{\circ}\text{C}$ )
- $T_{FNR+1}$  Temperature of makeup flowrate (F) ( $^{\circ}\text{C}$ )
- $T_{Fm}$  Temperature of the brine in feed entering recovery stage ( $^{\circ}\text{C}$ )
- $T_{Vj}$  Temperature of flashed vapour at stage  $j$  ( $^{\circ}\text{C}$ )
- $T_s$  Absolute surface temperature
- $T_{\text{steam}}$  Steam temperature ( $^{\circ}\text{C}$ )
- $T_{\text{seawater}}$  Seawater temperature ( $^{\circ}\text{C}$ )
- $U_H$  Overall heat transfer coefficient in brine heater ( $\text{Kcal} / \text{m}^2 \text{ h K}$ )
- $U_j$  Overall heat transfer coefficient in stage  $j$  ( $\text{Kcal} / \text{m}^2 \text{ h K}$ )
- $V_j$  Vapour flow rate leaving stage  $j$  ( $\text{kg/hr.}$ )
- $v_j$  Linear velocity of brine stream ( $\text{ft/s}$ )
- $V_t$  Total violation
- $W_j$  Width of stage (m)
- $W_R$  Seawater mass flow rate leaving stage 1 ( $\text{kg/s}$ )
- $W_S$  Seawater mass flow rate entering stage N ( $\text{kg/s}$ )
- $W_{\text{steam}}$  Steam mass flow rate ( $\text{kg/s}$ )

$x$	Deposit thickness
$X$	logarithmic mean temperature difference at stages
$X_{nc}$	Concentration of non-condensable gases (wt%)
$y$	Thermal resistance of brine film
$Z$	Thermal resistance

#### Greek Letters

$\Delta_j$	Temperature loss due to demister ( $^{\circ}\text{C}$ )
$\rho_v$	Flashed vapour density ( $\text{kg/m}^3$ .)
$\rho_l$	Brine density ( $\text{kg/m}^3$ .)
$\rho_j$	Brine density at stage ( $\text{kg/m}^3$ .)
$\lambda_s$	Latent heat of steam to the brine heater (kcal/kg)
$\lambda_v$	Latent heat of condensation (kcal/kg)
$\mu$	Viscosity (kg/m s)
$\Phi_d$	Deposition rate
$\Phi_r$	Removal rate.
$\Psi$	Strength of deposit
$\Omega^n$	Water quality factor

#### Index

- H Brine heater
- j Stage index
- \* Reference value

## Abbreviation

CAD Computer aided design

CFD Computational fluid dynamic

DPP Dual purpose desalination plant

ED Electrodialysis

GAMS General algebraic modeling system

GDP Generalised disjunctive programming

gPROMS general PROcess modeling system

HTC Heat transfer coefficient

$K_{sp}^{sw}$  Solubility constant of calcium carbonate in seawater

LP Low pressure steam

LSI Langelier saturation index

MEE Multieffect evaporation

MINLP Mixed integer nonlinear programming

MSF Multistage flash

MSF-BR Multistage flash-brine recirculation

MSF-OT Multistage flash-once-through

MVC Mechanical vapour compression

NCG Non-condensable gases

NLP Nonlinear programming

NN Neural network

RO Reverse Osmosis

RSI Ryznar stability index

SW Seawater

TDM Tri-diagonal matrix

TLC Total leveled cost

TOC Total operating cost

TVC Thermal vapour compression

UNDESA United Nation, department of economic and social affairs



# Chapter 1

## Introduction

### 1.1 Water Crisis and Need for Desalination

The world faces an increasing water crisis in recent years. Water shortage is one of the most important limitation of life, agriculture and industries. Like most other natural resources, fresh water is not evenly distributed across the earth. Although seawater is abundant, the available water in the ocean and sea is saline and is not suitable for normal human consumption. Moreover, 96% of the water on the earth is located in oceans and seas and 1.7 % groundwater, of which only 0.8% is considered to be freshwater (Assiry et al., 2010).

The world population is increasing at very rapid rates while the natural water resources such as rivers, lakes, subsurface, and aquifers remain constant. According to the UNDESA, 2011 report, the world population will reach 9 billion in 2043. Ninety-six percent of world population increase now occurs in the developing regions of Africa, Asia and Latin America, and this percentage will rise over the course of the next quarter century. At present, about 40% of the world's population is suffering from serious water shortages. By the year 2025, this percentage is expected to increase to more than 60% (Al-Fulaiji, 2011). This is because of the rapid increase of population, changes in the life-style, increased economic activities, and pollution that limit the use of fresh water resources. Moreover, common use of unhealthy water in developing countries causes 80-90% of all diseases and 30% of all deaths. Consequently, to resolve the water scarcity problem in many regions around the world, seawater desalination can be one of the solutions to overcome this problem. The desalination of salt water from the wells,

sea water and oceans and also from industrial, agriculture discharges is the best and main important substitutes in the world. Industrial desalination of seawater is a means of providing sustainable freshwater source for a large number of countries around the world. For example, the desalination industry becomes the main source of freshwater for domestic, industrial and agriculture use in Gulf countries and Middle East. At present, the multistage flash (MSF) and reverse osmosis (RO) desalination processes dominate the global desalination industry. For certain regions of the world, such as the Gulf countries, the MSF process accounts more than 80% of freshwater supplies (Khawaji et al., 2007).

In this chapter, the history of desalination, and brief description of different desalination processes are described. In addition, the scale formation fouling and non-condensable problems in MSF desalination plants are presented. Next, the state-of-art, scope, the aims and objectives of this research are summarised. Finally the thesis layout is outlined.

## **1.2 History of Desalination**

Desalination is a science where fresh water can be obtained from saline water. However, the scope of desalination technology nowadays is not only a water treatment technology to produce fresh water from seawater but also as a water treatment technology for effluent waters. In 1912, the six-effect (vessels) desalination plant was installed in Egypt (El-Dessouky and Ettouney, 2002). The six-effects desalination process works on the principles of inducing seawater evaporation and vapor condensation inside a series of effects (Al-Rawajfeh, 2004). After that several government and organisation gave attention to the development of desalination technology. In 1959, first thermal desalination process was developed in Kuwait

(Delyannis and Belessiotis, 2010). During the sixties and seventies, the most of the achievement has been found in the improvements in design of MSF plant with higher capacities, antiscalant, chemical additives, acid cleaning, corrosion prevention and construction of cogeneration plant (Temperley, 1995). During the seventies, specifications for plant construction, operation, chemical treatment, corrosion prevention, and control were compiled as a result of accumulated experience (Abu-Eid and Fakhoury, 1974). Development in the 1980's including the design and operation of single and multiple effect evaporation (MEE) processes at low temperature. In the mid 1990, large capacity of MSF and MEE with plant factor close to 90% and continued operation for periods varying between 2-5 years.

### 1.3 Types of Desalination Process

According to the type of energy it consumes and types of technology it uses, the commonly used industrial desalination processes (Figure.1.1) can be classified broadly into two categories:

- Heat consuming or thermal process
- Power consuming or membrane process

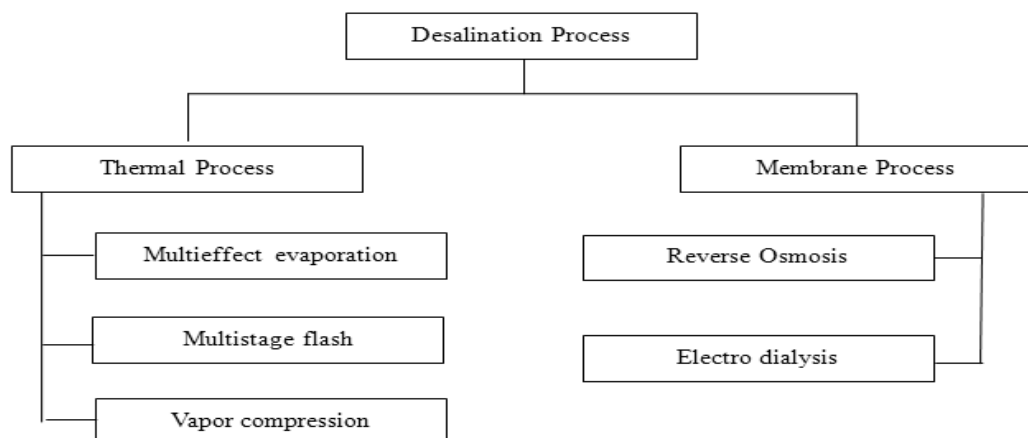


Figure 1.1 Types of desalination (Tanvir, 2007)

### 1.3.1 Thermal Process

Thermal process is the oldest desalination technology and reliable process because of good amount of experience. The thermal process is the combination of evaporation of water from brine and condensation of water vapour.

According to the phase change of the thermal process, it can be divided into:

- MEE
- MSF
- Thermal or mechanical vapour compression (TVC or MCV)

MEE and MSF are mainly dominant in the thermal desalination field. Vapour compression desalination uses power directly. (Tanvir, 2007)

#### MSF Process Desalination

The MSF distillation process is based on the principle of flash evaporation. In the MSF process, seawater is evaporated by reducing the pressure as opposed to raising the temperature (Khawaji et al., 2008). The MSF plant-brine recycle type consists of three sections: heat recovery section, rejection section and brine heater. The heat recovery and rejection sections consist of flashing chambers (stages) connected to one another. MSF process has many advantages, among them are; high quality freshwater, available knowledge of the technology, no waste from cleaning pretreatment filters, can use lower quality feedwater than RO and less scale than MEE. On the other hand, MSF process has some disadvantage such as extremely energy intensive and thermal discharge to the sea. The flashing flow system in the MSF process can be either a once through or with a recirculation.

The process description of the once-through system of MSF process is shown in Figure 1.2. The once-through MSF process has a heat recovery section and a brine heater. The heat recovery section consists of a condenser, the distillate collection trays and the flashing chamber. All the feed seawater flows through the condenser tubes and its temperature increases due to absorption of the heat of the condensing freshwater vapour. Then, the feed seawater enters the brine heater and heated to the top brine temperature by absorbing the latent heat of the condensing steam. After that, flashing of the hot brine stream and formation of the distillate product takes place across the flashing chambers. All the brine in the last stage after flashing is rejected to the sea. The main feature of the once-through system is operation at low salinity feed seawater. This reduces the fouling and scaling problem in the condenser tubes and brine heater (AlBahou et al., 2007). In addition, saving the equipment such as pumps, valves due to elimination of the rejection section is also other feature of this system (Baig et al., 2011). On the other hand, large seawater intake is the main problem facing the once-through system.

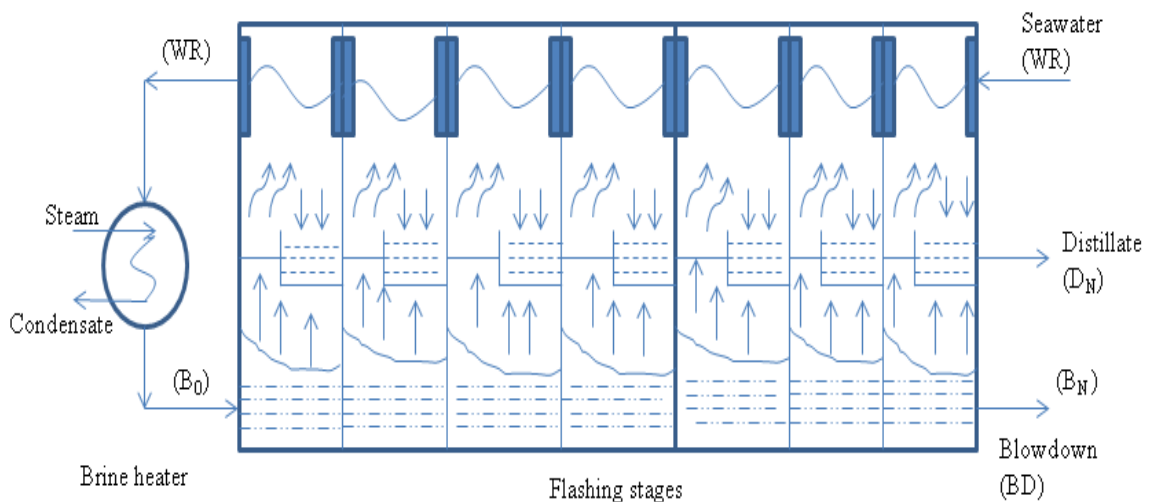


Figure 1.2 MSF-once through process type (El-Dessouky and Ettouney, 2002)

Figure 1.3 shows the brine recycle system of MSF process. The brine recycle MSF process has three sections: a heat recovery section, heat rejection section and a brine heater. The heat recovery section and heat rejection section consist of flashing stages connected to one another (more details in Chapter 2). The role of the heat rejection section is to remove the surplus thermal energy from the plant, thus cooling the distillate product and the concentrated brine to the lowest possible temperature. The brine recycle system has many advantages. Among them are; low temperature of the rejected brine due to the mixing in the stage, less pre-treatment facilities such as filtration and chemical treatment due to small seawater intake compared with once-through system (Ettouny and El-Dessouky, 1999).

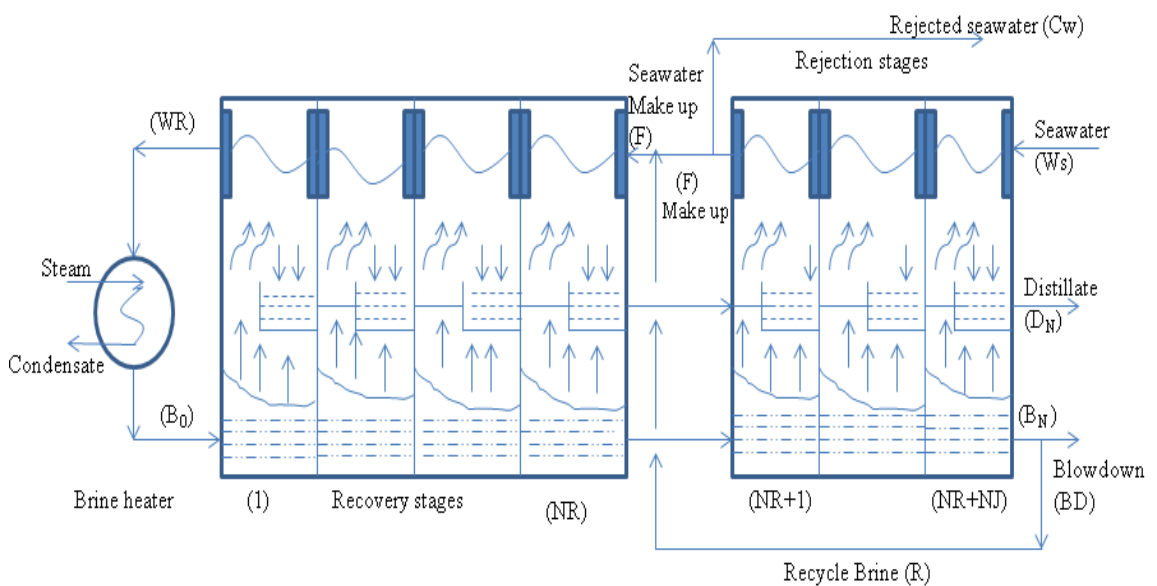


Figure 1.3 MSF-brine recycle process type (Rosso et al., 1996)

### MEE Desalination Process

MEE distillation was the first process used to produce a significant amount of water from the sea. This process takes place in a series of effects (vessels). Figure 1.4 shows the MEE process distillation. Vapor generated in the first effect gives up heat to the second effect for evaporation and is condensed inside the tubes. This continues for

several effects. The seawater is either sprayed, or otherwise distributed onto the surface of evaporator tubes in a thin film to promote rapid boiling and evaporation. The condensate from the boiler steam is recycled to the boiler for reuse. The larger the number of effects, the less heat that is required as heat sources. There are vertical and horizontal tube evaporation effects. The vertical tubes could be of the rising or the falling-film type. However, with horizontal effects, evaporation takes place on the outer surfaces of the heating tubes, steam for heating being condensed inside the tubes (Al-Shayji, 1998).

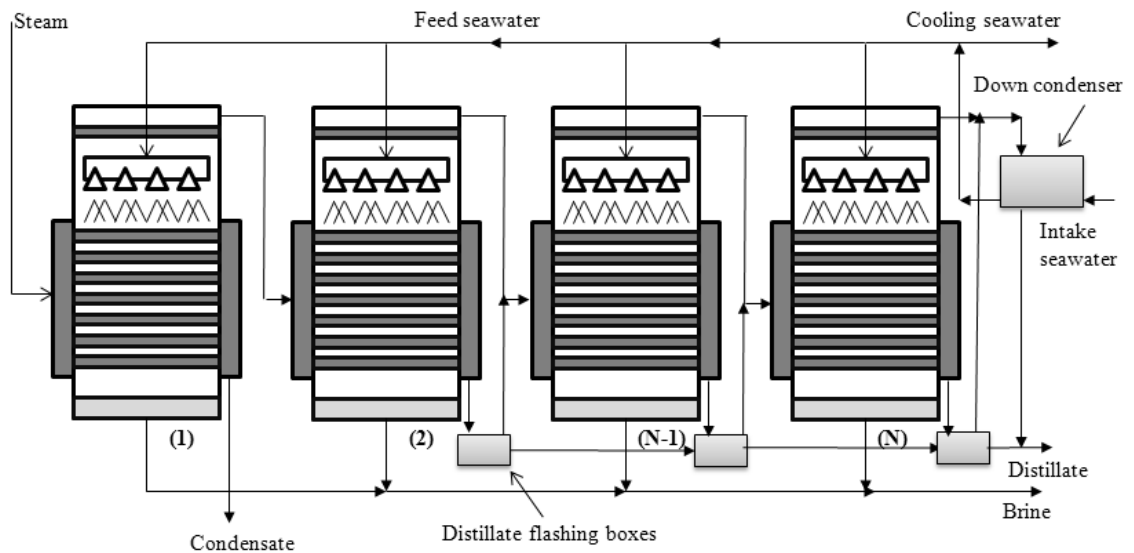


Figure 1.4 MEE desalination plant (El-Dessouky and Ettouney, 1999)

### 1.3.2 Membrane Process

In membrane process, the composition of desalted water depends on the membrane characteristics (Bowen, 1998), the feed composition and amount of recycle steam.

#### Reverse Osmosis Process

Reverse osmosis desalination process is pressure driven membrane separation process in which a dense membrane allows diffusion of the solvent and solutes. Diffusion of solutes, like salts is low compared to water results in a rejection for those substances.

When pressure is applied to the concentrated solution (seawater or brackish water), larger than the osmotic pressure, the flow of diffused solvent through the membrane is reversed as shown in Figure 1.5 and solvent flows from the concentrated solution side through the membrane to the diluted solution while dissolved ions and small molecules that contaminate aqueous solutions and impurities are rejected by the membrane. This process is called reverse osmosis (RO). The RO process depends on the quality of semi permeable membrane used and specific power consumption depends on the total dissolved solids in the seawater (Sassi and Mujtaba, 2011). The main attractive feature of the RO desalination process is the simplicity of its layout in comparison with the large-scale thermal desalination processes. Also, its modular design allows for simple expansion and increase of the production capacity (Al-Enezi and Fawzi, 2002)

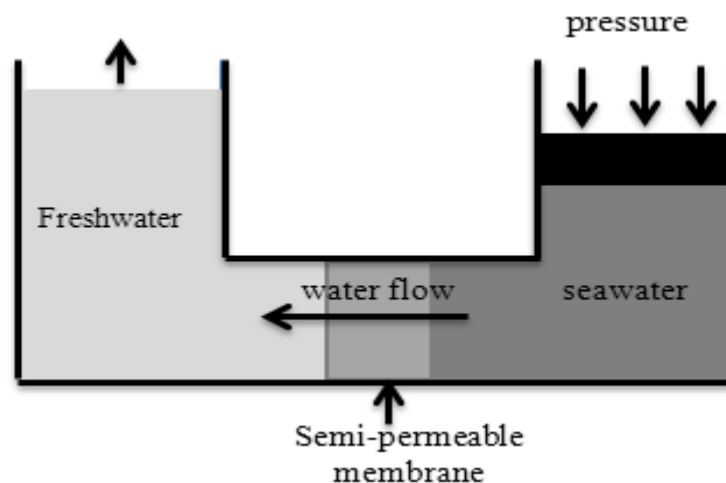


Figure 1.5 Representation of Reverse Osmosis (Sourirajan and Agrawal, 1996)

#### Electrodialysis (ED) Desalination Process

In electro dialysis process (Figure 1.6), two types of membranes are used. The action membrane allows only cations (positive ions) to permeate, and the anion membrane allows only anions (negative ions) to permeate. These exchange membranes are alternatively immersed in salty water in parallel, and an electric current is passed



through the liquid. The cations will migrate to the cathode, and the anions will migrate to the anode. Therefore, water passing between membranes is split into two streams. One is pure water, and the other is concentrated water (Al-Shayji, 1998). The main advantages of ED desalination are: higher water recovery rates for raw water with high sulfate content, longer operation life of membranes and less scale or membrane fouling. However, the ED desalination process has a limit to apply to the desalination of seawater with high salinity (Lee et al., 2009).

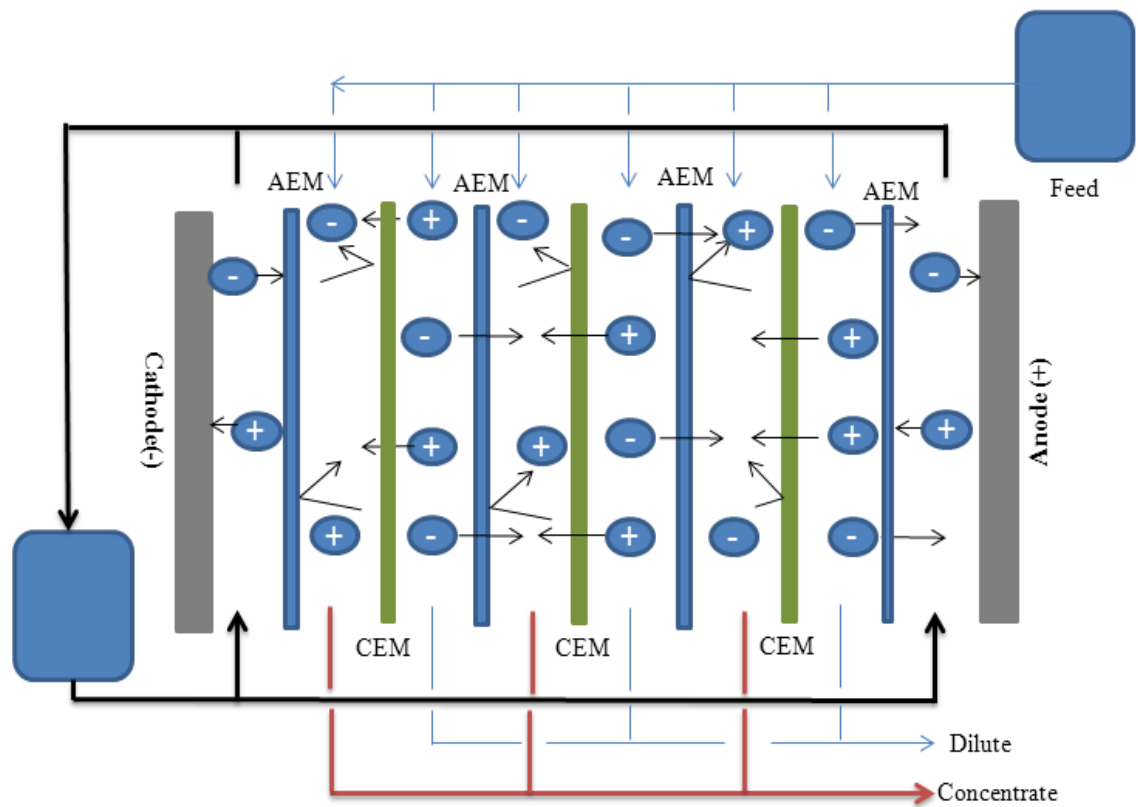


Figure 1.6 Representation of Electrodialysis (Fritzmann et al., 2007)

## **1.4 Scale Formation and Non-condensable Gases in MSF Desalination Plant**

### **1.4.1 Fouling Due to Scale Formation**

One of the problems encountered in the MSF process is that of scale formation inside the distiller and condenser tubes in heat rejection section and heat recovery section as shown in Figure 1.7 (Shams EL Din et al., 2002). The formation of scale inside the heat transfer surfaces is the major problem in the MSF distiller and results a serious loss of efficiency and production, and increase in the operating cost due to use the antiscaling chemical (Al-Rawajfeh et al., 2008). Scale formation is mainly produced by crystallization of alkaline scale such as calcium carbonate ( $\text{CaCO}_3$ ) and magnesium hydroxide ( $\text{Mg}(\text{OH})_2$ ) and non-alkaline scale like calcium sulfate ( $\text{CaSO}_4$ ). The most scales in MSF distillers are composed of  $\text{CaCO}_3$  and  $\text{Mg}(\text{OH})_2$  (El-Dahshan, 2001). The Alkaline scales result from the interaction between the decomposition and hydrolysis products of the bicarbonate ion of seawater with calcium and magnesium ions to produce  $\text{CaCO}_3$  and  $\text{Mg}(\text{OH})_2$  (Shams EL Din et al., 2005). The formation of  $\text{CaCO}_3$  and  $\text{Mg}(\text{OH})_2$  is strongly depend on temperature, pH, the release of  $\text{CO}_2$  as well as the concentration of  $\text{Ca}^{2+}$  and  $\text{Mg}^{2+}$  ions, and total dissolved solids (Al-Anezi and Hilal, 2007).

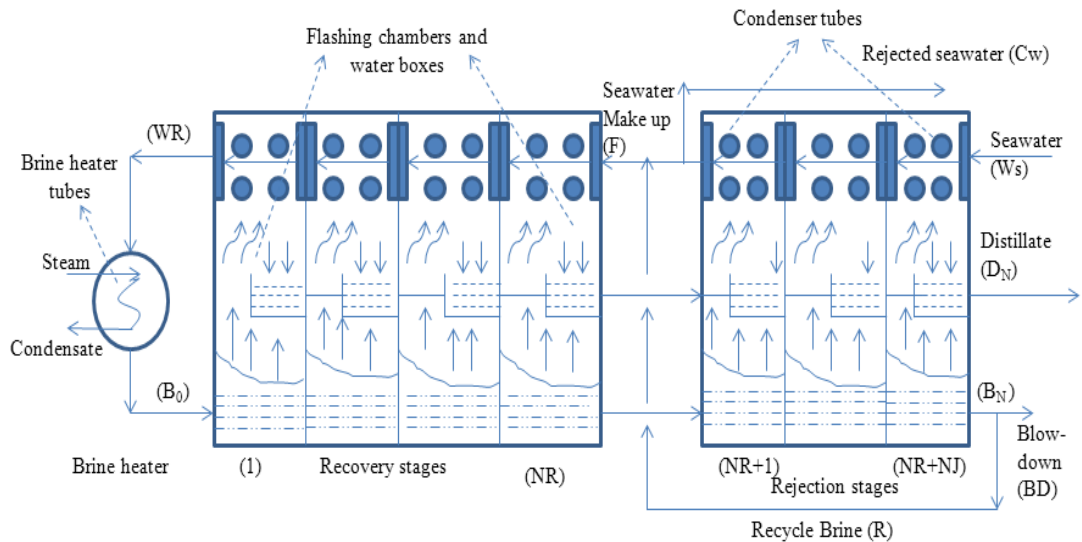


Figure 1.7 Scale formation regions in MSF plant (Shams EL Din et al., 2002)

### 1.4.2 Non-condensable Gases

Non-condensable gases (NCG) are a serious problem in MSF distillation (Al-Rawajfeh et al., 2003). The NCG consist mainly of air ( $N_2$  and  $O_2$ ) and  $CO_2$ . The presence of NCG in the MSF desalination plants is caused by:

1. Dissolved air in the seawater feed to the plant.
2. Carbon dioxide liberated by the break-down of bicarbonates dissolved in the feed. The seawater contains bicarbonate ion, when the sea water is heated or acidified with mineral acids, carbon dioxide is formed owing to decomposition of the bicarbonate ion.
3. The leakage of ambient air through flanges, man-holes, instrumentation nozzles, into the parts of the evaporating brine
4. Free carbon dioxide dissolved in the feed.

The NCG cause local reduction of performance, decrease of efficiency and hence a cost increase in most thermal desalination units. It was shown that even low concentrations of NCG gases significantly reduce the overall heat transfer coefficient (Khan, 1972).

This is happen due to the accumulation of the NCG at the interface between the vapour and condensate film. The rise in partial pressure of NCG near the film reduces the vapour pressure and condensation temperature and this produce an additional heat transfer resistance between film and vapour (Genthner et al., 1993). Therefore, additional heat transfer area is incorporated to handle the presence of non-condensable gases. In addition, in the MSF process, gas accumulation outside the design specifications would reduce the brine recycle temperature entering the brine heater. This will need to use larger amount of the heating steam, which will reduce the process thermal performance ratio of the plant (El-Dessouky and Ettouney, 2002).CO<sub>2</sub> dissolves in the condensate tubes lowers its pH value. In presence of O<sub>2</sub>, this may cause corrosion of the condenser tubes. Production losses due to plant shut-down for maintenance and reduction of lifetimes are the consequences (Oldfield, 1987). The release of CO<sub>2</sub> from the evaporating brine in seawater distillers considerably influences the concentrations of HCO<sub>3</sub><sup>-</sup>, CO<sub>3</sub><sup>-2</sup>, H<sup>+</sup>, and OH<sup>-</sup> ions in the carbonate system of the brine and plays an important role in alkaline scale formation. Furthermore, the accumulation of NCG in MSF distillers can lead to pressure losses for interstage brine transfer causing high brine level in brine pool.

## **1.5 State of the Art**

Modelling plays an important role in simulation, optimisation and control of MSF desalination plant process. The main issues in MSF desalination process are; improving the performance ratio which is the amount of product freshwater per unit mass of heating steam, improving the productivity, minimising the operating cost and optimising the design and operation parameters of the system. Furthermore, one of the more serious problems encountered in the MSF process is the scale deposition fouling inside the condenser tubes of the flashing stages and the brine heater, which reduce the

thermal performance of the plant, loss of water production, and increase in both operating and capital cost (Al-Ahmad, 2008). In the past, several studies have been done on the fouling problems in MSF desalination process. Most of these studies were experimental work to understand the scale formation process and antiscaling evaluation tests (Elliot et al., 1974; Casini, 1983; Shams El Din and Razak, 1989; Shams El Din and Mohamed, 1994; Hamed et al., 1999). However, only few publications were found in the literature which studies the scale formation modeling (Cooper et al., 1983; El-Dessouky and Khalifa, 1985; Al-Ahmad and Aleem, 1993; Al-Ahmad and Aleem, 1994). In addition, most of these studies did not include any effects of MSF operating parameters such as flow velocity, temperature and foulant concentration. In fact this may lead to excessive and unnecessary overdesign. More important, and as seen from the literature, varying scale formation fouling resistance in the developing of the steady state modelling and optimisation of MSF process has received little attention. Most of these studies carried out using fixed fouling factor in the calculating of overall heat transfer coefficient (Coleman, 1971; Khan, 1986; Helal et al., 1986; Hussain et al., 1993; El-Dessouky et al., 1995, Rosso et al., 1996; Aly and El-fiqi, 2003; Tanvir and Mujtaba, 2006; Alasfour and Abdulrahim, 2009; Alfulaiji et al., 2010). However, Hawaidi and Mujtaba (2010) developed a linear dynamic brine heater fouling factor and studied the role of fouling factor on the simulation and optimisation of MSF process. Therefore, part of this work is focused on investigating the role of varying fouling resistance and its effect on the operation and design of MSF process.

There are several studies which have been done on the optimisation of design and operation parameters of MSF process. Most of these studies were based on fixed water demand and fixed seawater temperature during a day and throughout the year (Wade et al., 1999; Mussati et al., 2001, Mussati et al., 2005, Mussati et al., 2008, Tanvir and Mujtaba 2008; Hawaidi and Mujtaba 2010). In reality, the freshwater demand (Alvisi et

al., 2007) and the seawater temperature (Yasunaga et al., 2008) vary throughout the day. Only Hawaidi and Mujtaba (2011) performed an optimisation of MSF desalination process involving a variable fouling factor in the brine heater, demand of freshwater throughout the day and throughout the year, with varying seawater temperatures throughout the day and year. However the scale deposition factor inside the condenser tubes of the flashing stages has an effect on the optimisation of the MSF process with varying seawater temperature and freshwater demand during the day and throughout the year. Therefore, in this work, the optimisation of the design and operation parameters of MSF process has been done to minimise the operating cost with varying fouling factor in the brine heat, recovery stages, and rejection stages and varying seawater temperature and freshwater demand during the day.

The other factor which has been neglected in the steady state modeling and simulation of the MSF process is the effect of NCG on the overall heat transfer coefficient and plant performance. Although there are many studies which have been done on the steady state modeling of MSF process (Coleman, 1971; El-Dessouky et al., 1985; Khan, 1986; Helal et al., 1986; Hussain et al., 1993; Rosso et al., 1996; Aly and El-fiqi, 2003; Tanvir and Mujtaba, 2006; Alasfour and Abdulrahim, 2009; Alfulaiji, 2011), only a very limited number of publications considered the effect of NCG in their models. The presence of NCG in the flashing chambers of MSF reduces the overall heat transfer coefficient and consequently reduces the performance and production capacity of MSF process. A few researches included the effect of NCG in their MSF models (El-Dessouky et al., 1995; Alasfour and Abdulrahim, 2009; Alfulaiji et al., 2011). However, they only carried out their models with fixed values of NCG and they did not study the effect of variation of NCG in the flashing stages on the design and operation parameters of MSF process (El-Dessouky et al., 1995; Alasfour and Abdulrahim, 2009). Alfulaiji,

2010 only included the effect of NCG in the mass balance equation of the flashed vapour in the flashing chambers.

Studying the release process of NCG in the MSF flashing stages is very important in calculating the mass flowrate of the NCG liberated from the flashing brine during the flashing process inside the brine pool. This also leads to understand the venting rate system design in the MSF process. A small venting rates lead to an accumulation of the NCG with the described adverse effect on the heat transfer and material life time and overestimation results in unnecessary vapour losses and higher energy consumption (Al-Rawajfeh, 2008). The release process of NCG in MSF evaporators are influenced by many factors. Among them is the composition of the carbonic acid at the entrance of the first flash chamber (Glade, 1995). Although there is some work which has been done on the release process of NCG (Lukin and Kalashnik, 1982; Glade and Genthner, 1995; Watzdorf and Marquardt, 1997; Glade et al., 2005; Al-Rawajfeh, 2008), only a few studies on the developing correlations to compute the dissociation constants of carbonic acid in seawater was found in the literatures (Mehrbach et al., 1973; Millero, 1995; Mojica et al., 2002). Small error in calculating the dissociation constant of carbonic acid in seawater can lead to considerable errors in the describing the release process of NCG during the flashing process.

In fact, to the author's best knowledge, no previous studies have been reported to date on the steady state model and simulation of MSF process with varying fouling resistance and at different amount of NCG and their effect on the design and operation parameters of the plant.

## 1.6 Scope of this Research

With previous background, the present research is focused on the following:

- To understand the role of calcium carbonate fouling factor resistance as a function of surface temperature with varying top brine temperature and seawater temperature. Furthermore to developed a MSF steady state model with varying calcium carbonate fouling in the brine heater, heat recovery and rejection section. Also, to study the effect of fouling factor with variation of seawater temperatures on the operating cost. The monthly operation cost is selected to minimise, while optimising the operation parameters such as rejected seawater flowrate, brine recycle flowrate for fixed water demand.
- To investigate the effect of variable freshwater demand throughout the day with varying fouling factor and seawater temperature without any shortage of freshwater access for the users) on design and operation of MSF desalination process. The role of an intermediate storage tank in meeting the variable demand and operation of the plant.
- To study the effect of presence of NCG on the overall heat transfer coefficient in MSF distiller chambers. Also to developed a MSF steady state model with vary effect of presence of non-condensable gases. In addition, to study the effect of presence of NCGs on the operation parameters of MSF processes for different plant configurations and with fixed freshwater demand.
- To develop the neural network (NN) based correlation to predict the first and second dissociation constant of carbonic acid in seawater as function of temperature and salinity. Also, to use these correlations to study the release



process of NCG (CO<sub>2</sub>) during the flashing process and calcium carbonated scale deposition in MSF distillers.

## **1.7 Aims and Objectives of This Work**

This research is focused on modeling and simulation and optimisation of MSF desalination process including the effect of NCG and variable fouling factor resistance for fixed/variable freshwater demand and variable seawater temperature during a day and night. The main objectives of this work can be summarised as follows:

- To carry out literature survey on the steady state modelling, simulation and optimisation of MSF desalination process.
- To develop comprehensive MSF process model using gPROMS modeling tool based on the mass and energy balances and physical properties correlations and to validate the model using the simulation results reported by Rosso et al. (1996) before it is extensively used for further investigation.
- To study the role of changing fouling factor resistance in the heat recovery section and heat rejection section and brine heater with surface temperature and effect of top brine temperature and seawater temperature on the fouling factor resistance.
- To optimise the design and operating parameters of the MSF process such as rejected seawater flow rate and brine recycle flow rate with variable fouling factor and seawater temperature while minimising total operating cost with a fixed freshwater demand.
- To include an intermediate storage tank between the MSF process and the client and to link the steady state process model for the MSF process with the dynamic

model for the storage tank. The model is then incorporated into the optimisation framework to find the optimal design and operation of the process to meet variable freshwater demand with varying seawater temperature throughout the day.

- To minimise the total operating cost of the process while optimising the design parameters such as total number of stages and some operating parameters such as rejected seawater and recycle brine at discrete time interval with different freshwater demand and seawater temperature during a day.
- To developed the correlations which take into consideration the effect of NCG on the calculations of overall heat transfer coefficient in recovery and rejection section and brine heater and implemented in the full MSF process model.
- To study the effect of variations in the NCG concentration on the MSF plant performance parameters. In addition how the design and operation are to be adjusted to maintain fixed demand of fresh water throughout the year for change the seawater temperature and steam temperature in the presence of different concentrations of NCG.
- Three NN based correlations are developed for estimating the first and second dissociation constants of carbonic acid in seawater for a given temperature and salinity. Note, the use of NN in all aspects of process engineering activities, such as modeling, design, optimisation and control, has been considerably increased in recent years (Mujtaba and Hussain, 2001).

## **1.8 Thesis Layout**

The layout of this thesis is presented below

### **Chapter 2: Literature Review**

The general description of multi stage desalination plants (brine recirculation) and the main parameters affecting the performance of MSF desalination process is carried out. Brief description of scale formation mechanism and the release process of non-condensable gases and their effects on MSF process are also discussed. In addition, literature review of the previous work on the modelling, simulation and optimisation of the MSF plant is outlined. In addition, the effect of fouling factor and non-condensable gases on MSF process is also presented in this chapter.

### **Chapter 3: Modelling, Simulation and Optimisation in gPROMS**

Important features of gPROMS model builder software package that has been used for modeling, simulation and optimisation are discussion in this chapter. The brief description of the composite model and connective of gPROMS tools with different software and MS Office software through gPROMS foreign process and object interface is highlighted. The comparison in terms of the benefit of using the gPROMS rather than other modelling package is also described.

### **Chapter 4: Modelling and Simulation of the MSF Process using gPROMS**

A detailed steady state mathematical modelling of MSF process using gPROMS software is presented in this chapter with validation results from the literature.

### **Chapter 5: Effect of Fouling Factors on The Optimisation of MSF Desalination Process for Fixed Water Demand using gPROMS**

Chapter five described a calcium carbonate fouling factor resistance models. This model has been implemented in full steady state MSF mathematical model. The effect of some MSF operation parameters such as top brine temperature and seawater temperature on the fouling factor resistance is also studied. In addition, optimisation of MSF operation parameters such as steam temperature, rejected seawater flowrate and recycle brine flowrate has been carried out while minimising the total operating cost for fixed water demand and variable seawater temperature and fouling factor resistance.

#### Chapter 6: Flexible Design and Operation of MSF Desalination Process: Coping with Different Freshwater Demand

Chapter six provided a polynomial correlation for predicting dynamic freshwater demand profiles at different time of the weekend and working days depending on actual data from the literature. A detailed steady state MSF process model incorporating polynomial correlation for predicting freshwater demand coupled with dynamic for the storage tank is outlined in this chapter. Economic optimisations are carried out for variable freshwater demand with changing seawater temperature throughout the day. Flexible design and operation of MSF desalination process is also carried out.

#### Chapter 7: Modelling and Simulation of the Effect of non-condensable Gases on MSF Process

A steady state mathematical MSF process model with effect of non-condensable gases on the overall heat transfer coefficient is presented here. The effect of changing process parameters on the MSF process performance to maintain the fixed water demand in the presence of NCG are presented and analysed in this chapter.

## Chapter 8: Neural network Based Correlations for Estimating Dissociation Constant of Carbonic acid in Seawater

A general overview of the neural network techniques and neural network based application in process engineering in this chapter. Three Neural network based correlations for predicting first and second dissociation constant of carbonic acid in seawater have been developed and validated with different experimental data sets.

## Chapter 9: Conclusion and Future Work

The final conclusions and suggested future recommendations of this work are presented.

## Chapter 2

### Literature Review

#### 2.1 Description of the MSF

Distillation is the oldest of all the desalination technologies. MSF distillation process has been used for many years (Hussain, 2003). An MSF process (Figure 2.1) mainly consists of three sections: brine heater section, recovery and rejection sections each with a number of flash chambers (stages). Seawater enters the last stage of the rejection stages and passes through series of tubes to remove heat from the stages. Before the recovery section, seawater is partly discharged into the sea to balance the heat. The other part is mixed with recycled brine from the last stage of the rejection section and fed before the last stage of the recovery section. Seawater is flowing through the tubes in different stages to recover heat from the stages and the brine heater raises the seawater temperature to the maximum attainable temperature (Top brine temperature, TBT). After that, it enters the first flashing stage and produce flashing vapour. The vapour then passes through the demisters, where the salt carried with the vapour is removed, condenses on the cooling tubes (water box) and is collected as distillate in the distillate tray.

Figure 2.2 shows the cross section of a single stage. This process continues until the last stage of the rejection section. The distillate is finally collected, disinfected, and treated for pH and hardness before going to storage vessels. The concentrated brine from the last stage is partly discharged to the sea and the remaining is recycled as mentioned before.

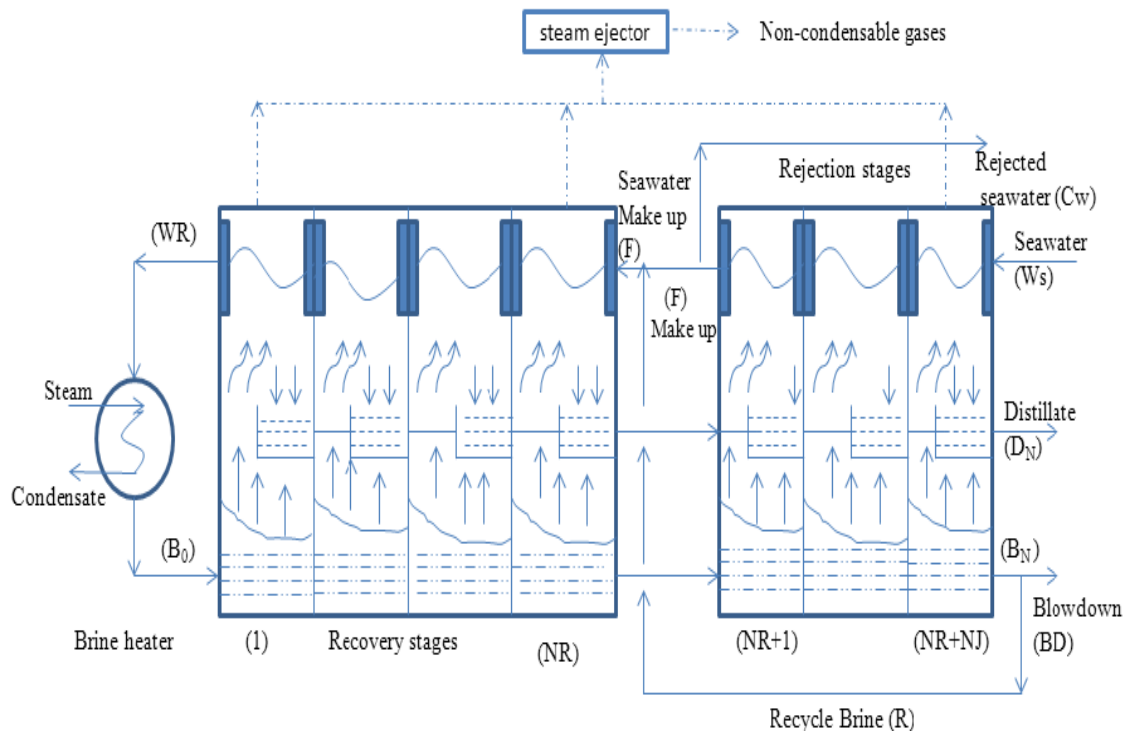


Figure 2.1 Typical MSF Process (Rosso et al., 1996)

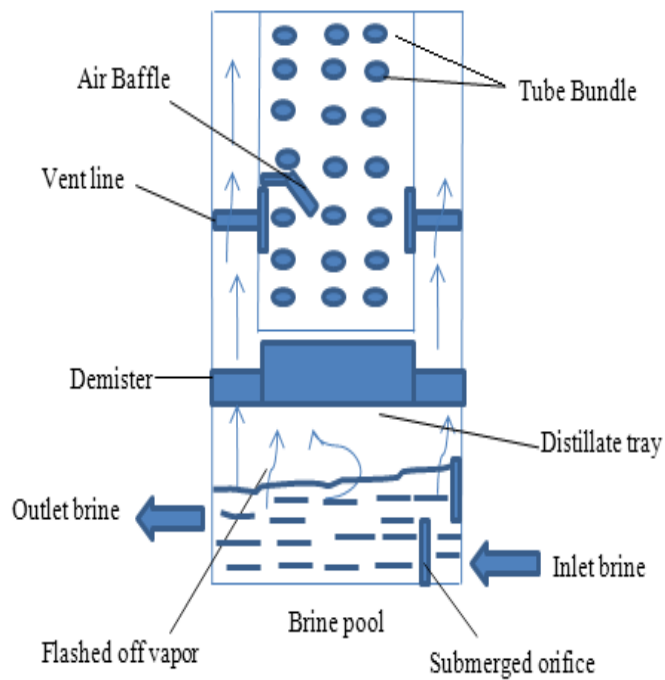


Figure 2.2 MSF flashing stage (El-Dessouky and Ettouney, 2002)

Several configurations of the MSF desalination systems are found in the literature, which developed over years.

- Single stage flash
- Once-through MSF
- Simple mixer brine recirculation
- Conventional MSF (such as one stage heat rejection brine circulation MSF, two stage/multiple brine recirculation).

As described, conventional MSF plant consists of three sections: the brine heater, the recovery section and heat rejection section and includes:

- A large brine pool
- The demister (formed of the wired mesh)
- The tube bundle of the condenser and preheated
- The distillate tray
- Water boxes at both ends of the tube bundle.
- Connections for venting system
- Instrumentation: thermocouple, level sensor and conductivity meter
- The number of stages in the heat recovery section is larger than the heat rejection section
- The brine heater.



## **2.2 Operation Variables in MSF Process**

### **2.2.1 Top Brine Temperature (TBT)**

The TBT plays an important role in determining the performance of a MSF plant. The brine concentration and the type of feed treatment determine the value of TBT. TBT cannot be raised above a certain value due to scaling problem. The upper limit of TBT depends on the types of chemicals and the brine concentration. However, reducing a TBT below a certain limit will cause insufficient pressure difference to vent the NCG from the flashing chambers and possible of vapor-side corrosion problems (Al-Shayji, 1998).

### **2.2.2 Make-Up Flowrate (F)**

As the make-up flow increases, the salt concentration in brine stream decreases. This will lower steam consumption and will decrease the blowdown salt concentration. The lower limit of the make-up flowrate depends on the salt concentration of the recirculating brine flow, and its upper limit changes with the cooling seawater flowrate and seawater supply-pump discharge pressure (Al-Shayji, 1998).

### **2.2.3 Recirculating Brine Flowrate (R)**

The recirculating brine flow rate is one of the most important operational variables affecting the performance of the MSF plant. Increasing the recirculating brine increases the distillate production, but adversely affects the performance ratio. Also, the recirculating brine flowrate determine the velocity inside the condenser tubes. This brine velocity has an effect on the scale formation, deposition, and removal. Recirculating brine flowrate also has influence on the degree of fouling occurring, as a

reduced recirculating flowrate can increase the fouling by reducing the scouring of deposits from the tube surfaces (Al-Shayji, 1998).

#### **2.2.4 Steam Flowrate ( $W_{\text{steam}}$ ) and Steam Temperature ( $T_{\text{steam}}$ )**

The steam flow rate entering brine heater affects the top brine temperature and distillate production  $D_N$ . In order to avoid the scale precipitation, the steam temperature and shell pressure regularly increase to maintain the desired TBT and distillate production (El-Dessouky and Ettouney, 2002).

#### **2.2.5 Seawater Feed Temperature ( $T_{\text{seawater}}$ )**

The seawater temperature varies from winter season to summer season. For example in the Arabian Gulf, the seawater water temperature varies between 14°C in winter and 35°C in summer. The efficiency of the MSF plant depends on the flashing range which is the difference between the top brine temperature and seawater temperature (El-Dessouky and Ettouney, 2002). Recent studies (Tanvir and Mujtaba, 2007) show that the production of fresh water from MSF process can vary with seasonal temperature variation of seawater producing more water in winter than in summer for a fixed design and operating conditions.

#### **2.2.6 Rejected Seawater Flowrate ( $C_w$ )**

In order to maintain the required seawater outlet temperature from the heat-rejection section, the cooling seawater flowrate ( $C_w$ ) reduces as the ambient temperature decrease. The lower limit of the seawater flowrate enters the heat rejection section corresponds to the requirement of specified rate of evaporation in the heat rejection section. The upper limit is restricted by the maximum available pump flow of the

seawater supply pump. Both limits are corresponding to the limits on the velocities in the tubes.

### **2.2.7 Concentration Ratio**

As the makeup flow increase, the salt concentration in brine stream decreases, which in turn will decrease the specific gravity of the brine and the boiling-point elevation. This lowers steam consumption and decrease the blowdown salt concentration (Al-Shayji, 1998).

## **2.3 Venting System in the MSF Desalination Plant**

In MSF, the NCG entering with the feed water are liberated during the evaporation process and have to be vented from each stage of the evaporator to the ejector system by adequate venting system as shown in Figure 2.1. Venting system in the MSF thermal desalination is driven by steam ejectors to removal of non-condensable gases during startup and operation. The flashing chambers in MSF are open to ambient air during shut-down processes. Therefore, air removal is one of the main activities in the startup procedure. During steady state operation, the main function of the ejectors is to remove of the NCG in order to reduce the concentration of these gases, which would accumulate around the condenser tubes (Al-Sum et al., 1993).

## **2.4 The Carbonate System in Seawater**

To describe the release process of the NCG in MSF distiller, the thermodynamic and the kinetics of the carbonate system in seawater is necessary.

The carbonate system (Figure 2.3) is a weak acid-base system which exists in seawater as dissolved carbon dioxide, carbonic acid, bicarbonate and carbonate ions and

complexes of these ions. Basically the system is derived from the dissolution of carbon dioxide gas and carbonate minerals into the water (Al-Rawajfeh, 2004).

Seawater is an aqueous mixed electrolyte. It reaches its chemical composition through a series of chemical reactions and physicochemical process. Among these are: acid-base reactions, gas absorption and desorption processes, precipitation and dissolution of solids and desorption processes at interfaces (Al-Rawajfeh, 2004). Table 2.1 shows the composition of standard seawater with a salinity of 35 g/kg. The specific concentration of species *i* is equal to its concentration in g/kg divided by the total concentration of seawater in g/kg.

The gas phase in the carbonate system forms an integral part of it. If the system is in equilibrium, any change in the partial pressure of CO<sub>2</sub> in the gas phase induces a state of non-equilibrium between gas and aqueous phases. This causes, with time, an exchange of CO<sub>2</sub> between the phases resulting in a shift in pH and the species concentration until equilibrium between the phases is re-established (Al-Anezi and Hilal, 2007).

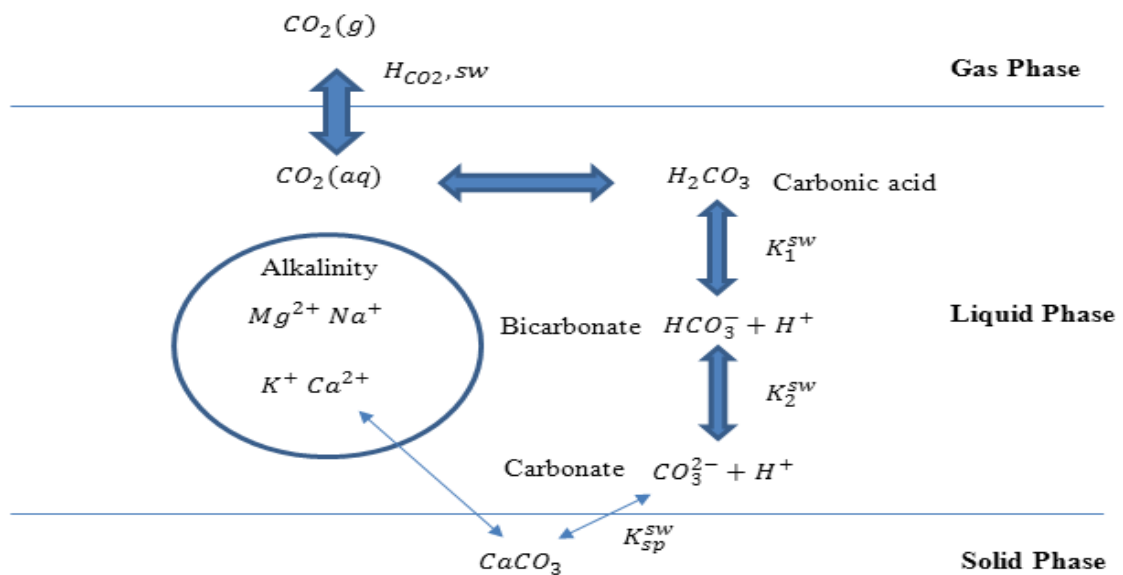


Figure 2.3 Schematic represent of the carbonate system in gas, liquid and solid phase

(Al-Rawajfeh, 2004)

Table 2.1 The composition of standard seawater (Al-Anezi and Hilal, 2007)

Species	Concentration		Specific concentration (g/kg)/s
	(g/kg seawater)	(gmole/kg seawater)	
Na <sup>+</sup>	10.7838	0.46907	0.30811
Mg <sup>2+</sup>	1.2837	0.05282	0.036678
Ca <sup>2+</sup>	0.4121	0.01028	0.01177
K <sup>+</sup>	0.3991	0.01021	0.01140
Sr <sup>2+</sup>	0.0079	0.00009	0.000227
Cl <sup>-</sup>	19.3529	0.54588	0.55294
SO <sub>4</sub> <sup>2-</sup>	2.4124	0.02824	0.07750
HCO <sub>3</sub> <sup>-</sup>	0.1070	0.00175	0.00306
Br <sup>-</sup>	0.0672	0.00084	0.00192
CO <sub>3</sub> <sup>2-</sup>	0.0161	0.00027	0.000459
B(OH) <sub>4</sub>	0.0079	0.00010	0.000225
F <sup>-</sup>	0.0013	0.000068	0.00037
B(OH) <sub>3</sub>	0.00193	0.00031	0.00051
Total	35.1707	1.1199	1.004877

Note, seawater with total dissolved solid (TDS) of 35,000 mg/l (ppm) is considered as 'standard seawater' (Millero et al., 2008).

### 2.4.1 Thermodynamics of the Carbonate System

The most abundant gases in seawater are nitrogen, oxygen, carbon dioxide and argon. The gases dissolved in seawater can be classified into two types: the first type is molecularly dissolved and does not react chemically such as N<sub>2</sub>, O<sub>2</sub> and Ar, while the other type chemically reacts in seawater such as CO<sub>2</sub>.

The carbon dioxide in seawater is governed by the following equilibria:



Subsequently, the dissolved gas combines with water to form carbonic acid H<sub>2</sub>CO<sub>3</sub>:



The carbonic acid dissociates to form bicarbonate HCO<sub>3</sub><sup>-</sup> and carbonate CO<sub>3</sub><sup>2-</sup> :



The water itself dissociates to form H<sup>+</sup> and OH<sup>-</sup> ions:



The carbonate system in seawater is characterized by the interaction of major cations (Na<sup>+</sup>, Mg<sup>2+</sup>, Ca<sup>2+</sup> and k<sup>+</sup>) and major anions (Cl<sup>-</sup>, SO<sub>4</sub><sup>2-</sup>, HCO<sub>3</sub><sup>-</sup> and CO<sub>3</sub><sup>2-</sup>).

Insoluble calcium carbonate and magnesium hydroxide can be formed:





## 2.4.2 Equilibrium Constants in Seawater

### *Dissociation Constant of water*

For the of water dissociation reaction (2.5):

The dissociation equilibrium constant of water in seawater can be expressed as

$$K_w^{\text{sw}} = [\text{H}^+]^{\text{sw}} [\text{OH}^-]^{\text{sw}} \quad (2.10)$$

Where  $[\text{H}^+]^{\text{sw}}$  and  $[\text{OH}^-]^{\text{sw}}$  are the concentration of the  $\text{H}^+$  and  $\text{OH}^-$  in seawater in mol/kg

The equilibrium constant of water in seawater was measured for temperatures up to 35°C and salinities up to 44 g/kg (Dickson and Riley 1979, Mehrbach et al., 1973).

Dickson and Riley (1979) proposed the following correlation:

$$\log K_w^{\text{sw}} = - \left( \frac{3441}{T} + 2.241 - 0.09415S^{0.5} \right) \quad (2.11)$$

Where  $K_w^{\text{sw}}$  mol/kg seawater, T in K and S in g/kg.

### *Dissociation Constant of Carbonic Acid*

Applying the law of mass action to the first dissociation of carbonic acid



$$K_1^{\text{sw}} = \frac{[\text{H}^+]^{\text{sw}} [\text{HCO}_3^-]^{\text{sw}}}{[\text{CO}_2]^{\text{sw}}} \quad (2.12)$$

Where  $[i]^{\text{sw}}$  is the concentration of the component ( i ) in seawater in mol/kg.

The second dissociation constant of the reaction  $\text{HCO}_3^- \leftrightarrow \text{CO}_3^{2-} + \text{H}^+$  can be written as

$$K_2^{\text{sw}} = \frac{[\text{H}^+]^{\text{sw}} [\text{CO}_3^{2-}]^{\text{sw}}}{[\text{HCO}_3^-]} \quad (2.13)$$

Where  $[i]^{\text{sw}}$  is the concentration of the component (i) in seawater in mol/kg.

Many researchers presented various correlations of  $K_1^{\text{sw}}$  and  $K_2^{\text{sw}}$  of carbonic acid in seawater. They investigated the parameters used to study the carbonate system such as pH, total alkalinity (TA),  $f_{\text{CO}_2}$  (fugacity) and  $T_{\text{CO}_2}$ , since a combination of at least two of these parameters is needed to characterize the carbonate system (Al-Anezi and Hilal 2007). Miellro (1995) suggested two correlations for computing the dissociation constants  $K_1^{\text{sw}}$  and  $K_2^{\text{sw}}$  and these correlations are based on the experimental data of Roy et al. (1993) and Goyet et al. (1989).

$$\begin{aligned} \ln K_1^{\text{sw}} = & 0.1886 - \frac{2275.036}{T} - 1.468591 \ln(T) + \left( -0.138681 - \frac{9.33291}{T} \right) S^{0.5} + \\ & + 0.0726483S - 0.00574938S^{1.5} \end{aligned} \quad (2.14)$$

$$\begin{aligned} \ln K_2^{\text{sw}} = & -0.84226 - \frac{3741.1288}{T} - 1.437139 \ln(T) + \left( -0.128417 - \frac{24.41239}{T} \right) S^{0.5} + \\ & 0.1195308S - 0.00912840S^{1.5} \end{aligned} \quad (2.15)$$

Where  $K_1^{\text{sw}}$  and  $K_2^{\text{sw}}$  are mol/kg seawater, T in K and S in g/kg.

Figures 2.4 and 2.5 show the dissociation constant  $K_1^{\text{sw}}$  and  $K_2^{\text{sw}}$  in seawater as function of temperature and salinities.



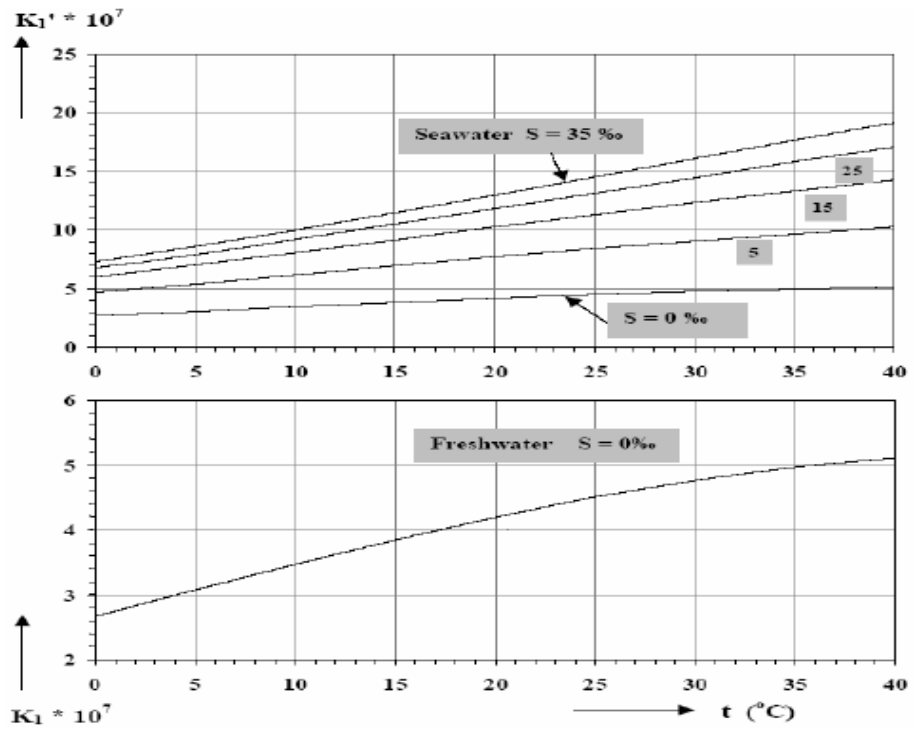


Figure 2.4 The first dissociation constant of carbonic acid in fresh and seawater as function of water temperature at salinities of 0, 5, 15, 25, and 35 % (Al-Anezi and Hilal, 2007)

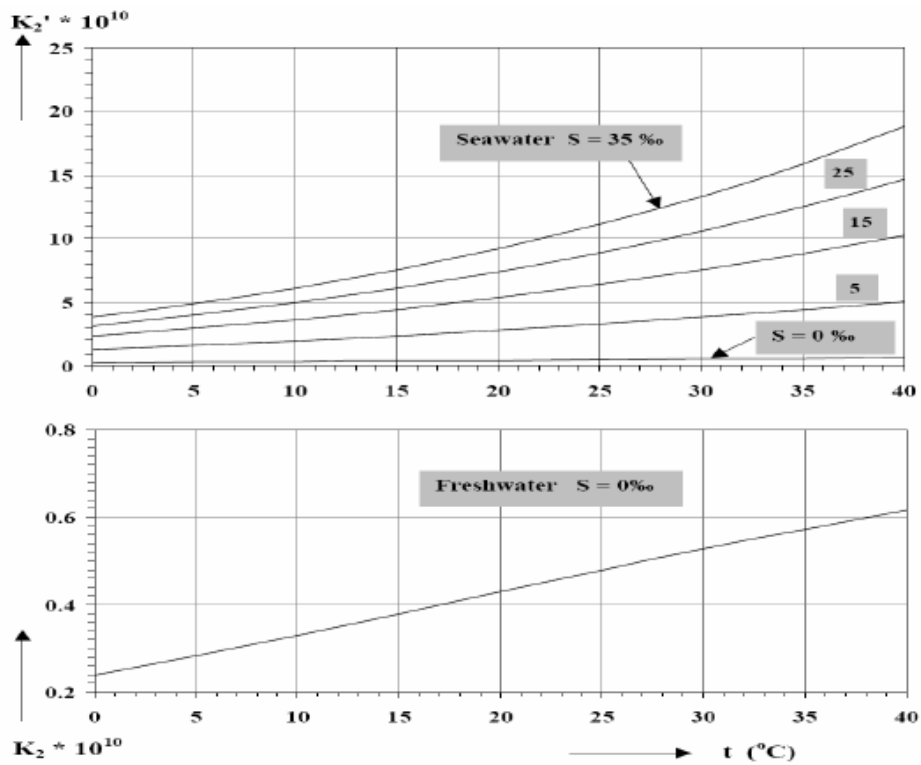


Figure 2.5 The second dissociation constant of carbonic acid in fresh and seawater as function of water temperature at salinities of 0, 5, 15, 25, and 35% (Al-Anezi and Hilal, 2007)

## 2.5 Scale Formation Process in MSF Desalination Plants

### 2.5.1 Alkaline Scale Deposition Process

The calcium carbonate and magnesium hydroxide scales in MSF plant are known as the alkaline scale. MSF plants usually operate at temperatures as high as 120°C, and consequently, the major risk of scaling is for minerals whose solubility decreases with increasing temperature.

The following mechanism for alkaline scale formation was proposed by Hillier (1952) and modified by Langelier (1954) and reported by Ellis et al. (1971):

On heating above 50°C, calcium carbonate is formed, which can precipitate and carbon dioxide is liberated.



CaCO<sub>3</sub> is often reported (Al-Sum and Hodgkiess, 1997) to precipitate in favour of Mg(OH)<sub>2</sub> at low temperature (i.e. 40 to 80°C).

At higher temperature (i.e. 80 -110 °C), the rate of carbonate hydrolysis increases and the pH increase with the release of CO<sub>2</sub> and this leads to the formation of magnesium hydroxide due to



Equation 2.17 is the net reaction of the predominant alkaline mechanism in the carbonate system and it is driven to the right direction with the release of CO<sub>2</sub>. This is the first step of scale formation (Al-Rawajfeh, 2004).

## **2.5.2 Factors Affecting CaCO<sub>3</sub> Scale Deposition Process**

The formation of alkaline scale inside the heat transfer surfaces of MSF distiller depends on many factors such as the CO<sub>2</sub> desorption rate, temperature, brine velocity and concentration of scale such as Ca<sup>2+</sup> and Mg<sup>2+</sup> ions, and total dissolved solids.

### 2.5.2.1 CO<sub>2</sub> desorption rate

The calcium carbonate deposition rate increases with increase the CO<sub>2</sub> desorption rate because the difference between CO<sub>2</sub> concentration in the bulk and at the phase interface increase with increase the top brine temperature (Al-Rawajfeh, 2008). The carbon dioxide and other NCG act as an insulating blanket around the condenser tubes and if it is left to accumulate it will reduce the vapor partial pressure and its temperature (Abdel-Jabbar et al., 2007).

### 2.5.2.2 Top brine temperature

The calcium carbonate deposition rates increase with increasing TBT due to the fact that the solubility of CaCO<sub>3</sub> decreases with increasing temperature. Super saturation is reached and is immediately followed by salt deposits. Due to increasing in the top brine temperature, the CO<sub>2</sub> desorption rate and pH will increase and consequently the reaction in equation (2.17) which is the main reaction in the deposition of calcium carbonate will move to the right (Al-Rawajfeh, 2008).

### 2.5.2.3 Flow velocity

In the MSF desalination process and at constant physical properties, the CaCO<sub>3</sub> deposition rate decreasing as the brine velocity increasing in the condenser tubes in the heat recovery section and heat rejection section and brine heater tube. This is because as the velocity increasing the rate of removal of the scale deposition increase. Smooth

heat transfer surface minimizes the presence of nucleation sites for scale deposits and crystallization. Higher flow velocity and enough turbulence also reduce scale deposition.

#### 2.5.2.4 Concentration of scale

The  $\text{CaCO}_3$  scale in MSF distiller depends on the concentration of  $\text{HCO}_3^-$ ,  $\text{CO}_3^{2-}$  and,  $\text{Ca}^{2+}$  ions. The primary reaction which causes  $\text{CaCO}_3$  formation is Equation (2.16) (Shams El Din and Mohammed, 1994).

### **2.6 Prediction of $\text{CaCO}_3$ Scale Deposition Tendency**

Various models and indices such as the Langelier Saturation Index (LSI) and the Ryznar Stability Index (RSI) have been introduced to infer the scale forming potential of an aqueous solution from its composition using easily measured parameters (Langelier, 1936; Ryznar, 1944). LSI only indicates if the solution is under-saturated or supersaturated with  $\text{CaCO}_3$ , RSI is a practical extension of the LSI based on experience. It attempts to quantify the relation between  $\text{CaCO}_3$  saturation and alkaline scale formation.

The LSI and RSI can be calculated from the difference between the pH (actual pH) value  $\text{pH}_s$  (calculated pH) of saturated calcium carbonate and the actual pH as follows:

$$\text{LSI} = \text{pH} - \text{pH}_s \quad (2.19)$$

$$\text{RSI} = 2\text{pH}_s - \text{pH} \quad (2.20)$$

The  $\text{pH}_s$  value of saturated calcium carbonate is defined as

$$\text{pH}_s = \text{pK}_2^{\text{sw}} - \text{pK}_{\text{SP}}^{\text{sw}} + \text{pTA} + \text{p}[\text{Ca}^{2+}] \quad (2.21)$$

Where  $K_2^{sw}$  is the second dissociation constant of carbonic acid,  $K_{SP}^{sw}$  is the solubility product of calcium carbonate, TA is the total alkalinity and  $[Ca^{2+}]$  is the concentration of calcium ions. The p-function designates the negative logarithm of that variable.

If a water has a negative LSI value ( $pH < pH_S$ ), it is under-saturated with respect to calcium carbonate and is potentially corrosive. Conversely, for waters with a positive LSI ( $pH > pH_S$ ), a protective layer of calcium carbonate can form as the water is supersaturated with  $CaCO_3$  and the water is scaling. Saturated water has LSI value of zero ( $pH = pH_S$ ). An evaluation of the LSI is given in Table 2.2.

Table 2.2 Interpretation of the Langelier Saturation Index (Carrier 1965)

LSI Value	Indication
2	Scale forming but non corrosive
0.5	Slightly scale forming and corrosive
0.02	Balanced
-0.5	Slightly corrosive but non-scale forming
-2	Serious corrosion

RSI is a correlation of an empirical data base on scale thickness observed in water system to the water chemistry. The RSI provides a closer correspondence between calculated predictions and results obtained in the field, and consequently has replaced the LSI in many applications. An evaluation of the RSI is given in Table 2.3.

Table 2.3 Interpretation of the Ryznar Stability Index (Carrier 1965)

RSI Value	Indication
4.0-5.0	Heavy scale
5.0-6.0	Light scale
6.0-7.0	Little scale or corrosion
7.0-7.5	Corrosion significant
7.5-9.0	Heavy corrosion
>9.0	Corrosion intolerable

## 2.7 Scale Deposition Control Methods

Control of scale formation on heat transfer surfaces is one of the main problems in the MSF desalination process. The driving force for scale formation is super saturation of scale-forming agents. The common methods which have been used to control the scale formation in the MSF process are either chemical methods such as addition of scale inhibitor and acid treatment or mechanical method like ball cleaning (Al-Ahmad and Abdul Aleem, 1993).

### 2.7.1 Addition of Acid

The addition of a strong acid such as sulphuric acid to seawater containing bicarbonate ions will result the following reaction:



This method is simple and effective of preventing the alkaline scale but the addition of acid has the following problems:

1. Additional equipment in the form of a decarbonator is needed to remove the carbon dioxide formed in equation (2.22) (Patel and Finan, 1999)
2. Safety problem due to large amounts of acid that must be added to the seawater.
3. Corrosion problems due to lower pH values.

### **2.7.2 Scale Inhibitor**

This method controls the scale formation by addition of less than stoichiometric quantities of certain chemicals which is known as threshold agent. These chemicals are inorganic or organic polymer compounds which, when adsorbed on a crystalline scale, interfere either with the nucleation or the crystal growth process (Hamed and Al-Sofi, 1997). One of the chemicals that can prevent the formation of calcium carbonate for substantial period of time is polyphosphate. However this type of scale inhibitor can prevent the precipitation of calcium carbonate up to operating temperature below 90°C. They are hydrolysed at higher temperature (Al-Ahmad and Abdul Aleem, 1993). Polymers based on polycarboxylic acid type chemistry have been used to prevent the scale formation at high temperature.

The selection of the dosing rate of scale inhibitor is one of the most important operating parameters. Under dosing leads to scale formation while overdosing will enhance sludge formation (Al-Sofi et al., 1989).

### **2.7.3 Mechanical Cleaning**

There are two basic mechanical cleaning systems that are currently used in desalination plants for scale removal. The first one is the off-cleaning system (by brush) while the plant is off. A second system is the on-line cleaning (by ball) with continuous plant operation (Al-Ahmad and Abul Aleem, 1993).

## **2.8 Process Modelling, Simulation and Optimisation of MSF**

### **Desalination Plant**

#### **2.8.1 Process Modelling of MSF Desalination Process**

In a model, real process that is being studied is represented using mathematical expression which predicts the real process behavior. In any chemical process model, the mass and energy balance, physical properties correlations, chemical kinetics can be described by a nonlinear set of algebraic equations to represent steady state operation or by differential algebraic equation to represent dynamic operation. A steady state model ignores the changes in process variable with time while the dynamic model considers dynamic characteristics. The dynamic models are used to understand the start-up and shutdown characteristic of the process (Tanvir, 2007).

Modeling is very important in the simulation, optimisation and control of MSF desalination process. These models are well established and developed using the basic laws of thermodynamics (Alasfour and Abdulrahim, 2009). Also, these models supported by equations to calculate the thermal and physical properties of fresh and salt water as functions of temperature and salinity (Said et al., 2010).

Models of MSF process can range from simple steady state models to rigorous models which consider properties variations and losses. Simple mathematical models of the MSF process are very useful to provide quick estimates of the main process characteristics such as performance ratio, heat transfer areas for the brine heater and condensers, and profiles of the temperature, pressures, salinity, and flow rate across the flashing stages. The common assumptions among simplified mathematical models for the MSF system include: constant physical properties, constant overall heat transfer coefficient, constant thermodynamic losses, negligible heat loss to the surrounding,



negligible heat of mixing and negligible heat and vapour losses due to venting of non-condensable gases. The past work on the modelling of the MSF process is shown in Table 2.4.

Table 2.4 Summary of past work on steady state modelling of MSF process

<b>Autor, year</b>	<b>Description of Model</b>
Mandil&Ghafour,1970	Approximate Lumped Parameter Model based on constant physical properties, constant heat transfer coefficient and constant stage temperature drop.
Coleman, 1971	Simple stage to stage model with linear and simplified TE (boiling point temperature elevation) correlation for different temperature range, no fouling/scaling included.
Helal et al.,1986	Rigorous stage to stage Model, nonlinear TF correlation and other physical properties as function of (Temperature, seawater composition), temperature loss due to demister included, heat transfer co-efficient (HTC) via polynomial fit (fouling included by assuming fixed values).No non-condensable gases effect included.
El-Dessouky et al., 1995	Model based on Helal et al. (1986) with constant inside/outside tube fouling factors, constant pressure drop across demister, constant number of tubes in the condenser and constant non-equilibrium allowance Effect of non-condensable gases effect included but with one fixed value.
Rosso et al., 1996	Model similar to Helal et al. (1986) and carried out different simulation studied. Model validation with plant data. (fouling included by assuming fixed values).No non-condensable gases effect included.
Mussati et al., 2001	Detailed Stage to Stage Model but with constant thermophysical properties.
Tanvir and Mujtaba, 2006	Model based on Helal et al. (1986) but included NN (Neural Network) based correlation for TE calculation. Constant inside/outside tube fouling factors. No non-condensable gases effect included.
Alasfour and Abdulrahim (2009)	The Model based on variable physical properties as function on temperature and salinity. Energy loss is included. Constant inside/outside tube fouling factors, The variation of thermal conductivity of tube material with tube temperature is also considered Effect of non-condensable gases effect included but with one fixed value.
Hawaidi and Mujtaba, 2010	Model based on Helal et al. (1986) but included dynamic brine heater fouling and dynamic seawater temperature profile. Also included dynamic intermediate storage tank to enhance flexibility in operation.
Al-Fulaij et al., 2011	Rigorous modelling, CFD based demister modelling

Mandil and Ghafour (1970) developed a lumped parameter model with constant physical properties (independent of seawater composition and temperature), constant heat transfer coefficient (HTC) and constant stage temperature drop.

Colman (1971) developed a simple stage to stage model with constant physical properties, specific heat transfer capacity, HTC in condensers and simplified TE (boiling point elevation) correlation for stage temperature range (112-168°C) with seawater temperature 38°C and steam temperature 268°C. Constant HTC in condensers and no fouling/scale model equations reformulated for easy sequential or iterative solution.

Soliman (1981) developed a steady state mathematical model for MSF brine recycle type; he considered different operating parameters for each plant section. The assumptions used by the author were: constant value of specific heat, temperature difference per stage, HTC and heat transfer area. Also, constant value of boiling point elevation losses and neglected the non-equilibrium allowance effect. The model was used to examine the effect of varying cooling water temperature and/or flow rate on plant performance, at constant distillate production or constant steam consumption, his results showed a good agreement with other complex models.

The simple models developed by Darwish (1991) focused on obtaining closed form equations that can be used to study the effect of operating and design parameters such as TBT, cooling seawater temperature, temperature range and number of stage. He used constant and average values for the following properties: the specific heat of distillate, feed and brine streams and for the latent heat of vapour in all stages and steam supply to the brine. Also, he neglected the effect of fouling factor and presence of non-condensable by using a constant value of overall heat transfer coefficient. The main outcome of the analysis presented by the author is the development of design equations

for determining the brine circulation flow rate, the performance ratio, and heat transfer area.

El-Dessouky et al. (1998) used simple models to determine the main features of the MSF systems which include single stage flashing, once-through MSF, and MSF with brine circulation. They developed their model based on the following assumption: specific heat is constant for all liquid streams, brine, distillate and seawater. The overall HTC in brine heater and preheater is constant (neglected the effect of fouling factor and NCG on HTC). The main points discussed in their basic model are:

- Increase in the TBT increase the system performance ratio and reduces the required specific heat transfer area.
- Minimum number of stages in the heat rejection section required to heat the intake seawater to the same temperature as that of the brine of the last stage. This is essential to prevent the decomposition of the bicarbonates salts and formation of carbonate precipitates and carbon dioxide gases which will reduce the heat transfer efficiency around the condenser tubes and has harmful effect on the steam jet ejector.

The other category of MSF models are steady state rigorous models, where the effect of temperature and salinity on the stream thermo-physical properties are considered. The stage temperature difference is calculated from the stage energy balance with nonlinear temperature profiles. In addition, the HTC is calculated at each stage, while temperature losses and pressure drop are considered.

Helal et al. (1986) developed a steady state rigorous model which considered several thermodynamic losses such as non-equilibrium allowance, boiling point elevation and temperature losses due to the drop in pressure across the demister and condenser tube

bundle. The assumptions used by the authors were: constant fouling factor in brine heater and flashing stages, salt free product, adiabatic processes, neglecting heat of mixing brine solution, no sub cooling of condensate leaving the brine heater and neglecting the presence of non-condensable gases in the MSF flashing chambers and their effect on the overall HTC. The model also considered the variation of thermophysical properties of the brine as a function of temperature and salinity. The results were compared with actual data at Al-Khobar II MSF plant and showed a good agreement.

Husain et al. (1993) presented a steady state mathematical rigorous model for MSF–BR (brine recirculation) plants. In their model, the authors divided the flashing stage into four components: brine pool, product tray, vapor space and tube bundle. Through their rigorous model they balance mass flow, salt content and flow enthalpy for each component, in addition they considered heat transfer between tube bundle and vapour space. They used correlations for brine densities, boiling temperatures, brine and vapor enthalpies and HTC, temperature losses due to boiling point elevation; non-equilibrium allowance and pressure losses in demister were included in the model. The authors explained that there were 10% difference between the actual data and the predicted values of heat transfer coefficient and non-equilibrium allowance. The differences were due to the presence of NCG and accumulation of fouling on heat transfer surfaces which they are not included in their model.

Aly et al. (1995) suggested a steady state rigorous model which takes into consideration the conservation of mass and energy in all MSF–BR sections, with additional correlations for heat transfer and thermophysical properties. The authors used their model to simulate an existing desalination plant at Al- Khobar-II, in order to investigate the possibility of increasing plant production rate and minimum cost. The model was

used to test the plant performance over an extended TBT range from 88 to 115°C and seawater temperature from 10 to 40°C.

El-Dessouky et al. (1995) developed a steady state mathematical rigorous model to analyse an MSF–BR system. The developed model was suitable for either design of a new plant or for evaluation of the performance of an existing plant under different operating conditions. The variation of thermo-physical properties of seawater with temperature and salt concentration was considered. The model considered flashing of the accumulated condensate in the distillate tray due to the pressure drop from one stage to another. The fouling resistance and NCG effect on heat transfer area were also considered in the calculation of the overall heat transfer coefficient, where constant values of fouling resistance and NCG were used in each plant section. The model results were verified against actual data at Doha West plant and showed a good agreement. The energy balance equations were based on specific heat and stage temperature difference. The authors assumed constant specific heat which evaluated at average plant temperature.

Rosso et al. (1996) presented a steady state mathematical rigorous model for MSF–BR (brine recirculation) plants based on Helal et al. (1986) model. It accounted for the geometry of the stages, the variation of physical properties of water with temperature and salinity, the mechanism of heat transfer and the role of constant fouling factor for all the heat exchangers of the plant. The model was developed based on some assumptions. Among them was neglecting the effect of non-condensable gases on the overall heat transfer coefficient calculation. Their model was used to analyse the role of operating and design variables in determining the process performance in terms of steady state behaviour.

Thomas et al. (1998) developed a steady state mathematical rigorous model to simulate both steady and dynamic behaviour of the MSF–BR system. They used steady state model to predict the effect of the operating parameters on the system performance. The flashing stage was divided into four control volumes: flashing brine tray, distillate tray, vapor space and condenser tubes. The model accounted for the temperature losses due to boiling point elevation, non-equilibrium allowance, and pressure losses in the demister and tube bundle. Results were compared against real operating data at unit five of Umm Al-Nar East Extension. The predicted temperatures of the flashing brine and vapor showed an excellent agreement.

Aly et al. (2003) developed a steady state mathematical rigorous model to analyses an MSF plant. The model accounted for the geometry of the stages, the mechanism of heat transfer and the variation of the thermophysical properties of brine with temperature and salinity. In addition, the model took into consideration the role of fouling and its effect on plant performance ratio. Model assumptions were: constant specific heat, adiabatic processes, and salt free distillate. They neglected the flashing process from the distillate tray, no subcooling for the condensate and assumed no effect of non-condensable gases on the mass and energy balance of the system. On the other hand, they included the effect of boiling point elevation, non-equilibrium allowance and temperature losses in the demister and tube bundle for flashed vapor temperature calculation. The authors used semi-empirical formulas for HTC and assumed constant value for fouling resistance. Their results were verified against actual data at Sidi-Krir plant, results showed a good agreement between model output and plant vendor data.

Tanvir and Mujtaba (2006a) developed a steady state mathematical rigorous model based on Rosso et al. (1996) using gPROMS model builder. Instead of using empirical correlation for temperature elevation (TE), a neural network based correlation is used.

The model results were validated against results obtained by Rosso et al. (1996) and showed a good agreement. They reported the sensitivity of operating parameters such as changing the seawater temperature in brine heater on the plant's performance, the total amount of fresh water, TBT and final bottom brine temperature (BBT) of the MSF process.

Alasfour and Abdulrahim (2009) developed a steady state mathematical rigorous model for a MSF brine recycle plant which took into consideration the dependence of thermo-physical properties on both temperature and salinity. In addition, the energy losses from the flashing stage and the brine heater to the environment were included. The variation of thermal conductivity of tube material with tube temperature was also considered in the heat transfer analysis. Different types of losses due to boiling point elevations, nonequilibrium allowance, and temperature losses due to pressure losses in the demister and tube bundle been considered in this model. In addition, the fouling factor was assumed to be constant in each section of the plant: heat input section, heat recovery section and heat rejection section. The non-condensable gas amount was also assumed to be constant in all stages. The results obtained were verified and validated against the actual data at MSF-BR Azzour South Plant in Kuwait. They concluded that the calculation of the heat transfer coefficient plays an important role in the model and has a great effect on numerical results.

Hawaidi and Mujtaba (2010) developed a steady state mathematical rigorous model based on Helal et. al. (1986) but included dynamic brine heater fouling and dynamic seawater temperature profile. In addition, the developed model included dynamic intermediated storage tank to enhance flexibility in operation. The model is validated against the simulation results reported by Rosso et al. (1996) and showed a good agreement. The model is then used to study the role of a changing brine heater fouling

factor with varying seawater temperatures and its effect on the plant performance for fixed water demand, for a given steam and top brine temperature.

Al-Fulaij (2011) developed a steady state and dynamic mathematical model rigorous for both MSF-OT (once through) and MSF-BR process. The developed model included many features such as distillate flashing, demister losses and venting system. In addition, the developed model was based on four assumption included: lumped parameter analysis, negligible heat loss to the surrounding, salt free distillate and negligible subcooling and superheating on the system energy balance. The model is validated against several sets of data obtained from large MSF plants. The validation results showed good agreement between measure and predicted data. In addition, CFD modelling of the demister was also developed in their work.

### **2.8.2 Simulation of MSF Desalination Process**

Simulation can be described as a science that deals with the study of a process or its parts by changing its mathematical or physical models. Any experimental work is expensive and the real plant operation is expensive and time consuming. Solution of the model equations utilising computers is known as computer simulation (Khalfalla, 2009). Figure 2.6 shows the typical modeling approach in for simulation and optimization using numerical solvers. The numerical solvers may include SQR based methods or any other non-gradient based optimizer such as GA, SA algorithm and in simulation the solver may contain Newton-Raphson method. Several methods have been used for solving the MSF process equation. Among them are: Sequential Iterative Method, Tri-diagonal Matrix (TDM) and Equation Oriented Solvers in Commercial Software.



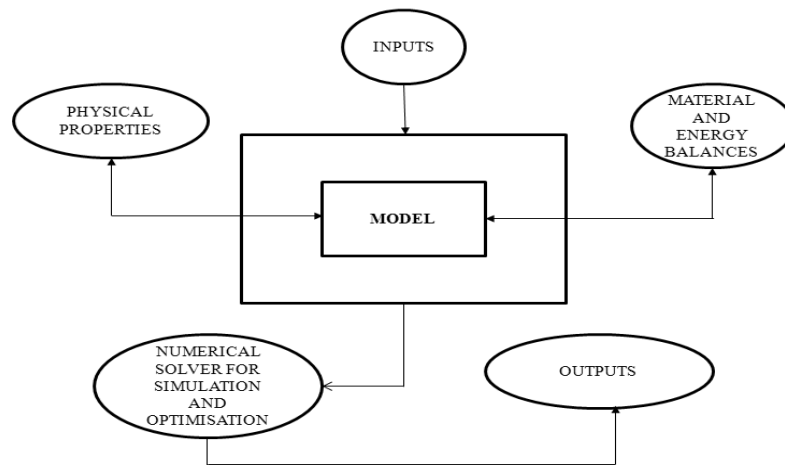


Figure 2.6 Typical Simulations and Optimisation Architecture (Tanvir, 2007)

Table 2.5 shows the past work on the simulation of the MSF process. Omar (1983) developed a simulation programme to solve the MSF process mathematical model. The solution procedure was based upon the stage to stage calculation to solve the mass and energy balance equations. The mathematical model was transferred into a Fortran IV computer code for the design or simulation of MSF desalination plant. The programme was used to simulate the Al-Khober I desalination I plant.

Helal et al. (1986) developed an efficient and reliable technique to solve a detailed MSF model. The proposed technique formulated the model equations in a tri-diagonal matrix (TDM) form, via; (a) linearization of the non-linear equations and (b) decomposes the equations into subsets grouped by type rather than by stage. The TDM was solved using Thomas algorithm. One of the advantages of the developed TDM algorithm was its minimum loop nesting and high convergence stability and reliability. Although the algorithm was very efficient and ensured rapid convergence, the linearization process was very complicated, not straightforward and required many mathematical manipulation steps.

Table 2.5 Summary of past work on simulation of MSF process

<b>Author, year</b>	<b>Simulation Solution Method</b>
Omer, 1983	Successive approximation is used to solve the system's equations (stage-to-stage calculations)
Helal et al., 1986	Decomposition of large set of equations into smaller subsets followed by iterative sequential solution of these subsets. Reduced the equations to generate a tri-diagonal matrix (TDM) and used an efficient method of solution based on Thomas algorithm (a modification of Newton's method).
AlMutaz and Soliman, 1989	Orthogonal collocation method where, the selected stages are chosen to be at the roots of a suitable orthogonal polynomial
Hussien et al., 1993	The model was solved using TDM technique and a commercial software SpeedUp. Also specially designed FORTRAN code was developed based on TDM algorithm to solve the model.
El-Dessouky et al., 1995;	Successive approximation is used to solve the system's equations (stage-to-stage calculations)
Rosso et al., 1997	Each flashing stage is modeled by a set of mass and energy balance equations. Successive approximation is used to solve the system's equations (stage-to-stage calculations)
Thomas et al., 1998	The nonlinear equations obtained in the model were solved in a global manner by linearising them and arranging them in the form suitable for tri-diagonal matrix algorithm.
Ettouney, 2002	Newton's method has been used as an iterative solution scheme to solve simultaneously the entire set of mass and energy balance equations in all flashing stages of MSF process.
Tanvir and Mujtaba, 2006	The nonlinear algebraic equations which presented. The steady state mathematical model of MSF-BR process has been solved using gPROMS software.
Abdel-Jabbar et al., 2007	Each flashing stage is modeled by a set of mass and energy balance equations. Used Newton's method to solve simultaneously the entire set of mass and energy balance equations in all flashing stages.
Hawaidi and Mujtaba, 2010	gPROMS has been used to solve the nonlinear algebraic equations which presented. The steady state mathematical model of MSF-BR process.
Al-Fulaij et al., 2011,	The nonlinear algebraic equations which presented. The formulated model of MSF-OT and MSF-BR process has been solved using gPROMS software. CFD software used to solve a demister model.

Almutaz and Soliman (1989) proposed a steady state simulation method for MSF systems. In their model, very few stages were solved instead of solving mass and energy balance for all stages. The application of the new method showed that it is remarkably efficient and at least twice faster than the method based on simultaneous solution for all

stages. The proposed method was used to simulate an existing MSF plant at Al-Khobar II, and results showed good agreement. The results of the proposed method were also compared against the TDM method used by Helal et al. (1986) and showed very good agreement. The proposed method needs less computational time compared to the TDM method.

Husain et al. (1993) solved their model using TDM technique and a commercial software SpeedUp by fixing the system degree of freedom. Also specially designed FORTRAN code was developed based on TDM algorithm to solve the model. The results were compared between TDM using FORTRAN code and SpeedUp software; their results showed a large difference in the temperature profile between the design data and the predicted ones, it reached 13% in the cooling brine temperature in the first stage, and with minimum error of 5% at low temperature side of the plant. When an arbitrary fouling factor was introduced, the maximum error was reduced to 12.5%. SpeedUp software showed better performance than the TDM using FORTRAN code.

El-Dessouky and Bingulac (1996) developed an algorithm to solve the equations simulating the steady-state behaviour of the multi-stage flash desalination process. The developed algorithm belongs to the class of stage-by-stage approach and starts from the high temperature flashing stage. The equations are broken down into three subsets. The equations in the three subsets are solved by a reliable and efficient one-dimensional fixed- point iteration. The developed algorithm was implemented using the computer-aided design (CAD) interactive package L-A-S.

Thomas et al. (1998) presented a mathematical model to simulate the steady state and dynamic behavior of multistage flash desalination plants. The solution procedure was numerically stable and easy to implement. The nonlinear equations obtained in the model were solved in a global manner by linearising them and arranging them in the

form suitable for tri-diagonal matrix algorithm. The steady state model was simulated for a real plant operating conditions and a close results has been observed between the predicted results and the actual plant operating parameters.

Ettouney et al. (2002) and Abdel Jabbar et al (2007) used a Newton's method as an iterative solution scheme to solve simultaneously the entire set of mass and energy balance equations in all flashing stages of MSF process. Newton-Raphson is one of the simplest multidimensional root finding methods. This method is capable of converging rapidly to a feasible solution provided that a sufficiently good initial guess is given.

Tanvir and Mujtaba (2006a) used gPROMS software to simulate the steady state and dynamic model of MSF desalination plant. The gPROMS software solves the simulation problem based upon the equation-oriented approach with a simultaneous approach incorporating an iterative procedure.

Hawaidi and Mujtaba (2010) simulated the MSF process developed a model using gPROMS model builder. In addition, they used the gPROMS software to simulate the developed MSF model included dynamic intermediated storage tank. The gPROMS software facilitates solution of the non-linear set equations forming of the steady state model for MSF .

The MSF-OT and MSF-BC process models (steady state and dynamics) developed by Al-Fulaiji (2011) were solved using gPROMS. This computer package enables constructing the model in a hierarchical structure where the lower hierarchy includes the flashing stages while the higher hierarchy combines the flashing stages together and also combine them with the brine heater. The author also used CFD software (FLUENT) to simulate three approaches developed pressure demister model. Then the predicted pressure drop by FLUENT for the demister were fed as input values to the

gPROMS simulator to predict their effect on the MSF-OT and MSF-BC plant performance.

### **2.8.3 Optimisation of MSF Desalination Process**

MSF desalination industry is facing the challenges to improve the market shares (profitability) due to increase in cost of energy, environmental regulations. The only way to achieve the target is by reducing the operating cost such as labour, utility, etc. (Tanvir and Mujtaba, 2008). Optimisation techniques provide an efficient way to minimise the cost of operation or maximizing the profit by better operation and management. For any optimisation problem, there are some basic steps to develop the optimisation model (Husain et al., 1993):

- An objective function.
- A mathematical model describing the process
- Inequality constraints defining the parameter limits
- An optimisation procedure.

The optimisation of an MSF plant can be accomplished for two purposes. Firstly, design of a new plant or modification of an existing plant (design optimisation), and secondly, operation of an existing plant (optimisation of operating conditions) (Husain et al 1993).

The aims of MSF process optimisation are to:

- Minimise energy consumption: this means high performance ratio (PR), which is defined as the ratio of distillate production rate to the heating steam flowrate.
- Avoid equipment fouling: which is related the TBT and tube side velocities.

- Provide stable operation: this means reasonable brine levels in flashing stages.
- Reduce chemical consumptions such as antiscaling and antifoaming in process operation) (Al-Shayji, 1998).

Clelland and Stewart (1966) developed a qualitative experience based procedure for optimisation of large scale MSF. Minimising the total operating cost was the objective function while optimising the unit size of the desalination plant.

Mandil and Ghafour (1970) presented a new approach to the optimisation of multi stage flash desalination plant. The approach presented involves the use of relative values of economic parameters rather than their absolute values. They used quantitative short-cut model based analytical optimisation (minimisation by setting first derivative to zero).

Coleman (1971) developed a dynamic programming based cost optimisation within a simple stage to stage model. In their models, all flowrates, heat transfer surface area, flashing temperature, number of stages are allowed to vary in determined cost of producing water.

Husain et al. (1993) discussed the steady-state optimisation on of the operation of MSF desalination plant. The purpose of optimization is to find the optimal adjustment of the set-points, which is needed due to changed seawater conditions and steam supply or load. The objective function was to minimise energy cost by assuming the other costs are invariable.

El-Nashar (1998) described the set point optimisation system. He used a simple MSF mathematical model to perform the optimisation problem. The objective function was to minimise the operation cost which is the sum of LP steam, power consumption, and antiscaling chemical while optimising the operating plant parameters such as TBT,

recirculated brine flowrate, cooling seawater flowrate and the inlet seawater temperature to the rejection section. The Steepest Descent method was used to solve the nonlinear optimisation problem. The values of fouling factors were estimated by minimising the sum of square errors between the measured and reconciled values over one-day interval.

Mussati et al. (2001) presented a rigorous model for MSF process based on nonlinear programming (NLP). In this study, the optimal design of MSF plant was performed. The objective function in the optimisation formulation was to minimise the cost of the heat transfer area and the cost of consumed energy while optimised the MSF design parameters. The pumping cost and pretreatment cost were neglected. In the MSF model, the HTC values were constant and neglected the effect of non-condensable gases. MSF model were implemented using General Algebraic Modelling System (GAMS) and the general reduced gradient algorithm CONOPT 2.041 was used to solve the problems in their work.

Mussati et al. (2004a) presented a novel iterative algorithm to solve non convex and nonlinear optimisation problem. The proposed algorithm is applied to MSF once-through (MSF-OT) and brine mixed (MSF-M) system. The total annualised cost for dual purpose plant (desalination and electricity) was minimising while optimising the flow pattern of strams and the number of stages for fixed water demand. In addition, the effect of the main parameters such as maximum admissible temperature, number of stages, heat consumption, and heat transfer area were also studied. Mussati et al (2004b) presents a rigorous mixed-integer nonlinear programming (MINLP) model for optimal synthesis and design of dual-purpose seawater desalination plants. More detailed description of different equipment and rigorous chemico-physical properties of the streams have been introduced in their model.

Mussati et al. (2005) presented an optimization mathematical model of a superstructure of alternative configurations of Dual Purpose desalination Plants (DPP). The superstructure of optional arrangements (optimization problem) is modeled as MINLP model where binary variables are used to select the equipment for the cogeneration plant. For a given electric power requirement, fresh water production and seawater condition (temperature and composition), the optimisation problem was to determine the optimal configuration and design of the desalter at minimum total leveled cost (TLC) while optimizing the heat consumption of the desalter, total heat transfer area including the main heaters, preheaters, and flashing stages, geometric design of stages, temperature and salinity profiles of the streams. The DPP model was implemented in General Algebraic Modelling System, GAMS. Outer approximation algorithm with equality relaxation strategies algorithm DICOPT is used as MINLP solver.

Tanvir and Mujtaba (2007) performed simultaneous optimisation of design and operation parameters of MSF desalination using MINLP techniques within gPROMS software. In gPROMS v2.3.4 the “CVP\_SS” solver was used in MINLP based optimization solver to optimise the design and operating parameters. For fixed freshwater demand throughout the year and with seasonal variation of seawater temperature, the external heat input (a measure of operating cost) to the process was minimised. The optimisation problem formulation was to optimise the number of stages in the recovery section, steam temperature, recycle flowrate and rejected seawater flowrate while minimising the amount of external heat supplied by steam.

Mussati et al (2008) presented a new formulation model for the optimal synthesis and design of DPP considered by Mussati et al (2005). The new formulation was based on the Generalised Disjunctive Programming (GDP). The Logic-Based Outer Approximation (LOA) algorithm developed by Turkay and Grossmann (1996) with the



modifications introduced by Yeomans and Grossmann (2000) was implemented in the solution procedure. This algorithm solves the disjunctive programming problem by iterating between reduced NLP subproblems and MILP (Mixed Integer Linear Programming) master problems. The optimisation problem was to determine the optimal configuration and design at minimum total leveled cost. They conclude that, despite that the MINLP formulation presented recently in Mussati et al. (2005) has efficiently solved the problem for different demands of freshwater and electricity, the proposed GDP formulation resulted to be more flexible and robust than the MINLP formulation which convergence is strongly dependent on a good initial solution.

Tanvir and Mujtaba (2008) performed an optimal design and operation of MSF desalination process using MINLP techniques within gPROMS model builder 2.3.4. In this work, for three fixed water demand, the total annualised cost (including capital, utility and pumping cost) was minimising while optimising the number of flashing stages, steam temperature, recycle flowrate, and rejected seawater flowrate. They concluded that a flexible scheduling of individual flash stages and operation is possible to supply freshwater at a fixed demand throughout the year.

Hawaidi and Mujtaba (2010) developed a linear dynamic brine heater fouling factor profile based on actual MSF plant operation data. The sensitivity of the fouling factor on the optimal performance of MSF process was studied at discrete time zone corresponding to different seawater temperature and fixed water demand using optimisation techniques in gPROMS model builder 2.3.4. Two different operations in terms of top brine temperature and anti scale dosing were considered. With freshwater demand fixed throughout the year, for each discrete time interval (season), the operating parameters such as make up flow rate, brine recycle flow rate and steam temperature are optimized while minimising the total operation costs (including steam cost, chemical

cost, power cost, and labour cost). They concluded that variation in seawater temperature throughout the year together with changes in the brine heater fouling factor adds further changes in the operating parameters, costs and GOR (Gained Output Ratio).

Abduljawad and Ezzeghni (2010) performed an optimization study of a once through multi-stage flash (MSF) desalination process with simple mixer. The optimization problem was to maximize the gained output ratio (GOR) at different plant capacities by varying the top brine temperature. A simple MSF model with constant heat transfer coefficient developed by Soliman (1981) was used with slightly modified to take into account the variation of average boiling point elevation. The optimization problem was solved using Microsoft Excel software utilizing the SOLVER tool.

Hawaidi and Mujtaba (2011) performed an optimisation of design and operation parameters of MSF desalination processes in order to meet variable demands of freshwater with changing seawater temperature throughout the day and throughout the year. A steady state process model for the MSF process coupled with a dynamic model for the storage tank was developed which was incorporated into the optimization framework within gPROMS modeling software. For a given design (process configuration), the operation parameters such as recycle brine and seawater makeup at a discrete time interval are optimised at discrete time intervals (based on the storage tank level) while the total daily cost (including capital plant cost, total operating cost and storage tank cost) is minimised. They summarised that the summer operation requires the desalination process to use more flash stages than in other seasons to meet the variable demand of freshwater. The past work on the optimisation of the MSF process is shown in Table 2.6.

Table 2.6 Summary of past work on optimisation of MSF process

Authors, Year	Variable studied	Objectives	Problem type
Coleman (1971)	-Number of stages -Heat transfer surface area -flashing temperature	Minimising the cost of producing water	NLP
El-Nashar (1998)	-Top brine temperature -Recycle brine flowrate -Inlet seawater temperature	Minimising the operating cost of the MSF process.	NLP
Mussati et al. (2001)		Minimising the cost of heat transfer area of MSF-once through process.	NLP solved using GAMS software
Mussati et al. (2004a) and (2004b)	-Number of stages -Total heat transfer area -Heat consumption	Minimising the total annulised cost for dual purpose plant (DPP) for fixed water demand	NLP plus MINLP problem solved using GAMS software
Mussati et al. (2005)	-Temperature and salinity -Total heat transfer area -Heat consumption	Minimising the total levelised cost (TLC) for dual purpose plant (DPP) for fixed water demand	MINLP problem solved using GAMS software
Tanvir and Mujtaba (2007)	-Total number of stages -Steam tmperature -Brine recycle flowrate -Rejected seawater flowrate	Minimising the external heat input to the MSF-BR process for fixed water demand	MINLP problem solved using gPROMS software
Mussati et al. (2008)	Temperature and salinity -Total heat transfer area -Heat consumption	Minimising the total levelised cost (TLC) for dual purpose plant (DPP) for fixed water demand	Generalised disjunctive programming problem solved using GAMS software
Tanvir and Mujtaba (2008)	-Total number of stages -Steam tmperature -Brine recycle flowrate -Rejected seawater flowrate	Minimising the total annualized cost of the MSF-BR process for fixed water demand	MINLP problem solved using gPROMS software

Table 2.6 Summary of past work on Optimisation of MSF

<b>Authors, Year</b>	<b>Variable studied</b>	<b>Objectives</b>	<b>Problem type</b>
Hawaidi and Mujtaba (2010)	-Total number of stages -Steam temperature -Brine recycle flowrate -Make up flowrate	Minimising the total operating cost of the MSF-BR process for fixed water demand (including dynamic fouling resistance into MSF process model)	NLP solved using gPROMS software
Abduljawad and Ezzeghi (2010)	Top brine temperature	Maximize the gain output ratio (GOR) for a MMSF-oncethrough process.	NLP solved using Microsoft Excel Solver
Hawaidi and Mujtaba (2011)	-Total number of stages -Steam temperature -Brine recycle flowrate -Make up flowrate	Minimising the total operating and capital cost of the MSF-BR process for variable freshwater demand during a day and throughout the year (including dynamic fouling resistance into MSF process model)	NLP solved using gPROMS software

(cont'd)

## **2.9 Previous Work on the Modelling, Simulation of MSF Process: Impact of Non-condensable Gases and Scale Deposition Fouling**

### **2.9.1 Effect of Scale Deposition Fouling**

The precipitation of  $\text{CaCO}_3$  scale inside the distiller chambers of the MSF desalination plants is a function of many variables such as TBT, pH and concentration of salts. In the past, several modelling, simulation and optimisation studies of MSF process have been carried out using fixed fouling factor in the calculating of overall HTC. In fact, this may lead to excessive and unnecessary overdesign. In addition, the fouling constant value does not consider any effects of operating conditions (flow velocity, temperature, foulant concentration) on the extent of fouling. The deposition layer, with low thermal conductivity, decreases the overall heat transfer coefficient which may further lead to significant loss of thermal exchange capacity (Malayeri and Muller-Steinhagen 2007). Modeling the effect of  $\text{CaCO}_3$  scale precipitation in the process modeling and simulation of MSF plants will help the design engineer to predict the effects of such problem on the performance of the desalination plants (Al-Ahmad and Abdul Aleem 1993).

In the past, several studies have been done on the fouling problems in MSF desalination process. Most of these studies are experimental work. Elliot et al. (1974) Casini (1983) performed a laboratory work on the developing and testing of anti-scale agent at temperature.

Cooper et al., (1983) studied the development of fouling in MSF plants which cannot be explained by a linear relationship by introduced the concept of a deposition-removal model. They examined the effect of changing parameters on the rate of fouling and

steady state value. They concluded that the model can be applicable to MSF plants treated with a polyphosphate based system as well as high performance additives.

El-Dessouky and Khalifa (1985) developed a mathematical model to investigate the effect of fouling due to scale formation of preheater tubes on the thermal performance of once through multi-stage desalination plant. The model was used to find the decrease in the plant performance ratio, and the increase of the ratio of makeup water to the product. In addition, the performance of the materials used for the condenser tubes after ten years of intermittent operation was investigated.

Shams El Din and Mohammed (1989) investigated the mechanisms of the alkaline scale formation process by performed an experimental work. They concluded that the bicarbonate ion ( $\text{HCO}_3^-$ ) and the supersaturation with calcium carbonate ( $\text{CaCO}_3$ ) is the key factor in the developing of alkaline scale.

Al-Ahmad and Aleem (1993) investigated various models and mechanisms of scale deposition fouling and their effect on the performance of desalination plant. They presented a simplified model for fouling resistance at any time and based on basic scale model. They summarised that the precise control on the operating conditions like temperature, pH, solids content and flow velocity is of significant importance to achieve smooth operation with minimum scale problem.

Al-Ahmad and Aleem (1994) applied the asymptotic fouling model of Keren and Seaton to correlate the actual fouling data taken from actual desalination plant. The interaction between scale formation and corrosion problems is also considered.

Shams El Din and Mohamed (1994) performed an experimental work to study the alkaline scale formation process. Their laboratory study was on the analysis of brine and scale samples which is mainly caused by crystallisation of the inversely soluble salts

calcium carbonate and magnesium hydroxide from different locations of MSF distiller. They found that the nature of scaling is decided by distiller top-temperature, volume, material, deaeration, and depends also on type of anti-scalant additive and ball cleaning.

Mubarek (1998) studied the kinetics of scale formation in MSF plants at a TBT of 90 °C and developed a kinetic model for  $\text{HCO}_3^-$  decomposition/ $\text{CaCO}_3$  formation. He concluded that the rate of scaling depended on the concentrations of the bicarbonates, calcium ions as well as the partial pressure of  $\text{CO}_2$ . In addition he found in the presence of antiscalants the reaction rates slow down and nearly inhibit the precipitation of calcium carbonate scale.

Hamed et al. (1999) reported a study on both qualitative and quantitative performance tests of three types of antiscalants in MSF plant. The types of inhibitors were polycarboxylate, polymaleic and polyphosphate. They performed the threshold effects of these scale inhibitors on laboratory scale while the variation of the fouling factor with time is examined and quantified on pilot plant. They concluded that all the examined antiscalants were successful in inhibiting alkaline scale formation and improving plant performance at TBT ranging between 105°C and 110 °C and with respective dosing rates of 1.5 and 3 ppm.

Malayeri and Muller-Steinhagen (2007) described the fouling mechanisms and introduced some prediction methods as well as new online mitigation methods and surface treatment based on ion implantation or sputtering techniques. They also highlighted some of the recent advances in fouling research and addressed the areas that required closer industrial and academic research collaboration.

Al-Anezi and Hilal (2007) studied the role of the solubility of  $\text{CO}_2$  and scale formation in desalination plants. Also, they presented the correlations used to characterize the

CO<sub>2</sub>-sewage system. In addition they summarised that the fouling in the MSF plants occurs as a result of alkaline scale formation and it is known that the rate of formation of calcium carbonate and magnesium hydroxide in seawater depends on temperature, pH, concentration of bicarbonate ions, rate of CO<sub>2</sub> release, concentration of Ca and Mg ions, and total dissolved solids.

Hawaidi and Mujtaba (2010) developed a linear dynamic brine heater fouling factor profile based on actual MSF plant operation data. The effect of fouling factor on the optimal performance of MSF process was studied at discrete time zone corresponding to different seawater temperature and fixed water demand using gPROMS software. They concluded that the changes in the brine heater fouling factor adds further changes in the MSF operating parameters.

Baig et al. (2011) investigated the effect of brine heater fouling resistance on overall heat transfer coefficient and surface area of once-through MSF desalination plant. They concluded that the fouling resistance has a significant effect in decreasing the overall heat transfer coefficient, which reduce the production rate as the fouling increases with time. In addition, increasing the fouling resistance from 0 to 0.001 m<sup>2</sup> k/W resulted in a 400% decreases in the overall heat transfer coefficient. In contrast, the surface area increases with increasing fouling resistance for a given top brine temperature.

Hawaidi and Mujtaba (2011) used the dynamic brine heater fouling factor correlations developed in Hawaidi and Mujtaba (2010) in the calculation of the overall heat transfer coefficient in brine heater of the MSF process model. The MSF process model and dynamic model for the storage tank were used to optimise the design and operation parameter of multistage flash (MSF) desalination processes while minimise the total annual cost to meet the variable demands of freshwater with changing seawater temperature throughout the day and throughout the year.



## 2.9.2 Effect of NCG

Although there is some work which has been done on the steady state modeling and simulation of MSF desalination plants, there are a very limited number of publications considered the effect of NCG on the overall HTC, mass and energy balance equations and flashing process of MSF desalination plants. These models only involved the thermodynamic losses from stage to stage, tube velocity, tube materials, and chamber geometry. The presence of NCG reduces the overall heat transfer coefficient for the condensing vapor and the temperature at which it condenses at given pressure in the vapor space (El-Dessouky et al. 1995). There are only a few investigations which included the effects of NCGs on steady state mathematical models either simple or details models of MSF process. Although some of these studied included the effect presence of non-condensable gases in their model, only constant values of NCGs had been considered.

In addition the developed models did not show the effect on NCGs on the heat transfer coefficient and consequent the plant performance parameters. The other investigations related to the presence of NCGs in the flashing stages of MSF desalination plants were about the release process of NCGs in the flashing chambers. These studies were performed to understand the release process of NCGs and to calculate the amount of release gases in the flashing chambers.

El-Dessouky et al. (1995) developed a steady state mathematical model to analyse the MSF desalination process. The developed model considered the effect of the presence of non-condensable gases on the overall heat transfer coefficient. The author performed his model at fixed value of percentage of NCGs and did not show the effect of this value on the overall heat transfer coefficient and the plant performance.

Alasfour and Abdulrahim (2009) developed MSF brine recycle model which took into consideration the effect of non-condensable gases on the heat transfer coefficient calculation in recovery and rejection stages only. The presence of non-condensable gases in the brine heater was neglected. Constant values for the percentage of NCGs accumulated in the flashing stages (4% wt.) were considered in the calculation of the overall heat transfer coefficient. They found difference between the predicted values of the overall heat transfer coefficient and the actual plant values. They explained that the difference between the model prediction and the actual plant data was mainly due to using constant values NCGs.

Al-Fulaiji (2011) developed a steady state and dynamic mathematical model for both MSF-OT (once through) and MSF-BR (brine recycle) process. The developed model contained correlations which used to calculate the flowrate of the releases of NCG through the venting system. The calculated non-condensable gases flowrates were used in the overall mass and energy balance of the flashed of vapor in the brine pool.

Other studies which have been done on the problem of the presence of NCG in the flashing stages of the MSF desalination plants are studying the release process itself and trying to understand the process mechanism and calculate the release flowrate of the non-condensable gases. The CO<sub>2</sub> release process in MSF is poorly understood and there is no approach available to reliably predict the release rates in individual stages and the effects of influencing parameters.

The first investigation into CO<sub>2</sub> release in desalination distillers relied on simple reaction models and sparse experimental data. Only chemical reactions in the brine were considered (Geigy, 1978; Watson, 1979). Mass transfer was completely neglected.

Lukin and Kalashnik (1982) developed the first physical models that allowed the calculation of the CO<sub>2</sub> release rates in individual MSF distiller stages. The model are based on the assumption that mass transfer phenomena in the brine rather than the reaction kinetics control the desorption process. Chemical reaction kinetics was scarcely investigated.

Glade and Genthner (1995) developed CO<sub>2</sub> release model to estimate for the total release of CO<sub>2</sub> in the MSF distiller and for the distribution of these releases between the individual stages. The developed model was based on the assumption that mass transfer in the brine and phase equilibrium by Henry's law at the brine/vapour interface controls the release process. They mentioned that the composition of the carbonic acid at the entrance of the first flash chamber influence the release of CO<sub>2</sub>.

Watzdorf and Marquardt (1997) applied the rigorous electrolyte thermodynamic to the simulation of MSF distillers. The brine considered as a multi-component electrolyte system of varying complexity. Scale formation and CO<sub>2</sub> release are predicted assuming equilibrium conditions.

Glade (1999) proposed a model that described the problem of CO<sub>2</sub> release in MSF distiller as problem of chemical desorption. The coupling of mass transfer and chemical kinetics was investigated and the rate-controlling steps in the CO<sub>2</sub> release process were determined.

Al-Rawajfeh et al. (2004) have modelled the CO<sub>2</sub> desorption rates in ME distillers. These simulations have not accounted for the deposition of alkaline scale and its effort on CO<sub>2</sub> desorption rates. Calcium carbonate and magnesium hydroxide were assumed to precipitate at negligible rates.

Glade et al. (2005) developed a model based on the model developed by Al-Rawajfeh et al (2004) to calculate the CO<sub>2</sub> release rates from the evaporating brine in MSF and MEE distillers. The developed model was used to study the use of the CO<sub>2</sub> release from the flashing stages to recarbonate the distillate.

Al-Rawajfeh (2008) simulated a CO<sub>2</sub> desorption rates, CaCO<sub>3</sub> deposition rates and fouling resistance at different top brine temperature for two MSF once-through and recycle distillers. The CaCO<sub>3</sub> deposition rates correlated to the CO<sub>2</sub> desorption rates in a developed model were based on coupling of mass transfer with chemical reaction.

## **2.10 Conclusions**

This chapter described the MSF desalination process and the main factors affected its performance such as TBT, steam flow rate , and brine recycle flow rate , etc. Special attention is given to the problem of NCG on the scale formation and plant operation of MSF process. In addition, the carbonate system in seawater and how to calculate the scaling tendency is also outlined. In addition, this section summaries the literature review that has been carried out in this chapter and highlights areas that have not been covered in the literature which this aims to address. The main contributions of this work are listed below.

- The majority of the literature investigates of problem of the scale deposition fouling inside the condenser tubes of the flashing stages and the brine heater of the MSF experimentally. Only few publications were found which studies the scale formation modeling but did not include any effects of MSF operating parameters such as flow velocity, temperature and foulant concentration. In fact this may be lead to excessive and unnecessary overdesign. In this study, a

steady state calcium carbonate fouling deposition model as a function of the surface temperature has been developed.

- Most of the recent works on the steady state modelling and optimisation of MSF process consider constant values of fouling resistance in the calculating of the overall heat transfer coefficient. Only, Hawaidi and Mujtaba (2010) developed a linear dynamic brine heater fouling factor in their MSF model. In this research, the investigating the role of varying fouling resistance and its effect on the operation and design of MSF process has been studied.
- There are several works which have been done on the optimisation of design and operation parameters of MSF process for fixed water demand. In reality, the freshwater demand and the seawater temperature vary throughout the day. Only few researchers performed an optimisation of MSF desalination process involving a variable demand of freshwater and varying seawater temperature throughout the day and throughout the year. The scale deposition factor inside the condenser tubes of the flashing stages has an effect on the optimisation of the MSF process with varying seawater temperature and freshwater demand during the day and throughout the year. Therefore, in this work, the optimisation of the design and operation parameters of MSF process has been done to minimise the operating cost with varying fouling factor in the brine heat, recovery stages, and rejection stages and varying seawater temperature and freshwater demand during the day.
- From the literature, it is seen that there are many work on the steady state mathematical model and simulation of MSF desalination plants in order to maximising performance and minimizing operating cost. However, a few studies considered the effect of NCG in their models. The overall heat transfer

coefficient dependence affected by the presence of non-condensable gases in the flashing chambers of MSF process. A few researches developed their models with fixed value of NCG when calculate the overall HTC in the energy balance equations. In this work, the steady state mathematical model include the effect of the presence of the NCG is developed. Furthermore, the effect of variation of NCG in the flashing stages on the design and operation parameters of MSF process has been studied.

- Studying the release process of NCG is very important in calculating the release flowrate and to understand the venting rate system design in the MSF process. The composition of the carbonic acid in seawater affects the CO<sub>2</sub> release process during the flashing process (Glade 1995). Although there is some work done on the release process of NCG, only a few studies on the developing correlations to compute the dissociation constants of carbonic acid in seawater was found in the literatures. In this research, a NN based correlations has been developed to calculate the dissociation constant of carbonic acid in seawater as function of temperature and salinity.

## Chapter 3

### Modelling, Simulation and Optimisation using gPROMS

#### 3.1 Introduction

This chapter briefly discusses the features of the software used for the modeling, simulation and optimisation of the multistage flash desalination process systems carried out in this work. gPROMS is **g**eneral **PRO**cess Modeling **S**ystem with proven capabilities for the simulation, optimisation and parameter estimation (both steady-state and dynamic) of highly complex processes. gPROMS allows the user to write equations almost as they would appear on paper. In addition gPROMS allows user to model the transient behavior of individual unit operations to be described in terms of mixed system of integral, partial differential and algebraic equations (IPADES).

The gPROMS has been used for a wide variety of applications in petrochemicals, food, pharmaceuticals, specialty chemicals and automation. Furthermore, it has the potential to be used for any process that can be described by a set of mathematical equations.

gPROMS can be used for (PSE, 2004):

- Steady state and dynamic simulation.
- Steady-state optimisation.
- Dynamic optimisation.
- Steady-state parameter estimation.
- Dynamic parameter estimation.

## 3.2 Features of gPROMS

gPROMS software was developed by Process System Enterprise (PSE) and has largely been employed for industrial applications. According to the developer of this software, gPROMS have many advantages compared to other commercial software in market today. Following are some advantages of gPROMS among of them:

- All solvers within gPROMS are specifically designed for large scale system and there are no limits regarding problem size. This unparalleled modelling powers with the generality of the software means that it can be used for any processes that can be described by mathematical model.
- Project tree structure is a comprehensive project environment which all element of a modelling project can be easily accessed and maintained. Besides that, a palette view can be used for steady-state and dynamic simulation, parameter estimation, optimisation and experiment design. There are multiple activities can be done using the same model.
- Models can be written to be steady-state or dynamic or both. It is not like steady state simulators which have added dynamic capabilities or dynamic simulator which have to iterate to steady state. gPROMS can always solve for a steady state providing the models and specifications allow this.
- gPROMS's optimisation facilities can be used for steady state or dynamic model to find the optimal answer to any design or operation questions directly rather than by trial and error iteration .



Because of the advantages of gPROMS described above, and many others not mentioned here, gPROMS (version 2.3.4 and 3.03) has been chosen as the software of choice for modelling, simulation and optimisation of MSF desalination process as carried out in this work. The details for utilising gPROMS for model improvement, simulation and optimization as described in this work are presented in the rest of the chapter.

### **3.3 Model Development using gPROMS**

In gPROMS model builder, the project –tree shows all the currently opened projects and cases.

The project (Figure 3.1) has several sub sections, among them the important sections are:

- VARIABLE TYPES
- MODELS
- TASKS
- PROCESS
- OPTIMISATION
- PARAMETER ESTIMATION
- EXPERIMENTAL DESIGN

In VARIABLES TYPES section, the types and range of the variables are specified for different MODEL, PROCESS. Equipment unit equations, physical properties equations and flowsheet equations are written in MODEL section. PROCESS section contains specification for simulating the process. Optimizing the operation of the process is written in OPTIMISATION section.

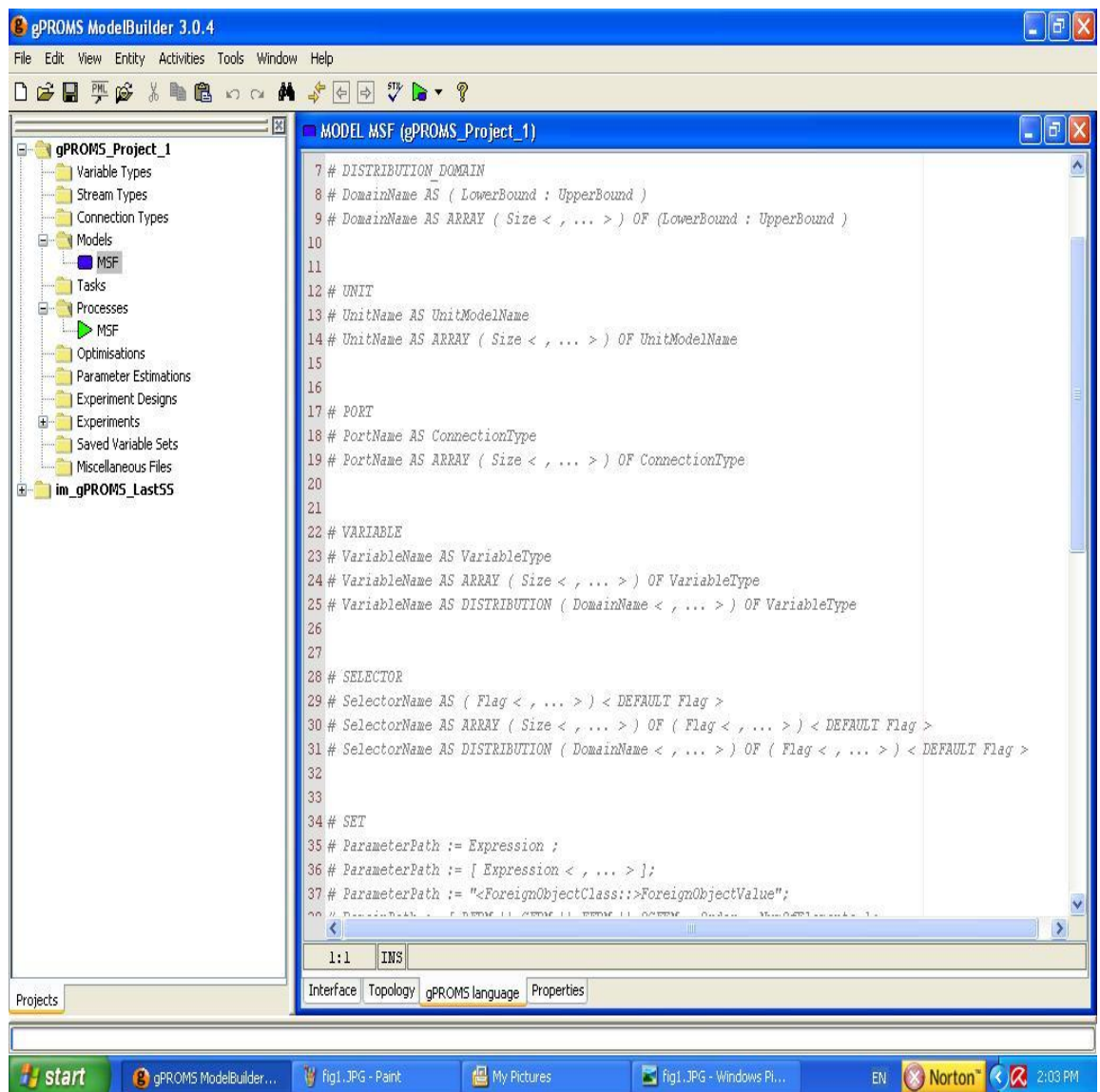


Figure 3.1 Model builder in gPROMS

### 3.4 Defining a Model

Model is defined as the modelling of physical, chemical and biological plant behavior.

The model consists of the following sections:

- PARAMETER
- VARIABLE
- UNIT
- STREAM and PORT
- EQUATION

Three types of constant (REAL, INTEGER, LOGICAL) are declared in PARAMETER section. Parameters are constant values, which cannot be estimated by the simulation. Their values must be fixed before simulation begin, and remain fixed throughout. An example of a parameter from the MSF process model is the heat transfer area of the tubes in the brine heater  $A_h$ , which is declared in the model file as

```
AH      AS      REAL  #  heat transfer area in brine heater
```

REAL refers to the type of parameter (i. e. a real value), and # is the comment sign in gPROMS after which a description of the parameter may be written in long hand. The diameter of the tubes in the heat recovery section ( $D_j^i$ ) is also example of parameters declared for MSF process model in this work.

In VARIABLES section, variables and corresponding variables type of the model are declared. Variables may or may not vary with time. Values of the variables may be

assigned or calculated by simulation. An example of a variable from the MSF process model is seawater feed temperature (Tseawater), which is declared in the model as

```
Tseawater      AS      tempfeed  #  seawater temperature
```

tempfeed is the name given to the process Tseawater in the above example. The variable type is defined in the VARIABLE folder as

Name	Lower bound	Default value	Upper bound
tempfeed	1.0	60.0	100.0

tempfeed is the variable type and the numbers after it are lower bound, default value and upper bound, respectively.

The specific piece of equipment of the process is referred in the Unit section. In EQUATION and BOUNDARY sections, equipment equations are specified. Equations are differential (differential operator \$ is the derivative sign in gPORMS) or algebraic operators. It has some built in functions for partial equations and integral functions by using the PARTIAL and INTEGRAL operator respectively. Conditional equations (for reversible & systematic discontinuities, reversible & asymmetric discontinuities, irreversible discontinuities) in MODEL and PROCESS is handled by the deferent operator such as WHEN...END, CASE...END. An example is the equation for heat transfer in the heat rejection section

$$W_R S_{Rj} (T_{Fj} - T_{Fj+1}) = U_j A_j X$$

The above equation is represented in the model file as

$$WR * SRj (TFj - TFj+1) = Uj * AJ * X$$

A part of the gPROMS model file for MSF desalination process model is shown in Figure 3.2.

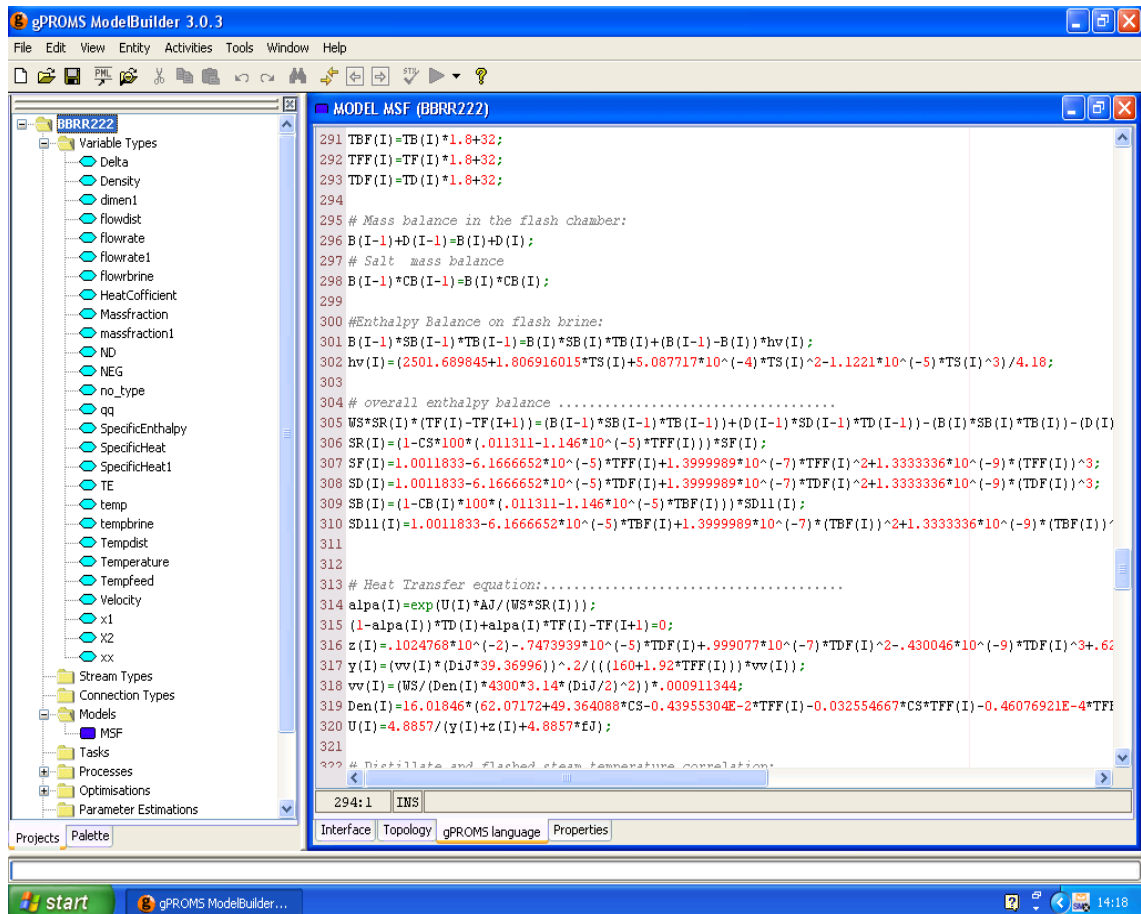


Figure 3.2 VARIABLES TYPES for gPROMS MODEL

### 3.5 Composite Models

Many systems in industries are much more complex than that, and their models involve many thousands or even tens of thousands of variables and equations. Although in principle all of these could be written in a single MODEL, in practice such an undertaking would be extremely tedious and error-prone. gPROMS has an “object-oriented” approach to modelling that applies to both process models and operating procedures. In this way, a user can easily construct models of complex flowsheets and procedures by decomposing them into sub-models that call on other sub-models and can even inherit values of parameters. For example if we consider the example shown in Figure 3.3, one approach would be to construct a single, primitive MODEL that would

contain the declarations of all parameters, variables and equations for the entire flowsheet. However, in practice it may be very inefficient and error-prone.

The flowsheet described above can be decomposed into different interconnected sections. The development of the models for each of these sections can initially be considered in isolation. Once these models are developed and tested, we can connect instances of each one of them in an appropriate way to construct the flowsheet model. This procedure is called hierarchical sub-model decomposition as shown in Figure 3.4.

The gPROMS language encourages hierarchical sub-model decomposition by offering mechanisms that support:

- The declaration of high-level MODELS that contain instances of lower-level MODELS
- The connection of the above instances to represent flows of material, energy and information between them.

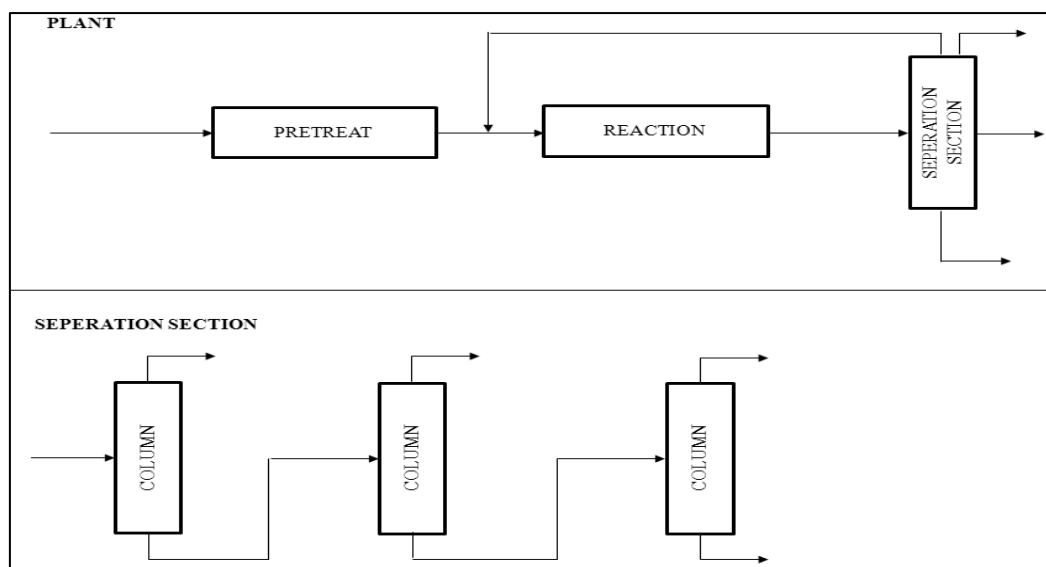


Figure 3.3 Hierarchical sub-model decomposition

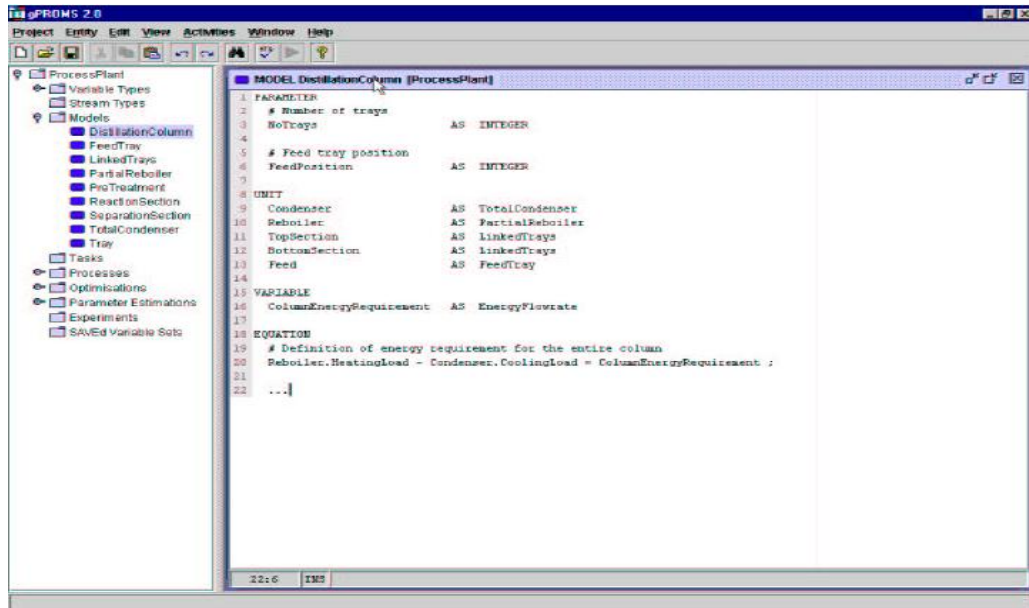


Figure 3.4 Composite model features in gPROMS software

### 3.6 Defining a Process

In the Processes entity, the specifications for running simulations with the MSF processes are defined. A Process is separated into sections that contain information necessary to define a simulation activity. The major Process sections utilised for carrying out simulation studies in this work are:

- UNIT
- SET
- ASSIGN
- INITIAL
- SOLUTION PARAMETERS
- SCHEDULE

The roles of these parts are discussed in the following subsections:

### 3.6.1 UNIT Section

As earlier stated, gPROMS can be used to model a complete process. In such a case, the various equipment units in the process are modelled and simulated separately. These different units can be linked to one another to give a complete picture of the overall process. In the unit part, the specific item of equipment to which the process files refers to is indicated. Equipment items are declared as instances of MODELS.

### 3.6.2 SET Section

In this part, the values of the parameters declared under the PARAMETERS section in the model file are assigned. For example, the value of heat transfer area of the tubes in the brine heater Ah, is assigned under the SET section as

```
AH      := 3530; # m2
```

### 3.6.3 ASSIGN Section

In the ASSIGN section, the input parameters to the model are specified. In a typical model, the number of variables is commonly more than the number of equations. In order to make the number of equations equal to the number of variables to avoid over or under specifying the system, some the extra variables are assigned in this section. For example, in the MSF process model, the variables assigned in the ASSIGN section are the seawater feed temperature (Tseawater)

```
ASSIGN
```

```
Tseawater:=34; # C
```

Note that through the optimization process, the value assigned in the ASSIGN section are overridden as the software searches for the best control values to satisfy a given set of process constraints.



### 3.6.4 INITIAL Section

The INITIAL section is used for specifying the initial conditions of a simulation activity. For example, in the tank model for MSF process model, the initial conditions are the values of the level of the tank (h) at time =0.

INITIAL

T101.Height=2.1; # m

In gPROMS, initial conditions are treated as general equations in gPROMS and as such, it is possible to estimate the value of an initial state by an equation rather than by assigning it a fixed value.

### 3.6.5 SOLUTION PARAMETERS

The SOLUTION PARAMETERS section of the PROCESS allows the specification of parameters of the results and the mathematical solvers for each type of activity (simulation, optimization and parameter estimation). As the number of solvers and subsolvers available in gPROMS for the solution of simulation, optimization and parameter calculation activities for both steady state and dynamic models are enormous.

gPROMS provides a range of the mathematical solvers for simulation, optimisation and parameter estimation. gPROMS supports an open software architecture regarding the mathematical solvers simulation, optimization and parameter estimation (Gosling, 2005). There are three standard mathematical solvers for the solution of sets of nonlinear algebraic equation in gPROMS: BDNLSOL, NLSOL and SPARSE: BNDLSOL (Block Decomposition Non Linear solver). NLSOL is nonlinear solver, with and without block decomposition. SPARSE is sophisticated implementation of Newton-type method without block decomposition. Two mathematical solvers namely (DASOLV and

SRADAU) solve mixed sets of differential and algebraic equations in gPROMS. DASOLV solver has been used in this work for the MSF process model. These two solvers are able to handle the partial derivatives.

### 3.6.6 SCHEDULE Section

In the SCHEDULE section, the operating schedule of the process is specified. One objective of modelling is to study a model's behaviour under several operating conditions (i.e. external manipulations). The information on these manipulations is specified in this section. A part of the gPROMS Processes file for the MSF process model is shown in Figure 3.5.

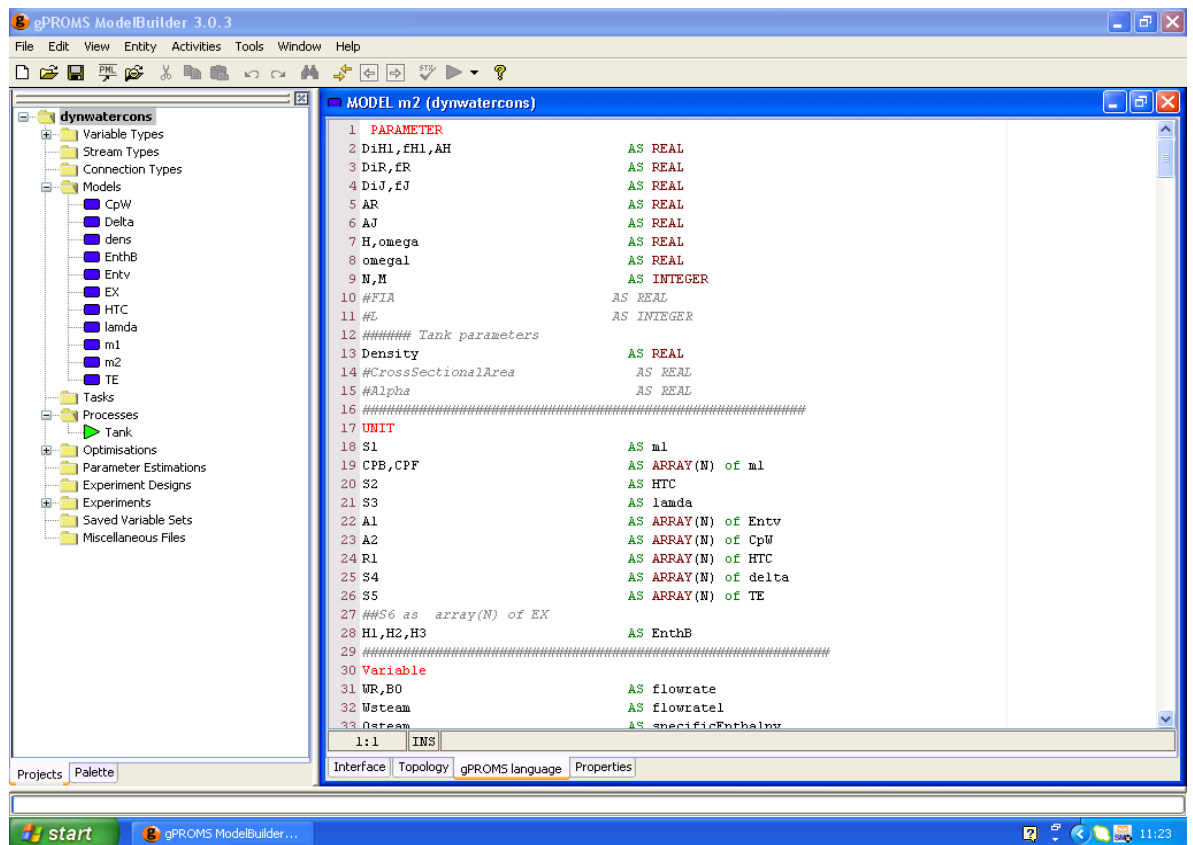


Figure 3.5 Part of the process file for the MSF process model

### 3.7 Optimisation in gPROMS

In the optimization entity, the parameters for steady state or dynamic optimization problems are specified. In various cases, the values are expressed in the form: [guessed value, lower bound, upper bound]. Some of the specifications for the optimization process involve the length horizon or time horizon for the process, the number of intervals, the numerical values of the intervals, the values of the control variables within the intervals and the end point constraints. The objective function to be maximized or minimised is also specified within the optimisation file. gPROMS provides a general numerical solver manager for the steady state and dynamic optimization problem called DOSOLV.

Mathematical solvers for optimization are specified in PROCESS entry SOLUTION PARAMETER subsection as:

```
DOSolver='' CVP_SS''
```

```
DOSolver='' CVP_MS''.
```

A part of the gPROMS Optimization file for the MSF process model is shown in Figure 3.6.

### 3.8 Connecting to MS Excel Software

gPROMS provides a built in feature to plot different variables in MS Excel. This feature makes the gPROMS more user friendly. However, Microsoft Excel Foreign object and Foreign Process interface provide better flexibility to send and receive data from the MS Excel. They are designed to let gPROMS to interact dynamically with calculations performed in Microsoft Excel. Different commands like SENT, RECEIVE are used to connect both software. The Microsoft Excel foreign Object inter interface

can be used to provide values for PARAMETERS and VARIABLES in gPROMS simulation. Different commands like SENT, RECEIVE are used to connect both software.

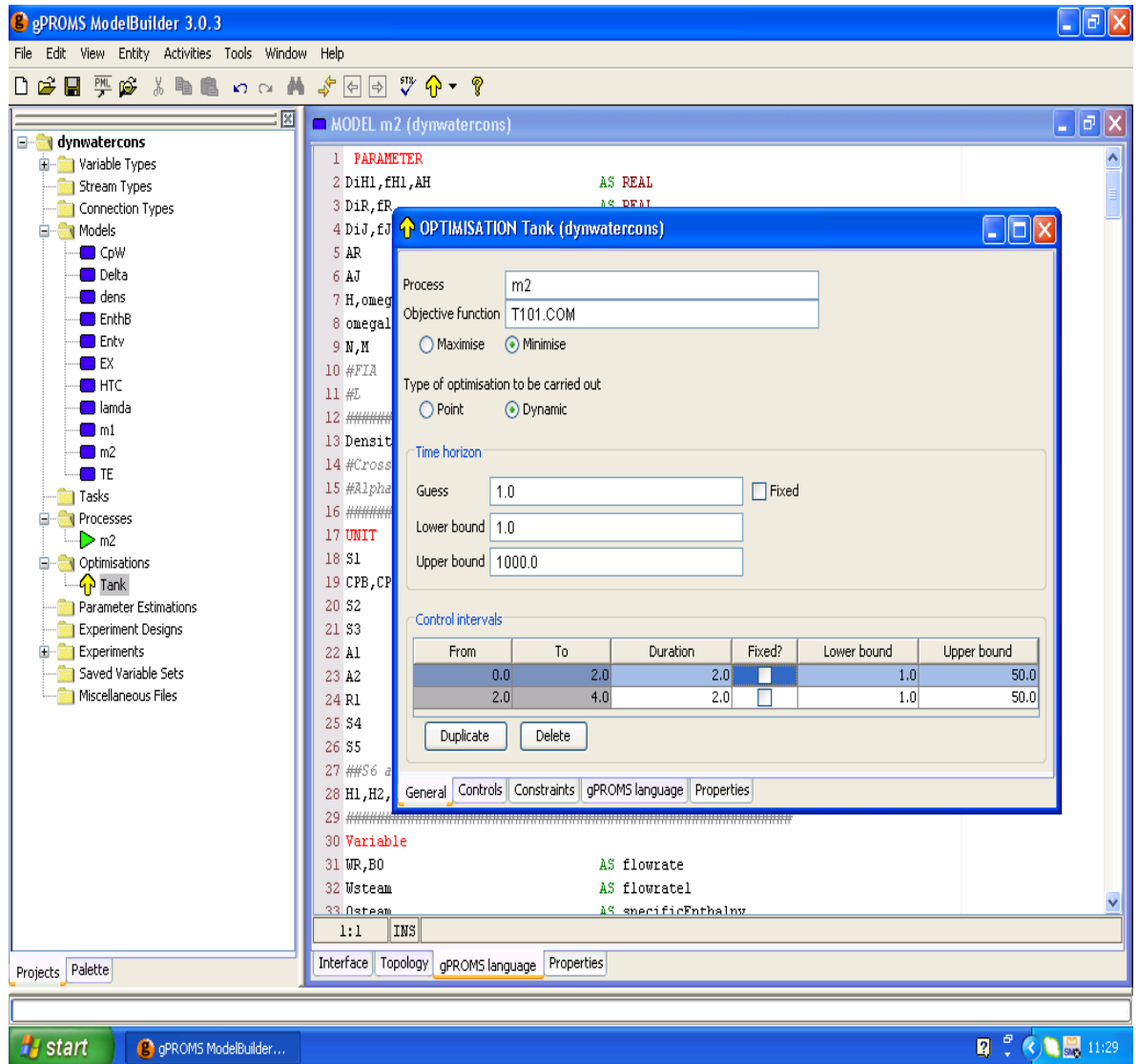


Figure 3.6 Part of the optimisation file for tank model in MSF process model

### 3.9 Comparison of gPROMS with other Commercial Software

Several commercial software packages for simulation, optimization, optimal control and design such as Hysys, CEMCAD, Matlab, PROII, ASCEND, SpeedUp and OMOLA are widely available these days to provide modelling languages that allow the transient behavior of individual unit operations to be described in terms of mixed systems of

ordinary differential and algebraic equations (DAEs). Each of these commercial packages is developed with different features. Some of them have high-quality application flexibility. Therefore, looking for appropriate software for a specific purpose is quite important in order to achieve the required target and to provide modelling languages that allow us to describe many operations.

Tjil (2005) compared the performance of Aspen Custom Modeller (ACM) with the performance of gPROMS to optimize the Sec-Butyl Alcohol (SBA) stripper. The SBA model was built in both softwares to perform parameter estimation and assesses their capabilities. CAPE-OPEN was utilised to use some physical and thermodynamic properties of the components in both softwares (ASC and gPROMS). Different features of parameter estimation were evaluated for both softwares such as: experimental data input, output interpretation, combination of objective functions and optimization solvers and their ability. Tjil (2005) concluded that the parameter estimation capabilities of gPROMS were better than ACM.

### **3.10 Conclusions**

The gPROMS software package used for modelling, simulation and optimization of the MSF process model in this work has been discussed in this chapter. The gPROMS is robust and open structure software. gPROMS has several features that make it an attractive and suitable tool for the modelling and simulation of any plant process (steady state and dynamic). The features of gPROMS have been discussed briefly in this chapter. Some of its numerous advantages include; clear and concise language, unparalleled modelling power and the ability to model process discontinuities and operating conditions among many others. Due to robustness and flexibility of this

software as mentioned in detail in this chapter, gPROMS has been chosen to use for modelling, simulation and optimisation in this work.

Further information can be found in developer's websites ([www.psenterprise.com](http://www.psenterprise.com)) and gPROMS user guide (gPROMS, 2005).

## Chapter 4

### Modelling and Simulation of the MSF Process using gPROMS

#### 4.1 Introduction

The objective of modelling of any industry process is to obtain a plausible mathematical description which adequately characterises the effect of important process parameters on its productivity. The MSF process models have been improved dramatically to improve the plant performance. Modeling is very important in the simulation, optimisation and control of MSF desalination process. Many models have been developed to find a functional relationship between the MSF process design variables and the effect of different operating parameters on the plant performance. All these models are well developed from the basic laws of total and component mass balances and enthalpy balances coupled with heat and mass flowrate coefficients. Furthermore, new models started to introducing equations to calculate the thermal and physical properties of fresh and salt waters as function of temperature and salinity.

In this chapter, a steady state mathematical model of MSF process is developed based on the basic laws of mass balance, energy balance, and heat transfer equations. The correlations for the thermal and physical properties of the brine and water such as heat capacity, densities, enthalpies, and HTC has been used. These correlations are function of temperature and salinity. gPROMS model builder 2.3.4 software is used to develop the model and simulation. The model is then validated against the simulation results reported by Rosso et al. (1996) (which was based upon real plant data). The real plant data was first used by Helal et al. (1986).

## 4.2 MSF Process Description

As described, MSF process mainly consists of three sections: brine heater section, recovery section with NR stage and rejection sections with NJ stage (Figure 4.1). Seawater enters the last stage of the rejection stages ( $W_s$ ) and passes through series of tubes to remove heat from the stages. Before entering the recovery section, seawater is partly discharged to the sea ( $C_w$ ) to balance the heat. The other part ( $F$ ) is mixed with recycled brine ( $R$ ) from the last stage of the rejection section and fed ( $W_R$ ) into the last stage of the recovery section. Seawater is flowing through the tubes in different stages to recover heat from the stages and the brine heater raises the seawater temperature to the maximum attainable TBT. After that it ( $B_0$ ) enters into the first flashing stage and produce flashing vapour. This process continues until the last stage of the rejection section. The concentrated brine ( $B_N$ ) from the last stage is partly discharged to the sea ( $B_D$ ) and the remaining ( $R$ ) is recycled as mentioned before. The vapour from each stage is collected in a distillate tray to finally produce the fresh water ( $D_N$ ).

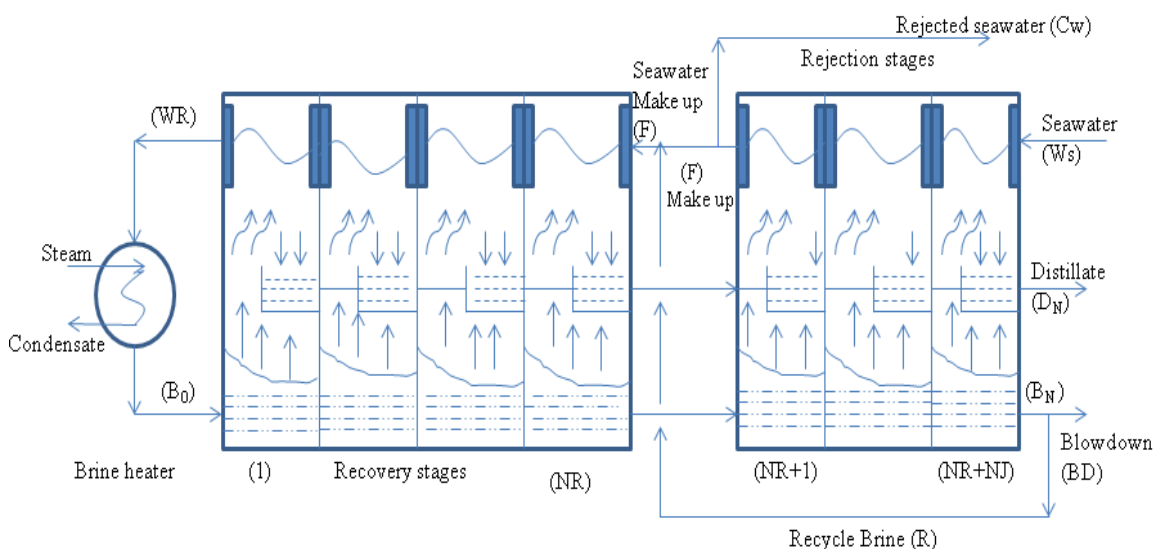


Figure 4.1 Typical MSF Process (Rosso et al., 1996)



### 4.3 Steady State MSF Process Model

The following assumptions are made in the model:

- The distillate from any stage is salt free
- Heat of mixing are negligible
- No sub cooling of condensate leaving the brine heater
- There are no heat losses and
- There is no entrainment of mist by the flashed vapour.

#### 4.3.1 Model Equations

The model equations for stage number  $j$  (Figure. 4.2) and physical properties (Table 4.1) correlations presented are reported by Helal et al., (1986), Rosso et al., (1996) and Hussain et al., (1993). Note, Tanvir and Mujtaba (2006) used NN based correlations to calculate the temperature elevation (TE). Hawaidi and Mujtaba (2010) used correlations developed by EL-Dessouky and Ettouney (2002) to calculate the TE.

##### 4.3.1.1 Stage model

Mass Balance in the flash chamber:

$$B_{j-1} = B_j + V_j \quad (4.1)$$

Mass Balance for the distillate tray:

$$D_j = D_{j-1} + V_j \quad (4.2)$$

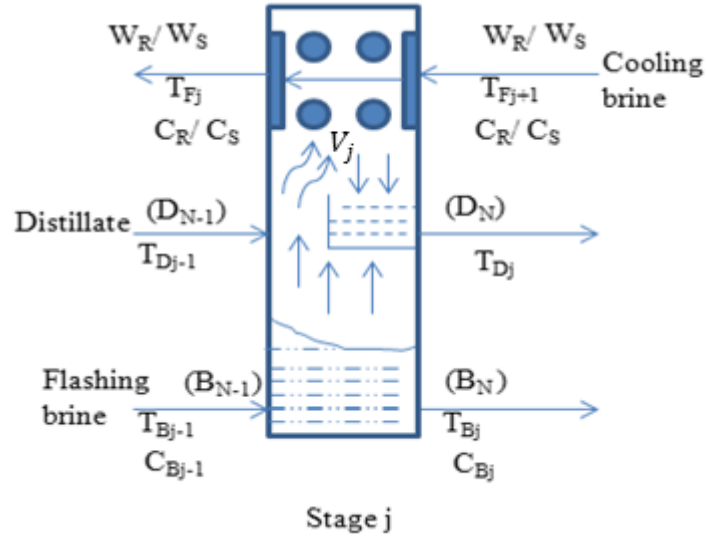


Figure 4.2 MSF flashing stage

Enthalpy balance on flash brine:

$$B_j = (h_{B_{j-1}} - h_{v_j}) / (h_{B_j} - h_{v_j}) B_{j-1} \quad (4.3)$$

$$h_{v_j} = f(T_{V_j}) \quad (4.4)$$

$$h_{B_j} = f(C_{B_j}, T_{B_j}) \quad (4.5)$$

Overall Energy Balance:

$$W_R S_{Rj} (T_{F_j} - T_{F_{j+1}}) = D_{j-1} S_{D_{j-1}} (T_{D_{j-1}} - T^*) + B_{j-1} S_{B_{j-1}} (T_{B_{j-1}} - T^*) - D_j S_{D_j} (T_{D_j} - T^*) - B_j S_{B_j} (T_{B_j} - T^*) \quad (4.6)$$

Heat transfer equation:

$$W_R S_{Rj} (T_{F_j} - T_{F_{j+1}}) = U_j A_j \text{LMTD}_j \quad (4.7)$$

(replace  $W_R$  for  $W_S$  rejection stage)

The logarithmic mean temperature difference in the recovery and rejection stages:

$$\text{LMTD}_j = (T_{F_j} - T_{F_{j+1}}) / \ln\{(T_{D_j} - T_{F_{j+1}}) / (T_{D_j} - T_{F_j})\} \quad (4.8)$$

(replace  $W_R$  for  $W_s$  rejection stage)

$$SR_j = f(T_{Fj}, T_{Fj+1}, C_R) \quad (4.9)$$

$$SD_j = f(T_{Dj}) \quad (4.10)$$

$$SB_j = f(T_{Bj}, CB_j) \quad (4.11)$$

Distillate and flashing brine temperature correlation:

$$T_{Bj} = T_{Dj} + TE_j + EX_j + \Delta_j \quad (4.12)$$

Distillate and flashing steam correlation:

$$T_{Vj} = T_{Dj} + \Delta_j \quad (4.13)$$

$$\Delta_j = f(T_{Dj}) \quad (4.14)$$

$$TE_j = f(T_{Dj}, C_{Bj}) \quad (4.15)$$

$$EX_j = f(H_j, w_j, T_{Bj}) \quad (4.16)$$

#### 4.3.1.2 Brine heater model

Mass and salt balance for the brine heater (Figure 4.3)

$$B_o = W_R \quad (4.17)$$

$$C_{Bo} = C_R \quad (4.18)$$

Overall enthalpy balance

$$B_o S_{RH} (T_{Bo} - T_{F1}) = W_{\text{steam}} \lambda_S \quad (4.19)$$

$$\lambda_S = f(T_{\text{steam}}) \quad (4.20)$$

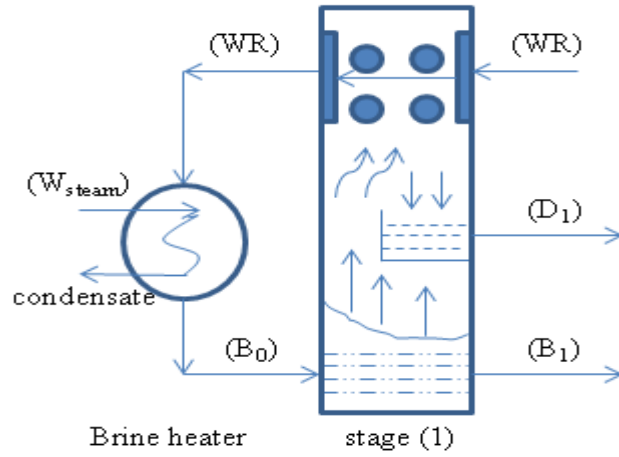


Figure 4.3 Brine heater and stage (1)

Heat transfer equation

$$W_R S_{RH} (T_{B_0} - T_{F1}) = U_H A_H \text{LMTD}_H \quad (4.21)$$

The logarithmic mean temperature difference in brine heater ( $\text{LMTD}_H$ )

$$\text{LMTD}_H = \frac{(T_{\text{steam}} - T_{F1}) - (T_{\text{steam}} - T_{B_0})}{(T_{\text{steam}} - T_{F1}) - (T_{\text{steam}} - T_{B_0})} \quad (4.22)$$

$$U_H = f(T_{\text{steam}}, T_{B_0}, T_{F1}, T_{\text{steam}}, D_H^i, D_H^o, f_H^i) \quad (4.23)$$

$$S_{RH} = f(T_{B_0}, T_{F1}) \quad (4.24)$$

#### 4.3.1.2 Splitter model

Mass balance on seawater splitter (Figure 4.4):

$$B_D = B_N - R \quad (4.25)$$

$$C_W = W_S - F \quad (4.26)$$

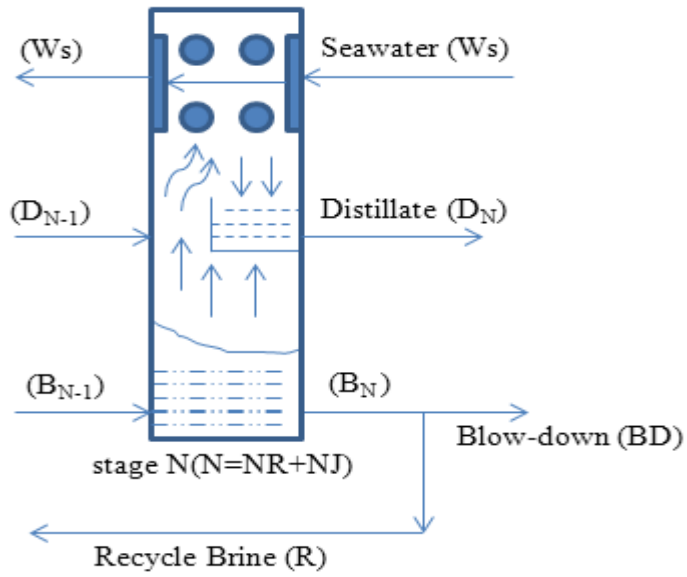


Figure 4.4 MSF Splitter and stage (N)

#### 4.3.1.3 Mixers model

Mass balance on mixer (Figure 4.5):

$$W_R = R + F \quad (4.27)$$

$$C_{BNS} + F C_S = W_R C_R \quad (4.28)$$

Enthalpy balance on mixer:

$$W_R h_W = R h_R + F h_F = f(T_{Fm}, C_R) \quad (4.29)$$

$$h_F = f(T_{FNR+1}, C_F) \quad (4.30)$$

$$h_R = f(T_{BNS}, C_{BNS}) \quad (4.31)$$

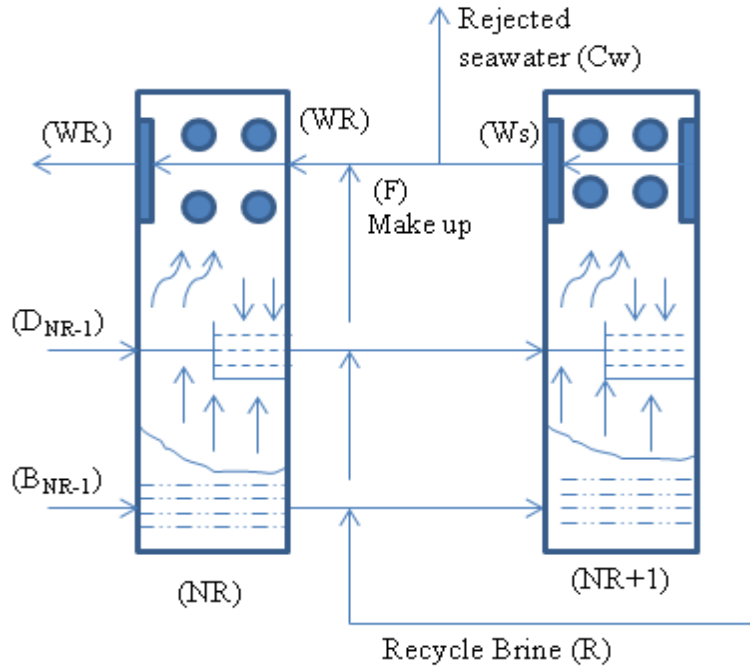


Figure 4.5 MSF Mixers

The Physical and chemical properties correlations are listed below.

Specific enthalpy of vapour

$$h_{vj} = 596.912 + 0.46694 \times T_V - 0.000460256 \times T_V^2 \quad (4.32)$$

For brine heater,  $h_v = h_{vj}$ ,  $T_V = T_{\text{steam}}$  in °F

Latent heat of vapour:  $\lambda_s = h_v - h_D$

Specific enthalpy of saturated water:

$$h_D = 1.8 \times (-31.92 + 1.0011833 T_{\text{steam}} - 3.0833326 \times 10^{-5} \times T_{\text{steam}}^2 + 4.66666 \times 10^{-8} \times T_{\text{steam}}^3 + 3.1333334 \times 10^{-10} \times T_{\text{steam}}^4) \quad (4.33)$$

Specific heat capacity of pure water:

$$S_{Dj}=1.001183-6.1666652\times 10^{-5}T_D+1.3999989\times 10^{-7}\times T_D^2+1.3333336\times 10^{-9}\times T_D^3 \quad (4.34)$$

For brine heater, seawater  $S_{Dj}=S_{Dj}$ ,  $T_D=T_{Bj}$  in °F

Specific heat capacity of seawater/brine

$$S_{Bj}=[1-C_B\times (0.011311-1.146\times 10^{-5}T_B)]\times S_{Dj} \quad (4.35)$$

For  $S_{Rj}=S_{Bj}$ ,  $C_B=C_S$  in wt%,  $C_B=C_R$  in wt %,  $T_B=T_{Fj+1}$  in °F,

For brine heater,  $S_{RH}=S_{Bj}$ ,  $C_B=C_R$  in wt%,  $T_B=T_{Fo}$  in °F

Specific enthalpy of seawater/brine

$$h_{Bj}=4.186\times ((4.185-5.381\times 10^{-3}\times C_{Bj}+6.26\times 10^{-6}\times C_{Bj}^2)\times T_{Bj}-$$

$$(3.055\times 10^{-5}+2.774\times 10^{-6}\times C_{Bj}-4.318\times 10^{-8}\times C_{Bj}^2)\times$$

$$\frac{T_{Bj}^2}{2} + \frac{(8.844\times 10^{-7}+6.527\times 10^{-8}\times C_{Bj}-4.003\times 10^{-10}\times C_{Bj}^2)\times T_{Bj}^3}{3} \quad (4.36)$$

For Mixer,  $h_w=h_{Bj}$ ,  $T_{Bj}=T_{Fm}$ ,  $C_{Bj}=C_R$ ,  $h_F=h_{Bj}$ ,  $T_{Bj}=T_{BNS}$ ,  $C_{Bj}=C_{BNS}$

Overall heat transfer Coefficient

The overall heat transfer coefficient has been calculated using Griffin and Keller (1965):

$$U_j = \frac{4.8857}{(y_j+Z_j+4.8857\times R_{fj})} \quad (4.37)$$

Where,

$$Z=0.102 \times 10^{-2} - 0.747 \times 10^{-5} \times T_{Dj} + 0.997 \times 10^{-7} \times T_{Dj}^2 - 0.430 \times 10^{-9} \times T_{Dj}^3 + 0.620 \times 10^{-12} \times T_{Dj}^4 \quad (4.38)$$

$$y = \frac{[v \times ID]^2}{[(160 + 1.92 \times TF_j) \times v]} \quad (4.39)$$

Density of Brine:

$$\rho_j = 16.01846 \times (62.707172 + 49.364088 \times C_{Bj} - 0.43955304 \times 10^{-2} \times T_B - 0.032554667 \times C_{Bj} \times T_B - 0.46076921 \times 10^{-4} \times T_B^2 + 0.63240299 \times 10^{-4} \times C_B \times T_B^2) \quad (4.40)$$

Boiling point elevation

$$TE_j = C_j \times TB_j / (266919.6 - 379.669 \times TB_j + 0.334169 \times TB_j^2) \times [565.757 / TB_j - 9.81559 + 1.54739 \times \ln TB_j + C_j (337.178 / TB_j - 6.41981 + 0.922753 \times \ln TB_j) + C_j^2 (32.681 / TB_j - 0.55368 + 0.079022 \times \ln TB_j)] \quad (4.41)$$

$$C_j = (19.819 \times C_{Bj}) / (1 - C_{Bj}) \quad (4.42)$$

Temperature loss due to demister

$$\Delta_j = \exp(1.885 - 0.02063 \times T_D) / 1.8 \quad (4.43)$$

Non equilibrium allowance

$$EX_j = \left( 195.556 \times \frac{H_j^{1.1} (\omega_j \times 10^{-3})^{0.5}}{\Delta T_{Bj}^{2.5}} \times T_{Vj}^{2.5} \right) \quad (4.44)$$



$\omega_j = \frac{W}{w}$ ,  $\Delta T_{Bj} = (T_{Bj} - T_{Bj-1})$  in °F, where ,  $W = W_R$  (recovery stage) in lb/h ,  $W = W_S$  (reject stage) in lb/h=(kg/h)

### 4.3.2 Degree of Freedom Analysis

For a total number of stages  $N = N_R + N_J$  ( $N_R$  is number of stages in the recovery section,  $N_J$  is the number stages in rejection section, the total number of equation (TNE) is  $25N + 27$ , the total number of variables (TNV) is :  $18NS + 16$ . Therefore the degree of freedom (D.F= $TNV - TNE$ ) is:  $7NS + 11$ . This means  $7NS + 11$  variables must be specified in the model equation could be solved.

The variables in the model are:

$V_j, CB_j, D_j, TD_j, TF_j, TB_j, f_j^i, D_j^i, D_j^o, w_j, H_j, L_j, SR_j, SD_j, SB_j, U_j, T_{Vj}, TE_j, EX_j,$   
 $h_{vj}, h_{Bj}, A_j, WR, CR, T,, B_o$

$CB_o, W_{steam}, \lambda_s, T_{steam}, TB_o, SR_H, U_H, A_H, D_H^i, D_H^o, f_H^i, L_H, B_D, R, C_W, hF, hR, TF_m$

With  $j=1, 2, \dots$  (N),  $N = N_R + N_J$

Total number of variables (TNV)= $24N + 26$

Total number of equations (TNE)= $17N + 15$

So the degree of freedom (D.F)= $TNV - TNE = 7N + 11$

Specifications to satisfy D.F are:

$A_H, D_H^i, D_H^o, f_H^i, L_H, A_j, f_j^i, D_j^i, D_j^o, w_j, H_j, L_j, WS, T_{steam}, T_{f_{NS+1}}, CS, R, CW = 7N + 11$

## 4.4 Model Implementation in gPROMS

An overview of the gPROMS MSF process model developed in gPROMS is shown in Figure 4.6. On the left hand panel of Figure 4.6 are a number of gPROMS entries corresponding to MSF process model such as (variable types, model, process and optimization). On the right hand panel, a set of constant parameters that characterizes the system are declared in the parameter section. A set of variety that describe the independent behavior of the system are declared in the VARIABLE

Section and a set of equation involving the declared variables and parameters are written in the EQUATION section of a model.

A process is partitioned into sections (UNIT, SET, ASSIGN, INITIAL, SOLUTION PARAMETERS and SCHEDULE). The unit section here refers to the process. Constant parameters are declared in the SET section includes variables specification satisfying the degree of freedom.

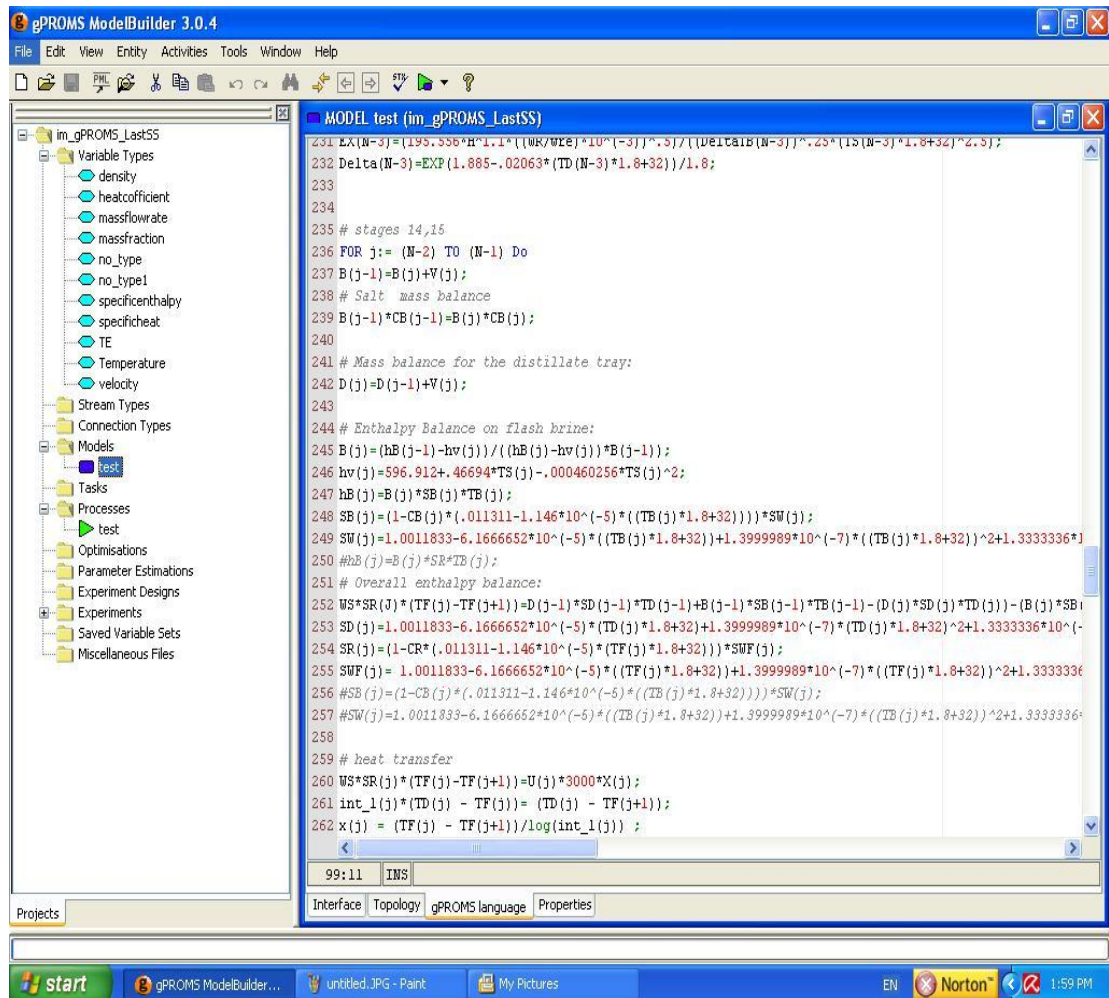


Figure 4.6 MSF simulation plants using gPROMS

## 4.5 Model Validation

In this work, the case study reported by Rosso et al., (1996) and Tanvir and Mujtaba (2006a) is considered for model validation. Rosso et al., (1996) developed their model based on real plant data used by Helal et al. 1986. There are total of 16 stages with NR=13 recovery and NJ=3 rejection stages. The specifications (satisfying the degree of freedom) used by Rosso et al., (1996) are shown in Table 4.1. The summary of the simulation results by Rosso et al., (1996) is given in Table 4.2. Using the same specifications as in Table 4.1, the simulation results of this work are also presented in Table 4.2 (as shown in italic). The simulation results for both models including, the flowrates of brine and distillate streams and temperature profiles for all stages are also

presented in Table 4.2. Comparison of the results presented in Table 4.2 clearly show that they are in good agreement as shown also in Figures 4.7-4.10. The temperature of the outlet brine ( $T_{Bj}$ ), cooling brine inside the condenser tubes ( $T_{Fj}$ ), and the distillate ( $T_{Dj}$ ) are decreasing through the flashing process (Figures 4.7-4.9). In contrast, the flashing brine salinity increase across the stages as shown in Figure 4.10.

Table 4.1 Constant Parameters and Input Data (Rosso et al., 1996)

	$A_j/A_H$	$D_j^i/D_H^i$	$D_j^o/D_H^o$	$f_j^i/f_H^i$	$w_j/L_j/L_H$	$H_j$
Brine heater	3530	0.022	0.0244	$1.86 \times 10^{-4}$	12.2	
Recovery stage	3995	0.022	0.0244	$1.4 \times 10^{-4}$	12.2	0.457
Rejection stage	3530	0.024	0.0254	$2.33 \times 10^{-5}$	10.7	0.457
$W_S$ (kg/s)	$T_{\text{steam}}$ (°C)	$T_{\text{seawater}}$ (°C)	$C_S$ (wt%)	$R$ (kg/s)	$C_w$ (kg/s)	
31416.67	97°C	35 °C	5.7	1763.89	1561.11	

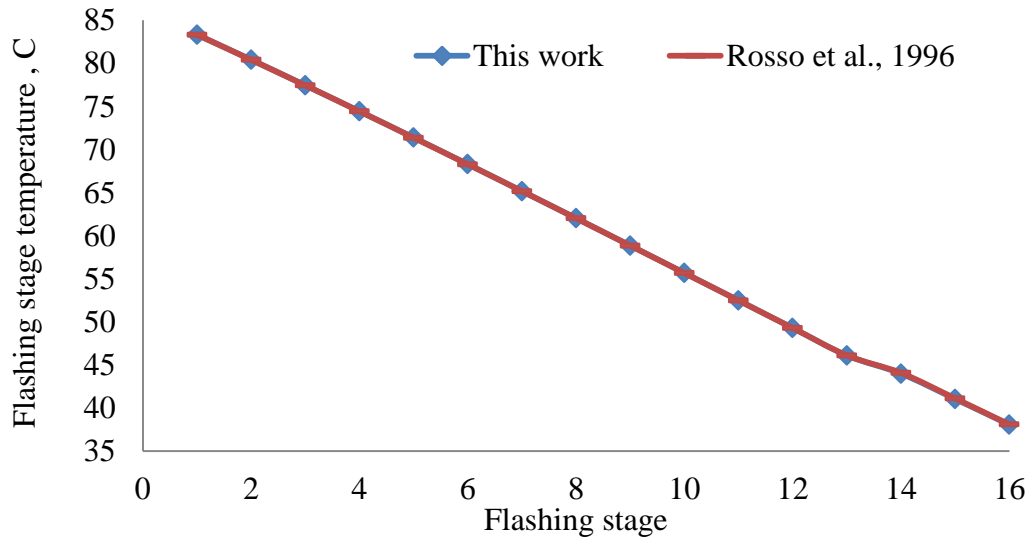


Figure 4.7 Comparison of this work results with Rosso et al., (1996) results of flashing stage temperature ( $T_{Bj}$ )

Table 4.2 Summary of the simulation Results by (Rosso et al., 1996) and this work

	F(kg/s)	BD(kg/s)	WR(kg/s)	$W_{\text{steam}}$ (kg/s)	CR%
	1577.78	1319.44	3333.33	33.06	6.29
	<i>1577.77</i>	<i>1315.59</i>	<i>3341.66</i>	<i>37.49</i>	<i>6.29</i>

Stage	$B_j$ (kg/s)	$D_j$ (kg/s)	$CB_j$ %	$TF_j$ (°C)	$TD_j$ (°C)	$TB_j$ (°C)	$U_j$ (kcal/hm <sup>2</sup> K)
0	3.34E+03		6.29	0	0	89.74	2040.9
	<i>3.32E+03</i>	<i>0</i>	<i>6.29</i>	<i>0</i>	<i>0</i>	<i>89.74</i>	<i>2043.8</i>
1	3.33E+03	16.50	6.32	83.33	85.75	86.89	2250
	<i>3.31E+03</i>	<i>16.82</i>	<i>6.33</i>	<i>83.33</i>	<i>85.75</i>	<i>86.93</i>	<i>2253.6</i>
2	3.31E+03	32.78	6.35	80.41	82.87	84.01	2246.4
	<i>3.29E+03</i>	<i>33.76</i>	<i>6.36</i>	<i>80.42</i>	<i>82.87</i>	<i>84.07</i>	<i>2250.1</i>
3	3.29E+03	49.44	6.38	77.44	79.95	81.08	2243
	<i>3.27E+03</i>	<i>50.80</i>	<i>6.39</i>	<i>77.45</i>	<i>79.95</i>	<i>81.15</i>	<i>2246.8</i>
4	3.28E+03	66.11	6.41	74.43	76.97	78.11	2239.9
	<i>3.26E+03</i>	<i>67.90</i>	<i>6.43</i>	<i>74.43</i>	<i>76.97</i>	<i>78.19</i>	<i>2243.7</i>
5	3.26E+03	82.78	6.45	71.37	73.94	75.09	2236.9
	<i>3.24E+03</i>	<i>85.04</i>	<i>6.46</i>	<i>71.38</i>	<i>73.94</i>	<i>75.18</i>	<i>2240.9</i>
6	3.24E+03	99.72	6.48	68.28	70.88	72.04	2234.2
	<i>3.22E+03</i>	<i>102.18</i>	<i>6.49</i>	<i>68.29</i>	<i>70.88</i>	<i>72.14</i>	<i>2238.2</i>
7	3.23E+03	116.67	6.51	65.16	67.78	68.95	2231.7
	<i>3.21E+03</i>	<i>119.30</i>	<i>6.53</i>	<i>65.16</i>	<i>67.78</i>	<i>69.06</i>	<i>2235.7</i>
8	3.21E+03	133.33	6.55	62.01	64.65	65.84	2229.2
	<i>3.19E+03</i>	<i>136.36</i>	<i>6.56</i>	<i>62.01</i>	<i>64.65</i>	<i>65.96</i>	<i>2233.3</i>
9	3.19E+03	150.28	6.58	58.84	61.49	62.7	2226.6
	<i>3.17E+03</i>	<i>153.33</i>	<i>6.60</i>	<i>58.84</i>	<i>61.49</i>	<i>62.85</i>	<i>2230.9</i>
10	3.18E+03	166.94	6.62	55.65	58.32	59.55	2224.0
	<i>3.15E+03</i>	<i>170.17</i>	<i>6.63</i>	<i>55.66</i>	<i>58.31</i>	<i>59.71</i>	<i>2228.4</i>
11	3.16E+03	183.33	6.65	52.46	55.13	56.39	2221.0
	<i>3.14E+03</i>	<i>186.84</i>	<i>6.67</i>	<i>52.47</i>	<i>55.12</i>	<i>56.58</i>	<i>2225.5</i>
12	3.14E+103	199.72	6.69	49.27	51.93	53.24	2217.6
	<i>3.12E+03</i>	<i>203.31</i>	<i>6.70</i>	<i>49.27</i>	<i>51.93</i>	<i>53.45</i>	<i>2222.2</i>
13	3.13E+03	216.11	6.72	46.09	48.74	50.09	2213.6
	<i>3.11E+03</i>	<i>219.53</i>	<i>6.74</i>	<i>46.09</i>	<i>48.73</i>	<i>50.33</i>	<i>2218.3</i>
14	3.11E+03	230.28	6.75	44.06	45.87	47.28	2917.3
	<i>3.09E+03</i>	<i>233.61</i>	<i>6.77</i>	<i>43.97</i>	<i>45.90</i>	<i>47.60</i>	<i>2779.8</i>
15	3.10E+03	244.72	6.78	41.10	42.95	44.42	2905.9
	<i>3.08E+03</i>	<i>247.85</i>	<i>6.80</i>	<i>41.03</i>	<i>43.02</i>	<i>44.81</i>	<i>2765.7</i>
16	3.08E+03	259.44	6.82	38.07	39.98	41.51	2892.3
	<i>3.32E+03</i>	<i>262.18</i>	<i>6.83</i>	<i>38.04</i>	<i>40.07</i>	<i>41.97</i>	<i>2749.4</i>

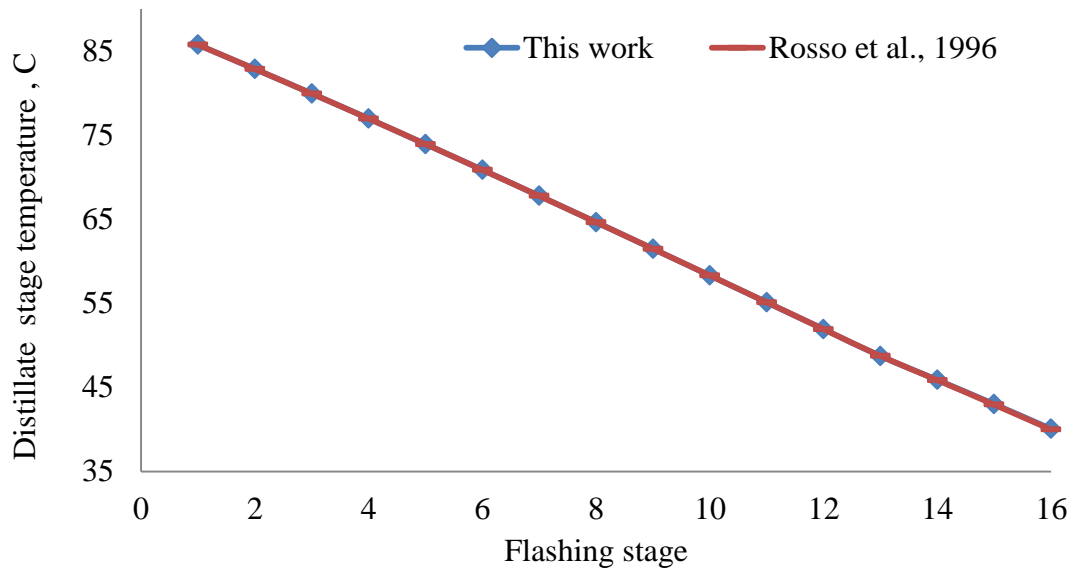


Figure 4.8 Comparison of this work results with Rosso et al., (1996) results of distillate stage temperature (TDj)

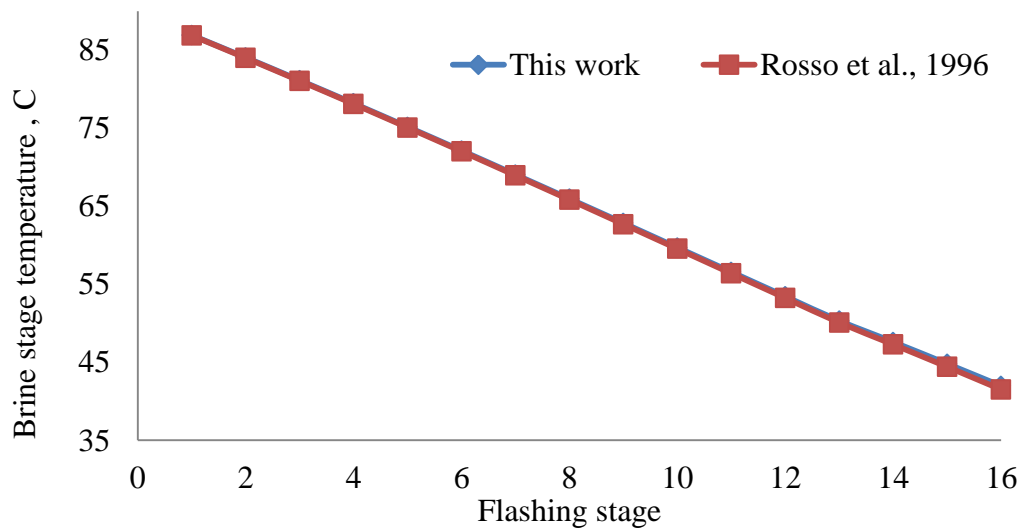


Figure 4.9 Comparison of this work results with Rosso et al., (1996) results of distillate stage temperature (TFj)

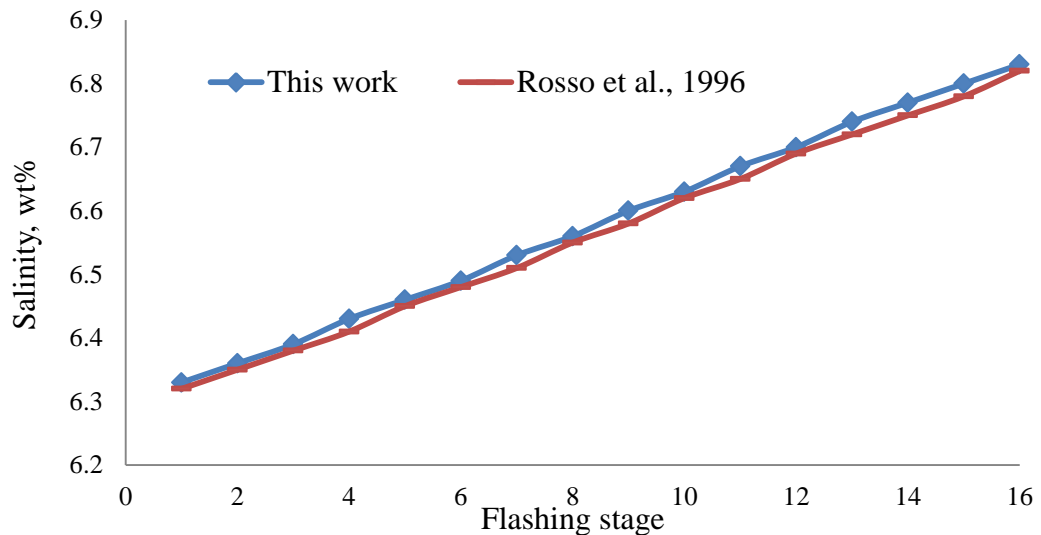


Figure 4.10 Comparison of this work results with Rosso et al., (1996) results of brine rejected salinity CBj

## 4.6 Conclusions

In this chapter, detailed steady state mathematical model is presented for MSF brine recycle (BR) process. The developed model is based on mass balance, energy balance, and heat transfer equations coupled with the correlations for physical properties for all the streams of brine and distillate. The physical properties accounts in the developed model were function of temperature and salinity. In addition the developed model included the geometry of the stages, the different non-idealities involved in the process, the temperature loss across the demister and condenser tubes.

The gPROMS modelling tool has been used to model and simulate the MSF-BR process. The model is validated against the simulation results from the literature. The predictions using the new model are in good agreement with the published results. The developed model in this chapter will be used in Chapters 5, 6 and 7.

## **Chapter 5**

# **Effect of Fouling Factors on the Optimisation of MSF Desalination Process for Fixed Water Demand using gPROMS**

### **5.1 Introduction**

The precipitation of  $\text{CaCO}_3$  scale inside the condenser tubes of MSF desalination plants is a function of many variables such as temperature, pH and concentration of salts. Modeling and simulation of  $\text{CaCO}_3$  scale precipitation in MSF plants will help the design engineer to predict the effects of such problem on the performance of the desalination plants (Al-Ahmad and Abdul Aleem 1993). In the past, several studies have been done on the fouling problems in MSF desalination process. Most of these studies were experimental work to understand the scale formation process and antiscaling evaluation tests. However, only few publications have mentioned the scale formation modeling. In addition, most of these works did not include any effects of MSF operating parameters such as flow velocity, temperature and foulant concentration on the scale fouling resistance models (Malayeri and Muller-Steinhagen 2007). More important, and as seen from the literature, varying scale formation fouling resistance in the developing of the steady state modelling and optimisation of MSF process has received little attention. Most of these studies carried out using fixed fouling factor in the calculating of overall heat transfer coefficient. However, Hawaidi and Mujtaba (2010) developed a linear dynamic brine heater fouling factor and studied the role of fouling factor on the simulation and optimisation of MSF process. Therefore, in this chapter, a steady state calcium carbonate fouling resistance model has been developed and implemented in the



full MSF mathematical model developed in chapter 4 using gPROMS software. This model takes into consideration the effect of surface temperature on the calcium carbonate fouling resistance in the flashing chambers in the heat recovery section, heat rejection section, and brine heaters of MSF process at fluid velocity 1 m/s. The effect of seasonal variation of seawater temperature and top brine temperature on the calcium carbonate fouling resistance has been studied throughout the flashing stage using gPROMS software. In addition, the total annual operating cost of the MSF process is selected to minimise, while optimising the operating parameters such as seawater rejected flow rate, brine recycle flow rate and steam temperature at different seawater temperature and fouling resistance.

## 5.2 Calcium Carbonate Fouling Process

Fouling is the accumulation of undesired solid materials at the phase interfaces. One of the major fouling encountered in the MSF desalination plants is calcium carbonate ( $\text{CaCO}_3$ ) scale formation. Thermal decomposition of bicarbonate ion at high temperatures causes the precipitation of  $\text{CaCO}_3$  once its solubility limits are reached (Al-Anezi et al., 2008).

Calcium carbonate fouling inside the condenser tubes in the MSF process is inherent to the composition of seawater which contains  $\text{HCO}_3^-$  and  $\text{Ca}^{2+}$  ions. The primary reaction which causes  $\text{CaCO}_3$  formation is the thermal decomposition of the  $\text{HCO}_3^-$  ion as follows:



The calcium ions present in the seawater react with the carbonate ions to form calcium carbonate.



### 5.3 Modelling of Calcium Carbonate Fouling deposition

At any time the Kern and Seaton Model (Cooper et al., 1983) postulates that the net rate of deposition of fouling is usually given in the form of:

$$\frac{dR_f}{dt} = \Phi_d - \Phi_r \quad (5.4)$$

Where  $\frac{dR_f}{dt}$  the rate of change in fouling resistance,  $\Phi_d$  is the deposition rate, and  $\Phi_r$  is the removal rate.

For water basically

$$\Phi_d = C_{11} P_d \Omega^n \exp\left(\frac{-E}{R_g T_s}\right) \quad (5.5)$$

$$\Phi_r = C_{22} \tau^{\frac{x}{\psi}} \quad (5.6)$$

Where,

$\tau$  is the shear stress (shear force) near the fouling deposit layer. In addition, it refers to the force for the removal of solid material from the surface as shown in Figure 5.1. The removal rate of the deposit depends on the velocity of the fluid flowing through the pipe. In deed if the velocity across the fouling deposit increases the deposit thickness decrease (Bott, 1995).

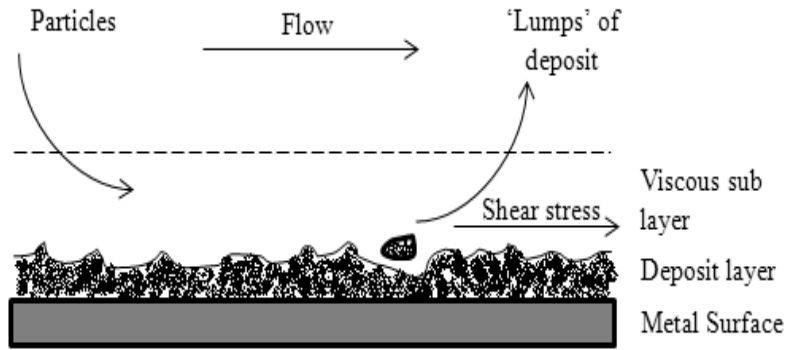


Figure 5.1 Removal of deposit from the metal surface (Bott, 1995)

$C_{11}, C_{22}$  : constant

$x$  : deposit thickness

$\Psi$  : strength of deposit

$P_d$  : deposition of factor related to velocity and stickiness of deposit

$\Omega^n$  : water quality factor

$\exp\left(\frac{-E}{R_g T_s}\right)$  : Arrhenius reaction rate function

$E$  : activation energy

$T_s$  : absolute surface temperature

$R_g$  : gas constant

Integration of Equation (5.4) with substitute of Equations (5.5) and (5.6) leads to

$$R_f = \frac{C_{11} P_d \Omega^n}{C_{22} \tau_{\Psi}^x} \exp\left(\frac{-E}{R_g T_s}\right) \left[1 - \exp\left(-\frac{C_{22} \tau x t}{\Psi}\right)\right] \quad (5.7)$$

$$R_f = \frac{\Phi_d}{\Phi_r} \left[1 - \exp(-\Phi_r t)\right] \quad (5.8)$$

As time becomes large, then

$$R_f = \frac{C_1 P_d \Omega^n}{C_2 \tau \bar{\Psi}} \exp\left(\frac{-E}{RT_s}\right) \quad (5.9)$$

Various aspects of Equation (5.9) have been studied by Knudsen and Story (1978) who have obtained the following equation for  $\text{CaCO}_3$  fouling deposition from water flowing at 1 m/s

$$R_f = 3 \times 10^{11} e^{-\left(\frac{42,000}{R_g T_s}\right)} \quad (5.10)$$

Equation (5.10) is a function of the surface temperature but due to the unavailable data for the surface temperature of the condenser tubes in the flashing stages for the case study under investigated; therefore the temperature of the brine inside the condenser tubes ( $T_{Fj}$ ) in each stage of heat recovery section and heat rejection section and also in the brine heater has been considered. Then Equation 5.11 has been used to calculate the overall heat transfer coefficient ( $U_j$ ) in the heat recovery section, heat rejection section, and brine heater according to the following correlations developed by Griffin and Keller (1965):

$$U_j = \frac{4.8857}{(y_j + Z_j + 4.8857 \times R_{fj})} \quad (5.11)$$

Where,

$$Z = 0.102 \times 10^{-2} - 0.747 \times 10^{-5} \times T_{Dj} + 0.997 \times 10^{-7} \times T_{Dj}^2 - 0.430 \times 10^{-9} \times T_{Dj}^3 + 0.620 \times 10^{-12} \times T_{Dj}^4 \quad (5.12)$$

$$y = \frac{[v \times ID]^2}{[(160 + 1.92 \times T_{Fj}) \times v]} \quad (5.13)$$

Equation 5.11 has been implemented in the steady state MSF process model described in chapter 4 to study the effect of some MSF operation such as seawater feed temperature and top brine temperature on the  $\text{CaCO}_3$  fouling resistance. In addition the effect of  $\text{CaCO}_3$  fouling resistance on the optimization of MSF process parameters has been described.

## **5.4 Effect of MSF Operation Parameters on $\text{CaCO}_3$ Fouling Resistance**

The MSF process model developed in chapter 4 and the case study reported by Rosso et al., (1996) (chapter 4) has been considered in the investigations of this section . The MSF process model and  $\text{CaCO}_3$  fouling resistance model has been applied to 16 stages MSF recycle brine desalination plant with NR=13 recovery stages and NJ=3 rejection stages. The specifications are shown in Table 5.1. In this section, the effect of MSF operating parameters such as seawater temperature and TBT on the  $\text{CaCO}_3$  fouling resistance has been studied.

### **5.4.1 Effect of Seawater Feed Temperature on the $\text{CaCO}_3$ Fouling Resistance**

The seawater temperature is varied due to seasonal time between winter and summer. The effect of variation in the seawater temperature on the  $\text{CaCO}_3$  fouling resistance has been investigated in this section. The seawater temperature was varied between 25°C and 45°C at top brine temperature 89°C. The  $\text{CaCO}_3$  fouling resistance increases as the seawater temperature increases as shown in Figure 5.2 for stage (1). The fouling resistance increased from 8.42E-5 m<sup>2</sup> K/w at  $T_{\text{seawater}}=25^\circ\text{C}$  to 1.12E-4 m<sup>2</sup> K/kw at  $T_{\text{seawater}} = 45^\circ\text{C}$ . The fouling resistance has increased by 24% due to increase the seawater temperature from 25°C to 45°C. This is due to the decrease in the solubility of the  $\text{CaCO}_3$  scale as the temperature inside the condenser tube increase due to the increase in the seawater feed temperature.

Table 5.1 Constant Parameters and Input Data (Rosso et al., 1996)

	$A_j/A_H$	$D_j^i/D_H^i$	$D_j^o/D_H^o$	$w_j/L_j/L_H$	$H_j$
Brine heater	3530	0.022	0.0244	12.2	
Recovery stage	3995	0.022	0.0244	12.2	0.457
Rejection stage	3530	0.024	0.0254	10.7	0.457
$W_S$ (kg/s)	$T_{\text{steam}}$ (°C)	$T_{\text{seawater}}$ (°C)	$C_S$ (wt%)	$R$ (kg/s)	$C_w$ (kg/s)
31416.67	97	35	5.7	1763.89	1561.11

Figure 5.3 shows the effect of seawater temperature on the  $\text{CaCO}_3$  fouling resistance in the individual stages of the MSF distillers. The seawater temperature was varied between 25°C and 45°C at top brine temperature at 89°C. The  $\text{CaCO}_3$  fouling resistance increases as the seawater temperature increases for any stage. On the other hand, the  $\text{CaCO}_3$  fouling resistance decreases with the number of stages. At seawater 45°C, the fouling resistance was  $1.12 \times 10^{-4} \text{ m}^2 \text{ K/w}$  in the first stage of the heat recovery section and declined to  $1.78 \times 10^{-6} \text{ m}^2 \text{ K/w}$  in the last stage of the heat rejection section (stage 16) at the same seawater temperature. This is due the decrease in the  $\text{CaCO}_3$  solubility with increasing the brine inside in the condenser tubes from stage 1 to stage 16.

#### 5.4.2 Effect of Top Brine Temperature on the $\text{CaCO}_3$ Fouling Resistance

The effect of TBT which is one of the MSF control parameters on the  $\text{CaCO}_3$  fouling resistance has been studied. The TBT was varied between 90, 100, 110, and 120°C at seawater temperature at 25°C. The results show that the fouling resistance increased with increased TBT as described in Figure 5.4 for stage (1). The  $\text{CaCO}_3$  fouling resistance increased from  $8.28 \text{E-}5 \text{ m}^2 \text{ K/w}$  at TBT 90°C to  $8.73 \text{E-}4 \text{ m}^2 \text{ K/w}$  at TBT 120 °C, i.e. a 90 % increase. The increase in the TBT led to increasing in the vapor

flashing temperature and the seawater temperature inside the condenser tubes of the flashing stages due to the heat transfer process.

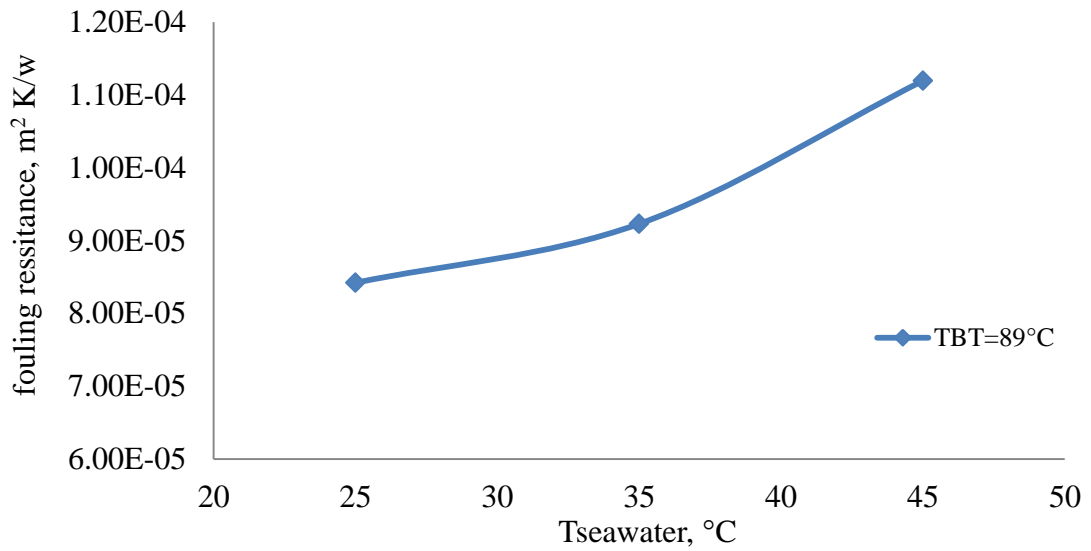


Figure 5.2 Effect of seawater temperature on fouling resistance in stage (1) of MSF recycle distiller

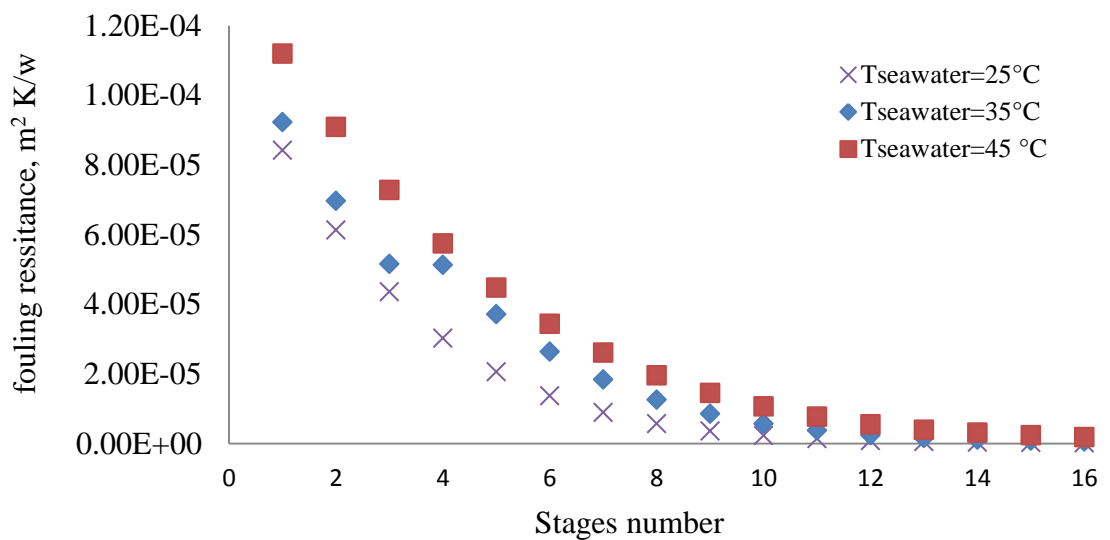


Figure 5.3 Effect of seawater temperature on fouling resistance in stage (1) of MSF recycle distiller

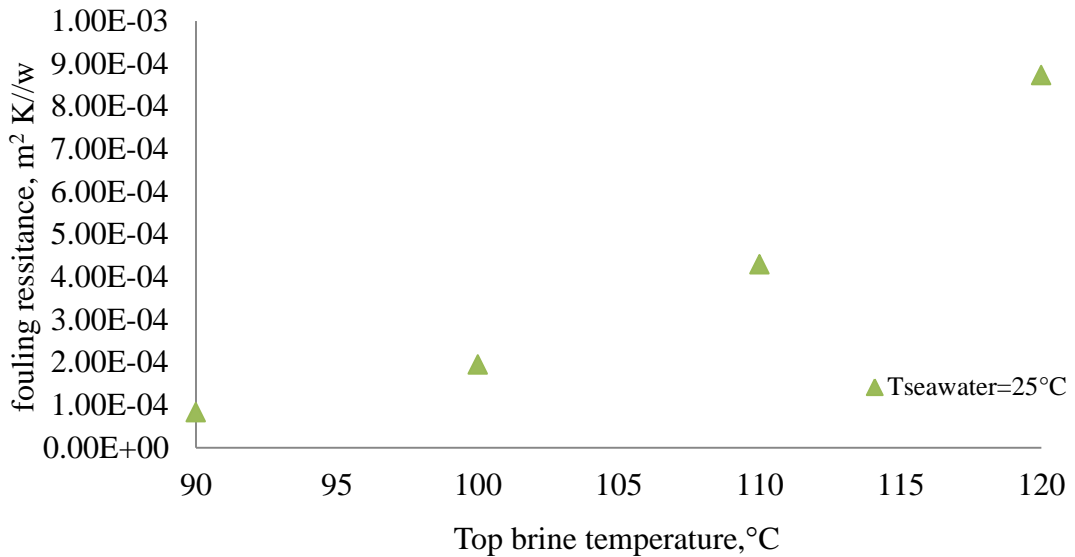


Figure 5.4 Effect of TBT on fouling resistance in stage (1) of MSF recycle distiller

Figure 5.5 shows the effect of TBT on the CaCO<sub>3</sub> fouling resistance in the individual stages of the MSF distillers. The TBT was varied between 90, 100, 110, and 120°C at seawater temperature at 25°C. The CaCO<sub>3</sub> fouling resistance increases as the top brine temperature increases for fixed stage. Conversely, the CaCO<sub>3</sub> fouling resistance decreases with the number of stages. For example at top brine temperature 100°C, the fouling resistance was  $1.95 \times 10^{-4}$  m<sup>2</sup> K/w in the first stage of the heat recovery section and declined to  $2.16 \times 10^{-7}$  m<sup>2</sup> K/w in the last stage of the heat rejection section (stage 16) at the same TBT. Note, the fouling resistance remaining the same value at last stages of the heat rejection section for different TBT. Again here, as the top brine temperature increase, the vapor flashing temperature increase and as result the seawater temperature inside the condenser tubes of the flashing stages increase and cause the solubility of the calcium carbonate decreases.



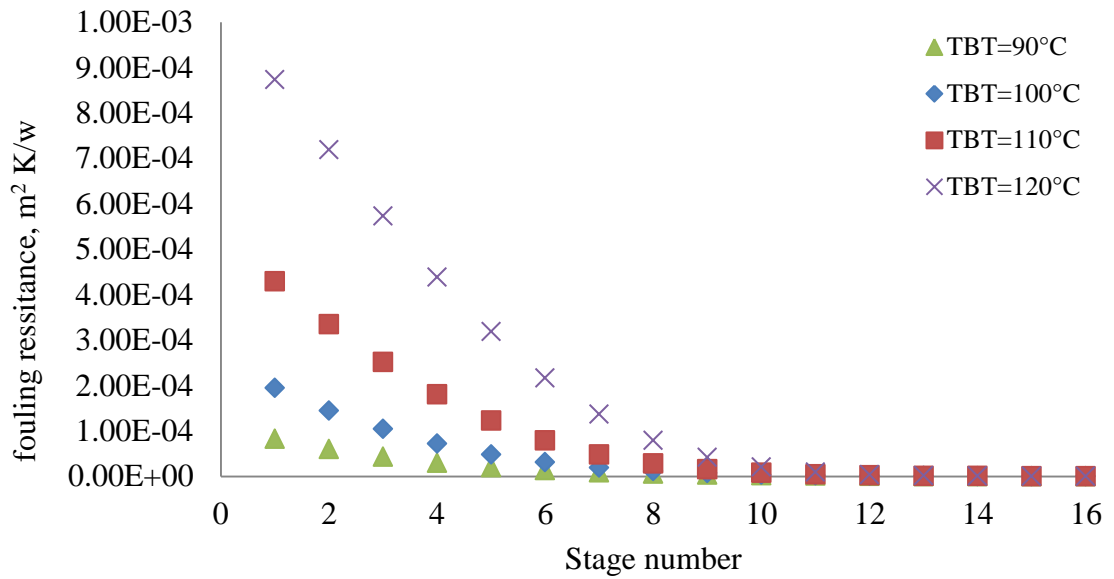


Figure 5.5 Effect of TBT on fouling resistance in stages of MSF recycle distiller

## 5.5 Optimisation of MSF Process: impact of CaCO<sub>3</sub> Fouling

### Resistance for Fixed Water Demand

As seen from the previous section the seawater feed temperature has an effect on the CaCO<sub>3</sub> fouling resistance. In addition, the fouling deposition affects the performance of the MSF desalination process by reducing the overall HTC and consequently cause reduction in the freshwater production. Therefore, to supply freshwater meeting a fixed demand, the operation parameters of the MSF process have to be adjusted with the variation of CaCO<sub>3</sub> fouling resistance and seawater temperature. In this section, the total operating cost (including steam cost, chemical cost, power cost, spare cost, and labor cost) of MSF desalination was chosen to minimise while optimising the operating parameters such as steam temperature, recycle brine flowrate and rejected seawater flowrate with the variation of CaCO<sub>3</sub> fouling resistance and seawater temperature.

### 5.5.1 Optimisation Problem Formulation

The optimisation problem is described as:

Given: Fixed water demand throughout the year, fixed number of stages, fixed amount of seawater Flow, heat exchanger areas in stages, design specifications of each stage.

Optimise: The steam temperature, recycle brine flowrate, rejected seawater flowrate.

To minimise: The total operation cost (TOC).

Subject to: Any constraints.

The optimisation problem (OP) can be described mathematically by:

$$\text{OP} \quad \text{Min} \quad \text{TOC} \\ T_{\text{steam}}, R, C_w$$

Subject to:

$$D_{\text{end}} = D_{\text{end}}^*$$

$$(93^\circ\text{C}) T_{\text{steam}}^L \leq T_{\text{steam}} \leq T_{\text{steam}}^U (98^\circ\text{C})$$

$$(6.66 \text{ kg/s}) R^L \leq R \leq R^U (3041 \text{ kg/s})$$

$$(3.33 \text{ kg/s}) C_w^L \leq C_w \leq C_w^U (1693.33 \text{ kg/s})$$

The TOC for the MSF process can be calculated as follows (Helal, 2004). Note, the constant unit cost values in the Equations (5.11-5.15) has been reported by Al-Mutaz et al., (200) and Wade, (2001). These unit costs refer to plants with a capacity of 31,822 m<sup>3</sup>/d (the same specifications of the current case study).

The TOC includes:

- Steam cost ( $C_1$ )

$$C_1 = 8000 \times W_{\text{Steam}} \left( \frac{T_s - 40}{85} \right) \times (0.00415) \quad \$/y \quad (5.11)$$

Where,  $W_{\text{Steam}}$  is steam consumption in kg/hr,  $T_s$  is steam temperature in °C

- Chemical treatment ( $C_2$ )

$$C_2 = 8000 \times \left( \frac{F}{\rho_B} \right) \times (0.024) \quad \$/y \quad (5.12)$$

Where,  $F$  is make-up flow rate in kg/hr,  $\rho_B$  is brine density in  $\text{kg/m}^3$

- Power cost ( $C_3$ )

$$C_3 = 8000 \times \left( \frac{D_N}{\rho_w} \right) \times (0.109) \quad \$/y \quad (5.13)$$

Where,  $D_N$  is distillate product in kg/hr,  $\rho_w$  is water density in  $\text{kg/m}^3$

- Spares cost ( $C_4$ )

$$C_4 = 8000 \times \left( \frac{D_N}{\rho_w} \right) \times (0.082) \quad \$/y \quad (5.14)$$

- Labor cost ( $C_5$ )

$$C_5 = 8000 \times \left( \frac{D_N}{\rho_w} \right) \times (0.1) \quad \$/y \quad (5.15)$$

$$\text{TOC} = \sum_{i=1}^{i=5} C_i \quad \$/y \quad (5.16)$$

### 5.5.2 Case Studies

The effect of  $\text{CaCO}_3$  fouling resistance ( $R_f$ ) on optimization of MSF process parameters has been studied here. Two cases are considered. In case 1, the increasing in  $\text{CaCO}_3$  fouling resistance ( $R_f$ ) by 25%, 50% and 75% is considered. In case 2, decreasing the  $\text{CaCO}_3$  fouling resistance ( $R_f$ ) by 25%, 50% and 75% is considered. In both cases, the total annual operating cost (TOC) of the MSF process is selected to minimise, while optimising the operating parameters such as seawater rejected flow rate ( $C_w$ ), brine recycle flow rate ( $R$ ) and steam temperature ( $T_{\text{steam}}$ ).

All the optimisation problem have been solved for a set of seawater temperature (ranging from 20 to 45°C) and for fixed water demand at 194.44 kg/s. For all cases, the seawater feed flow rate is 3138.88 kg/s with salinity 5.7 wt.% and the TBT is 89°C. For both cases, the total number of stage is 16, with 13 stages in the recovery section and 3 in the rejection section. The plant specifications and input data are the same as in the case described in Table 5.1. For different seawater temperatures the  $\text{CaCO}_3$  fouling resistances ( $R_f$ ) has been calculated are using Equation 5.11.

Table 5.2 shows the optimal results of the TOC, steam flowrate ( $W_{\text{steam}}$ ), external heat supplied ( $Q_{\text{steam}}$ ), steam temperature ( $T_{\text{steam}}$ ), recycle flowrate ( $R$ ) and rejected seawater flowrate ( $C_w$ ) for case 1. The TOC increases with increasing  $\text{CaCO}_3$  fouling resistance and seawater temperature from 25 °C to 45 °C as shown in Table 5.1 and Figure 5.6. The increasing percentage in the TOC was 3.7% at 0% fouling resistance (clean condition) and 4.65% at 75% fouling resistance for the same seawater change. Furthermore, the highest value of TOC is when the seawater temperature is 45 °C and fouling resistance increased by 75%. However, the lowest value of the TOC is obtained when the seawater temperature 25 and fouling resistance increased by 25%.

Table 5.2 Summary of the optimisation results (Case 1)

CaCO <sub>3</sub> fouling resistance (R <sub>f</sub> ) 0% FF(clean)							
Tseawater,°C	R,kg/sec	Cw,kg/s	Qsteam,kj/kg	WR,kg/s	Tsteam,	Wsteam	TOC,\$/y
20	445.20	1693.33	50681.29	1890.76	93	22.27	4274991
25	589.48	1693.33	48408.66	2035.04	93	21.28	4215344
35	916.75	1693.33	52129	2362.31	93	22.91	4304521
45	1510.60	1693.33	54166.16	2956.15	93	23.81	4379851
CaCO <sub>3</sub> fouling resistance (R <sub>f</sub> ) increased by 25% FF							
20	456.88	1693.33	51008.33	1902.44	93	22.42	4285729
25	603.40	1693.33	48788.03	2048.96	93	21.44	4228109
35	936.81	1693.33	52638.36	2382.36	93	23.13	4320732
45	1548.0	1693.33	54999.70	2993.63	93	24.17	4407140
CaCO <sub>3</sub> fouling resistance (R <sub>f</sub> ) increased by 50% FF							
20	468.24	1693.33	51323.6	1913.8	93	22.56	4296096
25	616.95	1693.33	49154.02	2062.51	93	21.60	4240424
35	956.41	1693.33	53130.47	2401.97	93	23.35	4336433
45	1585.13	1693.33	55811.88	3030.68	93	24.53	4433752
CaCO <sub>3</sub> fouling resistance (R <sub>f</sub> ) increased by 75% FF							
20	479.28	1693.33	51627.8	1924.84	93	22.69	4306115
25	630.149	1693.33	49507.44	2075.70	93	21.76	4252316
35	975.58	1693.33	53606.78	2421.14	93	23.56	4351650
45	1621.73	1693.33	56604	3067.28	93	24.88	4459701

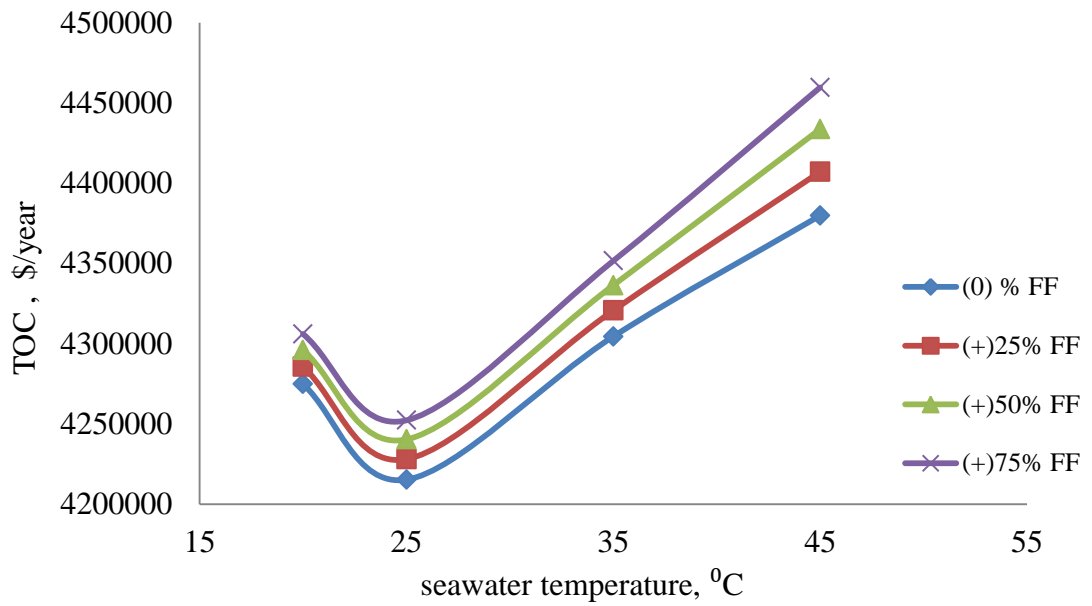


Figure 5.6 Effect of % increasing in fouling factor on TOC at different seawater temperature

In case 1, and for the seawater temperature varies from 20 to 45 °C and fouling resistance varies from 25%-75%, the steam temperature hits the lower values while the seawater rejected ( $C_w$ ) flowrate hits the upper bound. In addition, the brine recycle flow rate (R) increase by 24-39% and brine flowrate to the recovery stages ( $W_R$ ) varies between 7-20 % for different seawater temperature. So the effect of seawater temperature and fouling resistance on the recycle brine flowrate is more pronounced. As shown in Figures 5.7 and 5.8, the steam cost (C1) increases as  $CaCO_3$  fouling resistance increases for the seawater changes from 25°C to 45 °C. This increasing due to the increases in steam consumption ( $W_{steam}$ ) and the external heat supplied  $Q_{steam}$ .

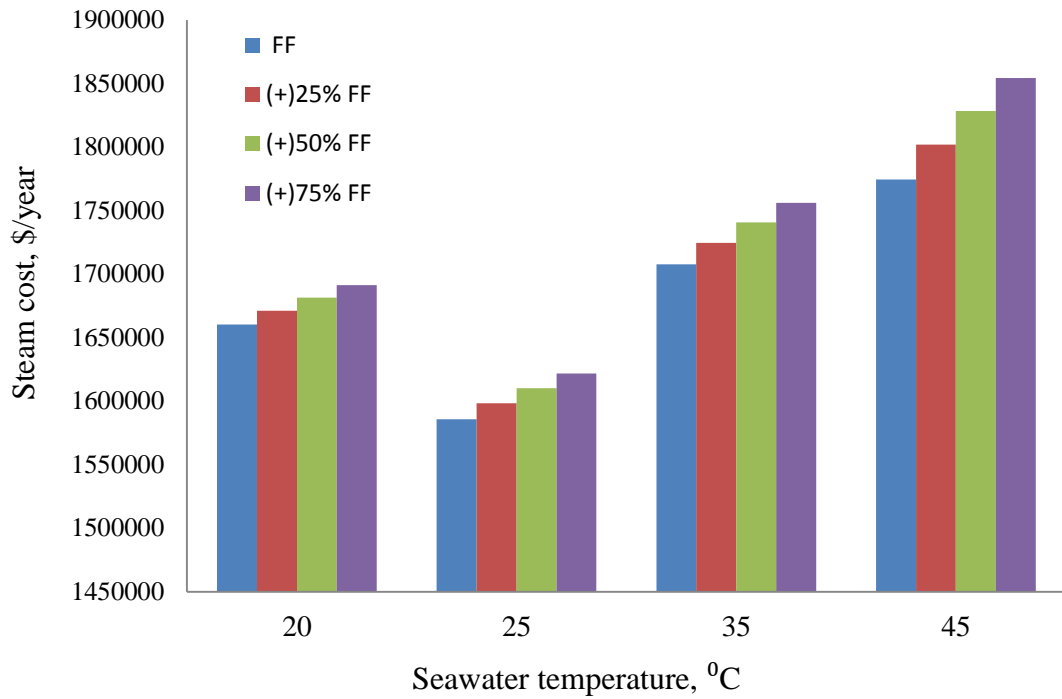


Figure 5.7 Effect of % increasing in fouling factor on steam cost at different seawater temperature

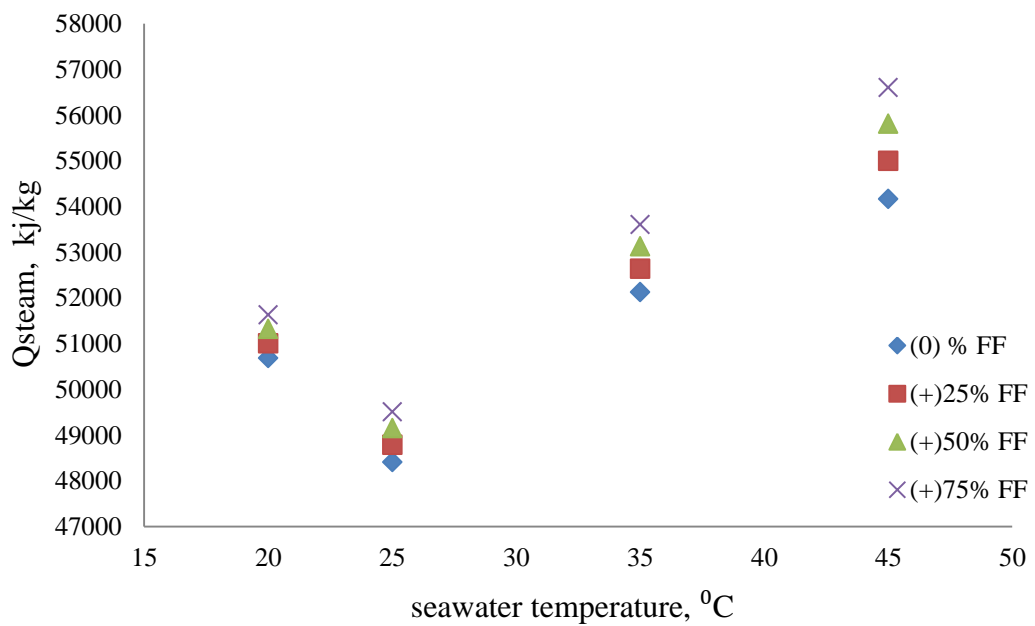


Figure 5.8 Effect of % increasing in fouling factor on Q steam at different seawater temperature

The optimal results of the annual operating cost (TOC), steam flowrate ( $W_{\text{steam}}$ ), external heat supplied ( $Q_{\text{steam}}$ ), steam temperature ( $T_{\text{steam}}$ ), recycle flowrate (R) and rejected seawater flowrate ( $C_W$ ) for case 2 are shown in Table 5.3. The TOC decreases with decreasing in both the  $\text{CaCO}_3$  fouling resistance and seawater temperature from (25-45 °C) as shown in Figure 5.9. The decreasing percentage in the TOC was 3.53% at 25% fouling resistance and 2.8 % at (75%) fouling resistance for the same seawater change. Furthermore, the highest value of TOC is when the seawater temperature is 45 °C and fouling resistance increased by 75%. However, the lowest value of the TOC is obtained when the seawater temperature 25 °C and fouling resistance increased by 25%.

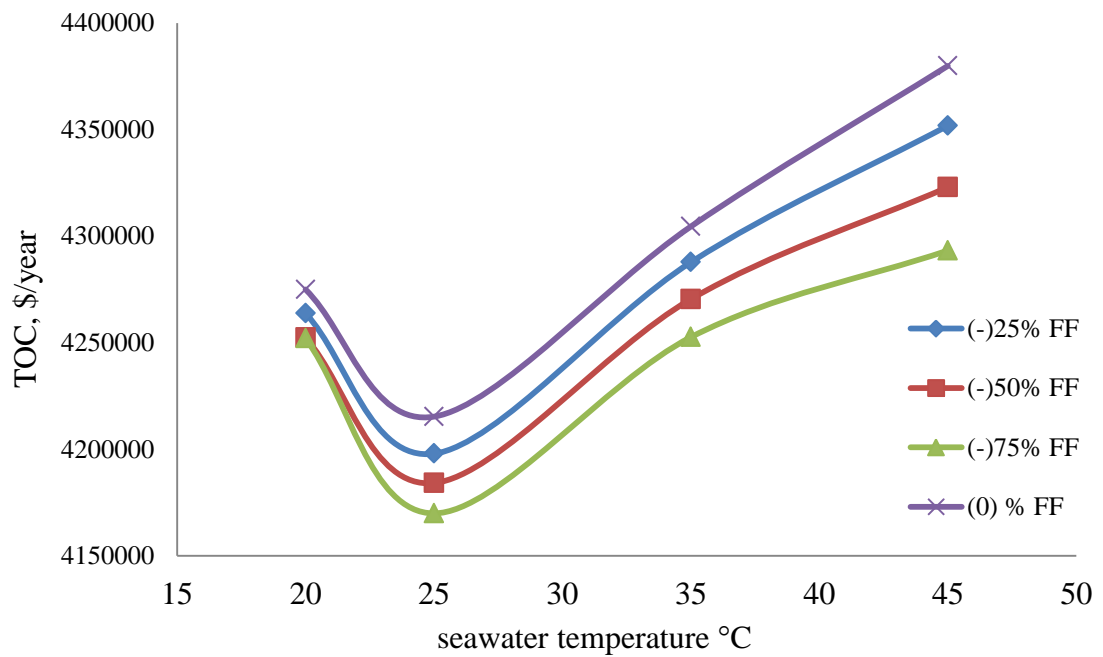


Figure 5.9 Effect of % decreasing in fouling factor on TOC at different seawater temperature



Table 5.3 Summary of optimisation results (Case 2)

Tseawater, °C	R, kg/sec	C <sub>w</sub> , kg/sec	Q <sub>steam</sub> , kJ/kg	W <sub>R</sub> , kg/hr	T <sub>steam</sub> ,	W <sub>steam</sub>	TOC, \$/y
CaCO <sub>3</sub> fouling resistance (R <sub>f</sub> ) decreased by 25% FF							
20	433.19	1693.33	50341.93	1878.75	93	22.13	4263869
25	572.56	1693.33	47946.65	2018.12	93	21.07	4197960
35	896.23	1693.33	51602.48	2341.79	93	22.68	4287765
45	1472.65	1693.33	53310.29	2918.21	93	23.43	4351799
CaCO <sub>3</sub> fouling resistance (R <sub>f</sub> ) decreased by 50% FF							
20	420.88	1693.33	49990.12	1866.44	93	21.97	4252368
25	557.92	1693.33	47538.61	2003.48	93	20.89	4184195
35	875.32	1693.33	51057.22	2320.88	93	22.44	4270479
45	1434.29	1693.33	52429.52	2879.85	93	23.04	4322945
CaCO <sub>3</sub> fouling resistance (R <sub>f</sub> ) decreased by 75% FF							
20	414.95	1693.33	49816.01	1860.51	93	21.89	4252052
25	542.99	1693.33	48116.55	1988.55	93	20.71	4169956
35	854.04	1693.33	50493.09	2299.60	93	22.19	4252629
45	1395.60	1693.33	51523.6	2841.16	93	22.64	4293265

The same results obtained in Case 1, the steam temperature hits the lower values while the seawater rejected (C<sub>w</sub>) flowrate hits the upper bound for the seawater temperature various from 20 to 45 °C and decreasing in fouling resistance. On the other hand, the brine recycle flow rate (R) and brine flowrate enters the recovery stages (W<sub>R</sub>) varied slightly for the same changes in the seawater temperature and fouling resistance. As shown in Figures 5.10 and 5.11, for seawater temperature (25-45 °C), the steam cost decreases as CaCO<sub>3</sub> fouling resistance decreases. This decreasing due to the decreases in steam consumption (W<sub>steam</sub>) and the external heat supplied Q<sub>steam</sub>.

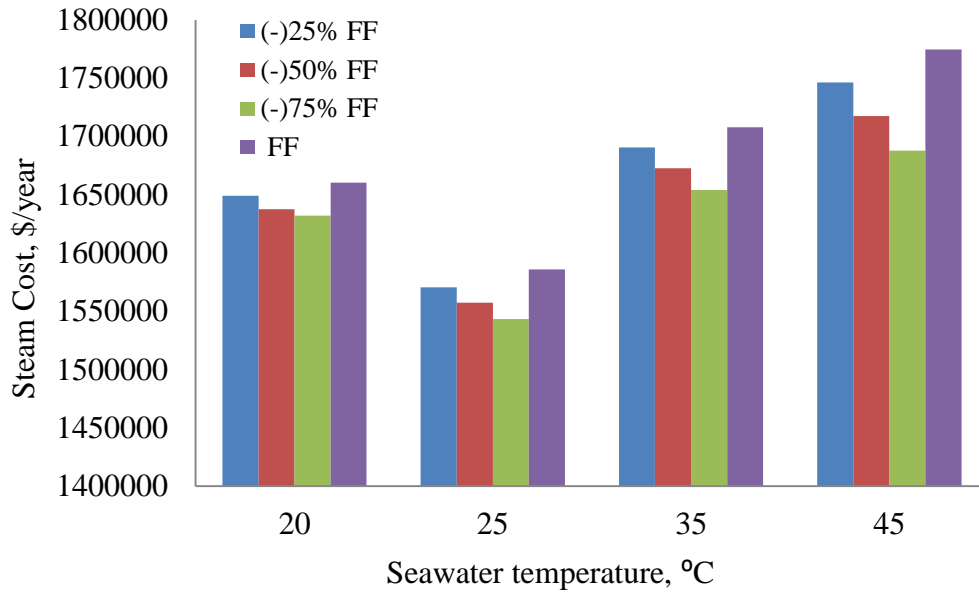


Figure 5.10 Effect of % decreasing in fouling factor on steam cost at different seawater temperature

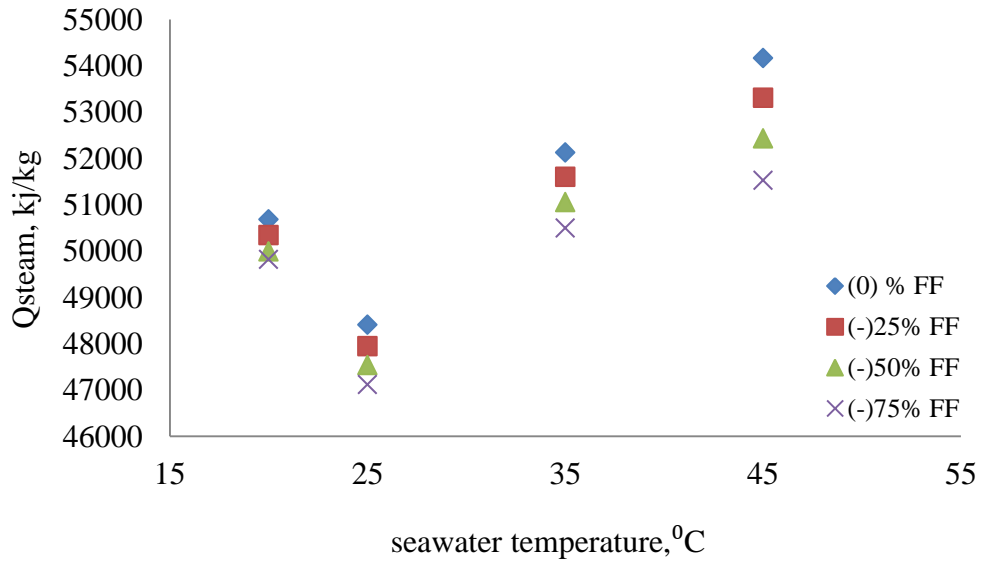


Figure 5.11 Effect of % decreasing in fouling factor on Q steam at different seawater temperature

## 5.6 Conclusions

In this work, the steady state  $\text{CaCO}_3$  fouling resistance model has been developed and implemented in full MSF process model using gPROMS software. The  $\text{CaCO}_3$  fouling resistance ( $R_f$ ) were investigated at different seawater temperature ( $T_{\text{seawater}}$ ) and top brine temperature (TBT). The results show increasing in the  $\text{CaCO}_3$  fouling resistance with increased seawater temperature and top brine temperature by 8 % and 50 % respectively. In addition, the MSF operating parameters such as steam temperature, recycle brine and seawater rejected flowrate are optimised while minimising the total operating cost of the process for fixed water demand throughout the year by assuming increasing and decreasing in the  $\text{CaCO}_3$  fouling resistance ( $R_f$ ). The results clearly show that for any seawater temperature the total annual operating cost increases as fouling resistance increases. On the other hand, as the fouling resistance decrease the total operating cost decrease. Furthermore, the steam cost show increasing trend as the fouling resistance increase due to the increase in steam consumption. Also the optimisation results show increasing in the brine recycle flow rate ranged from (24-39%) while the steam temperature and rejected seawater flow rate remains constant for different seawater temperature.

## Chapter 6

### **Flexible Design and Operation of MSF Desalination Process:**

### **Coping with Different Freshwater Demand**

#### **6.1 Introduction**

Optimisation of operating variables in MSF desalination plant is useful as it leads to an increase in distillate production rates and lower operating costs. The top brine temperature, brine recirculation rate, intake flow rate, and steam condition and flow rate can be manipulated to better plant performance and achieve an incremental increase in plant capacity. In addition, the selection of optimum design and operation of MSF desalination is aimed at reducing energy and operation costs such as steam, electric power, anti-scale, etc.

Recent studies (Tanvir and Mujtaba, 2007) show that for a fixed design and operating conditions the production of fresh water from MSF process can significantly vary with seasonal temperature variation of seawater producing more water in winter than in summer. However, the fresh water demand is continuously increasing and of course there is more demand in summer than in winter. To supply fresh water meeting a fixed demand, the operation of MSF process has to be adjusted with the variation of seawater temperature to reduce the energy and operation cost such as steam and antiscaling (Tanvir and Mujtaba, 2008; Hawaidi and Mujtaba, 2010) . However, the seawater temperature varies during the day (Yasunaga et al., 2008). More important, the freshwater demand subject to variation during a day and throughout the year (Alvisi et al., 2007). These variations in the seawater temperature and freshwater demand will affect the rate of production of freshwater using MSF process during a day and throughout the year.

Therefore, an optimal design and operation of MSF processes should be performed to coping these variations. Most recently, (Hawaidi and Mujtaba, 2011) provided a study on the design and operation of the MSF process with variable fouling resistance in the brine heater and variable seawater temperature and freshwater demand during a day and throughout the year. However, the dynamic variation in fresh water demand during the week days is not the same. Herrera et al., (2010) showed a variation in the freshwater demand in the working days which is different than during weekends. More important, as described in chapter 5 the seawater temperature has an effect on the calcium carbonate fouling resistance and consequence on the total operating cost. Therefore, the variation in the fouling resistance as function of cooling seawater temperature ( $T_{Fj}$ ) in the heat recovery section, heat rejection section and brine heater developed in chapter 5 is considered in this chapter. So, to avoid dynamic changes in operating conditions of the MSF process due to dynamic variation in freshwater demand throughout the day, the dynamic optimisation of design and operating parameters of MSF desalination process is considered.

In this chapter, an intermediate storage tank between the plant and the client is considered as shown in Figure 6.1 to provide additional flexibility in operation and maintenance of the MSF process throughout the day. Also, a simple polynomial based dynamic seawater temperature and freshwater demand correlations based on working day and weekends are developed based on actual data. These correlations with a dynamic model for the storage tank and the  $\text{CaCO}_3$  fouling resistance model developed in chapter 5 are implemented in the full steady state MSF mathematical model developed in chapter 4 using gPROMS. For different number of flash stages, operating parameters such as seawater rejected flow rate and brine recycle flow rate are optimised, while the total annual operating cost of the MSF process is selected to minimise.

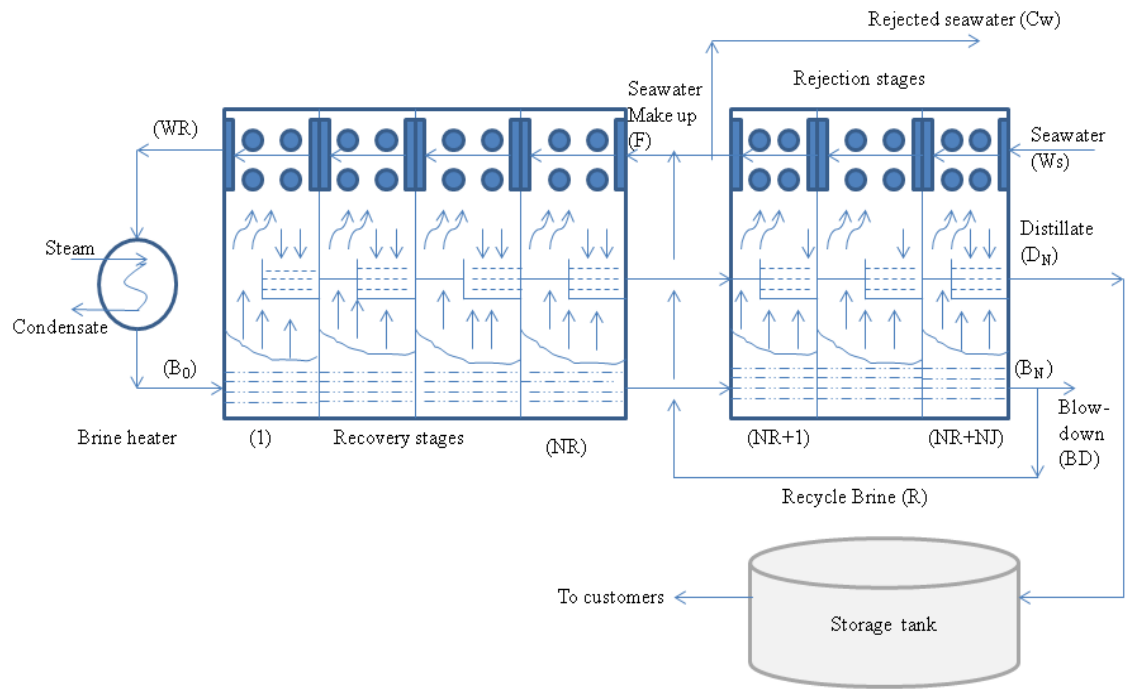


Figure 6.1 MSF desalination process with storage tank

## 6.2 Dynamic Freshwater Demand

### 6.2.1 Dynamic Freshwater Demand during Weekends

Figure 6.2 shows the average freshwater consumption for the 24 hrs of a weekend (Herrera et al 2010). The average consumption slope down from 0.00 to 6.00 and grows up from 6:00 am till 12:00 am. From 14:00 the curve goes down till 24:00. In addition and by using linear regression analysis, the following polynomial relationship is obtained with a correlation coefficient greater than 90%.

$$\left\{ \begin{array}{l} \text{Demand}_1 = 16.46 + 1.71 \times t - 2.15 \times t^2 + 0.35 \times t^3 - 0.014 \times t^4 \quad 0 \leq t \leq 13 \\ \text{Demand}_2 = -1351.77 + 315.8 \times t - 26.3 \times t^2 + 0.95 \times t^3 - 0.012 \times t^4 \quad 13 \leq t \leq 24 \end{array} \right\} \quad (6.1)$$

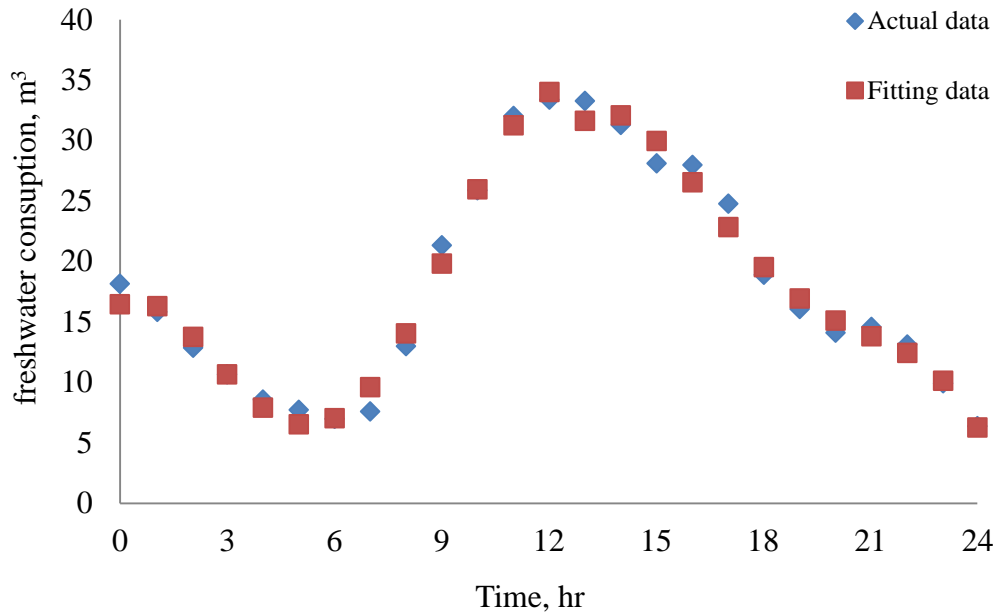


Figure 6.2 Fresh water consumption profile on weekend (Saturday) (Herrera et al 2010).

### 6.2.2 Dynamic Freshwater Demand during Working Days

The dynamic variation of freshwater demand on working day (Monday) (Herrera et al., 2010) is shown in Figure 6.3. The consumption goes down from 0.00 to 6.00 and then from 6:00 am till 10:00 am, the average consumption grows up the same as in the holiday profile. Then the consumption goes down again from 10.00 to 12.00 and goes up again during lunch time from 12:00 till 15:00. In the afternoon and till 18:00, the curve first go decreasing and then increasing from 18.00 to 24.00. As seen from Figure 6.3, there is fluctuation in the freshwater demand profile in working days comparing to the weekend days (Figure 6.2). Furthermore, the following polynomial relationship is obtained using linear regression analysis as shown in Figure 6.3 with a correlation coefficient greater than 90%.

$$\left\{ \begin{array}{l} \text{Demand}_1=13.84-3.81\times t+0.84\times t^2-0.17\times t^3+0.017\times t^4 \quad 0 \leq t \leq 8 \\ \text{Demand}_2=-400.41+155.89\times t-21.03\times t^2+1.21\times t^3-0.025\times t^4 \quad 8 \leq t \leq 16 \\ \text{Demand}_3=5392.7-1012.25\times t+70.75\times t^2-2.1836\times t^3+0.0252\times t^4 \quad 16 \leq t \leq 24 \end{array} \right\} (6.2)$$

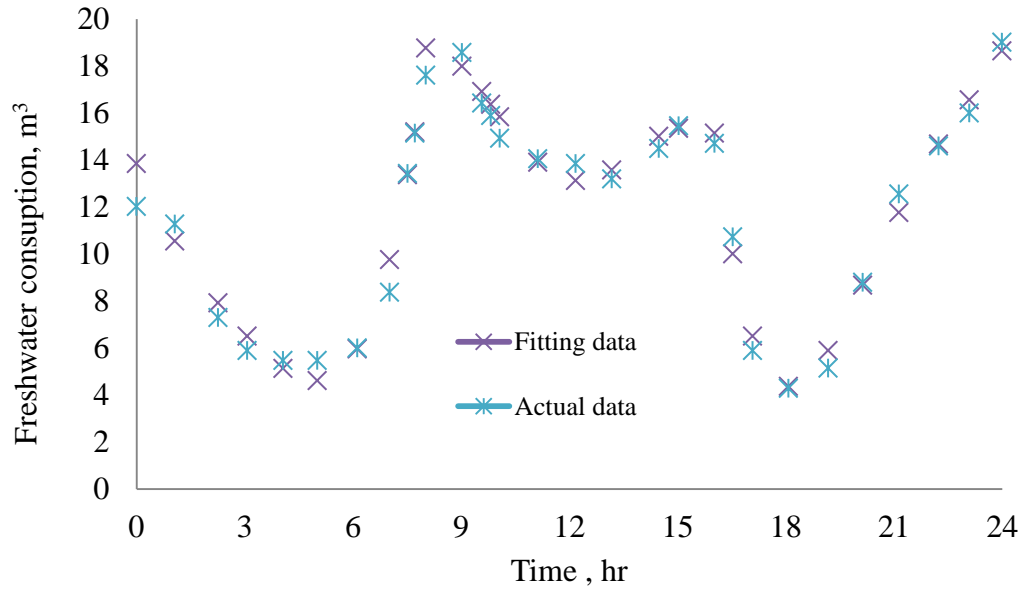


Figure 6.3 Fresh water consumption profile on working day (Monday) (Herrera et al 2010)

### 6.3 Seawater Temperature Dynamic Profile

The variation in seawater temperature throughout the day is shown in Figure 6.4 (Yasunaga et al 2008). By using regression analysis, the relationship between the seawater temperature and time (hr) can be represented by Equation 6.3. The temperature at  $t = 0$  represents the seawater temperature at night-time.

$$\left\{ \begin{array}{l} T_{\text{seawater}1}=-0.0001\times t^5+0.0029\times t^4-0.0259\times t^3+0.0913\times t^2-0.116\times t+28.84 \quad 0 \leq t \leq 13 \\ T_{\text{seawater}2}=-0.0009\times t^4+0.0649\times t^3-1.73\times t^2+20.14\times t-55 \quad 13 \leq t \leq 24 \end{array} \right\} (6.3)$$



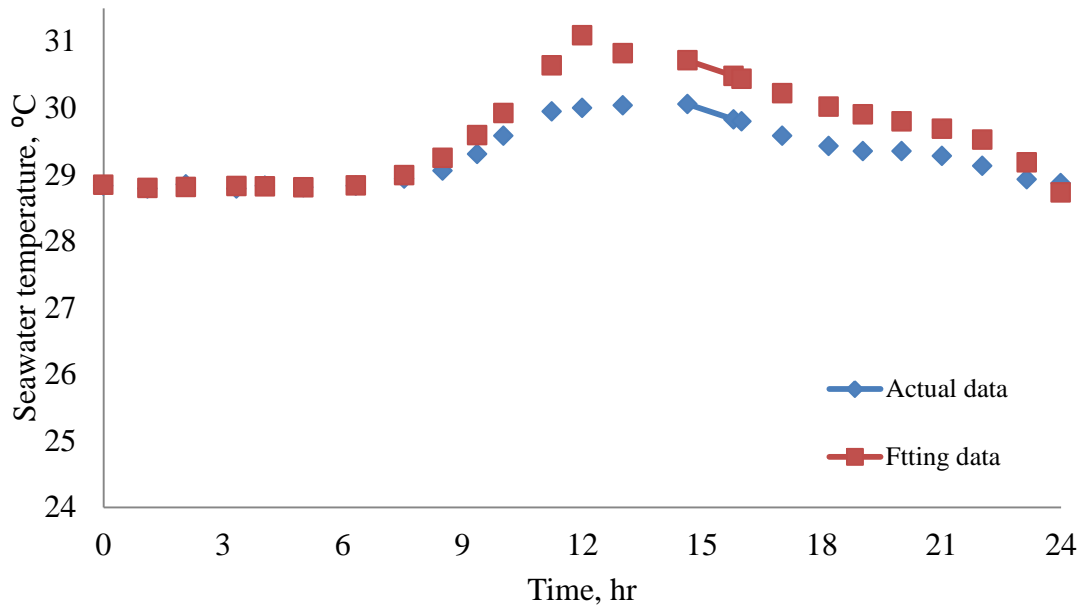


Figure 6.4 Seawater temperature profile during the day and night (Yasunaga et al 2008)

## 6.4 Storage Tank and Level Control Models

### 6.4.1 Storage Tank Model

The dynamic mathematical model of the tank process shown in Figure 6.5 is as the follows:

Mass balance

$$\frac{dM}{dt} = \text{Flow}_{\text{in}} - \text{Flow}_{\text{out}}$$

Relation between liquid level and holdup:

$$M = \rho A_s h$$

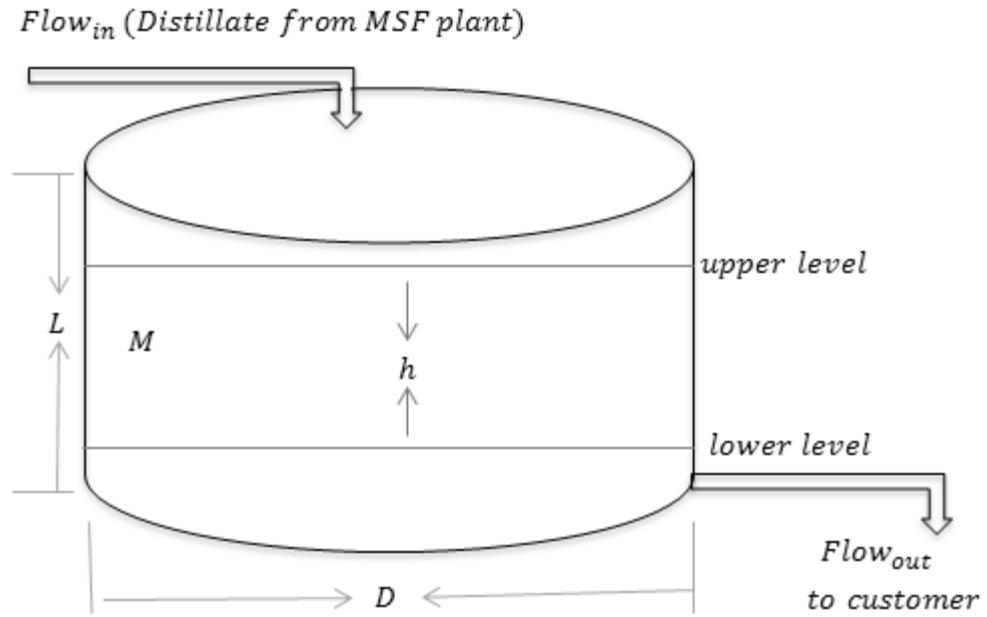


Figure 6.5 Storage tank

#### 6.4.2 Storage Tank Level Control Model

The storage tank described above is assumed to operate without any control on the level( $h$ ), therefore and during the MSF operation process, the tank level goes above the maximum level ( $h_{\max}$ ) or below the minimum level ( $h_{\min}$ ) as shown in Figure 6.6 (a). At any time, this violation ( $V_1, V_2$ ) of safe operation can be defined as (Hawaidi and Mujtaba, 2011):

$$V_1 = \begin{cases} (h(t) - h_{\max})^2 & \text{if } h > h_{\max} \\ 0 & \text{if } h < h_{\max} \end{cases} \quad (6.4)$$

and

$$V_2 = \begin{cases} (h(t) - h_{\min})^2 & \text{if } h > h_{\min} \\ 0 & \text{if } h < h_{\min} \end{cases} \quad (6.5)$$

A typical plot of  $V_1$  and  $V_2$  versus time  $t$  is shown in Figure 6.6 (b). The total accumulated violation for the entire period can be written using

$$V_t = \int_{t=0}^{t_f} (V_1(t) + V_2(t)) dt \quad (6.6)$$

Therefore,

$$\frac{dV_t}{dt} = (V_1(t) + V_2(t)) = (h(t) - h_{\max})^2 + (h(t) - h_{\min})^2 \quad (6.7)$$

Equation 6.7 is added to the overall process model equations presented in chapter 4.

Also the following additional terminal constraint is added in the optimisation problem formulations.

$$0 \leq V_T(t_f) \leq \varepsilon \quad (6.8)$$

where  $\varepsilon$  is a very small finite positive number. The above constraint will ensure that  $h(t)$  will always be  $\leq h_{\max}$  and  $\geq h_{\min}$  throughout the 24 hr.

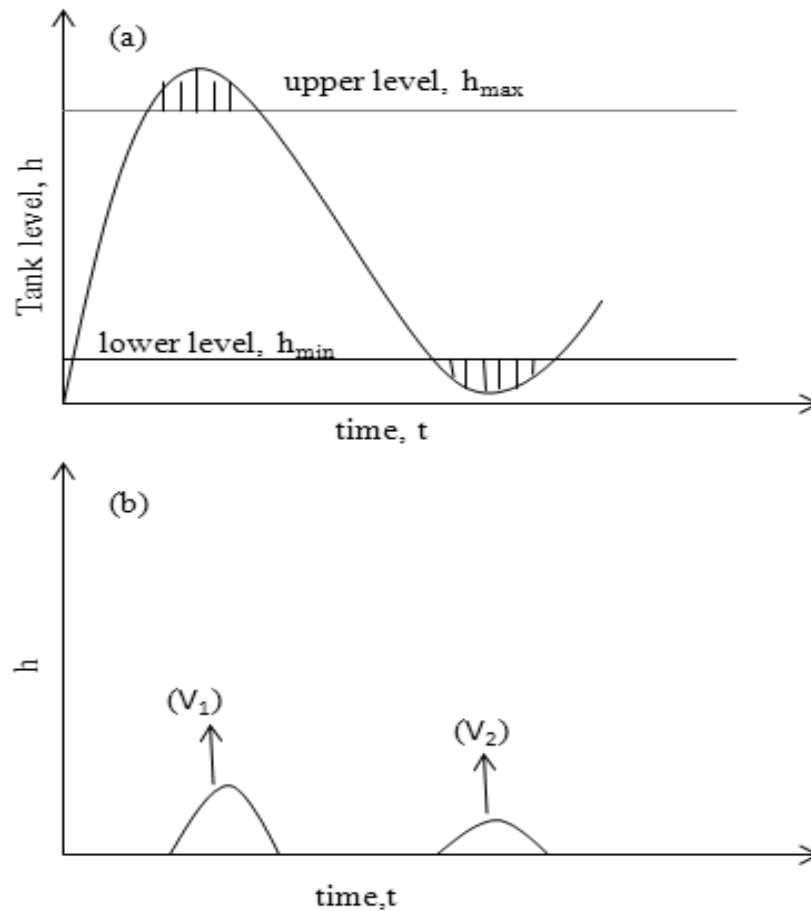


Figure 6.6 (a) Tank level profile and (b) tank level violations during the MSF operation

## **6.5 Optimisation of MSF parameters**

As described in chapter 5 the seawater feed temperature has an effect on the  $\text{CaCO}_3$  fouling resistance and consequent on total operating cost of MSF process for fixed water demand. In addition, the seawater temperature and the freshwater demand are subject to vary during a day. Therefore, to supply freshwater meeting a variation in the seawater temperature and variable freshwater demand throughout the day, the operation parameters of the MSF process has to be adjusted. In this section, the MSF process model developed in chapter 4 and the  $\text{CaCO}_3$  fouling resistance model coupled with the storage tank model developed in this chapter has been used to adequate the variations in the seawater temperature and freshwater demand during a day. For different number of flash stages, operating parameters such as seawater rejected flow rate and brine recycle flow rate are optimised, while the total annual operating cost of the MSF process is selected to minimise using gPROMS models builder 3.0.3.

### **6.5.1 Optimisation Problem Formulation**

The optimisation problem is described as:

Given: Design specifications of each stage, fixed amount of seawater flow, heat exchanger areas in stages, variable seawater temperature, steam temperature, freshwater demand profile, and volume of the storage tank.

Optimise: Recycle brine flow rate, rejected seawater flow rate, number of stage at different time intervals within 24 hrs.

To minimise: The total operation cost (TOC).

The optimisation problem (OP) can be described mathematically by:



salinity 5.7 wt%. The intermediate storage tank has diameter ( $D=18\text{m}$ ), and aspect ratio:  $=L/D=0.5$ .

Table 6.1 Constant parameters and input data

	$A_j/A_H$	$D_j^i/D_H^i$	$D_j^o/D_H^o$	$w_j/L_j/L_H$	$H_j$
Brine heater	3530	0.022	0.0244	12.2	
Recovery stage	3995	0.022	0.0244	12.2	0.457
Rejection stage	3530	0.024	0.0254	10.7	0.457
$W_S$ (kg/s)	$T_{\text{steam}}(^{\circ}\text{C})$	$T_{\text{seawater}}(^{\circ}\text{C})$	$C_S$ (wt%)	$R$ (kg/s)	$C_w$ (kg/s)
31416.67	97	35	5.7	1763.89	1561.11

### 6.6.1 Case Study 1

In this case, the freshwater demand correlation developed in section 6.2.1 (Equation 6.1) for a weekend and the seawater temperature correlation developed in section 6.3 (Equation 6.3) has been considered. In addition, in this section one interval within 24 hrs is considered within which  $R$  and  $C_w$  are optimised with interval length.

The total operating cost on daily basis and the other plant cost (steam cost ( $C_1$ ), chemical cost ( $C_2$ ), power cost ( $C_3$ ), spare cost ( $C_4$ ) and labor cost ( $C_5$ )) for three different number of stages (16, 17 and 18) are listed in Table 6.2. The total operating cost (TOC) decreases as the number of stage increases. This is due to higher increase in the steam consumption compared and the higher value of  $C_w$  as shown in Figure 6.7. There is a small change in the  $C_2$ ,  $C_3$ ,  $C_4$  and  $C_5$  while a change in the  $C_1$  is relatively high.

Table 6.2 Summary of optimization results (case 1)

N	C1, \$/d	C2, \$/d	C3, \$/d	C4, \$/d	C5, \$/d	TOM, \$/d
16	46184583	37498047	17220256	12954688	15798400	129655973
17	44026301	37597628	17358817	13058927	15925521	127967194
18	41403746	37222956	17250642	12977547	15826277	124681167

Figures 6.7 and 6.8 show the optimum results of recycle flow rate (R) and seawater rejected flow rate ( $C_w$ ) throughout the day for 24 hrs at different number of stages. The plant operates at the high flowrate of rejected seawater (Figure 6.7 and 6.9) until the 8:00 where the water demand is low (Figure 6.10) and the tank level increased gradually during this time as shown in Figures 6.11. In contrast, the brine recycle flow rate remaining at the minimum level in this period (Figure 6.8).

For the time interval between 10:00 and 16:00 where the freshwater consumption is high, optimum results show slightly decreasing in the rejected seawater flowrate and tank level while the plant appears increase in the freshwater product and brine recycle flow rate to replace the decreasing in the tank level as shown in Figure 6.11. Furthermore and for the remaining time interval after 16:00 till 24:00, there is decreasing in the freshwater demand while the plant production and the rejected seawater flowrate increased and consequently the tank level goes up.

However, the intermediate storage tank adds the operational flexibility, and maintenance could be carried out without interrupting the production of water or full plant shut-downs at any time throughout the day by adjusting the number of stage. Note, the optimal results in this case are almost the same for the all number of stage.

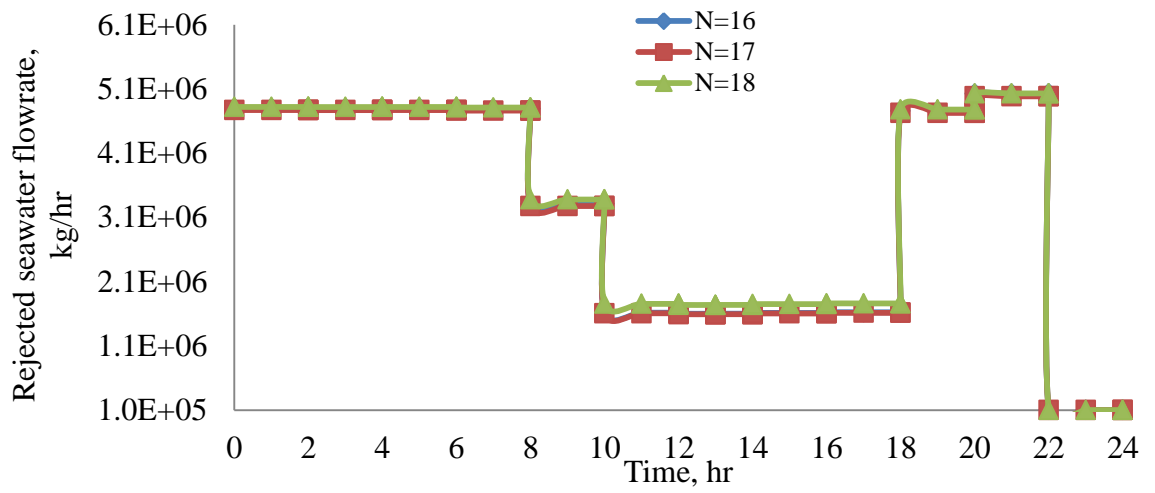


Figure 6.7 Optimum rejected seawater flow rate throughout profile (case 1)

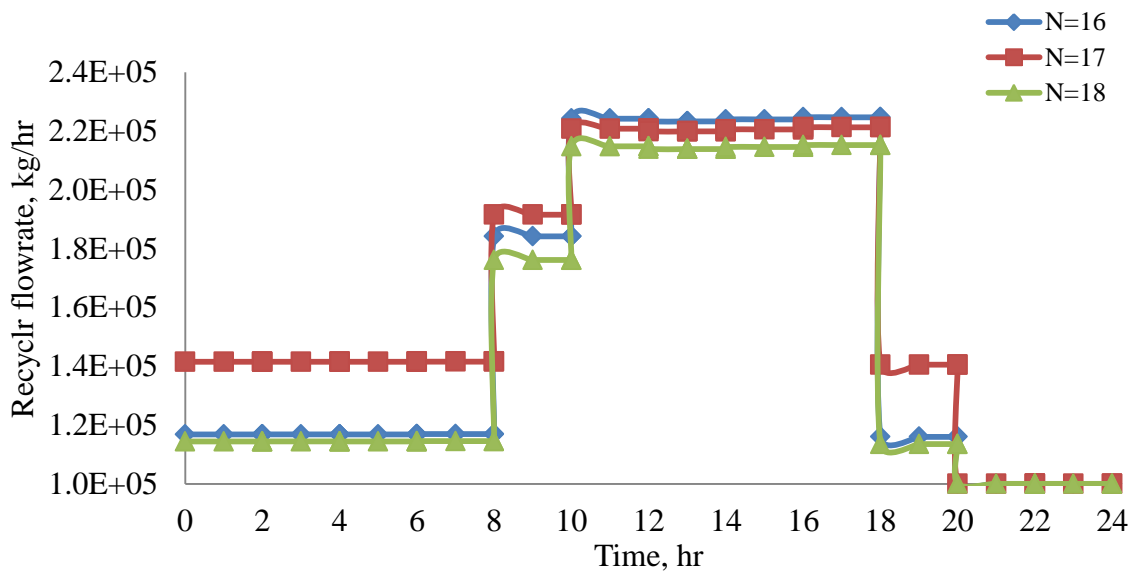


Figure 6.8 Optimum brine recycle flow rate throughout profile (case 1)



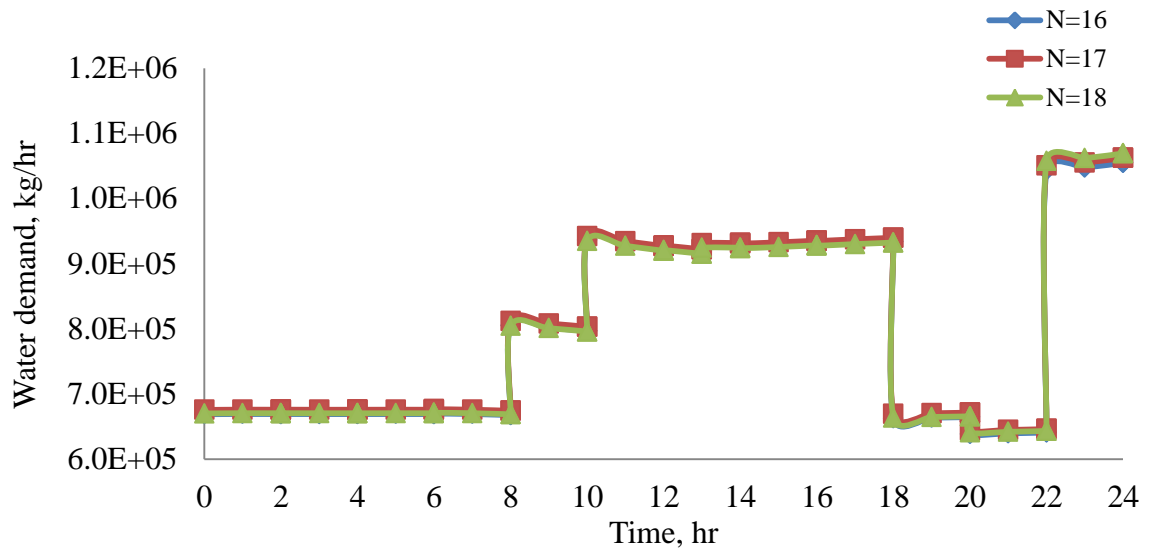


Figure 6.9 Fresh water plant production flow rate profile (case 1)

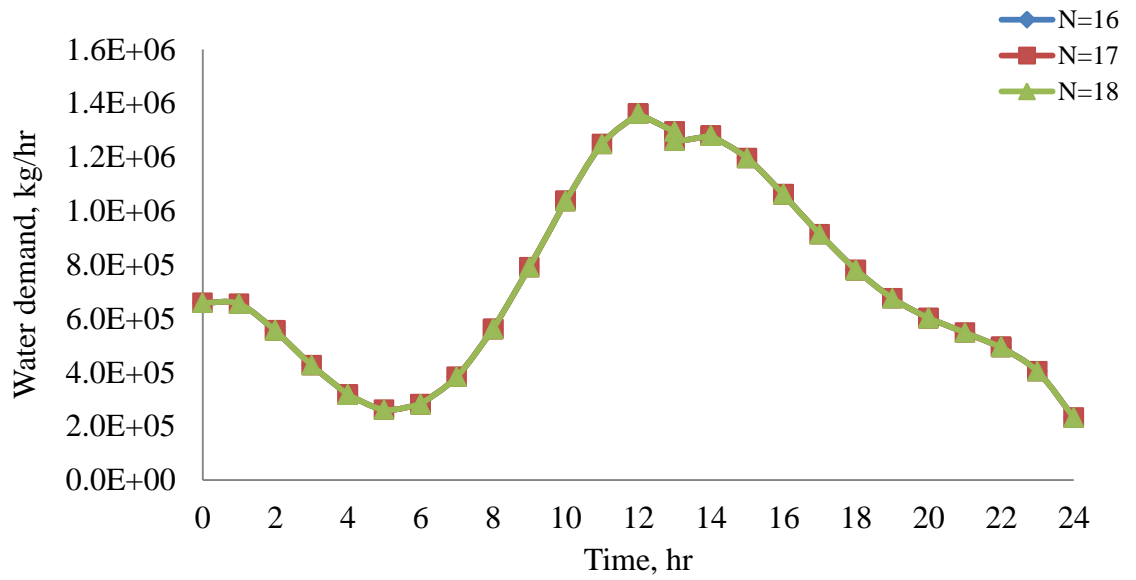


Figure 6.10 Fresh water demand profile (case 1)

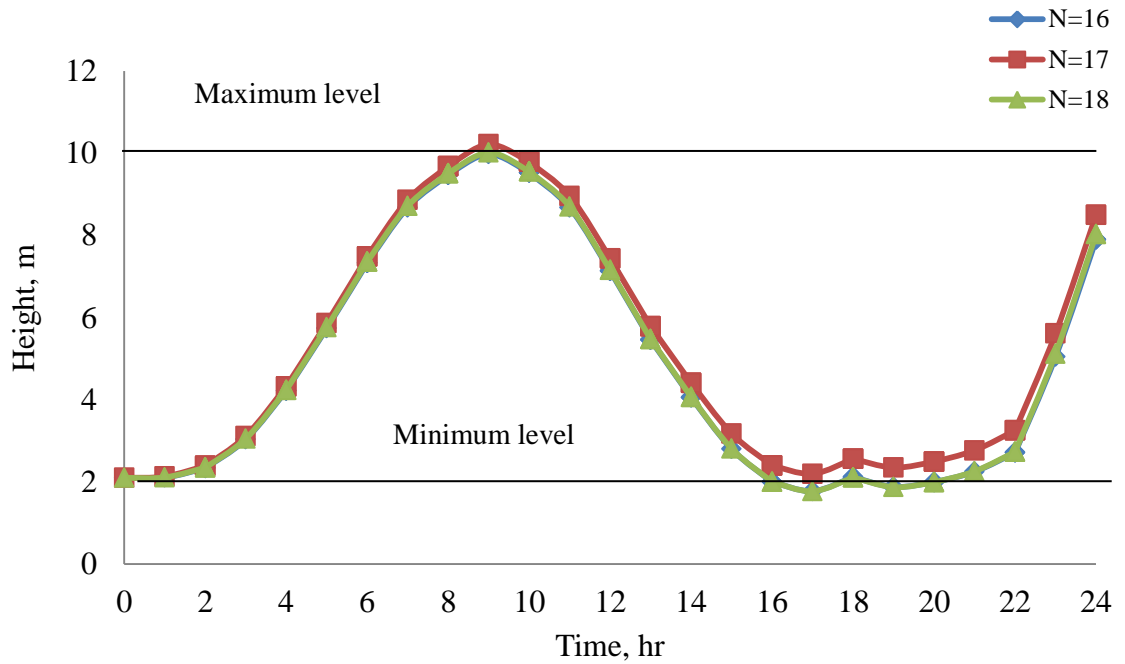


Figure 6.11 Storage tank level profiles (case 1)

### 6.6.2 Case Study 2

The dynamic freshwater demand correlation (during working days) (Equation 6.2) and the seawater temperature correlation (Equation 6.3) has been considered in case 2. For three different number of stages ( $N=16, 17$  and  $18$ ), Table 6.3 listed the results of the total operating cost and the other plant cost ( $C_1, C_2, C_3, C_4$  and  $C_5$ ). The total operating cost (TOC) decreases as the number of stage increases (the same results obtained in case 1). The steam cost shows increasing with increased number of stage while the other costs show small changes.

The optimum results of recycle flow rate ( $R$ ) and seawater rejected flow rate ( $C_w$ ) throughout the day for 24 hr at different number of stages are shown in Figures 6.12 and 6.13 respectively. For the time interval between, 0:00 till 8:00, the freshwater consumption is low (Figure 6.16) the plant operates at the high flow rate of rejected seawater flow rate until the 8:00 (Figure 6.12 and 6.14). The tank level increased gradually during this time as shown in Figure. 6.15.

Table 6.3 Summary of optimisation results (case 2)

N	C1,\$/d	C2,\$/d	C3,\$/d	C4,\$/d	C5,\$/d	TOM,\$/d
16	44798724	34887280	16298856	12261525	14953079	123199465
17	44354229	35061974	16915867	12725698	15519144	122740574
18	41848980	34891011	16897123	12711597	15501948	121850659

In contrast, the brine recycle flow rate remaining constant at the minimum level during the same time interval (Figure 6.13). In addition, for the time interval between 10:00 and 16:00 where the freshwater consumption is high, optimum results show slightly decreasing in the rejected seawater flow rate and increasing in the brine recycle flow rate for all stages. The tank level is goes down during this time interval while the freshwater production is going up as shown in Figure 6.14 to makeup the decreasing in the tank level as shown in Figure 6.15.

For the time between 16:00 and 24:00, the optimum  $C_w$  flow rate hit the upper value up to hour 22:00 while the recycle flow rate (R) remaining at the lower value for all number of stages. Furthermore there is decreasing in plant production and consequently the tank level goes up. The optimal results show that, the plant should operate at high seawater rejected flowrate and minimum brine recycle flowrate to overcome the variation in the freshwater demand during the day.

The same as in case 1, the intermediate storage tank adds the operational flexibility, and maintenance could be carried out without interrupting the production of water or full plant shut-downs at any time throughout the day by adjusting the number of stage. Note,

again here the optimal results in this case are almost the same irrespective of the number of stages.

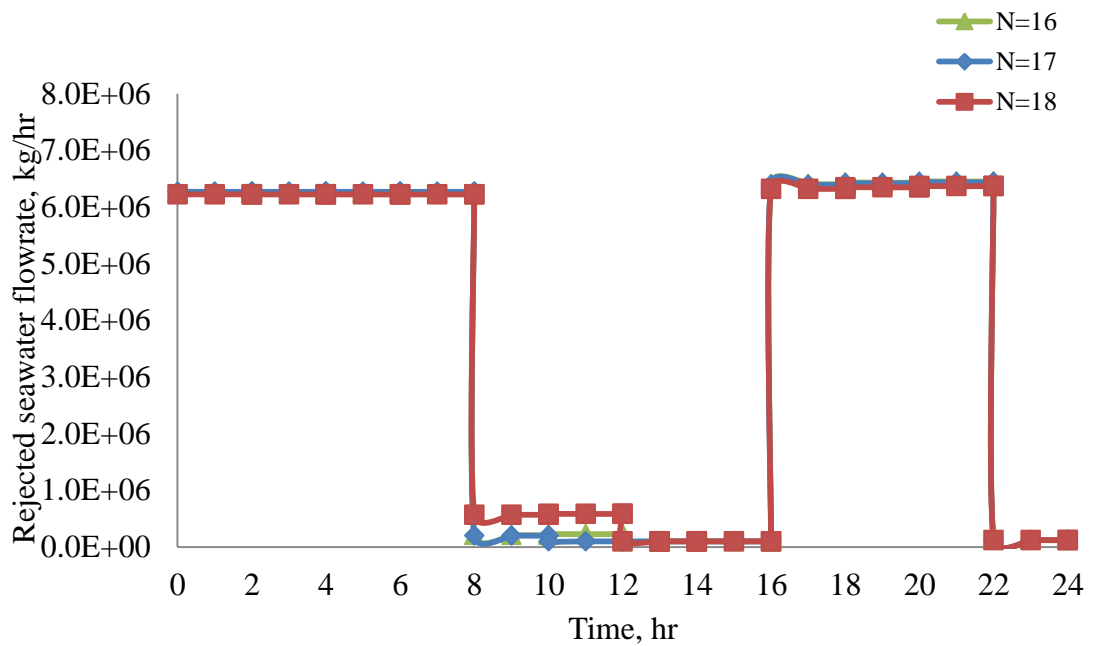


Figure 6.12 Optimum rejected seawater ( $C_w$ ) flow rate throughout profile (case 2)

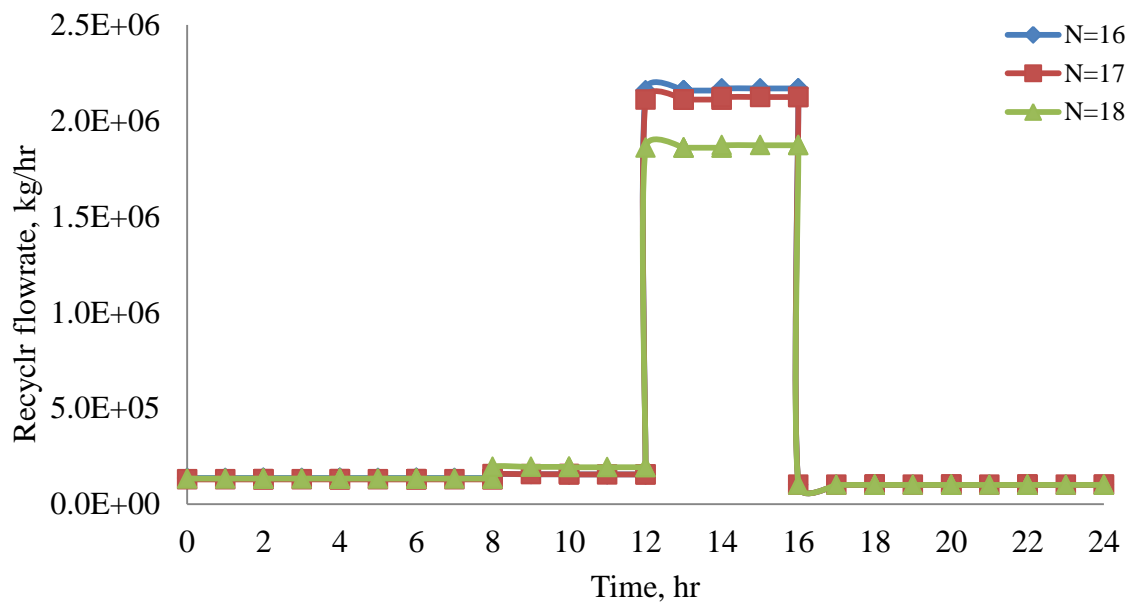


Figure 6.13 Optimum brine recycle (R) flow rate throughout profile (case 2)

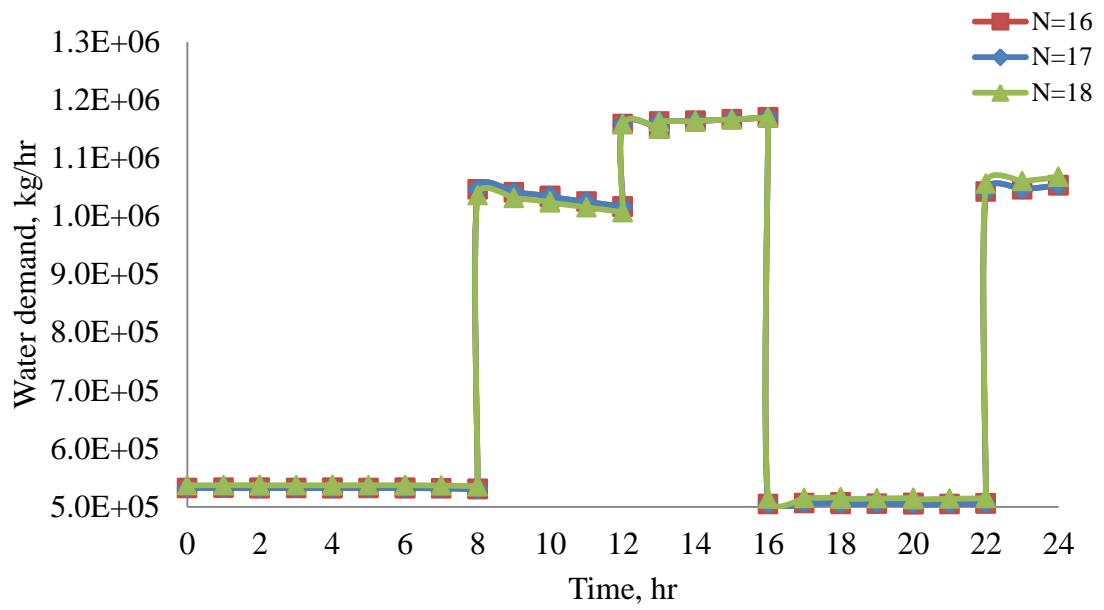


Figure 6.14 Fresh water production profile (case 2)

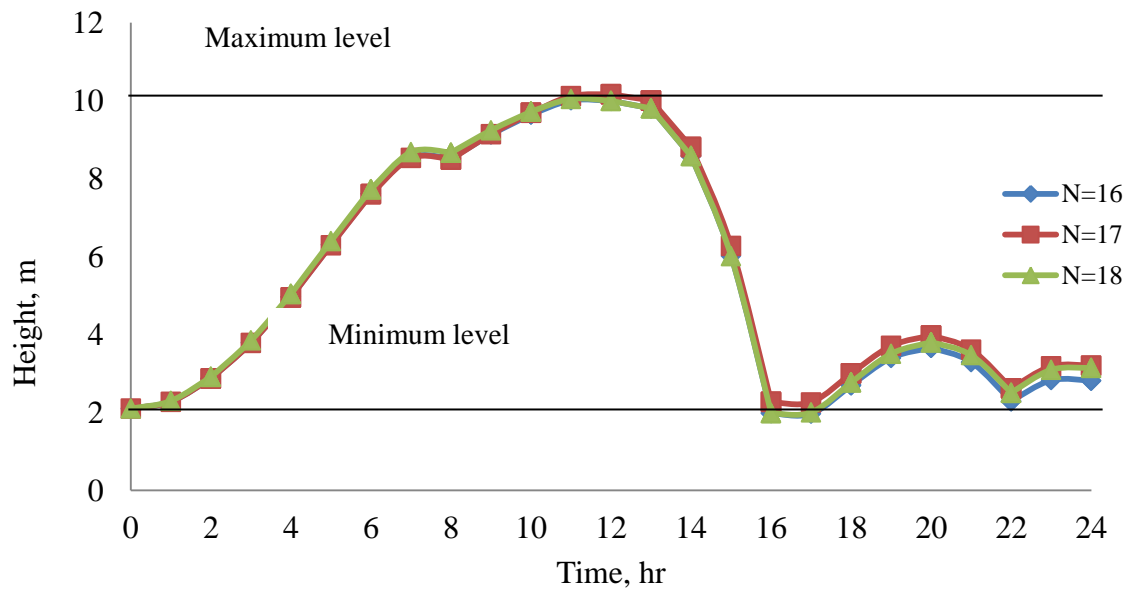


Figure 6. 15 Storage tank level profiles (case 2)

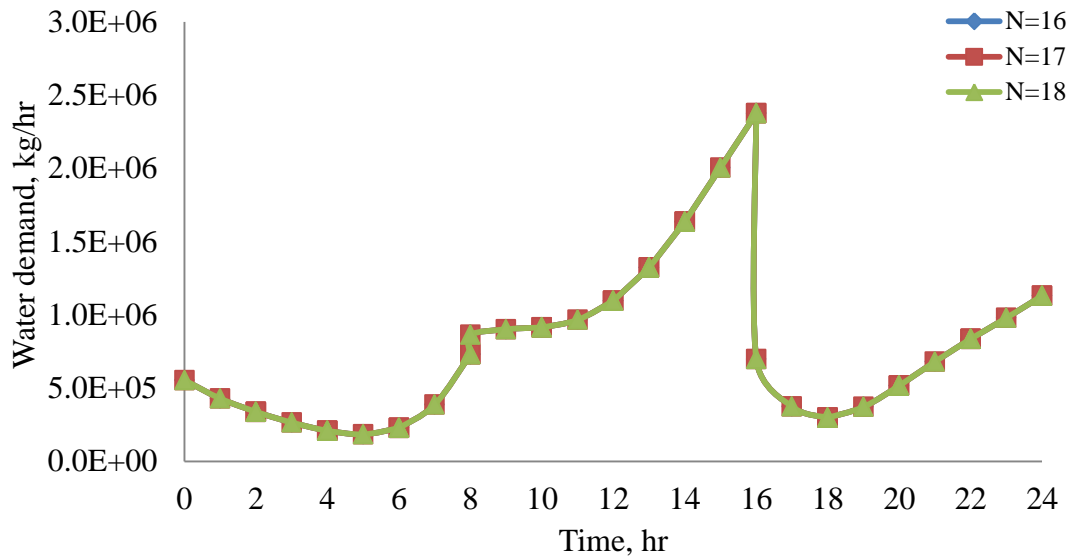


Figure 6.16 Fresh water demand profile (case 2)

## 6.7 Conclusion

In this work, for a given design, an optimal operation scheme for MSF desalination process dependent on variable seawater temperature is considered to cope with different freshwater demand dynamic profiles. An intermediate storage tank is considered between the MSF process and the customer to add flexibility in meeting the customer demand. A dynamic model for the storage tank level has been implemented with steady state MSF process model using gPROMS 3.0.3 model builder. Two cases of dynamic fresh water demand have been included in this study. Case 1 considers the fresh water demand during weekend days while the fresh water demand during working days has been considered in case 2.

For several process configuration (the design), some of the operation parameters of the MSF process such as seawater recycle flow rate and brine recycle flow rate at discrete time interval are optimised, while minimised the total operating costs. For both cases, the optimisation results show increase in the total operating cost with decrease the number of stage of MSF. During the low consumption of freshwater for cases, there is

increasing in the tank level and plant production consequently the plant operate at maximum value of seawater rejected flowrate and at minimum value of brine recycle flowrate. On the other hand, optimum results decreases in the plant production and tank level when there is increase in the freshwater consumption and consequently the plant operate at minimum value of seawater rejected flowrate and slightly increase in recycle brine flowrate. The results clearly also show that the advantage of using the intermediate storage tank adds flexible scheduling in the MSF plant design and operation parameters to meet the variation in freshwater demand with varying seawater temperatures without interrupting or fully shutting down the plant at any time during the day by adjusting the number of stage.

## Chapter 7

# Modelling and Simulation the Effect of Non-condensable Gases on the MSF Process

### 7.1 Introduction

In the thermal desalination plants, the release of non-condensable gases from an evaporating solution and the in-leakage of air affect the performance, the material and energy balances and material life-time of the desalination distillers. However, many models of MSF desalination process did not consider any effect of non-condensable gases on the overall heat transfer coefficient and consequent on the plant performance. These assumptions cause a larger discrepancy between the results obtained through simulation and those of the actual plant data.

Here, the effect of NGC on the overall heat transfer coefficient is studied first. The MSF process model developed in chapter 4 is refined with the new correlation for the overall heat transfer co-efficient featuring the effect of NCG. The model is then used to study the effect of the presence of NCG on the operation parameters of MSF processes for different plant configurations and with fixed freshwater demand.

### 7.2 Modelling of MSF Process Model: Impact of NCG

In the past, there are many works which has been done on the steady state of MSF process modelling and simulation. However there are a very limited number of publications which take into consideration the effect of non-condensable in their steady state model. The presence of non-condensable gases in the flashing chambers of MSF reduces the overall heat transfer coefficient and consequence reduces the performance



and production capacity of MSF process. Although a few researches included the effect of non-condensable gases in their MSF models (El-Dessouky et al., 1995; Alasfour and Abdulrahim, 2009; Alfulaiji, 2011), they only carried out their models with fixed value of non-condensable gases and they did not study the effect of variation of non-condensable gases in the flashing stages on the design and operation parameters of MSF process. In this chapter, the steady state mathematical model which includes the effect of the presence of the non-condensable gases is developed. Furthermore, the effect of variation of non-condensable gases in the flashing stages on the design and operation parameters of MSF process has been studied.

### **7.2.1 Developing MSF Process Model with Effect of NCG**

The MSF process model developed in chapter 4 is used in this section. However, the correlations which have been used to calculate the overall heat transfer coefficient in chapter 4 (Equations 4.37-4.39) which do not include any effect of non-condensable gases are substituted by the correlations reported by (Wangnick, 1995) and El-Dessouky et al. (1995) as described in Equations (7.1-7.7). These correlations take into consideration the effect of the presence of NCG on the overall heat transfer coefficient in the heat recovery section, heat rejection section, and brine heaters. These correlations calculate the inside and outside overall heat transfer coefficients which depend on the fouling factors, flowrate, temperature and physical properties such as thermal conductivity, viscosity, density and specific heat of the condensing vapour and the brine inside the condenser.

### Overall heat transfer coefficient

$$\frac{1}{U_o} = \frac{1}{h_o} + \frac{1}{h_i} + r_t + R_{fi} + R_{fo} \quad (7.1)$$

### Steam Side Heat Transfer Coefficient

$$h_o = 0.725 \left( \frac{K^3 \rho_l (\rho_l - \rho_v) g \rho \lambda_v}{D_j^o \mu \Delta T} \right)^{0.25} C_1 C_2 \quad (7.2)$$

$$C_1 = 1.23795 + .353808 N_1 - .0017035 N_1^2 \quad (7.3)$$

$$C_2 = 1 - 34.313 X_{nc} + 1226.8 X_{nc}^2 - 14923 X_{nc}^3 \quad (7.4)$$

$$N_1 = 0.564 \sqrt{N_t} \quad (7.5)$$

$$N_t = \frac{4W_R}{\pi d_i^2 \rho_f V} \quad (7.6)$$

### Water side heat transfer coefficient

$$h_i = (3293.5 + T(84.24 - 0.1714T) - C_R(8.471 + .1161C_R + .2716T)) \left( \frac{D_j^i}{.017272} \right)^{0.2} \times (0.656V)^{0.8} \left( \frac{D_j^i}{D_j^o} \right) \quad (7.7)$$

The case study described in chapter 4 with the specifications shown in Table 7.1 has been used here. The presence of 0.015wt% concentration of NCG in the heat recovery section, heat rejection section and brine heater is assumed (Genthner et al., 1993) to study the effect of NCG on the simulation results of the MSF process model.

Table 7.1 Constant Parameters and Input Data

	$A_j/A_H$	$D_j^i/D_H^i$	$D_j^o/D_H^o$	$f_j^i/f_H^i$	$w_j/L_j/L_H$	$H_j$
Brine heater	3530	0.022	0.0244	$1.86 \times 10^{-4}$	12.2	
Recovery stage	3995	0.022	0.0244	$1.4 \times 10^{-4}$	12.2	0.457
Rejection stage	3530	0.024	0.0254	$2.33 \times 10^{-5}$	10.7	0.457
(0.015% of NCG)						
$W_S$ (kg/s)	$T_{\text{steam}}(^{\circ}\text{C})$	$T_{\text{seawater}}(^{\circ}\text{C})$	$C_S$ (wt%)	$R$ (kg/s)	$C_w$ (kg/s)	
31416.67	97 <sup>o</sup> C	35 <sup>o</sup> C	5.7	1763.89	1561.11	

The simulation results of MSF process model with the effect of non-condensable gases are presented in Table 7.2. The results including the flowrates of brine and distillate streams and temperature profiles for all stages. The results show increasing in the top brine temperature (TBT), brine temperature ( $T_{Bj}$ ) and distillate ( $T_{Dj}$ ) temperature when compared with the results obtained in the MSF process model developed without effect of the non-condensable (compare Table 4.2 with Table 7.2). This increasing was due to the increases in the overall heat transfer coefficient ( $U_j$ ) due to the presence of NCG in MSF distiller.

### 7.2.2 Effect of NCG on Overall Heat Transfer Coefficient and Plant Performance

In this section, the effect of the variation in the non-condensable gases in the flashing chambers on the overall heat transfer coefficient and plant performance parameters has been studied. First, the effect of the presence of the NCG in the flashing chambers in the heat recovery section and heat rejection section on the overall heat transfer coefficient is calculated. The NCG concentrations were assumed to be varied from 0.015 - 0.06 wt %

Table 7.2 Simulation results of gPROMS model with effect of 0.015 % of NCGs

F(kg/s)	BD(kg/s)	WR(kg/s)	$W_{\text{steam}}$ (kg/s)	CR%				
1577.78	1313.89	3341.66	37.49	6.29				
Stage	$B_j$ (kg/s)	$D_j$ (kg/s)	$CB_j$ %	$TF_j$ (°C)	$TD_j$ (°C)	$TB_j$ (°C)	$U_j$ (kcal/hm <sup>2</sup> K)	
0	3.34E+03	0.0	6.29	0	0	90.35	2102.5	
1	3.33E+03	17.33	6.35	84.24	86.26	87.45	2599.15	
2	3.31E+03	34.72	6.38	81.23	83.29	84.49	2591.87	
3	3.29E+03	52.22	6.42	78.16	80.26	81.47	2584.09	
4	3.27E+03	70.00	6.45	75.04	77.18	78.4	2575.78	
5	3.25E+03	87.78	6.49	71.88	74.05	75.29	2566.91	
6	3.24E+03	105.28	6.52	68.68	70.88	72.14	2557.44	
7	3.22E+03	123.06	6.56	65.45	67.67	68.96	2547.34	
8	3.20E+03	140.56	6.6	62.19	64.44	65.76	2536.56	
9	3.18E+03	158.06	6.63	58.92	61.19	62.55	2525.08	
10	3.17E+03	175.28	6.67	55.64	57.92	59.33	2512.86	
11	3.15E+03	192.22	6.7	52.36	54.65	56.12	2499.84	
12	3.13E+03	208.89	6.74	49.08	51.38	52.92	2486.01	
13	3.12E+03	225.28	6.78	45.83	48.12	49.74	2471.33	
14	3.10E+03	240.28	6.81	44.51	45.12	46.86	5448.89	
15	3.09E+03	255.28	6.84	41.41	42.06	43.9	5336.17	
16	3.07E+03	270.28	6.87	38.24	38.9	40.87	5336.54	

Figures 7.1 and 7.2 described the variation in the overall heat transfer coefficient in the heat recovery section and heat rejection section flashing stages at different NCG concentrations respectively. In the heat recovery section and heat rejection section, the

overall heat transfer coefficient decrease as the concentration of the NCG increases. The decreasing in overall heat transfer coefficient was up to 6% in heat recovery section and 13% in heat rejection section.

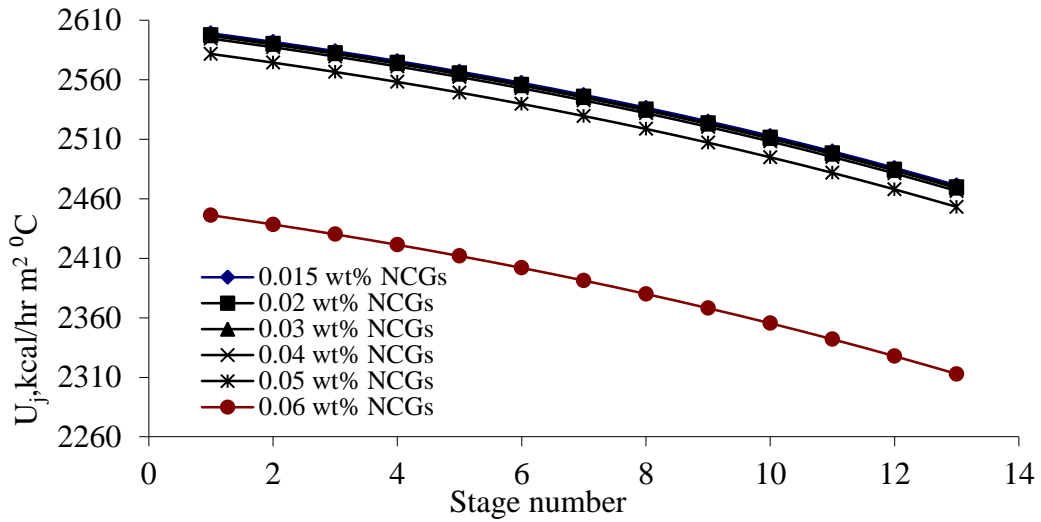


Figure 7.1 Overall heat transfer coefficient through recovery stages at different NCG wt %

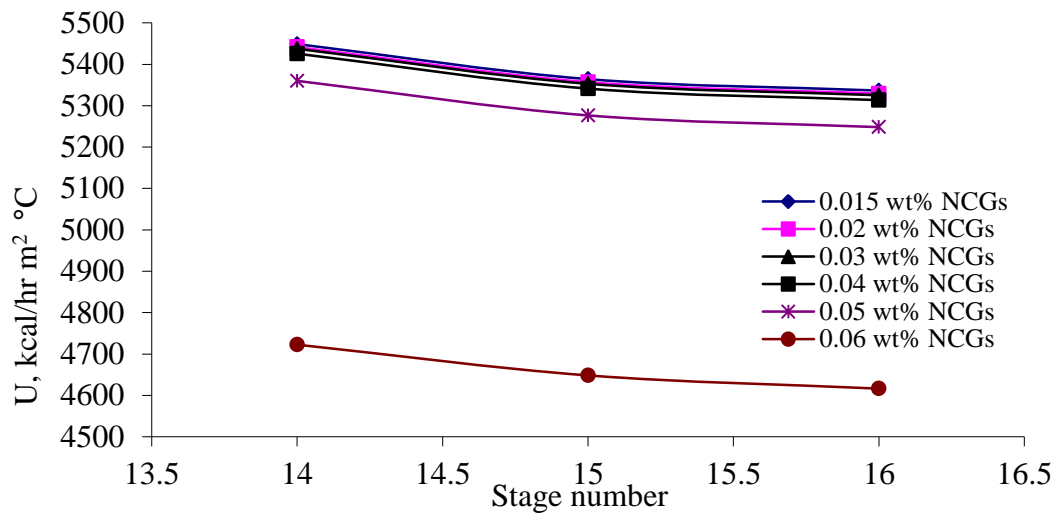


Figure 7.2 Overall heat transfer coefficient through rejection stages

Furthermore, the effect of different NCG concentration on the plant performance parameter has been studied. These simulation studies were performed at different concentration of NCGs (0.015, 0.02, 0.03, 0.04, 0.05 and 0.06) in the heat recovery section and heat rejection section. The purpose of this investigation is to know how the MSF plant performance parameters gained output ratio(GOR), steam flowrate ( $W_{steam}$ )

and distillate product ( $D_{NS}$ ) affecting by the presence of NCG. The GOR is the ratio of the flowrate of product of the MSF plant to the steam consumption. Table 7.3 shows the effect of the increasing in the NCG concentration on the GOR,  $W_{steam}$  and  $D_{NS}$ . The simulation results showed decrease in the gained output ratio and distillate product as the concentration of NCG increases. This evidenced by increasing amount of steam distillate product due to increase in the overall heat transfer coefficient.

Table 7.3 Effect of NCG on MSF Plant Performance

NCGs	GOR	$W_{steam}$	$D_{NS}$
% wt		(kg/s)	(kg/s)
0.015	7.571	35.721	270.517
0.02	7.569	35.734	270.480
0.03	7.567	35.737	270.460
0.04	7.560	35.747	270.400
0.05	7.542	35.806	270.061
0.06	7.305	36.445	266.241

$$\text{Gained Output Ratio (GOR)} = \frac{\text{Total Distilled}(D_{NS})}{\text{Steam Needed}(W_{steam})}$$

## 7.3 Sensitivity of Design and Operation Parameters in the presence of NCG

### 7.3.1 Effect of Seawater and Steam Temperature on Freshwater Production (Fixed Design)

At the presence of 0.015 % of the NCG and fixed design of MSF process in terms of number of stages and stage dimension specification in the heat recovery section and heat rejection section, the sensitivity of the seawater temperature ( $T_{seawater}$ ), and steam temperature ( $T_{steam}$ ) on the gained output ratio (GOR), distillate product( $D_{NS}$ ), top brine

temperature (TBT) and final bottom brine temperature (BBT) is studied. The simulation results are summarized in Table 7.4. For a given NCGs (0.015 wt %) and steam temperature ( $T_{\text{steam}}$ ) ( $97^{\circ}\text{C}$ ) simulations are carried out at different seawater temperature ( $T_{\text{seawater}}$ ). The seawater temperature was assumed to vary from 22 to  $45^{\circ}\text{C}$  as shown in Table 7.4. The variation in the seawater temperature was subject to the season variation from summer to winter. The results also show decrease in plant production, performance ratio, steam flowrate and increase in the top brine temperature and brine blowdown temperature as seawater temperature increases from  $22^{\circ}\text{C}$  to  $45^{\circ}\text{C}$  (similar pattern was observed by Tanvir and Mujtaba, 2006a). Comparison of the results at  $T_{\text{seawater}} = 35^{\circ}\text{C}$  with those of Rosso et al. (1996) and Tanvir and Mujtaba (2006a) clearly show the effect of NCG. The amount of steam consumption goes very high due to change in overall heat transfer coefficient. Further simulations are carried out for a given seawater temperature ( $45^{\circ}\text{C}$ ) with steam temperature varying from  $110^{\circ}\text{C}$  -  $120^{\circ}\text{C}$ . The results showed increases in all the operation variables (again a similar pattern was observed but with different values by Tanvir and Mujtaba, 2006a).

Table 7.4 Effect of  $T_{\text{seawater}}$  and  $T_{\text{steam}}$  on DNS, GOR, TBT, and BBT at 0.015 % wt of NCG

$T_{\text{seawater}}, ^{\circ}\text{C}$	$D_{\text{NS}}, \text{kg/s}$	$W_{\text{steam}}, \text{kg/s}$	GOR	TBT, $^{\circ}\text{C}$	BBT, $^{\circ}\text{C}$
22	320	42.8	7.48	89	29.24
35	270	35.7	7.57	90	40.87
45	230	30.4	7.56	91	50.00
$T_{\text{steam}}, ^{\circ}\text{C}$					
110	293	36.3	8.07	103	50.90
115	317	38.5	8.24	108	51.26
120	342	40.7	8.40	112	51.64

### 7.3.2 Effect NCG on MSF Operation Parameters at Different Number of Stages and Seawater Temperature for Fixed Water Demand

Finally for 3 different sets of plant configuration (different values of number of stages in the recovery section), a series of simulations were carried out to study the effect of NCG on the operation parameters at different seawater temperature ( $T_{\text{seawater}}$ ) but with fixed water demand ( $D_{\text{NS}}$ ) of 277.77kg/s. The seawater temperature is assumed to vary from 20 to 35°C (20, 25, 30 and 35). The total number of stages is varied from 16 to 20 (16, 17, 18, and 20). The number of stage in the rejection section is composed of 3 stages and the number of stages in the heat recovery section is varied. In the presence of 0.015% of NCG in the heat recovery section and heat rejection section, the effect of seawater temperature ( $T_{\text{seawater}}$ ) and total number of stage ( $N$ ) on the steam flowrate ( $W_{\text{steam}}$ ), steam temperature ( $T_{\text{steam}}$ ), recycle flowrate ( $R$ ) and final brine blowdown temperature (BBT) are shown in the Figures 7.3-7.6. The simulation results in this section are compared with those obtained by Tanvir and Mujtaba (2006b) who did not consider the effect of NCGs in their model. For a given number of stages, as the seawater temperature changes from 20 to 35, the steam flowrate increases (Figure 7.3). Higher steam consumption (9 % increase at  $T_{\text{seawater}}=35^{\circ}\text{C}$  compared to that at  $T_{\text{seawater}}=20^{\circ}\text{C}$ ) compared to 13 % increasing obtained by Tanvir and Mujtaba (2006b). The increasing in the steam temperature ( $T_{\text{steam}}$ ) as the seawater temperature varied from 20 to 35 °C for given number of stages is show in Figure 7.4. The results show for a fixed water demand, there is slightly increasing in the  $T_{\text{steam}}$  with changing  $T_{\text{seawater}}$ . Figure 7.5 shows the increasing in the brine recycle flowrate ( $R$ ) with increase seawater temperature for given number of stages. The ( $R$ ) increases up 70% at seawater temperature 35°C compared to that at 20°C (the same results obtained by Tanvir and Mujtaba (2006b). higher amount of recycle will increase the total operating cost by



increase the pumping recycle. In addition, for given number of stages and as the seawater temperature changes from 20 to 35°C, the brine blowdown temperature (BBT) increases as shown in Figure 7.6. 58% increase in BBT at  $T_{\text{seawater}}=35^{\circ}\text{C}$  compared to that at  $T_{\text{seawater}}=20^{\circ}\text{C}$  (again here, the same results obtained by Tanvir and Mujtaba, (2006b)). It can be seen that, no significant changes are noticed in the amount of brine recycle and brine blowdown temperature when changing number of stages (Figure 7.5 and 7.6). Note, although the observations (pattern) are very similar to those of Tanvir and Mujtaba, (2006b) the actual values of the parameters are quite different which are due to the consideration of the effect of NCG in the model considered in this work.

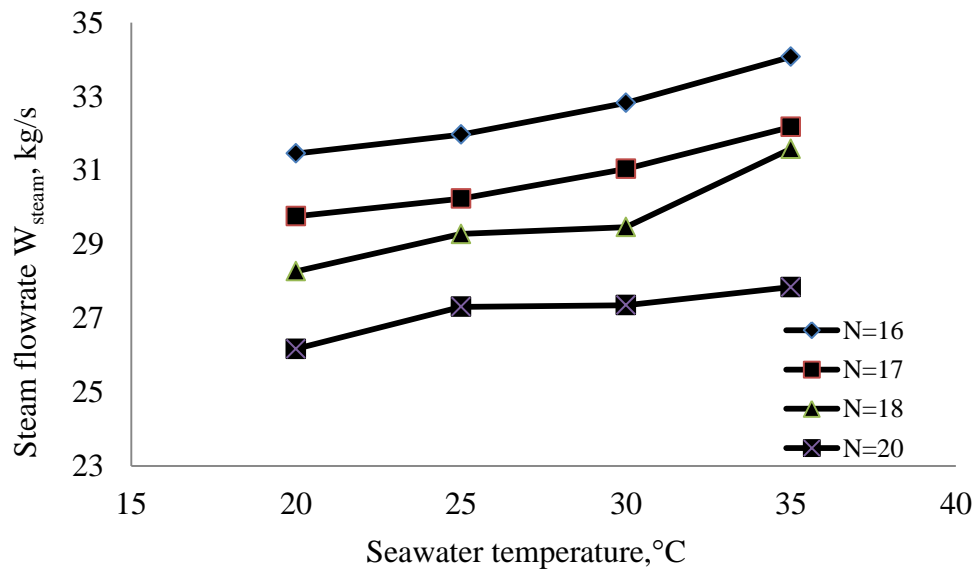


Figure 7.3 Effect of seawater temperature on steam flowrate for different number of stages at 0.015 % wt of NCG

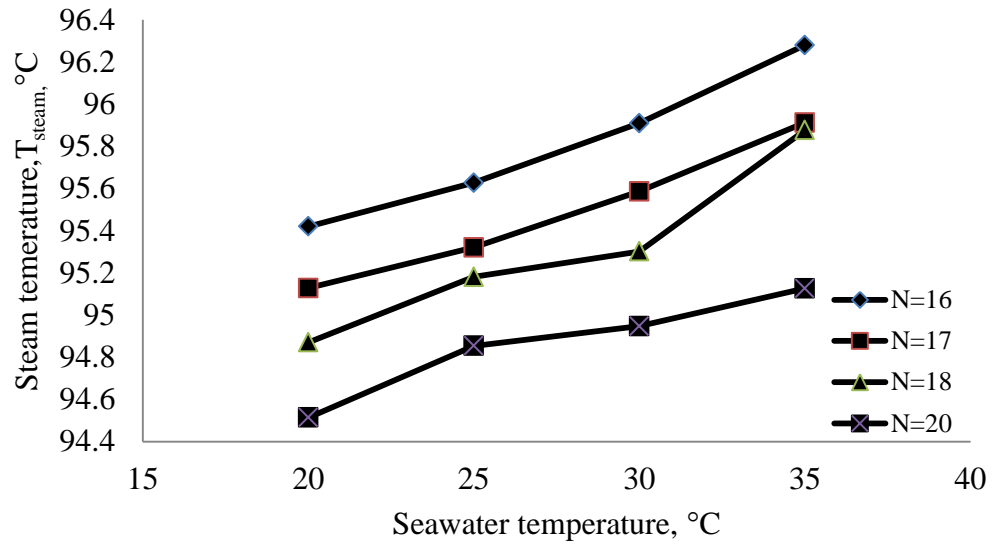


Figure 7.4 Effect of seawater temperature on steam temperature for different number of stages at 0.015 NCG

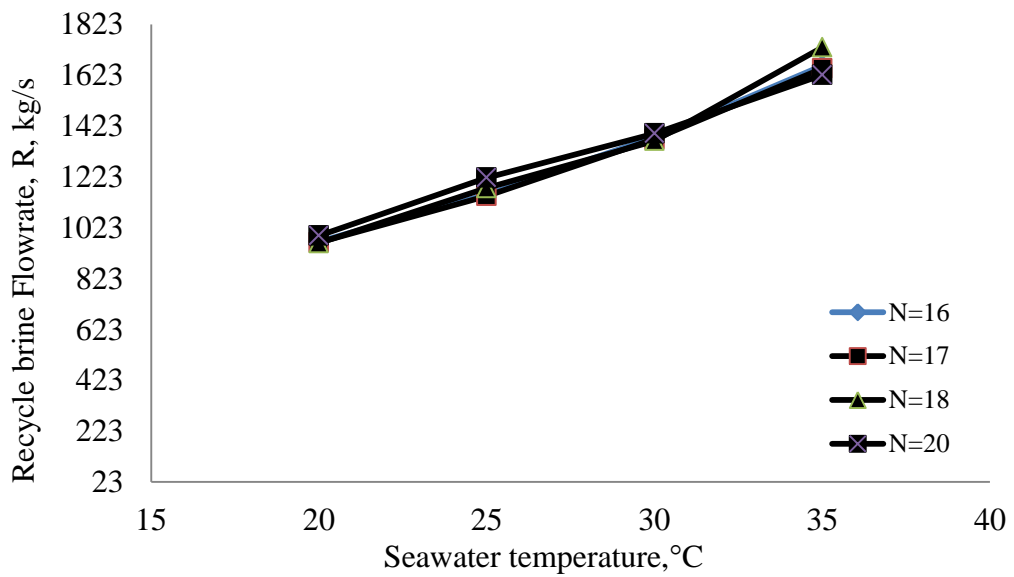


Figure 7.5 Effect of seawater temperature on recycle brine flowrate for different number of stages at 0.015 % wt of NCG

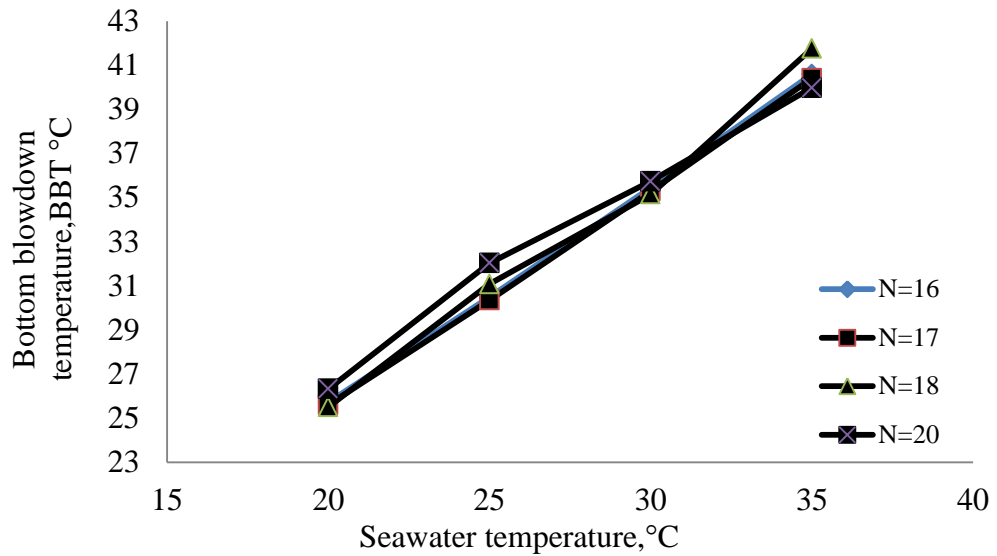


Figure 7.6 Effect of seawater temperature on blow down temperature for different number of stages at 0.015 % wt of NCG

## 7.4 Conclusions

Furthermore, the effect of non-condensable gases on the overall heat transfer coefficient correlations have been modelled and incorporated within an MSF process model developed using gPROMS modelling tool. First the developed model has been used simulate the MSF process at 0.015% NCG. The simulation results show increasing in the flowrates of brine and distillate streams and temperature profiles in the flashing stages compared with the simulation results developed without consider the effect of NCGs. Then model has been used to study the effect of variation concentrations (0.015, 0.02, 0.03, 0.04, 0.05 and 0.06 %) of NCGs in the flashing chambers on the overall heat transfer coefficients in the flashing stages. The simulation results show decrease in overall heat transfer coefficient up to 6% in heat recovery section and 13% in heat rejection section. The model is then used to study how the process and design parameters affect due to the changes in overall heat transfer coefficient. The results show increase in steam flowrate and plant production in the presence of 0.015 wt % of

NCG compared with the same results obtained by Rosso et al. (1996) and Tanvir and Mujtaba, (2006). Also, in the presence of 0.015 wt % of NCG and to maintain a fixed water demand , a 70% increases in recycle flowrate and 57% increases in brine blowdown temperature obtained when we change the number of stages from 16 to 20 and at seawater temperature between 20°C and 35°C.

## Chapter 8

# Neural Network Based Correlations for Estimating Dissociation Constants of Carbonic Acid in Seawater

### 8.1 Introduction

As described in chapter 7, the NCG affects the overall heat transfer coefficients, operation, and design of MSF process. To describe the CO<sub>2</sub> release process and the carbonate system of seawater in MSF distiller, better knowledge of the first and the second dissociation constant in seawater water ( $K_1$  and  $K_2$ ) are needed.  $K_1$  and  $K_2$  depend on the temperature and salinity of seawater. Several correlations have been developed in the past to calculate  $K_1$  and  $K_2$ . Small error in calculating  $K_1$  and  $K_2$  can lead to considerable errors in the describing the carbonate system in seawater and calculation of calcium carbonate scaling tendency.

In this chapter, neural networks (NN) are used to develop new correlations for calculating  $K_1$  and  $K_2$  for given salinity (in terms of weight percent.) and temperature (in terms of degree centigrade). Three NN based correlations based on three source of experimental data are developed and the results are compared with those obtained by the experiments. It is found that the NN based correlations can predict the dissociation constant very closely.

### 8.2 Application of Neural Networks

In the recent years neural networks have become the focus of attention in many technology disciplines including chemical engineering where they can be used to solve highly nonlinear and complex problems. A number of applications such as process

modeling and identification, design, optimisation, sensor data analysis, adaptive control and nonlinear internal model predictive control for nonlinear systems have appeared in the literature. Neural networks have ability to approximate any nonlinear function relationship between variables, and this has triggered many applications including those in the nonlinear identification and control chemical processes.

In chemistry, neural networked determines the molecular structure by comparing the data obtained by spectroscopic analysis. In process control, NN determine the complex relationship between the controlled and manipulated variable comparing the data obtained from the monitoring of the process and fault detection (Zupan and Gasteiger, 1999; Mujtaba and Hussain, 2006).

In manufacturing, NN can be used in process control, product design, product design and analysis, process and machine diagnosis, real time particle identification, visual quality inspection systems, welding quality analysis, paper quality prediction, computer chip quality analysis, analysis of grinding operations, chemical product design analysis, machine maintenance analysis, project bidding, planning and management, dynamic modeling of chemical process systems (Hagan et al., 1996). Also, NN have been applied in other many fields such as aerospace, automotive, banking, electronics, financial, insurance, and medical (Hagan et al., 1996).

.In the past, there are many works which has been done in use of NN in the process engineering activities such as modeling, design, optimization and control. Aziz et al. (2001) implemented a Generic Model Control (GMC) plan for controlling reactor temperature by manipulating the temperature of the heating jacket, using neural networks to calculate the heat released in an exothermic batch reactor system. Greaves et al., (2003) proposed a framework process model using NN techniques to optimise the operation of pilot-plant middle vessel batch column (MVBC). Mujtaba et al., (2006)

developed three different types of nonlinear control strategies and implemented in batch reactors using NN techniques. Tanvir and Mujtaba (2006a) developed three NN based correlations for estimating temperature elevation (TE) of MSF desalination process for given seawater salinity and boiling point temperature (BPT). The developed correlations were implemented in the MSF process model for further study. Ekpo and Mujtaba, (2008) developed an algorithms of two advanced nonlinear controllers (GMC-NN and IMBC) using NN to control the batch reactor temperature set point during the dynamic optimization of polymerization process. Hawaidi and Mujtaba, (2011) developed a NN based correlations to calculate the dynamic freshwater demand profiles at different times of the day and season. The developed correlations are implemented in a steady state MSF process model using gPROMS software.

### **8.3 Introduction to Neural Network Architecture**

The name of neural networks comes from the simple processors in the brain, called neurons, which are interconnected by network that transmits signals between them. A brain is made up of large number neurons, coupled to receptors and effectors. The major components of a typical nerve cell (neuron) in the central nervous system are shown in Figure 8.1. The major structure of a typical nerve cell includes dendrites, cell body, and axon. Dendrites are the receptive zones and the axon is transmission (output) line. Synapses are the units that connect the axon of the neuron to various parts of other neurons (Al-Shayji, 1998).

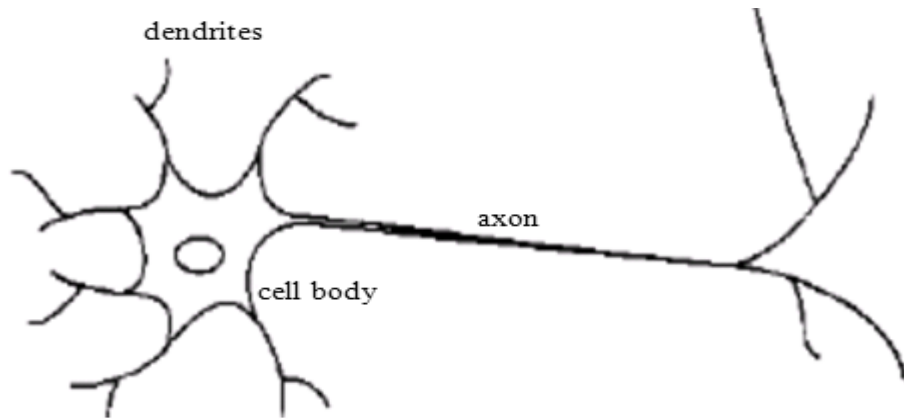


Figure 8.1 A single neuron

Neural network (NN) is extremely simplistic models of the brain. Figure 8.2 shows a simplified model of an artificial neuron, which may be used to simulate some important aspects of the real biological neuron. The node receives weighted value of other nodes through its incoming connections. Firstly, these are added, and then passed through an activation function. The activation value is multiplied with the specific weight and transferred to the next node (Gao et al, 2007). One major difference between real neural networks and artificial neural networks is that neural networks use parallel processing. In this chapter, the NN are implemented using MATHLAB 7.

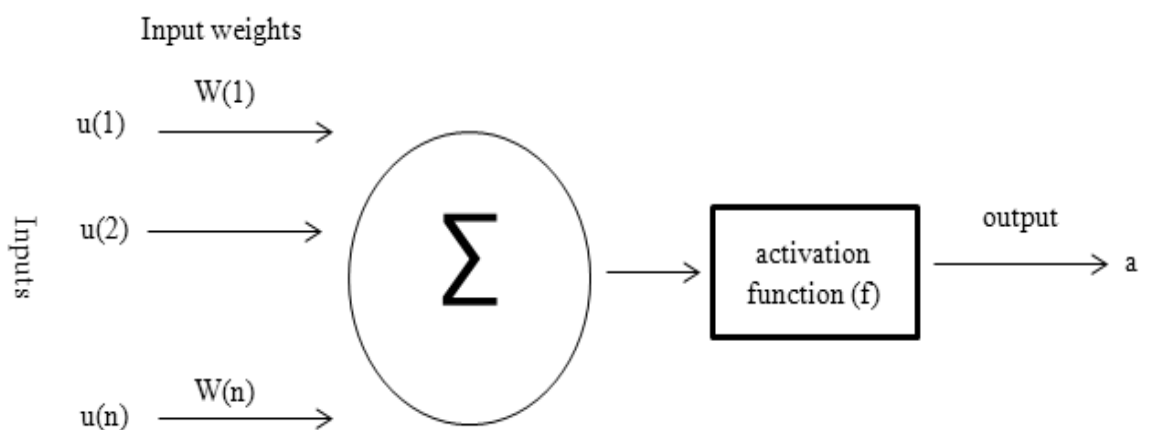


Figure 8.2 An artificial neuron



As shown in Figure 8.3, a typical neural network architecture is contained of a number of layers, a number of neurons, weights, biases and how layers are connected between themselves.

*Neuron:*

A mathematical processing element of the neural network is called a neuron. The neurons in the input layer are called the input. Also, the neurons in the output layer are output. The neurons in the input layer receive information from external sources and pass them to network for processing. This information may be either sensory inputs or signals from other systems. A layer of neurons that receives information from input layer and processes them in a hidden way is called a hidden layer. Hidden layer neuron has no direct connections to the outside world, receives information from the input layer and processes them in a hidden way. Output layer neurons receive processed information and sends output signals out of the system.

*Weights and biases:*

Weights are adaptive coefficients within the network that determine the intensity of the input signal. Each neuron connection is associated to a quantity, called weight factor, which act relative connection strength among the neurons to one another. The weight factor is positive if the associated connection is excitatory and negative if the connection is inhibitory.

The bias input is connected to each of the hidden and output neurons a network. Function of the bias is to act as an offset for the activation of neurons (Tanvir and Mujtaba, 2006).

*Transfer function:*

A transfer function can be used to determine the node's output using a mathematical operation on the total activation of the node. The transfer function can transform the node's activation in a linear or nonlinear manner. Common types of transfer function are show in Table 8.1

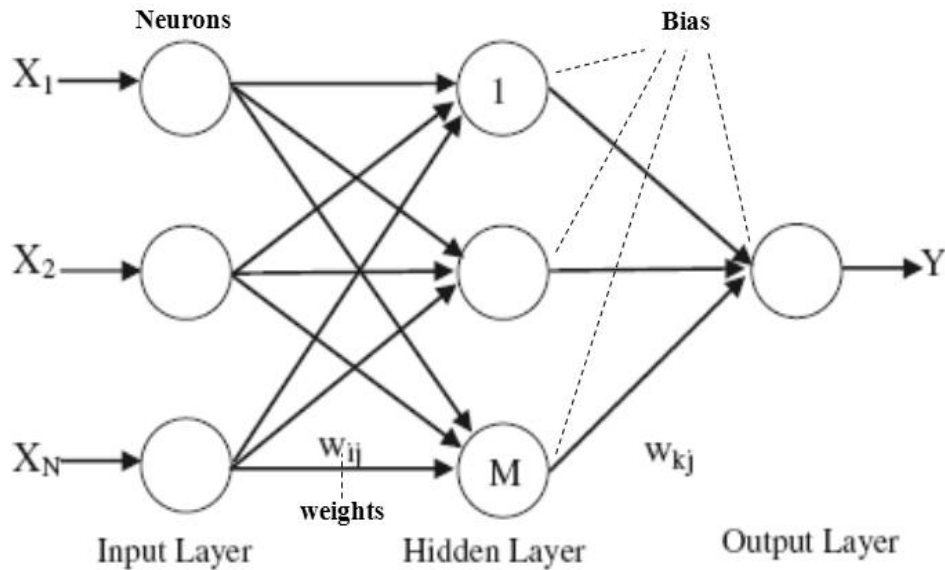


Figure 8.3 Structure of a typical multilayer neural network.

### 8.3.1 Back Propagation Training Algorithm

There are many different types of training algorithms. One of the most common classes of training algorithms for feedforward interlayer networks is called backpropagation. Back propagation algorithm was introduced by Werbos and published by Rumelhart and co-worker (Hagen et al., 1996). In a backpropagation algorithm, a set of inputs is fed to the network and outputs are returned. Then, the network compares its output with the output of the actual data source. The network calculates the amount of error between its predicted output and the actual output. The network works backwards through the layers, adjusting the weight factors according to how much error it has calculated in its output. Once all of the weight factors have been adjusted, the network works in a

forward path, taking the same input data to predict the output, based on the new weight factors. The network again calculates the error between the predicted and actual outputs. It adjusts the weight factors and the process continues, iteratively, until the error between the predicted and actual outputs has been minimised.

The following steps have been taken to increase the efficiency of neural network training in Matlab neural network Toolbox (Math Works, 2007).

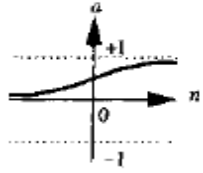
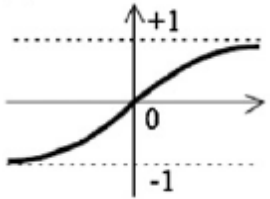
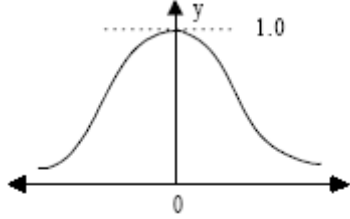
*a. Generalization and processing of data*

It is useful to scale the inputs and targets before training so that they always fall within a specified range. The data sets are divided into training, validation and test subsets. One fourth of the data is taken for the validation set, one fourth is taken for the test set and one-half is taken for the training set.

*b. Optimum network architecture*

The next step after processing the data is the selection of the architecture (the number of layer and nodes in each layer). Transfer function of each layer is then selected. Then the weights and biases are randomly initialised. Train the network using various configurations to determine the optimal number of layer, select the one that gives the optimum value. Due to the fact that as the number of neurons increase the accuracy of the computation increases, the chosen number of neurons is an important factor.

Table 8.1 Commonly used transfer function (Hagan et al., 1996)

Name of the Transfer Function	Mathematical function	
Sigmoid transfer function	$f(x) = \frac{1}{1 + e^{-x}}$ $[0 \leq f(x) \leq 1]$	
Hyperbolic transfer function	$f(x) = \tanh(x) = \frac{e^x + e^{-x}}{e^x - e^{-x}}$ $[-1 \leq f(x) \leq 1]$	
Gaussian transfer function	$f(x) = \exp\left(\frac{-x^2}{2}\right)$ $[0 \leq f(x) \leq 1]$	

*c. The training, validation and testing of neural network using back propagation-training algorithm*

Levenberg-Marquardt algorithm is widely used training algorithms within back propagation training in process engineering. The back propagation converges slowly with the increase of number of hidden layer. It can produce the local minima report. The LMS error converges to solution where learning rate is not large (such as quadratic function). Back propagation learning rate updates weights and biases by optimisation techniques such as gradient descent algorithm. This training normally takes much time

to minimise the square error. To achieve the faster training variable learning rate can be applied that is available in Matlab Neural Network toolbox.

#### d. Visualisation and statistical analysis

To visualize the relationship between the neural net output and targets, a linear regression between the network outputs will be performed and the network prediction for corresponding targets are plotted. Visualisation and statistical analysis help to understand network response easily.

### **8.4 Dissociation Constants of Carbonic Acid in Seawater**

A better knowledge of CO<sub>2</sub> release and of the interaction with the carbonate system in desalination distillers is very important for the design of the venting system and a stable distiller operation (Donner et al., 2008). Since CO<sub>2</sub> release and scale formation are closely related to the carbonate system of the brine, a better understanding of CO<sub>2</sub> release may contribute to the knowledge of scale formation in desalination distillers and improve scale prediction and prevention methods. The release process of non-condensable gas in MSF evaporators are influenced by many factors. Among them is the composition of the carbonic acid at the entrance of the first flash chamber (Glade, 1995). Better understanding of first dissociation constant ( $K_1$ ) and second dissociation constant ( $K_2$ ) of carbonic acid in seawater water are essential to describe the carbonate system of seawater, release process of CO<sub>2</sub>, and calculating of scaling tendency of CaCO<sub>3</sub> in multiple effect evaporator (MEE) and MSF distillers. Calculation of  $K_1$  and  $K_2$  depend on the temperature and salinity of the seawater (Said et al, 2011).

#### **8.4.1 Chemistry of Dissociation Constant of Carbonic Acid in Seawater**

The carbon dioxide in seawater is governed by the following equilibria:



Subsequently, the dissolved gas combines with water to form carbonic acid  $\text{H}_2\text{CO}_3$ :



The carbonic acid dissociates in seawater to form bicarbonate  $\text{HCO}_3^-$  and carbonate  $\text{CO}_3^{2-}$  :



The water itself dissociates to form  $\text{H}^+$  and  $\text{OH}^-$  ions:



calcium carbonate can be formed:



Applying the law of mass action to the first dissociation of carbonic acid



$$K_1^{\text{sw}} = \frac{[\text{H}^+]^{\text{sw}} [\text{HCO}_3^-]^{\text{sw}}}{[\text{CO}_2]^{\text{sw}}} \quad (8.7)$$

Where  $K_1^{\text{sw}}$  is the first dissociation constant of carbonic acid in seawater and  $[i]^{\text{sw}}$  is the concentration of the component  $i$  in seawater in mol/kg.

The second dissociation constant of the reaction  $\text{HCO}_3^- \leftrightarrow \text{CO}_3^{2-} + \text{H}^+$  can be written as

$$K_2^{SW} = \frac{[H^+]^{SW} [CO_3^{2-}]^{SW}}{[HCO_3^-]^{SW}} \quad (8.8)$$

Where  $K_2^{SW}$  is the second dissociation constant of carbonic acid in seawater and  $[i]^{SW}$  is the concentration of the component  $i$  in seawater in mol/kg.

Better understanding of first dissociation constant ( $K_1$ ) and second dissociation constant ( $K_2$ ) of carbonic acid in seawater water are essential to describe the carbonate system of seawater, release process of  $CO_2$ , and calculating of scaling tendency of  $CaCO_3$  in multiple effect evaporator (MEE) and MSF distillers. Calculation of  $K_1$  and  $K_2$  depend on the temperature and salinity of the seawater (Said et al, 2011).

#### 8.4.2 Empirical Correlations for Dissociation Constants of Carbonic Acid in Seawater

There are several correlations as shown below have been developed in the past to calculate  $K_1$  and  $K_2$  as described by Equations (8.9-8.14). Small error in calculating  $K_1$  and  $K_2$  can lead to considerable errors in describing the carbonate system in seawater and calculation of calcium carbonate scaling tendency.

Correlation 1: Mehrbach et al (1973)

$$pK_1 = -13.721 + 0.031334 \times T + 3235.76/T + 1.3 \times 10^{-5} \times S \times T - 0.1032 \times S \quad (8.9)$$

$$pK_2 = 5371.96 + 1.671221 \times T + 0.22913 \times S + 18.3802 \times \log(S) - 128375.28/T - 2194.30 \times \log(T) - 8.0944 \times 10^{-4} \times S \times T - 5617.11 \times \log(S)/T + 2.136 \times S/T \quad (8.10)$$

$pK_1$  and  $pK_2$  in  $\frac{\text{mol}}{\text{kg}}$ ,  $T$  in  $^{\circ}\text{K}$ ,  $S$  in ppt.

Correlation 2: Millero (1995)

$$pK_1^{sw} = 2.18867 - 2275.036/T - 1.468 \ln(T) + (-0.138681 - 9.33291/T) \times S^{0.5} \\ + 0.0726483 \times S - 0.00574938 \times S^{1.5} \quad (8.11)$$

$$pK_2^{sw} = -0.84226 - 3741.1288/T - 1.437 \ln(T) + (-0.128417 - 24.41239/T) \times S^{0.5} \\ + 0.1195308 \times S - 0.00912840 \times S^{1.5} \quad (8.12)$$

$pK_1^{sw}$  and  $pK_2^{sw}$  in mol/kgT in °K, S in g/kg.

Correlation 3: Mojica et al (2002)

$$pK_1 = -43.6977 - 0.012903 \times S + 3235.76/T + 1.3 \times 10^{-5} \times S \times T - 0.1032 \times S \quad (8.13)$$

$$pK_2 = -452.0940 - 13.14216 \times S - 8.101 \times 10^{-4} \times S^2 + 21263.61/T + 68.483143 \times \ln(T) \\ + (-581.4428 \times S + 0.259601 \times S^2)/T - 1.967035 \times S \times \ln(T) \quad (8.14)$$

$pK_1$  and  $pK_2$  in mol/kg, T in °C, S in g/kg.

## 8.5 Neural Network and Development of Correlations for $K_1$ and $K_2$

Neural Network (NN) has been used successfully in developing the seawater properties correlations and process modelling, simulation and optimisation of thermal desalination plants (Tanvir and Mujtaba, 2006a). In this work, three NN correlations based on three sources of experimental data have developed for calculating  $K_1$  and  $K_2$  of carbonic acid in seawater for different salinity and temperature. The overall objective is to implement these correlations in the full steady state MSF mathematical model developed in chapter 7 for the performance evaluation of the MSF process.



### 8.5.1 NN Architecture and Training

As shown in the Figure 8.3, the neural network architecture can be described by how many layers the network has, the number of neurons in each layer, and how the layers are connected to each other. Each neuron  $j$  in the  $i^{\text{th}}$  layer (except in the input layer) is connected with all the neurons of the  $(i-1)^{\text{th}}$  layer with bias  $(b_{ij})$  and through weights  $(w_{jk}^i)$ , where  $k$  denotes the neurons of  $(i-1)^{\text{th}}$  layer. The total number of neurons in layer  $i$  is  $n_j$  and transfer function for layer  $i$  and neurons  $j$  is  $f_{ij}$ . In each layer, the value of the neuron  $j$  is calculated by:

$$a_{jk}^i = f_j^i \left( \sum_{k=1}^{n_{i-1}} w_{jk}^i \times a_k^{i-1} + b_j^i \right) \quad (8.15)$$

Neural network based techniques usually requires a large number of data sets. For a given set of input data, NN are able to produce a corresponding set of outputs according to some mapping relationship. In this work, the back propagation method is used for training. In this method, the network calculates the error between the output and the target. This error is fed back to the network and weights and biases are adjusted according to Least Mean Square (LMS) error criteria. The process is continued until the network output is close to the target (As shown in Figure 8.4) (Tanvir and Mujtaba, 2006a).

All the input data has been scaled, so that they will have zero mean and standard deviation equal to 1, to find the most accurate neural network relationship between input and output relationship.

A training graph (LMS error vs time) is used to find how long it takes to get a good NN architecture and how many times the network needs to reinitialise the weights and biases (for a new architecture, according to Figure 8.5). The NN predicted output value

is rescaled to its original units. The statistical regression between predicted value and output data is plotted to find the overall trends of the data.

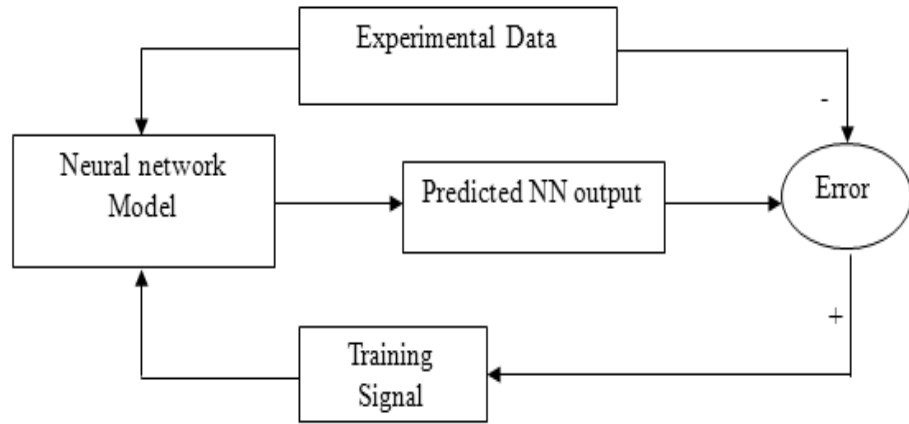


Figure 8.4 Neural network backpropagation training Scheme

### 8.5.2 Development of the Correlations

Once the optimum network architecture is found, the weights and biases are used to develop the NN based correlations. This is explained below.

The correlation estimate  $K_1$  and  $K_2$  in terms of temperature (T) salinity (S).  $K_1$  and  $K_2$  expressed in mol/kg, T in ° C and S in g/kg.

The input data is scaled up with mean and its standard deviation as:

$$T_{\text{scaleup}} = \frac{(T - \text{mean}T)}{\text{std}T} \quad (8.16)$$

$$S_{\text{scaleup}} = \frac{(S - \text{mean}S)}{\text{std}S} \quad (8.17)$$

Where meanT is the average of T and meanS is the average of S; stdT is standard deviation of T and stdS is the standard deviation of S data used to develop the correlation.

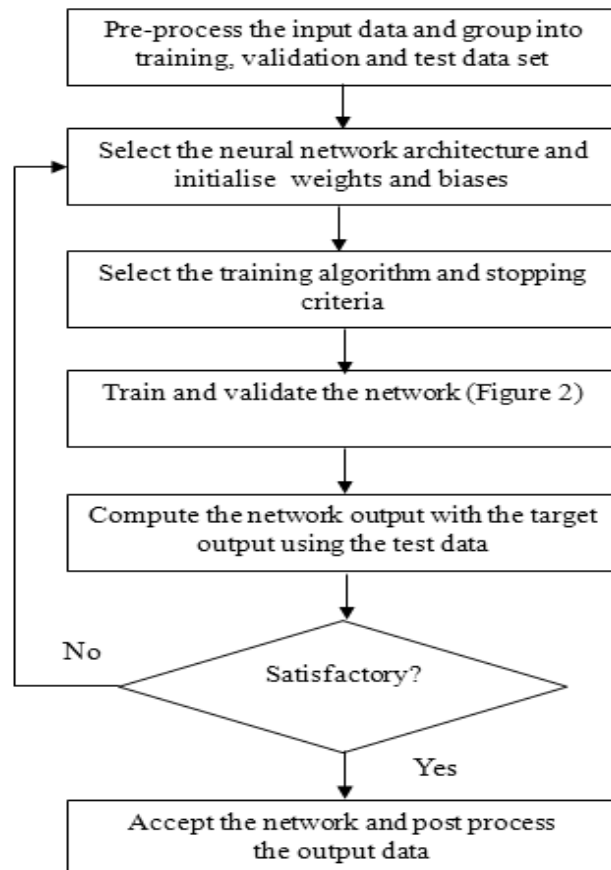


Figure 8.5 Determination of optimum network Structure

There are two input neurons in the NN based correlations. The values are:

$$a_1^1 = T_{\text{scaleup}} \text{ and } a_2^1 = S_{\text{scaleup}}$$

There is one output neuron in the NN based correlations:

$$a_j^l = K_i_{\text{scaleup}} \tag{8.18}$$

Where  $l$  is the output layer. The output value is rescaled to find the value in original units.

$$K_i = K_i_{\text{scaleup}} \times \text{std}K_i + \text{mean}K_i \tag{8.19}$$

Where  $\text{mean}K_i$  and  $\text{std}K_i$  are average and standard deviation respectively of the  $K_i$  data used for developing the correlations.

The NN based correlations developed in this work is explained with respect to 3 layers NN architecture. In 3 layers NN architecture there is one input, one hidden layer and one output layer (Figure 5.6).

For 3 layered network, the correlation is given by:

$$a_1^3 = f_l^3 \left( \sum_{k=1}^4 (w_{1k}^3 \times a_k^2) + b_1^3 \right) \quad (8.20)$$

Where  $a_k^2$  is given by:

$$a_1^2 = f_l^2 \left( \sum_{k=1}^2 (w_{1k}^2 \times a_k^1) + b_1^2 \right) \quad (8.21)$$

For  $j=1$  in layer 2, Equation (8.15) can be expressed as:

$$a_1^2 = f_l^2 \left( w_{11}^2 a_1^1 + w_{11}^2 a_2^1 + b_1^2 \right) \quad (8.22)$$

In this work we used  $f_j^2=1$  and Equation (8.16) becomes:

$$a_1^2 = (w_{11}^2 a_1^1 + w_{11}^2 a_2^1 + b_1^2) \quad (8.23)$$

In general, for the 2<sup>nd</sup> layer, the value of  $j$ -th neuron can be given by:

$$a_j^2 = (w_{j1}^2 a_1^1 + w_{j2}^2 a_2^1 + b_j^2) \quad (8.24)$$

$$a_j^1 = f_j^1 \left( \sum_{k=1}^2 (w_{jk}^1 a_k^0) + b_j^1 \right) \quad (8.25)$$

In this work, we used  $f_j^1 = \tanh$ ; Equation (8.19) becomes:

$$a_j^1 = \tanh \left( w_{j1}^1 T_{\text{scaleup}} + w_{j2}^1 S_{\text{scaleup}} + b_j^1 \right) \quad (8.26)$$

Equation (8.14) can be written now for  $Ki_{\text{scaleup}}$ :

$$Ki_{\text{scaleup}} = a_1^3 = w_{11}^3 \times a_1^2 + w_{12}^3 \times a_2^2 + w_{13}^3 \times a_3^2 + w_{14}^3 \times a_4^2 + b_1^3 \quad (8.27)$$

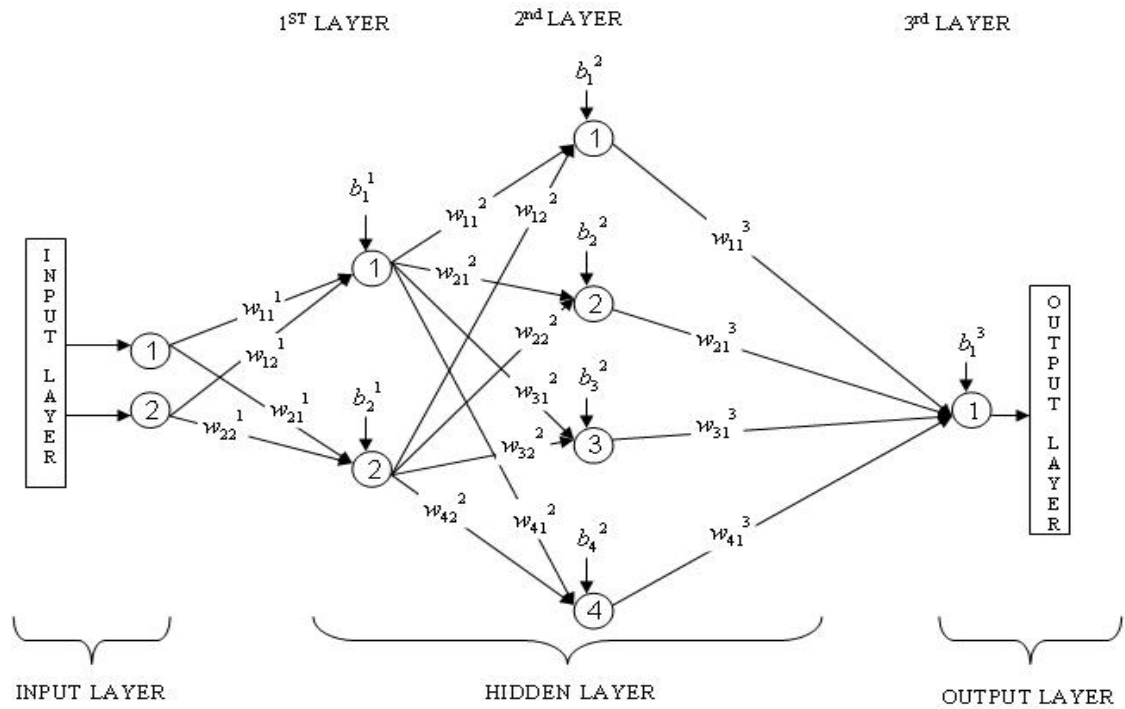


Figure 8.6 A four layer neural network

## 8.6 Experimental Data and Correlations

### 8.6.1 Experimental Data

The input data for NN based correlation are taken from three different experimental data sources. The experimental data are different due to the variation in seawater properties and experimental methods used. The input data range for the first 3 NN based correlations is shown in Table 8.2.

1. Millero et al (1997), 316 data points of temperature, salinity,  $K_1$  and  $K_2$  were used with temperature range (1-40 °C) and salinity at (5, 15, 25, 35 g/Kg). (Table 8.3 and Table 8.4).
2. Mehrbach et al. (1973), 288 data points of temperature, salinity,  $K_1$  and  $K_2$  were used with temperature range (0-35°C) and salinity at (19, 27, 31, 33, 35, 37, 39, 40, 43 g/Kg). (Table 8.5 and Table 8.6).

3. Millero et al (2006), 466 data points of temperature, salinity,  $K_1$  and  $K_2$  were used with temperature range (0-50 °C) and salinity range (1-50) (Table 8.7 and Table 8.8).

Table 8.2 The salinity (S) and temperature (T) data range for different NN based correlations

NN based Correlation	S range(wt%)	T range( $^{\circ}$ C)	Number of data used
NN1_K1	5.0-35.0	1.0-40.0	316
NN1_K2	5.0-35.0	1.0-40.0	316
NN2_K1	19.0-43.0	0.0-35.0	288
NN2_K2	19.0-43.0	0.0-35.0	288
NN3_K1	3.46-36.3	1.1-50.5	459
NN3_K2	3.46-36.3	1.1-50.5	459

Table 8.3 (K1×107) from Millero data (Millero et al., 1997) used in NN1\_K1

T(°C)	Salinity (%)				T(°C)	Salinity (%)				T(°C)	Salinity (%)			
	5	15	25	35		5	15	25	35		5	15	25	35
1	4.8796	6.2363	7.0414	7.5812	<i>14.5</i>	<i>6.909</i>	<i>9.0474</i>	<i>10.4277</i>	<i>11.3702</i>	<b>28</b>	<b>8.8348</b>	<b>11.9646</b>	<b>13.9631</b>	<b>15.4727</b>
1.5	4.9508	6.3397	7.1551	7.7158	15	6.9871	9.161	10.5609	11.5201	28.5	8.8955	12.0679	14.1036	15.6279
<b>2</b>	<b>5.0221</b>	<b>6.4431</b>	<b>7.2687</b>	<b>7.8505</b>	15.5	7.0651	9.2801	10.6969	11.67	29	8.9561	12.1711	14.2441	15.7831
<i>2.5</i>	<i>5.0934</i>	<i>6.5466</i>	<i>7.3824</i>	<i>7.9852</i>	<b>16</b>	<b>7.1432</b>	<b>9.3992</b>	<b>10.8329</b>	<b>11.8198</b>	29.5	9.0167	12.2743	14.3846	15.9383
3	5.1647	6.65	7.5004	8.1199	<i>16.5</i>	<i>7.2212</i>	<i>9.5183</i>	<i>10.9689</i>	<i>11.9696</i>	<b>30</b>	<b>9.0774</b>	<b>12.3775</b>	<b>14.5251</b>	<b>16.0935</b>
3.5	5.236	6.7535	7.6203	8.2545	17	7.2993	9.6375	11.1049	12.1195	30.5	9.138	12.4808	14.6656	16.249
<b>4</b>	<b>5.3072</b>	<b>6.8569</b>	<b>7.7404</b>	<b>8.3892</b>	17.5	7.3773	9.7566	11.2409	12.2693	31	9.1986	12.5821	14.8061	16.4095
<i>4.5</i>	<i>5.3785</i>	<i>6.9603</i>	<i>7.8604</i>	<i>8.5239</i>	<b>18</b>	<b>7.4553</b>	<b>9.8757</b>	<b>11.3769</b>	<b>12.4191</b>	31.5	9.2593	12.6759	14.9466	16.57
5	5.4498	7.0638	7.9805	8.6586	<i>18.5</i>	<i>7.5334</i>	<i>9.9948</i>	<i>11.5129</i>	<i>12.569</i>	<b>32</b>	<b>9.3193</b>	<b>12.7698</b>	<b>15.0871</b>	<b>16.7306</b>
5.5	5.5211	7.1672	8.1005	8.7932	19	7.6115	10.1059	11.6446	12.7187	32.5	9.3782	12.8637	15.2268	16.8911
<b>6</b>	<b>5.5924</b>	<b>7.2707</b>	<b>8.2205</b>	<b>8.9279</b>	19.5	7.6885	10.2092	11.7684	12.8685	33	9.437	12.9576	15.3544	17.0516
<i>6.5</i>	<i>5.6637</i>	<i>7.3741</i>	<i>8.3406</i>	<i>9.0665</i>	<b>20</b>	<b>7.7611</b>	<b>10.3124</b>	<b>11.8923</b>	<b>13.0182</b>	33.5	9.4958	13.0515	15.4801	17.2121
7	5.735	7.4769	8.4669	9.2067	<i>20.5</i>	<i>7.8339</i>	<i>10.4156</i>	<i>12.0161</i>	<i>13.168</i>	<b>34</b>	<b>9.5546</b>	<b>13.1454</b>	<b>15.6058</b>	<b>17.3726</b>
7.5	5.8082	7.5796	8.5964	9.3469	21	7.9068	10.5188	12.1399	13.3178	34.5	9.6134	13.2392	15.7315	17.5331
<b>8</b>	<b>5.8866</b>	<b>7.6824</b>	<b>8.726</b>	<b>9.4871</b>	21.5	7.9796	10.622	12.2638	13.4675	35	9.6722	13.3335	15.8571	17.6918
<i>8.5</i>	<i>5.9653</i>	<i>7.7851</i>	<i>8.8556</i>	<i>9.6273</i>	<b>22</b>	<b>8.0524</b>	<b>10.7252</b>	<b>12.3876</b>	<b>13.6174</b>	35.5	9.7311	13.4297	15.9828	17.8436
9	6.0441	7.8878	8.9851	9.7676	22.5	8.1253	10.8284	12.5114	13.7687	<b>36</b>	<b>9.7899</b>	<b>13.5258</b>	<b>16.1085</b>	<b>17.9952</b>
9.5	6.1228	7.9906	9.1147	9.9078	23	8.1981	10.9317	12.6369	13.9231	36.5	9.8487	13.6219	16.2342	18.1467
<b>10</b>	<b>6.2015</b>	<b>8.0933</b>	<b>9.2443</b>	<b>10.048</b>	23.5	8.269	11.035	12.7672	14.0779	37	9.9075	13.7181	16.3599	18.2983
<i>10.5</i>	<i>6.2803</i>	<i>8.1963</i>	<i>9.3739</i>	<i>10.1927</i>	<b>24</b>	<b>8.3323</b>	<b>11.1383</b>	<b>12.8976</b>	<b>14.2328</b>	37.5	9.9658	13.8142	16.4856	18.4499
11	6.359	8.3019	9.5047	10.3398	<i>24.5</i>	<i>8.3955</i>	<i>11.2416</i>	<i>13.028</i>	<i>14.3877</i>	<b>38</b>	<b>10.036</b>	<b>13.9103</b>	<b>16.6113</b>	<b>18.6015</b>
11.5	6.4377	8.4084	9.6366	10.4868	25	8.4587	11.3449	13.1583	14.5425	38.5	10.1066	14.0064	16.7315	18.7531
<b>12</b>	<b>6.5164</b>	<b>8.5148</b>	<b>9.7684</b>	<b>10.6339</b>	25.5	8.522	11.4482	13.2887	14.6974	39	10.1772	14.1026	16.8514	18.904
<i>12.5</i>	<i>6.5952</i>	<i>8.6213</i>	<i>9.9003</i>	<i>10.7809</i>	<b>26</b>	<b>8.5852</b>	<b>11.5516</b>	<b>13.4191</b>	<b>14.8523</b>	39.5	10.2478	14.1987	16.9714	19.0503
13	6.6739	8.7278	10.0321	10.928	26.5	8.6484	11.6549	13.5495	15.006	<b>40</b>	<b>10.305</b>	<b>14.2765</b>	<b>17.0786</b>	<b>19.1677</b>
13.5	6.7526	8.8343	10.164	11.075	27	8.7117	11.7582	13.6828	15.1624					
<b>14</b>	<b>6.8309</b>	<b>8.9408</b>	<b>10.2958</b>	<b>11.2221</b>	27.5	8.7742	11.8614	13.8227	15.3175					

Note: Training data in plain, validation data in bold, test data in italic

Table 8.4 (K2×1010) from Millero data (Millero et al., 1997) used in NN1\_K2

T(°C)	Salinity (%)				T(°C)	Salinity (%)				T(°C)	Salinity (%)			
	5	15	25	35		5	15	25	35		5	15	25	35
1	1.3793	2.4808	3.3345	4.0918	<i>14.5</i>	<i>2.3087</i>	<i>4.357</i>	<i>6.0451</i>	<i>7.4393</i>	<b>28</b>	<b>3.6861</b>	<b>7.1906</b>	<b>9.9718</b>	<b>12.4944</b>
1.5	1.4106	2.5463	3.4262	4.1944	15	2.3508	4.4462	6.1751	7.5887	28.5	3.7336	7.3002	10.1446	12.7091
<b>2</b>	<b>1.4419</b>	<b>2.6119</b>	<b>3.5179</b>	<b>4.2971</b>	15.5	2.3928	4.5499	6.3051	7.7383	29	3.789	7.4099	10.3175	12.9282
2.5	<i>1.4732</i>	<i>2.6775</i>	<i>3.6095</i>	<i>4.3997</i>	<b>16</b>	<b>2.4349</b>	<b>4.6535</b>	<b>6.435</b>	<b>7.9152</b>	29.5	3.8466	7.5195	10.4903	13.1695
3	1.5044	2.743	3.7012	4.5024	<i>16.5</i>	<i>2.4771</i>	<i>4.7571</i>	<i>6.565</i>	<i>8.0924</i>	<b>30</b>	<b>3.9042</b>	<b>7.6368</b>	<b>10.6631</b>	<b>13.4104</b>
3.5	1.5357	2.8086	3.7928	4.6051	17	2.534	4.8608	6.695	8.2695	30.5	3.9619	7.7655	10.8359	13.6513
<b>4</b>	<b>1.567</b>	<b>2.8742</b>	<b>3.8845</b>	<b>4.7106</b>	17.5	2.5911	4.9644	6.8249	8.4466	31	4.0195	7.8941	11.0087	13.8922
4.5	<i>1.5983</i>	<i>2.9398</i>	<i>3.9761</i>	<i>4.8205</i>	<b>18</b>	<b>2.6482</b>	<b>5.068</b>	<b>6.9549</b>	<b>8.6238</b>	31.5	4.0771	8.0227	11.1908	14.1331
5	1.6296	3.0053	4.0678	4.9303	<i>18.5</i>	<i>2.7053</i>	<i>5.1716</i>	<i>7.0849</i>	<i>8.8009</i>	<b>32</b>	<b>4.1347</b>	<b>8.1513</b>	<b>11.3877</b>	<b>14.374</b>
5.5	1.6608	3.0709	4.1595	5.0402	19	2.7624	5.2753	7.2148	8.978	32.5	4.1923	8.2799	11.5849	14.6148
<b>6</b>	<b>1.6921</b>	<b>3.1365</b>	<b>4.2511</b>	<b>5.15</b>	19.5	2.8194	5.3789	7.3448	9.1551	33	4.2499	8.4085	11.7821	14.8794
6.5	<i>1.7234</i>	<i>3.2021</i>	<i>4.3428</i>	<i>5.2598</i>	<b>20</b>	<b>2.8765</b>	<b>5.4825</b>	<b>7.4748</b>	<b>9.3326</b>	33.5	4.3075	8.5371	11.9792	15.148
7	1.7547	3.2676	4.4355	5.3697	<i>20.5</i>	<i>2.9336</i>	<i>5.5862</i>	<i>7.6047</i>	<i>9.5182</i>	<b>34</b>	<b>4.3651</b>	<b>8.6657</b>	<b>12.1764</b>	<b>15.4166</b>
7.5	1.7859	3.3332	4.5298	5.4795	21	2.9907	5.6898	7.7526	9.7032	34.5	4.4225	8.7943	12.3736	15.6853
<b>8</b>	<b>1.8172</b>	<b>3.3988</b>	<b>4.6241</b>	<b>5.5894</b>	21.5	3.0477	5.7934	7.9033	9.8883	35	4.4721	8.9245	12.5708	15.9539
8.5	<i>1.8485</i>	<i>3.4643</i>	<i>4.7183</i>	<i>5.7171</i>	<b>22</b>	<b>3.1048</b>	<b>5.8971</b>	<b>8.0541</b>	<b>10.0733</b>	35.5	4.5193	9.0549	12.7679	16.2225
9	1.8798	3.5299	4.8126	5.8536	<i>22.5</i>	<i>3.1621</i>	<i>6.0007</i>	<i>8.2049</i>	<i>10.2584</i>	<b>36</b>	<b>4.5664</b>	<b>9.1853</b>	<b>12.9651</b>	<b>16.4912</b>
9.5	1.9111	3.5967	4.9069	5.9902	23	3.2105	6.1043	8.3556	10.4434	36.5	4.6135	9.3157	13.1633	16.7598
<b>10</b>	<b>1.9423</b>	<b>3.6723</b>	<b>5.0013</b>	<b>6.1268</b>	23.5	3.2581	6.2079	8.5064	10.6284	37	4.6606	9.4462	13.3646	17.0284
10.5	<i>1.9738</i>	<i>3.7484</i>	<i>5.1137</i>	<i>6.2634</i>	<b>24</b>	<b>3.3056</b>	<b>6.3135</b>	<b>8.6571</b>	<b>10.8135</b>	37.5	4.7078	9.5776	13.5659	17.3198
11	2.0143	3.8245	5.2285	6.3999	<i>24.5</i>	<i>3.3532</i>	<i>6.4231</i>	<i>8.8079</i>	<i>10.9979</i>	<b>38</b>	<b>4.7549</b>	<b>9.7119</b>	<b>13.7672</b>	<b>17.6153</b>
11.5	2.0563	3.9006	5.3433	6.5427	25	3.4008	6.5327	8.9587	11.2064	38.5	4.802	9.8462	13.9685	17.9108
<b>12</b>	<b>2.0984</b>	<b>3.9767</b>	<b>5.4581</b>	<b>6.6922</b>	25.5	3.4483	6.6424	9.1081	11.4211	39	4.8491	9.9805	14.1697	18.2063
12.5	<i>2.1405</i>	<i>4.0528</i>	<i>5.5729</i>	<i>6.8416</i>	<b>26</b>	<b>3.4959</b>	<b>6.752</b>	<b>9.2806</b>	<b>11.6358</b>	39.5	4.8962	10.1148	14.3709	18.5018
13	2.1825	4.1288	5.6877	6.991	<i>26.5</i>	<i>3.5434</i>	<i>6.8617</i>	<i>9.4534</i>	<i>11.8504</i>	<b>40</b>	<b>4.9345</b>	<b>10.2351</b>	<b>14.5346</b>	<b>18.7207</b>
13.5	2.2246	4.2049	5.8025	7.1404	27	3.591	6.9713	9.6262	12.0651					
<b>14</b>	<b>2.2666</b>	<b>4.281</b>	<b>5.9172</b>	<b>7.2899</b>	27.5	3.6386	7.081	9.799	12.2798					

Note: Training data in plain, validation data in bold, test data in italic



Table 8.5 (K1×106) from Mehrbach data (Mehrbach et al., 1973) used in NN2\_K1

T, °C	Salinity (%)								T(°C)	Salinity (%)							
	19	27	33	35	37	39	40	43		19	27	33	35	37	39	40	43
0	0.498	0.569	0.617	0.633	0.648	0.662	0.669	0.69	<b>18</b>	<b>0.726</b>	<b>0.827</b>	<b>0.894</b>	<b>0.915</b>	<b>0.935</b>	<b>0.96</b>	<b>0.965</b>	<b>0.994</b>
1	0.512	0.585	0.634	0.65	0.665	0.68	0.687	0.708	<i>19</i>	<i>0.74</i>	<i>0.84</i>	<i>0.907</i>	<i>0.928</i>	<i>0.949</i>	<i>0.97</i>	<i>0.979</i>	<i>1.008</i>
<b>2</b>	<b>0.525</b>	<b>0.6</b>	<b>0.65</b>	<b>0.666</b>	<b>0.682</b>	<b>0.697</b>	<b>0.71</b>	<b>0.73</b>	20	0.748	0.851	0.919	0.941	0.962	0.982	0.992	1.022
3	<i>0.539</i>	<i>0.615</i>	<i>0.667</i>	<i>0.683</i>	<i>0.699</i>	<i>0.72</i>	<i>0.72</i>	<i>0.75</i>	21	0.758	0.862	0.932	0.954	0.975	0.995	1.005	1.035
4	0.552	0.63	0.683	0.7	0.716	0.732	0.74	0.763	<b>22</b>	<b>0.768</b>	<b>0.873</b>	<b>0.944</b>	<b>0.966</b>	<b>0.987</b>	<b>1.01</b>	<b>1.018</b>	<b>1.048</b>
5	0.565	0.645	0.699	0.716	0.733	0.749	0.757	0.781	23	<i>0.78</i>	<i>0.88</i>	<i>0.955</i>	<i>0.977</i>	<i>0.999</i>	<i>1.02</i>	<i>1.03</i>	<i>1.06</i>
<b>6</b>	<b>0.579</b>	<b>0.66</b>	<b>0.716</b>	<b>0.733</b>	<b>0.75</b>	<b>0.766</b>	<b>0.78</b>	<b>0.8</b>	24	0.787	0.895	0.966	0.989	1.01	1.032	1.042	1.072
7	<i>0.592</i>	<i>0.675</i>	<i>0.732</i>	<i>0.749</i>	<i>0.767</i>	<i>0.78</i>	<i>0.79</i>	<i>0.82</i>	25	0.796	0.905	0.977	0.999	1.021	1.043	1.053	1.084
8	0.605	0.69	0.747	0.766	0.783	0.8	0.809	0.833	<b>26</b>	<b>0.805</b>	<b>0.914</b>	<b>0.987</b>	<b>1.01</b>	<b>1.032</b>	<b>1.05</b>	<b>1.064</b>	<b>1.095</b>
9	0.618	0.705	0.763	0.782	0.799	0.817	0.826	0.851	27	<i>0.81</i>	<i>0.92</i>	<i>0.997</i>	<i>1.02</i>	<i>1.042</i>	<i>1.06</i>	<i>1.074</i>	<i>1.105</i>
<b>10</b>	<b>0.631</b>	<b>0.719</b>	<b>0.779</b>	<b>0.797</b>	<b>0.816</b>	<b>0.833</b>	<b>0.84</b>	<b>0.87</b>	28	0.821	0.932	1.006	1.029	1.052	1.073	1.084	1.115
<i>11</i>	<i>0.643</i>	<i>0.733</i>	<i>0.794</i>	<i>0.813</i>	<i>0.832</i>	<i>0.85</i>	<i>0.86</i>	<i>0.89</i>	29	0.829	0.941	1.015	1.038	1.061	1.083	1.093	1.125
12	0.656	0.747	0.809	0.828	0.847	0.866	0.875	0.901	<b>30</b>	<b>0.836</b>	<b>0.949</b>	<b>1.023</b>	<b>1.047</b>	<b>1.069</b>	<b>1.09</b>	<b>1.102</b>	<b>1.134</b>
13	0.668	0.761	0.824	0.844	0.863	0.881	0.891	0.917	<i>31</i>	<i>0.84</i>	<i>0.96</i>	<i>1.031</i>	<i>1.055</i>	<i>1.077</i>	<i>1.1</i>	<i>1.11</i>	<i>1.142</i>
<b>14</b>	<b>0.68</b>	<b>0.775</b>	<b>0.838</b>	<b>0.858</b>	<b>0.878</b>	<b>0.897</b>	<b>0.91</b>	<b>0.93</b>	32	0.849	0.963	1.039	1.062	1.085	1.107	1.118	1.15
<i>15</i>	<i>0.692</i>	<i>0.788</i>	<i>0.853</i>	<i>0.873</i>	<i>0.893</i>	<i>0.91</i>	<i>0.92</i>	<i>0.95</i>	33	0.855	0.97	1.045	1.069	1.092	1.114	1.125	1.157
16	0.704	0.801	0.867	0.887	0.907	0.927	0.936	0.964	<b>34</b>	<b>0.861</b>	<b>0.976</b>	<b>1.052</b>	<b>1.076</b>	<b>1.099</b>	<b>1.12</b>	<b>1.132</b>	<b>1.164</b>
17	0.715	0.814	0.88	0.901	0.921	0.941	0.951	0.979	<i>35</i>	<i>0.87</i>	<i>0.98</i>	<i>1.058</i>	<i>1.082</i>	<i>1.105</i>	<i>1.13</i>	<i>1.138</i>	<i>1.17</i>

Note: Training data in plain, validation data in bold, test data in italic

Table 8.6 (K2×1010) from Mehrbach data (Mehrbach et al., 1973) used in NN2\_K2

T,°C	Salinity (%)								T(°C)	Salinity (%)							
	19	27	33	35	37	39	40	43		19	27	33	35	37	39	40	43
0	1.67	2.69	3.34	3.53	3.71	3.87	3.94	4.14	<b>18</b>	<b>3.64</b>	<b>4.95</b>	<b>5.87</b>	<b>6.17</b>	<b>6.47</b>	<b>6.76</b>	<b>6.91</b>	<b>7.34</b>
1	1.73	2.76	3.43	3.62	3.8	3.96	4.04	4.24	<i>19</i>	<i>3.8</i>	<i>5.12</i>	<i>6.07</i>	<i>6.38</i>	<i>6.69</i>	<i>6.99</i>	<i>7.14</i>	<i>7.6</i>
<b>2</b>	<b>1.81</b>	<b>2.84</b>	<b>3.52</b>	<b>3.71</b>	<b>3.9</b>	<b>4.06</b>	<b>4.14</b>	<b>4.35</b>	20	3.96	5.3	6.27	6.59	6.91	7.23	7.39	7.87
3	<i>1.88</i>	<i>2.93</i>	<i>3.61</i>	<i>3.81</i>	<i>4</i>	<i>4.17</i>	<i>4.25</i>	<i>4.47</i>	21	4.13	5.48	6.47	6.8	7.13	7.47	7.63	8.14
4	1.96	3.03	3.72	3.92	4.11	4.29	4.37	4.6	<b>22</b>	<b>4.3</b>	<b>5.66</b>	<b>6.68</b>	<b>7.02</b>	<b>7.36</b>	<b>7.71</b>	<b>7.89</b>	<b>8.42</b>
5	2.05	3.13	3.83	4.04	4.23	4.41	4.5	4.73	23	4.5	5.85	6.89	7.24	7.6	7.96	8.14	8.7
<b>6</b>	<b>2.14</b>	<b>3.23</b>	<b>3.95</b>	<b>4.16</b>	<b>4.36</b>	<b>4.55</b>	<b>4.63</b>	<b>4.88</b>	24	4.65	6.03	7.1	7.46	7.83	8.21	8.4	8.98
7	<i>2.23</i>	<i>3.34</i>	<i>4.07</i>	<i>4.29</i>	<i>4.49</i>	<i>4.69</i>	<i>4.78</i>	<i>5.03</i>	25	4.82	6.22	7.31	7.68	8.07	8.46	8.66	9.27
8	2.34	3.46	4.2	4.43	4.64	4.84	4.93	5.2	<b>26</b>	<b>5</b>	<b>6.41</b>	<b>7.52</b>	<b>7.9</b>	<b>8.3</b>	<b>8.71</b>	<b>8.92</b>	<b>9.56</b>
9	2.44	3.59	4.34	4.57	4.79	4.99	5.09	5.37	27	<i>5.2</i>	<i>6.59</i>	<i>7.72</i>	<i>8.12</i>	<i>8.54</i>	<i>8.96</i>	<i>9.18</i>	<i>9.85</i>
<b>10</b>	<b>2.55</b>	<b>3.71</b>	<b>4.49</b>	<b>4.72</b>	<b>4.95</b>	<b>5.16</b>	<b>5.26</b>	<b>5.56</b>	28	5.36	6.77	7.93	8.34	8.77	9.21	9.44	10.15
<i>11</i>	<i>2.67</i>	<i>3.85</i>	<i>4.64</i>	<i>4.88</i>	<i>5.11</i>	<i>5.33</i>	<i>5.44</i>	<i>5.75</i>	29	5.53	6.95	8.13	8.56	9	9.46	9.69	10.43
12	2.79	3.99	4.8	5.05	5.29	5.52	5.63	5.95	<b>30</b>	<b>5.71</b>	<b>7.12</b>	<b>8.33</b>	<b>8.76</b>	<b>9.22</b>	<b>9.7</b>	<b>9.94</b>	<b>10.7</b>
13	2.92	4.14	4.96	5.22	5.47	5.71	5.82	6.16	<i>31</i>	<i>5.9</i>	<i>7.29</i>	<i>8.52</i>	<i>8.97</i>	<i>9.44</i>	<i>9.93</i>	<i>10.2</i>	<i>11</i>
<b>14</b>	<b>3.06</b>	<b>4.29</b>	<b>5.13</b>	<b>5.4</b>	<b>5.65</b>	<b>5.9</b>	<b>6.02</b>	<b>6.38</b>	32	6.04	7.45	8.7	9.16	9.65	10.16	10.43	11.27
<i>15</i>	<i>3.19</i>	<i>4.45</i>	<i>5.31</i>	<i>5.58</i>	<i>5.85</i>	<i>6.11</i>	<i>6.23</i>	<i>6.61</i>	33	6.2	7.61	8.88	9.35	9.85	10.38	10.66	11.54
16	3.34	4.61	5.49	5.77	6.05	6.32	6.45	6.84	<b>34</b>	<b>6.36</b>	<b>7.75</b>	<b>9.04</b>	<b>9.53</b>	<b>10</b>	<b>10.6</b>	<b>10.88</b>	<b>11.8</b>
17	3.49	4.78	5.68	5.97	6.25	6.54	6.68	7.09	35	6.5	7.89	9.2	9.69	10.2	10.8	11.1	12

Note: Training data in plain, validation data in bold, test data in italic

Table 8.7 Sample of (K1×107) from Millero data (Millero et al., 2006) used in NN3\_K1

T(C)	Salinity	K1	T(C)	Salinity	K1	T(C)	Salinity	K1	T(C)	Salinity	K1	T(C)	Salinity	K1	T(C)	Salinity	K1
25	39.011	14.89	30	8.305	10.33	30	30.045	15.35	35	30.116	16.71	40	22.149	16.18	45	25.66	18.45
25	40.39	15.14	30	10.29	11.14	30	30.045	15.24	35	30.116	16.75	40	24.818	16.33	44.9	27.13	18.75
<b>25</b>	<b>40.39</b>	<b>15.1</b>	<b>30</b>	<b>10.29</b>	<b>10.99</b>	<b>30</b>	<b>30.919</b>	<b>15.35</b>	<b>35</b>	<b>33.062</b>	<b>17.3</b>	<b>40</b>	<b>24.818</b>	<b>17.06</b>	<b>45</b>	<b>27.13</b>	<b>18.84</b>
25	<i>40.39</i>	<i>15.17</i>	30	<i>10.29</i>	<i>11.04</i>	30	<i>30.919</i>	<i>15.38</i>	35	<i>33.062</i>	<i>17.22</i>	40	<i>24.818</i>	<i>16.87</i>	<i>45.1</i>	<i>30.1</i>	<i>19.36</i>
25	40.39	15.14	30	13.277	11.89	30.1	33.133	15.74	35	34.881	17.62	40	26.997	16.9	45.1	30.1	19.45
25	42.67	15.38	30	13.277	11.89	30	33.133	15.81	35	34.881	17.62	40	26.997	17.34	45	32.95	20.04
<b>25</b>	<b>42.67</b>	<b>15.45</b>	<b>30</b>	<b>13.277</b>	<b>11.89</b>	<b>30</b>	<b>33.133</b>	<b>15.81</b>	<b>35</b>	<b>39.562</b>	<b>18.24</b>	<b>40</b>	<b>29.736</b>	<b>17.38</b>	<b>45.1</b>	<b>32.95</b>	<b>20.23</b>
25	<i>42.67</i>	<i>15.45</i>	30	<i>15.5</i>	<i>12.36</i>	30	<i>38.789</i>	<i>16.11</i>	<i>34.9</i>	<i>39.562</i>	<i>18.2</i>	40	<i>29.736</i>	<i>17.82</i>	<i>45.3</i>	35	<i>20.09</i>
25	44.008	15.45	30	15.5	12.45	30	38.789	16.26	35	42.509	18.49	40	31.008	17.91	45	36.2	20.75
25	44.008	15.45	30	15.5	12.36	30	38.789	16.18	35	42.509	18.71	40	31.008	18.24	45	36.3	20.75
<b>25</b>	<b>44.008</b>	<b>15.45</b>	<b>30.1</b>	<b>17.231</b>	<b>12.94</b>	<b>30</b>	<b>45.344</b>	<b>17.18</b>	<b>35</b>	<b>48.513</b>	<b>19.5</b>	<b>40</b>	<b>31.008</b>	<b>18.16</b>	<b>44.9</b>	<b>37.51</b>	<b>20.7</b>
25	<i>44.236</i>	<i>15.56</i>	<i>30.2</i>	<i>17.231</i>	<i>12.88</i>	30	<i>45.344</i>	<i>17.26</i>	35	<i>48.513</i>	<i>19.59</i>	40	<i>32.604</i>	<i>18.2</i>	45	<i>43.28</i>	<i>21.93</i>
25	44.236	15.6	30	17.676	12.85	30	45.344	17.22	35	0.967	7.24	40	32.604	18.49	50	9.53	13.52
25	44.236	15.6	30	17.676	12.94	30	0.823	6.89	40	1.761	7.87	40	38.48	18.54	50	9.53	13.61
<b>25</b>	<b>45.002</b>	<b>15.56</b>	<b>30</b>	<b>17.676</b>	<b>12.76</b>	<b>35</b>	<b>2.905</b>	<b>8.69</b>	<b>40</b>	<b>2.91</b>	<b>8.77</b>	<b>40</b>	<b>38.48</b>	<b>19.54</b>	<b>50.4</b>	<b>12.4</b>	<b>14.76</b>
25	<i>45.002</i>	<i>15.67</i>	30	<i>18.33</i>	<i>13.18</i>	35	<i>4.395</i>	<i>9.08</i>	40	<i>3.932</i>	<i>9.33</i>	40	<i>44.793</i>	<i>19.59</i>	<i>49.7</i>	<i>14.97</i>	<i>16.14</i>
25	45.002	15.89	30	18.33	13.15	35	5.476	9.89	40	9.584	12.33	40	44.793	20.56	50.2	14.97	15.78
25	45.985	16.07	30.1	19.216	13.27	35	8.413	11.43	40	9.584	12.42	45	14.513	20.84	50.2	17.73	16.83
<b>25</b>	<b>45.985</b>	<b>16</b>	<b>30.1</b>	<b>19.216</b>	<b>13.3</b>	<b>35</b>	<b>11.931</b>	<b>12.47</b>	<b>40</b>	<b>12.625</b>	<b>13.49</b>	<b>45.1</b>	<b>14.513</b>	<b>15.24</b>	<b>50.2</b>	<b>19.71</b>	<b>17.14</b>
25	<i>45.985</i>	<i>16</i>	30	<i>20.853</i>	<i>13.58</i>	35	<i>14.502</i>	<i>13.34</i>	40	<i>13.779</i>	<i>14</i>	45	<i>17.814</i>	<i>15.24</i>	50	<i>21.16</i>	<i>18.2</i>
30	0.953	6.5	30	20.853	13.61	35	14.502	13.3	40	13.779	13.93	45	17.814	16.14	50.1	21.16	18.11
30	2.435	7.66	30	21.429	13.71	35	14.502	13.24	40	16.462	14.76	45	19.519	16.11	50	21.25	17.99
<b>30</b>	<b>2.435</b>	<b>7.59</b>	<b>30</b>	<b>21.429</b>	<b>13.61</b>	<b>35</b>	<b>17.876</b>	<b>14.13</b>	<b>40</b>	<b>16.462</b>	<b>14.62</b>	<b>45</b>	<b>19.519</b>	<b>16.71</b>	<b>50.3</b>	<b>24</b>	<b>18.88</b>
30	<i>2.435</i>	<i>7.59</i>	30	<i>24.674</i>	<i>14.26</i>	35	<i>17.876</i>	<i>14.09</i>	40	<i>17.864</i>	<i>15.21</i>	45	<i>21.709</i>	<i>17.14</i>	<i>49.7</i>	<i>28.024</i>	<i>20.23</i>
30	3.804	8.45	30	24.674	14.32	35	21.521	15.1	40	17.864	15.14	45	21.709	17.26	49.8	28.024	20.42
30	3.804	8.45	30	25.236	14.49	35	21.521	15.07	40	20.501	15.63	44.9	22.935	17.74	50.1	32.66	21.13
<b>30</b>	<b>5.815</b>	<b>9.44</b>	<b>30</b>	<b>25.236</b>	<b>14.49</b>	<b>35</b>	<b>24.579</b>	<b>15.67</b>	<b>40</b>	<b>20.501</b>	<b>15.85</b>	<b>45.1</b>	<b>22.935</b>	<b>17.74</b>	<b>50.5</b>	<b>32.66</b>	<b>21.23</b>
30	8.305	10.33	30	27.281	14.93	35	24.579	15.67	40	20.501	15.89	45	25.66	18.37	50	36.3	22.39

Note: Training data in plain, validation data in bold, test data in italic

Table 8.8 Sample of (K2×1010) from Millero data (Millero et al., 2006) used in NN3\_K2

T(C)	Salinity	K2	T(C)	Salinity	K2	T(C)	Salinity	K2	T(C)	Salinity	K2	T(C)	Salinity	K2	T(C)	Salinity	K2
25	39.011	12.05	30	10.29	6.04	30	30.919	12.11	35	33.062	14.96	40	26.997	15.07	45	32.957	20.7
25	40.39	12.47	30	10.29	6.14	30	30.919	12.16	35	34.881	15.56	40	26.997	15.03	45.1	32.957	20.65
<b>25</b>	<b>40.39</b>	<b>12.47</b>	<b>30</b>	<b>10.29</b>	<b>6.04</b>	<b>30.1</b>	<b>33.133</b>	<b>12.68</b>	<b>35</b>	<b>34.881</b>	<b>15.56</b>	<b>40</b>	<b>29.736</b>	<b>16.22</b>	<b>45.3</b>	<b>35</b>	<b>22.7</b>
25	40.39	12.56	30	13.277	7.01	30	33.133	12.68	35	39.562	17.34	40	29.736	16.22	45	36.2	22.44
25	40.39	12.53	30	13.277	7.01	30	33.133	12.68	34.9	39.562	17.26	40	31.008	16.56	45	36.3	22.44
25	42.67	13.09	30	13.277	7.01	30	38.789	14.39	35	42.509	18.45	40	31.008	16.83	44.9	37.51	22.7
<b>25</b>	<b>42.67</b>	<b>13.06</b>	<b>30</b>	<b>15.5</b>	<b>7.57</b>	<b>30</b>	<b>38.789</b>	<b>14.39</b>	<b>35</b>	<b>42.509</b>	<b>18.41</b>	<b>40</b>	<b>31.008</b>	<b>16.83</b>	<b>45</b>	<b>43.289</b>	<b>25.94</b>
25	42.67	13.03	30	15.5	7.59	30	38.789	14.35	35	48.513	<i>a</i>	40	32.604	17.5	50	9.534	10.05
25	44.008	13.43	30	15.5	7.57	30	45.344	15.96	35	48.513	a	40	32.604	17.54	50	9.534	9.98
25	44.008	13.52	30.1	17.231	8.09	30	45.344	16.37	35	0.967	1.83	40	38.48	19.95	50.4	12.4	12.76
<b>25</b>	<b>44.008</b>	<b>13.49</b>	<b>30.2</b>	<b>17.231</b>	<b>8.02</b>	<b>30</b>	<b>45.344</b>	<b>16</b>	<b>40</b>	<b>1.761</b>	<b>2.44</b>	<b>40</b>	<b>38.48</b>	<b>20</b>	<b>49.7</b>	<b>14.975</b>	<b>14.79</b>
25	44.236	13.49	30	17.676	8.28	30	0.823	1.5	40	2.91	3.25	40	44.793	22.59	50.2	14.975	14.16
25	44.236	13.43	30	17.676	8.22	35	2.905	2.96	40	3.932	3.95	40	44.793	22.75	50.2	17.73	16.6
25	44.236	13.49	30	17.676	8.2	35	4.395	3.78	40	9.584	7.96	45	14.513	12.53	50.2	19.717	16.71
<b>25</b>	<b>45.002</b>	<b>13.71</b>	<b>30</b>	<b>18.33</b>	<b>8.32</b>	<b>35</b>	<b>5.476</b>	<b>4.65</b>	<b>40</b>	<b>9.584</b>	<b>7.89</b>	<b>45.1</b>	<b>14.513</b>	<b>12.08</b>	<b>50</b>	<b>21.163</b>	<b>17.42</b>
25	45.002	13.61	30	18.33	8.32	35	8.413	5.97	40	12.625	9.75	45	17.814	13.43	50.1	21.163	17.3
25	45.002	13.61	30.1	19.216	8.55	35	11.931	7.94	40	13.779	10.26	45	17.814	13.49	50	21.25	17.58
25	45.985	13.93	30.1	19.216	8.61	35	14.502	8.79	40	13.779	10.02	45	19.519	14.19	50.3	24	20.61
<b>25</b>	<b>45.985</b>	<b>13.9</b>	<b>30</b>	<b>20.853</b>	<b>9.12</b>	<b>35</b>	<b>14.502</b>	<b>8.97</b>	<b>40</b>	<b>16.462</b>	<b>11.43</b>	<b>45</b>	<b>19.519</b>	<b>14.22</b>	<b>49.7</b>	<b>28.024</b>	<b>21.33</b>
25	45.985	13.58	30	20.853	9.16	35	14.502	8.89	40	16.462	11.32	45	21.709	15.24	49.8	28.024	21.18
30	0.953	1.4	30	21.429	9.18	35	17.876	10	40	17.864	11.51	45	21.709	15.14	50.1	32.66	24.1
30	2.435	2.38	30	21.429	9.18	35	17.876	9.84	40	17.864	11.53	44.9	22.935	15.63	50.5	32.66	24.1
<b>30</b>	<b>2.435</b>	<b>2.35</b>	<b>30</b>	<b>24.674</b>	<b>10.09</b>	<b>35</b>	<b>21.521</b>	<b>11.46</b>	<b>40</b>	<b>20.501</b>	<b>12.53</b>	<b>45.1</b>	<b>22.935</b>	<b>15.6</b>	<b>50</b>	<b>36.3</b>	<b>27.48</b>
30	2.435	2.39	30	24.674	10.12	35	21.521	11.43	40	20.501	12.74	45	25.66	17.38	50	36.3	27.48
30	3.804	3.03	30	25.236	10.33	35	24.579	11.97	40	20.501	12.94	45	25.66	17.34	50.2	36.34	27.61
30	3.804	3.01	30	25.236	10.28	35	24.579	11.89	40	22.149	13.09	45	25.66	17.34	50	46.291	a
<b>30</b>	<b>5.815</b>	<b>4.15</b>	<b>30</b>	<b>27.281</b>	<b>10.86</b>	<b>35</b>	<b>28.39</b>	<b>13.18</b>	<b>40</b>	<b>22.149</b>	<b>13.58</b>	<b>44.9</b>	<b>27.133</b>	<b>17.82</b>			
30	8.305	5.38	30	27.281	10.91	35	30.116	13.93	40	24.818	14.69	45	27.133	17.58			

Note: Training data in plain, validation data in bold, test data in italic

## 8.6.2 NN Based Correlations for Different Data Sets

In this work, three different NN based correlations have been developed to estimate the first and the second dissociation constant  $K_1$  and  $K_2$  respectively. These correlations (NN1\_K1 and NN1\_K2) are based on the data source from Millero (1997), (NN2\_K1 and NN2\_K2) are based on the data source from Mehrbach et al. (1973) and (NN3\_K1 and NN3\_K2) are based on the data source from Millero et al. (2006).

In these NN based correlations, the number of neurons in the first layer, hidden layer and third layer were found 2, 4, and 1 respectively (Figure 8.6). Between the input and first layer, the transfer function was tangent function and between the first and second layer was purline. In addition, the transfer function between the second and third function was purline.

For each of the NN based correlations, first 2 input data points are selected for training, the next input data point for validation (shown in bold) and the fourth one is selected for testing (shown in italic ) (shown in Tables 8.3-8.8). This selection process continues sequentially until all the data points are exhausted. Thus, the total input data are divided into three sets: training (50%), validation (25%), and testing (25%) datasets.

### 8.6.2.1 The Correlations

With reference to Figure 8.3, the NN based correlations (NN1\_K1, NN1\_K2, NN2\_K1, NN2\_K2, NN3\_k1, and NN3\_K2) can be expressed as follows:

The values of the first layer, second and third layer neurons are:

$$a_1^1 = \tanh ( w_{11} \times T_{\text{scaleup}} + w_{11} \times S_{\text{scaleup}} + b_1 )$$

$$a_2^1 = \tanh ( w_{21} \times T_{\text{scaleup}} + w_{22} \times S_{\text{scaleup}} + b_2 )$$

$$a_1^2 = w_{11}^2 \times a_1^1 + w_{21}^2 \times a_2^1 + w_{31}^2 \times a_3^1 + w_{41}^2 \times a_4^1 + b_1^2$$

$$a_2^2 = w_{12}^2 \times a_1^1 + w_{22}^2 \times a_2^1 + w_{32}^2 \times a_3^1 + w_{42}^2 \times a_4^1 + b_2^2$$

$$a_3^2 = w_{13}^2 \times a_1^1 + w_{23}^2 \times a_2^1 + w_{33}^2 \times a_3^1 + w_{43}^2 \times a_4^1 + b_3^2$$

$$a_4^2 = w_{14}^2 \times a_1^1 + w_{24}^2 \times a_2^1 + w_{34}^2 \times a_3^1 + w_{44}^2 \times a_4^1 + b_4^2$$

$$a_1^1 = \tanh (w_{11} \times T_{\text{scaleup}} + w_{11} \times S_{\text{scaleup}} + b_1)$$

$$a_2^1 = \tanh (w_{21} \times T_{\text{scaleup}} + w_{22} \times S_{\text{scaleup}} + b_2)$$

$$K1_{\text{scaleup}} \times 10^7 = a_1^3 = w_{11}^3 \times a_1^2 + w_{12}^3 \times a_2^2 + w_{13}^3 \times a_3^2 + w_{14}^3 \times a_4^2 + b_1^3$$

$$K2_{\text{scaleup}} \times 10^{10} = a_1^3 = w_{11}^3 \times a_1^2 + w_{12}^3 \times a_2^2 + w_{13}^3 \times a_3^2 + w_{14}^3 \times a_4^2 + b_1^3$$

Table 8.9 shows the parameters used in scale up (Equations. 8.16, 8.17, 8.19) for different correlations. The different weights and biases for the different NN based correlations are shown in Tables 8.10-8.15.

The statistical regression between predicted data (A) values of  $K_1$  and  $K_2$  by NN correlations and experimental data (T) is plotted to find the overall trends of the predicted data (example Figure 8.7). The regression analysis plot is used to determine the optimum network. The network architecture is updated (according to Figure 8.3) until the regression value (R) is close to 1.

Table 8.9 Scaled up parameters for NN based correlations

	NN1	NN2	NN3
std_T	11.41	10.406	17.14
std_S	11.19	7.31	12.07
std_K1	3.4	0.157	4.185
std_K2	4	2.315	5.413
mean_T	20.5	17.5	21.11
mean_S	20	34.12	24.85
mean_k1	10.83	0.8768	11.6
mean_k2	6.76	6.15	8.07

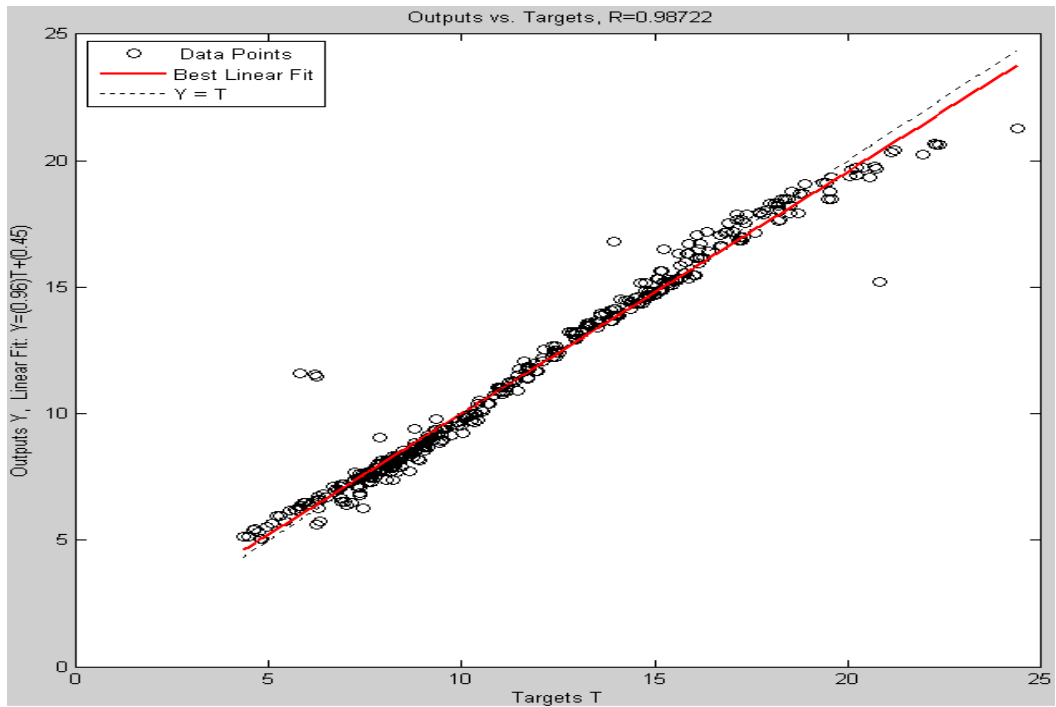


Figure 8.7 Regression of NN1\_K1 Predicted Data with Experiment K1

Table 8.10 Weights and Biases of the NN1\_K1

1 <sup>st</sup> Layer			2 <sup>nd</sup> Layer				3 <sup>rd</sup> Layer		
Weights	Bias	TF	Weights	Weights	Bias	TF	Weights	Bias	TF
$w_{11} = 0.0188$	$b_1 = -0.536$	tanh	$w_{11}^2 = -3.660$	$w_{21}^2 = 1.764$	$b_1^2 = -0.590$	1	$w_{11}^3 = -3.969$	$b_1^3 = 1.065$	1
$w_{21} = -0.064$	$b_2 = -0.520$	tanh	$w_{12}^2 = 0.470$	$w_{22}^2 = -1.179$	$b_2^2 = 0.339$	1	$w_{12}^3 = 1.145$		1
$w_{12} = 0.200$		tanh	$w_{13}^2 = -0.285$	$w_{23}^2 = -0.763$	$b_3^2 = 0.992$	1	$w_{13}^3 = 0.447$		1
$w_{22} = 0.379$		tanh	$w_{14}^2 = -2.704$	$w_{24}^2 = 0.355$	$b_4^2 = -0.806$	1	$w_{14}^3 = -2.662$		1

Table 8.11 Weights and Biases of the NN1\_K2

1 <sup>st</sup> Layer			2 <sup>nd</sup> Layer				3 <sup>rd</sup> Layer		
Weights	Bias	TF	Weights	Weights	Bias	TF	Weights	Bias	TF
$w_{11} = 0.2840$	$b_1 = -1.360$	tanh	$w_{11}^2 = -1.037$	$w_{21}^2 = 1.812$	$b_1^2 = 0.845$	1	$w_{11}^3 = 1.929$	$b_1^3 = 0.836$	1
$w_{21} = 0.2520$	$b_2 = -1.113$	tanh	$w_{12}^2 = -2.416$	$w_{22}^2 = 2.457$	$b_2^2 = 0.086$	1	$w_{12}^3 = 3.308$		1
$w_{12} = -0.148$		tanh	$w_{13}^2 = -0.795$	$w_{23}^2 = -0.125$	$b_3^2 = 0.765$	1	$w_{13}^3 = 0.711$		1
$w_{22} = 0.022$		tanh	$w_{14}^2 = -1.165$	$w_{24}^2 = 2.458$	$b_4^2 = -0.333$	1	$w_{14}^3 = 2.580$		1



Table 8.12 Weights and Biases of the NN2\_K1

1 <sup>st</sup> Layer			2 <sup>nd</sup> Layer				3 <sup>rd</sup> Layer		
Weights	Bias	TF	Weights	Weights	Bias	TF	Weights	Bias	TF
$w_{11} = 0.656$	$b_1 = -2.210$	tanh	$w_{11}^2 = 0.281$	$w_{21}^2 = 0.874$	$b_1^2 = 0.916$	1	$w_{11}^3 = 0.060$	$b_1^3 = 0.294$	1
$w_{21} = 0.522$	$b_2 = -0.216$	tanh	$w_{12}^2 = -0.776$	$w_{22}^2 = 1.151$	$b_2^2 = -0.034$	1	$w_{12}^3 = 1.038$		1
$w_{12} = -1.194$		tanh	$w_{13}^2 = -0.403$	$w_{23}^2 = -0.576$	$b_3^2 = 0.568$	1	$w_{13}^3 = 0.378$		1
$w_{22} = 0.133$		tanh	$w_{14}^2 = 0.0545$	$w_{24}^2 = 1.203$	$b_4^2 = -0.713$	1	$w_{14}^3 = 1.132$		1

Table 8.13 Weights and Biases of the NN2\_K2

1 <sup>st</sup> Layer			2 <sup>nd</sup> Layer				3 <sup>rd</sup> Layer		
Weights	Bias	TF	Weights	Weights	Bias	TF	Weights	Bias	TF
$w_{11} = 0.449$	$b_1 = -2.740$	tanh	$w_{11}^2 = 0.224$	$w_{21}^2 = 0.916$	$b_1^2 = 0.909$	1	$w_{11}^3 = 0.163$	$b_1^3 = 0.261$	1
$w_{21} = 0.371$	$b_2 = -1.225$	tanh	$w_{12}^2 = -2.074$	$w_{22}^2 = 1.846$	$b_2^2 = -0.119$	1	$w_{12}^3 = 2.636$		1
$w_{12} = -0.538$		tanh	$w_{13}^2 = -0.851$	$w_{23}^2 = -0.354$	$b_3^2 = 0.548$	1	$w_{13}^3 = 0.668$		1
$w_{22} = 0.146$		tanh	$w_{14}^2 = -1.030$	$w_{24}^2 = 1.786$	$b_4^2 = -0.771$	1	$w_{14}^3 = 2.037$		1

Table 8.14 Weights and Biases of the NN3\_K1

1 <sup>st</sup> Layer			2 <sup>nd</sup> Layer				3 <sup>rd</sup> Layer		
Weights	Bias	TF	Weights	Weights	Bias	TF	Weights	Bias	TF
$w_{11}=0.656$	$b_1 = -2.210$	tanh	$w_{11}^2 = 0.281$	$w_{21}^2 = 0.874$	$b_1^2 = 0.916$	1	$w_{11}^3 = -0.060$	$b_1^3 = 0.294$	1
$w_{21}=0.522$	$b_2 = -0.216$	tanh	$w_{12}^2 = -0.776$	$w_{22}^2 = 1.151$	$b_2^2 = -1.194$	1	$w_{12}^3 = 1.038$		1
$w_{12} = -1.194$		tanh	$w_{13}^2 = -0.403$	$w_{23}^2 = -0.576$	$b_3^2 = 0.568$	1	$w_{13}^3 = 0.378$		1
$w_{22} = 0.133$		tanh	$w_{14}^2 = 0.054$	$w_{24}^2 = 1.203$	$b_4^2 = -0.713$	1	$w_{14}^3 = 1.132$		1

Table 8.15 Weights and Biases of the NN3\_K2

1 <sup>st</sup> Layer			2 <sup>nd</sup> Layer				3 <sup>rd</sup> Layer		
Weights	Bias	TF	Weights	Weights	Bias	TF	Weights	Bias	TF
$w_{11}=0.449$	$b_1 = -2.740$	tanh	$w_{11}^2 = 0.224$	$w_{21}^2 = -0.916$	$b_1^2 = 0.909$	1	$w_{11}^3 = 0.163$	$b_1^3 = 0.261$	1
$w_{21}=0.371$	$b_2 = -1.22$	tanh	$w_{12}^2 = -2.074$	$w_{22}^2 = 1.846$	$b_2^2 = -0.11$	1	$w_{12}^3 = 2.636$		1
$w_{12} = -0.538$		tanh	$w_{13}^2 = -0.851$	$w_{23}^2 = -0.354$	$b_3^2 = 0.548$	1	$w_{13}^3 = 0.668$		1
$w_{22} = 0.146$		tanh	$w_{14}^2 = -1.038$	$w_{24}^2 = 1.786$	$b_4^2 = -0.771$	1	$w_{14}^3 = 2.037$		1

## 8.7 Results and Discussions

Sample experimental data from different sources and predictions by different NN based correlations are shown in Figures 8.8-8.13. For each data source, the corresponding NN based correlation predicted the  $K_1$  and  $K_2$  values are found to be close to the experiment data.

Each correlation was also used to predict  $K_1$  and  $K_2$  values based on (salinity, temperature) which were never used for training, validation or testing the correlation. For example, NN1\_K1 and NN1\_K2 are used to predict  $K_1$  and  $K_2$  at  $T=40$  °C at different salinity values (Figures 8.8 and 8.9); NN2\_K1 and NN2\_K2 is used to predict  $K_1$  and  $K_2$  at  $T=35$  °C = at different salinity values (Figures 8.10 and 8.11); and NN3\_K1 and NN3\_K3 is used to predict  $K_1$  and  $K_2$  at  $T= 50$  °C at different salinity values (Figure 8.12 and 8.13). The results clearly show that the predictions by the correlations follow the expected trends.

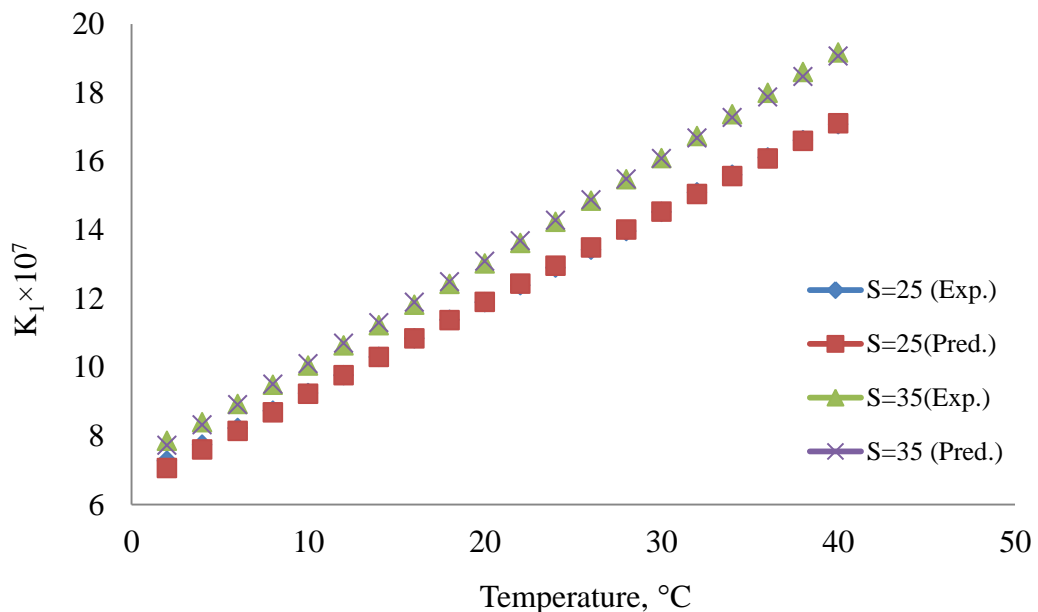


Figure 8.8 Experimental  $K_1$  by Millero et al. (1997) and Prediction by NN1\_K1

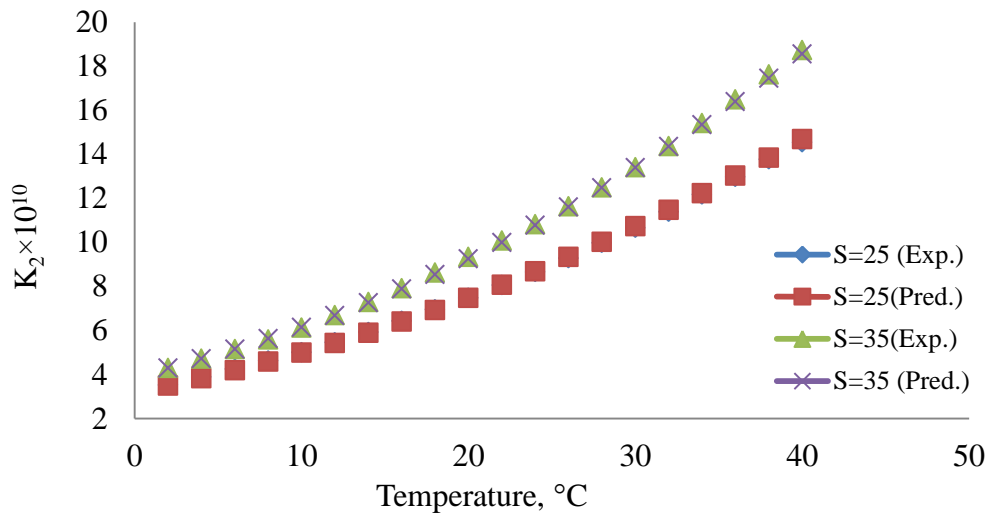


Figure 8.9 Experimental K2 by Millero et al. (1997) and Prediction by NN1\_K2

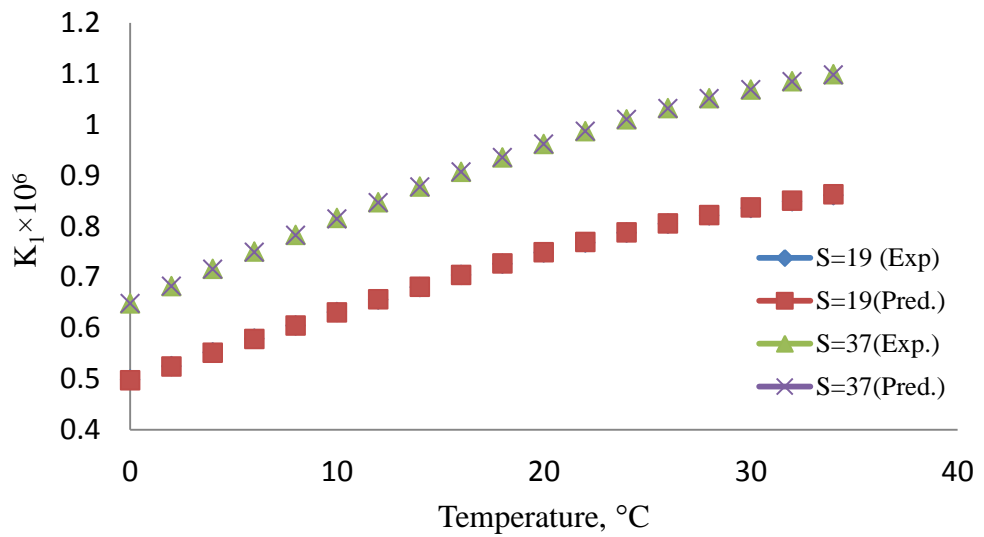


Figure 8.10 Experimental K1 by Mehrbach et al. (1973) and Prediction by NN2\_K1

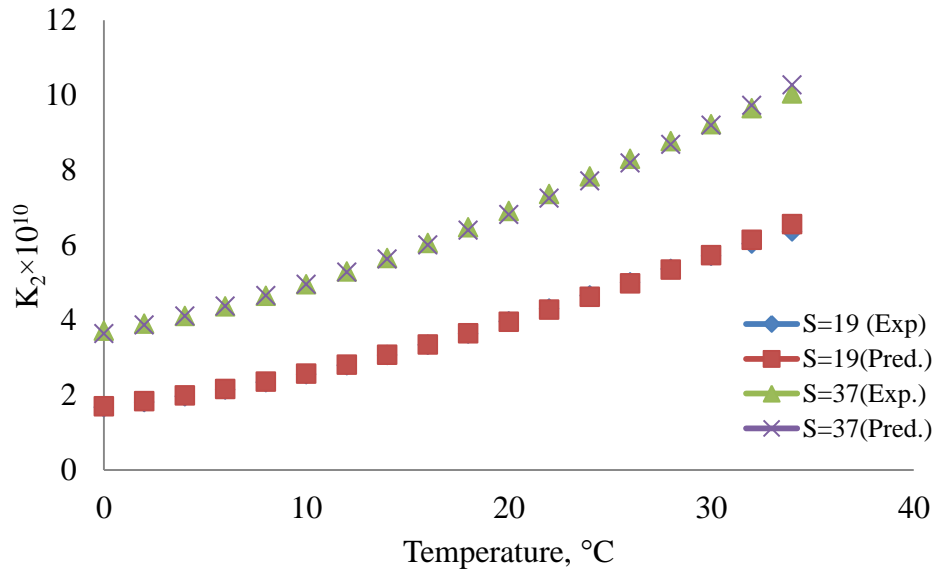


Figure 8.11 Experimental K2 by Mehrbach et al. (1973) and Prediction by NN2\_K2

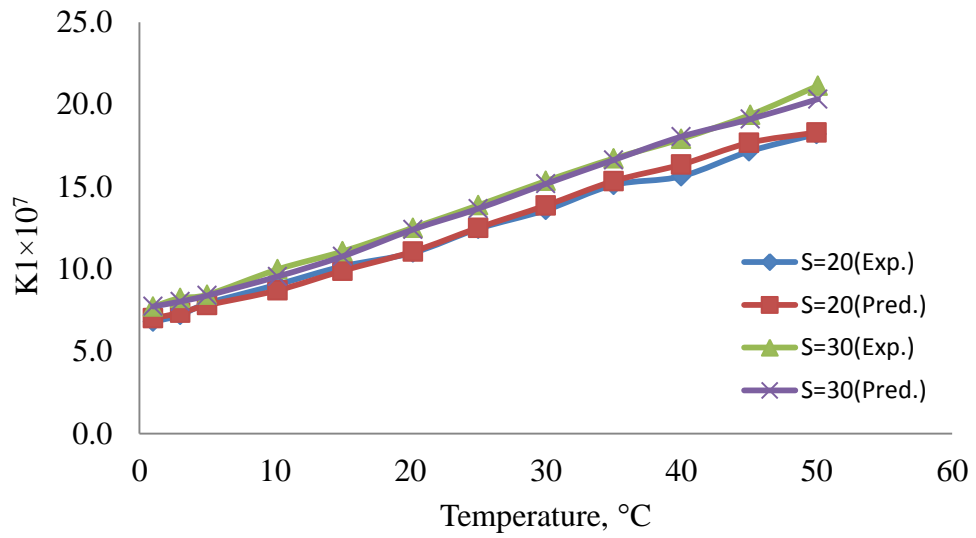


Figure 8.12 Experimental K1 by Millero et al. (2006) and Prediction by NN3\_K1

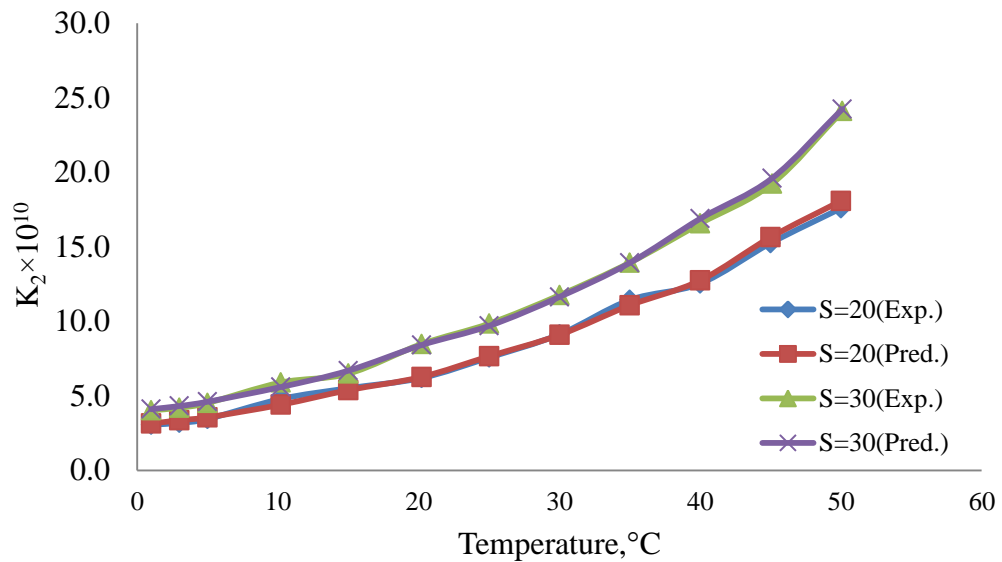


Figure 8.13 Experimental  $K_2$  by Millero et al. (1997) and Prediction by NN3\_K2

It would be interesting now to examine how different NN based correlations predict  $K_1$  and  $K_2$  values using the (temperature, salinity) data from sources other than the sources used to develop the correlation using the same range. For example NN1\_K1 and NN1\_k2 was developed using the temperature range  $1 < T < 40$   $^{\circ}\text{C}$ , and salinity  $5 < S < 35$  wt% (Tables 8.4 and 8.5). NN1\_K1 and NN1\_K2 are now used to predict  $K_1$  and  $K_2$  values using Mehrbach data within the range of  $0 < T < 30$   $^{\circ}\text{C}$ , and salinity  $19 < S < 43$  wt%. The results are shown in Tables 8.16 and 8.17. Similarly prediction of  $K_1$  and  $K_2$  by (NN1\_K1, NN1\_K2) using Millero (2006) data within the range of  $0 < T < 50$   $^{\circ}\text{C}$ , and salinity  $1 < S < 50$  wt. % are shown in Tables 8.18 and 8.19. Prediction of  $K_1$  and  $K_2$  by NN2\_K1 and NN2\_K2 for Millero (1997) and Millero (2006) within a given range of temperature and salinity are shown in Tables 8.20-8.23. In addition, prediction of  $K_1$  and  $K_2$  by NN3\_K1 and NN3\_K2 for Millero (1997) and Mehrbach (2006) within a given range of temperature and salinity are shown in Tables 5.24-5.27.

In each of Tables 8.16-8.27, the predicated  $K_1$  and  $K_2$  are compared with the experimental  $K_1$  and  $K_2$ . They are interesting to note that prediction of  $K_1$  and  $K_2$  by

NN1\_K1 and NN1\_K2 are close to Millero (2006) data (compare  $K_1$  and  $K_2$  in Tables 8.18 and 8.19). Also predictions of  $K_1$  and  $K_2$  by NN2\_K1 and NN2\_K2 are close to Millero (2006) data (compare  $K_1$  and  $K_2$  in Tables 8.22 and 8.23). However, predictions of prediction of  $K_1$  by NN1\_K1 were not as close as expected to the experimental by Mehrbach data (Table 8.17). Also predictions of  $K_1$  and  $K_2$  by NN3\_K1 and NN3\_K2 were not close to experimental  $K_1$  by Mehrbach data (Table 8.26 and 8.27).

## 8.8 Conclusions

Three NN based correlations for predicting the first dissociation constant ( $K_1$ ) and second dissociation constant ( $K_2$ ) of carbonic acid in seawater. For each correlation, a multi-layered feed forward network trained with back propagation method is used. The NN based correlations can predict the experimental  $K_1$  and  $K_2$  very closely to the values of  $K_1$  and  $K_2$  obtained by using correlations from literature. The proposed NN model structure (with one hidden and four neurons in hidden layer) is capable of predicting the experiment  $K_1$  and  $K_2$  very closely. It is found that, the NN1\_K1 and NN1\_K2 developed based on experimental data of Millero (1997) can predicted the values of  $K_1$  and  $K_2$  when compared with NN2\_K1, NN2\_K2, NN3\_K1 and NN3\_K2 correlations. The neural network based correlations developed in this chapter can predict the values of  $K_1$  and  $K_2$  for temperature less than or equal 50 °C based on the experimental data available. Multistage flash (MSF) plants usually operate at temperature as high as 90 °C. Therefore, the extrapolation of the NN correlations will be used when applying the correlations in further application to adequate the MSF temperature conditions.

Table 8.16 Comparison of  $K1 \times 10^7$  values prediction by NN1\_K1 and experiment data from Mehrbach et al. (1973) Range : T=<0-35 °C>, S=<19-43wt%>

Temp	Salinity	K1exp	NN1_K1	Temp	Salinity	K1exp	NN1_K1
0	19	0.630658	0.498	11	39	1.107647	0.85
1	19	0.65482	0.512	12	39	1.137347	0.866
2	19	0.678926	0.525	13	39	1.167088	0.881
3	19	0.702977	0.539	14	39	1.196871	0.897
4	19	0.726971	0.552	15	39	1.226693	0.912
5	19	0.750908	0.565	16	39	1.256554	0.927
6	19	0.774789	0.579	17	39	1.286453	0.941
7	19	0.798611	0.592	18	39	1.316387	0.955
8	19	0.822375	0.605	19	39	1.346358	0.969
9	19	0.846082	0.618	20	39	1.376362	0.982
10	19	0.869729	0.631	0	40	0.808083	0.669
0	27	0.656634	0.569	1	40	0.837055	0.687
1	27	0.684733	0.585	2	40	0.866086	0.705
2	27	0.712811	0.6	3	40	0.895174	0.722
3	27	0.740867	0.615	4	40	0.924318	0.74
4	27	0.768902	0.63	5	40	0.953517	0.757
5	27	0.796912	0.645	6	40	0.982771	0.775
6	27	0.824898	0.66	7	40	1.012077	0.792
7	27	0.852859	0.675	8	40	1.041437	0.809
8	27	0.880793	0.69	9	40	1.070848	0.826
9	27	0.9087	0.705	10	40	1.100309	0.842
10	27	0.936579	0.719	24	43	1.591242	1.072
0	35	0.713197	0.633	25	43	1.620863	1.084
1	35	0.742736	0.65	26	43	1.650533	1.095
2	35	0.772307	0.666	27	43	1.680251	1.105
3	35	0.801906	0.683	28	43	1.710017	1.115
4	35	0.831534	0.7	29	43	1.739829	1.125
5	35	0.86119	0.716	30	43	1.769687	1.134
6	35	0.890871	0.733	31	43	1.799589	1.142
7	35	0.920576	0.749	32	43	1.829535	1.15
8	35	0.950306	0.766	33	43	1.859522	1.157
9	35	0.980058	0.782	34	43	1.889551	1.164
10	35	1.009831	0.797	35	43	1.919621	1.17
Maximum deviation				0.21			



Table 8 17 Comparison of  $K2 \times 10^{10}$  values prediction by NN1\_K2 and experiment data from Mehrbach et al. (1973) Range: T=<0-35 °C >, S=<19-43wt %>

Temp	Salinity	K2exp	NN1_K2	Temp	Salinity	K2exp	NN1_K2
0	19	0.630658	0.498	11	39	1.107647	0.85
1	19	0.65482	0.512	12	39	1.137347	0.866
2	19	0.678926	0.525	13	39	1.167088	0.881
3	19	0.702977	0.539	14	39	1.196871	0.897
4	19	0.726971	0.552	15	39	1.226693	0.912
5	19	0.750908	0.565	16	39	1.256554	0.927
6	19	0.774789	0.579	17	39	1.286453	0.941
7	19	0.798611	0.592	18	39	1.316387	0.955
8	19	0.822375	0.605	19	39	1.346358	0.969
9	19	0.846082	0.618	20	39	1.376362	0.982
10	19	0.869729	0.631	0	40	0.808083	0.669
0	27	0.656634	0.569	1	40	0.837055	0.687
1	27	0.684733	0.585	2	40	0.866086	0.705
2	27	0.712811	0.6	3	40	0.895174	0.722
3	27	0.740867	0.615	4	40	0.924318	0.74
4	27	0.768902	0.63	5	40	0.953517	0.757
5	27	0.796912	0.645	6	40	0.982771	0.775
6	27	0.824898	0.66	7	40	1.012077	0.792
7	27	0.852859	0.675	8	40	1.041437	0.809
8	27	0.880793	0.69	9	40	1.070848	0.826
9	27	0.9087	0.705	10	40	1.100309	0.842
10	27	0.936579	0.719	24	43	1.591242	1.072
0	35	0.713197	0.633	25	43	1.620863	1.084
1	35	0.742736	0.65	26	43	1.650533	1.095
2	35	0.772307	0.666	27	43	1.680251	1.105
3	35	0.801906	0.683	28	43	1.710017	1.115
4	35	0.831534	0.7	29	43	1.739829	1.125
5	35	0.86119	0.716	30	43	1.769687	1.134
6	35	0.890871	0.733	31	43	1.799589	1.142
7	35	0.920576	0.749	32	43	1.829535	1.15
8	35	0.950306	0.766	33	43	1.859522	1.157
9	35	0.980058	0.782	34	43	1.889551	1.164
10	35	1.009831	0.797	35	43	1.919621	1.17
Maximum deviation				0.6			

Table 8.18 Comparison of  $K1 \times 10^7$  values prediction by NN1\_K1 and experiment data from Millero et al. (2006) Range: T=<1.1-50.5 °C>, S=<3.47-46.29wt %>

Temp	Salinity	K1exp	NN1_K1	Temp	Salinity	K1exp	NN1_K1
1.1	3.47	4.345102	4.549665	35	2.91	8.689604	8.944013
1.2	3.47	4.477133	4.56409	35	4.40	9.078205	9.514672
1	4.35	4.753352	4.711484	35	5.48	9.885531	9.924714
1.2	4.70	4.613176	4.809484	35	8.41	11.42878	11.01423
1.2	4.93	4.655861	4.853266	35	11.93	12.47384	12.25178
1	5.56	4.931738	4.941603	35	14.50	13.33521	13.09381
1	6.28	5.069907	5.072298	35	14.50	13.30454	13.09381
1.2	8.15	5.211947	5.426529	35	14.50	13.24342	13.09381
1.2	8.15	5.296634	5.426529	35	17.88	14.12538	14.10126
1.2	9.97	5.546257	5.705135	35	17.88	14.09289	14.10126
5	22.17	7.888601	7.723468	40	1.76	7.870458	9.099497
5	23.47	8.090959	7.794382	40	2.91	8.770008	9.569785
6	24.00	8.07235	8.088499	40	3.93	9.332543	9.986839
5	25.47	8.203515	7.894409	40	9.58	12.33105	12.23723
5	25.47	8.222426	7.894409	40	9.58	12.41652	12.23723
5	25.47	8.203515	7.894409	40	12.63	13.48963	13.37743
5	26.35	8.147043	7.936856	40	13.78	13.99587	13.79147
5	26.35	8.109611	7.936856	40	13.78	13.93157	13.79147
5	26.35	8.203515	7.936856	40	16.46	14.75707	14.70697
5.1	26.51	8.279422	7.972647	40	16.46	14.62177	14.70697
25	27.71	13.52073	13.60371	40	17.86	15.20548	15.15647
25	27.71	13.52073	13.60371	40	17.86	15.13561	15.15647
25	27.71	13.52073	13.60371	40	20.50	15.63148	15.94357
25	27.71	13.52073	13.60371	50	21.25	17.98871	18.43854
25	30.00	13.86756	13.90343	50.3	24.00	18.87991	19.39624
25	30.00	13.89953	13.90343	49.7	28.02	20.23019	20.37472
25	30.00	13.86756	13.90343	49.8	28.02	20.41738	20.40133
25	30.00	13.89953	13.90343	50.1	32.66	21.13489	21.57799
25	30.00	13.89953	13.90343	50.5	32.66	21.23244	21.69319
25	31.85	13.93157	14.1434	50	36.30	22.38721	22.31139
25	31.85	14.02814	14.1434	50	36.30	22.28435	22.31139
25	31.85	14.06048	14.1434	50.2	36.34	22.2331	22.37957
25	31.85	13.99587	14.1434	50	46.29	24.37811	24.59391
Maximum deviation				0.04			

Table 8.19 Comparison of  $K_2 \times 10^{10}$  values prediction by NN1\_K2 and experiment data from Millero et al. (2006.) Range: T=<1.1-50.5 °C>, S=<3.47-46.29 wt%>

Temp	Salinity	K2exp	NN2_K2	Temp	Salinity	K2exp	NN1_K2
1.1	3.47	1.135011	1.163907	35	14.50	8.892011	8.658414
1.2	3.47	1.161449	1.169738	35	17.88	10	10.00565
1	4.35	1.193988	1.266311	35	17.88	9.840111	10.00565
1.2	4.70	1.321296	1.321444	35	21.52	11.45513	11.38481
1.2	4.93	1.393157	1.348935	35	21.52	11.42878	11.38481
1	5.56	1.383566	1.410903	35	24.58	11.96741	12.48343
1	6.28	1.489361	1.495143	35	24.58	11.88502	12.48343
1.2	8.15	1.901078	1.726807	35	28.39	13.18257	13.78168
1.2	8.15	1.901078	1.726807	35	30.12	13.93157	14.34491
1.2	9.97	2.094112	1.929018	35	30.12	13.93157	14.34491
1.1	10.35	2.070141	1.961565	44.9	22.94	15.63148	15.77978
1.3	10.35	2.06538	1.980484	45.1	22.94	15.59553	15.86119
5	22.17	3.715352	3.725496	45	25.66	17.37801	17.17195
5	22.17	3.689776	3.725496	45	25.66	17.33804	17.17195
5	22.17	3.672823	3.725496	45	25.66	17.33804	17.17195
5	23.47	3.79315	3.859188	44.9	27.13	17.82379	17.83455
6	24.00	4.064433	4.092309	45	27.13	17.57924	17.88171
5	25.47	3.990249	4.060687	45.1	30.14	19.23092	19.33794
5	25.47	3.990249	4.060687	45.1	30.14	19.09853	19.33794
5	25.47	3.990249	4.060687	45	32.96	20.70141	20.54924
5	26.35	4.295364	4.146264	50.2	14.98	14.15794	13.04254
5	26.35	4.265795	4.146264	50.2	17.73	16.59587	14.78919
5	26.35	4.335109	4.146264	50.2	19.72	16.71091	16.01576
25	27.71	9.268298	9.632618	50	21.16	17.41807	16.81508
25	27.71	9.246982	9.632618	50.1	21.16	17.29816	16.85294
25	27.71	9.225714	9.632618	50	21.25	17.57924	16.86697
25	30.00	9.840111	10.13937	50.3	24.00	20.6063	18.60679
25	30.00	9.862795	10.13937	49.7	28.02	21.33045	20.5968
25	30.00	9.840111	10.13937	49.8	28.02	21.18361	20.64557
25	30.00	9.862795	10.13937	50.1	32.66	24.09905	23.26611
25	30.00	9.908319	10.13937	50.5	32.66	24.09905	23.48971
25	31.85	10.3992	10.53518	50	36.30	27.47894	25.04409
25	31.85	10.28016	10.53518	50	36.30	27.47894	25.04409
Maximum deviation				0.025			

Table 8.20 Comparison of  $K1 \times 10^7$  values prediction by NN2\_K1 and experiment data from Millero et al. (1997) Range: T=<1-40 °C>, S=<5-35wt %>

Temp	Salinity	K1exp	NN2_K1	Temp	Salinity	K1exp	NN2_K1
1.00	5	4.8796	3.610403	16.00	25	10.8329	7.783184
1.50	5	4.9508	3.660016	16.50	25	10.9689	7.846056
2.00	5	5.0221	3.709729	17.00	25	11.1049	7.908156
2.50	5	5.0934	3.759532	17.50	25	11.2409	7.969462
3.00	5	5.1647	3.809413	18.00	25	11.3769	8.029952
3.50	5	5.236	3.859361	18.50	25	11.5129	8.089607
4.00	5	5.3072	3.909365	19.00	25	11.6446	8.148407
4.50	5	5.3785	3.959415	19.50	25	11.7684	8.206333
5.00	5	5.4498	4.009499	20.00	25	11.8923	8.263367
5.50	5	5.5211	4.059606	20.50	25	12.0161	8.319491
1.00	15	6.2363	4.710131	21.00	25	12.1399	8.374689
1.50	15	6.3397	4.772817	21.50	25	12.2638	8.428946
2.00	15	6.4431	4.835528	22.00	25	12.3876	8.482246
2.50	15	6.5466	4.898243	22.50	25	12.5114	8.534576
3.00	15	6.65	4.960941	23.00	25	12.6369	8.585923
3.50	15	6.7535	5.0236	23.50	25	12.7672	8.636275
4.00	15	6.8569	5.0862	24.00	25	12.8976	8.685621
4.50	15	6.9603	5.14872	24.50	25	13.028	8.733951
5.00	15	7.0638	5.211138	25.00	25	13.1583	8.781255
5.50	15	7.1672	5.273433	33.50	35	17.2121	10.70854
6.00	15	7.2707	5.335584	34.00	35	17.3726	10.73912
6.50	15	7.3741	5.39757	34.50	35	17.5331	10.76842
7.00	15	7.4769	5.459368	35.00	35	17.6918	10.79645
7.50	15	7.5796	5.520958	35.50	35	17.8436	10.82322
8.00	15	7.6824	5.582318	36.00	35	17.9952	10.84873
8.50	15	7.79	5.643429	36.50	35	18.1467	10.873
12.50	25	9.9003	7.323398	37.00	35	18.2983	10.89602
13.00	25	10.0321	7.391021	37.50	35	18.4499	10.91781
13.50	25	10.164	7.458039	38.00	35	18.6015	10.93837
14.00	25	10.2958	7.524427	38.50	35	18.7531	10.95773
14.50	25	10.4277	7.590159	39.00	35	18.904	10.9759
15.00	25	10.5609	7.655212	39.50	35	19.0503	10.99288
15.50	25	10.6969	7.719562	40.00	35	19.1677	11.00869
Maximum deviation				0.26			

Table 8.21 Comparison of  $K_2 \times 10^{10}$  values prediction by NN2\_K2 and experiment data from Millero et al. (1997) Range: T=<1-40 °C>, S=<5-35wt %>

Temp	Salinity	K2exp	NN2_K2	Temp	Salinity	K2exp	NN2_K2
1.00	5	1.3793	1.170502	16.00	25	6.435	4.314554
1.50	5	1.4106	1.18686	16.50	25	6.565	4.387068
2.00	5	1.4419	1.203633	17.00	25	6.695	4.460641
2.50	5	1.4732	1.22083	17.50	25	6.8249	4.535299
3.00	5	1.5044	1.238463	18.00	25	6.9549	4.611068
3.50	5	1.5357	1.256541	18.50	25	7.0849	4.687971
4.00	5	1.567	1.275074	19.00	25	7.2148	4.766031
4.50	5	1.5983	1.294073	19.50	25	7.3448	4.84527
5.00	5	1.6296	1.31355	20.00	25	7.4748	4.925709
5.50	5	1.6608	1.333514	20.50	25	7.6047	5.007368
1.00	15	2.4808	1.519279	21.00	25	7.7526	5.090264
1.50	15	2.5463	1.545182	21.50	25	7.9033	5.174416
2.00	15	2.6119	1.571782	22.00	25	8.0541	5.259838
2.50	15	2.6775	1.599101	22.50	25	8.2049	5.346545
3.00	15	2.743	1.627158	23.00	25	8.3556	5.434551
3.50	15	2.8086	1.655976	23.50	25	8.5064	5.523868
4.00	15	2.8742	1.685575	24.00	25	8.6571	5.614506
4.50	15	2.9398	1.715978	24.50	25	8.8079	5.706475
5.00	15	3.0053	1.74721	25.00	25	8.9587	5.799783
5.50	15	3.0709	1.779293	33.50	35	15.148	9.683568
6.00	15	3.1365	1.812252	34.00	35	15.4166	9.817274
6.50	15	3.2021	1.846113	34.50	35	15.6853	9.951679
7.00	15	3.2676	1.880901	35.00	35	15.9539	10.08674
7.50	15	3.3332	1.916644	35.50	35	16.2225	10.22241
8.00	15	3.3988	1.953369	36.00	35	16.4912	10.35866
8.50	15	3.46	1.991104	36.50	35	16.7598	10.49542
12.50	25	5.5729	3.834271	37.00	35	17.0284	10.63266
13.00	25	5.6877	3.90016	37.50	35	17.3198	10.77034
13.50	25	5.8025	3.966907	38.00	35	17.6153	10.9084
14.00	25	5.9172	4.034542	38.50	35	17.9108	11.0468
14.50	25	6.0451	4.103096	39.00	35	18.2063	11.18548
15.00	25	6.1751	4.172596	39.50	35	18.5018	11.32441
15.50	25	6.3051	4.243073	40.00	35	18.7207	11.46353
Maximum deviation				0.15			

Table 8.22 Comparison of  $K1 \times 10^7$  values prediction by NN2\_K1 and experiment data from Millero et al. (2006) Range: T=<1.1-50.4 °C >, S=<3.47-36 wt %>

Temp	Salinity	K1exp	NN2_K1	Temp	Salinity	K1exp	NN2_K1
1.1	3.47	4.345102	3.437707	35	2.91	8.689604	6.497131
1.2	3.47	4.477133	3.447218	35	4.40	9.078205	6.690855
1	4.35	4.753352	3.533937	35	5.48	9.885531	6.833037
1.2	4.70	4.613176	3.594936	35	8.41	11.42878	7.225518
1.2	4.93	4.655861	3.621837	35	11.93	12.47384	7.705192
1	5.56	4.931738	3.676188	35	14.50	13.33521	8.060129
1	6.28	5.069907	3.759564	35	14.50	13.30454	8.060129
1.2	8.15	5.211947	3.995473	35	14.50	13.24342	8.060129
1.2	8.15	5.296634	3.995473	35	17.88	14.12538	8.528232
1.2	9.97	5.546257	4.198211	35	17.88	14.09289	8.528232
1.1	10.35	5.662393	4.229202	40	1.76	7.87	6.7702
5	22.17	7.906786	5.97477	40	2.91	8.77	6.9026
5	22.17	7.888601	5.97477	40	3.93	9.33	7.0219
5	23.47	8.090959	6.104281	40	9.58	12.33	7.7075
6	24.00	8.07235	6.301772	40	9.58	12.42	7.7075
5	25.47	8.203515	6.300279	40	12.63	13.49	8.0921
5	25.47	8.222426	6.300279	40	13.78	14.00	8.2405
5	25.47	8.203515	6.300279	40	13.78	13.93	8.2405
5	26.35	8.147043	6.38381	40	16.46	14.76	8.5895
5	26.35	8.109611	6.38381	40	16.46	14.62	8.5895
5	26.35	8.203515	6.38381	45	43.29	21.93	12.0940
25	31.85	13.93157	9.632099	50	9.53	13.52	8.2461
25	31.85	14.02814	9.632099	50	9.53	13.61	8.2461
25	31.85	14.06048	9.632099	50.4	12.40	14.76	8.5466
25	31.85	13.99587	9.632099	49.7	14.98	16.14	8.7864
25	34.00	14.39	9.88093	50.2	14.98	15.78	8.8030
25	34.00	14.38799	9.88093	50.2	17.73	16.83	9.0962
25	34.00	14.38799	9.88093	50.2	19.72	17.14	9.3139
25	34.00	14.38799	9.88093	50	21.16	18.20	9.4721
25	36.06	14.4544	10.11036	50.1	21.16	18.11	9.4737
25	36.06	14.58814	10.11036	50	21.25	17.99	9.4819
25	36.06	14.58814	10.11036	50.3	24.00	18.88	9.7999
25	36.06	14.55459	10.11036	49.7	28.02	20.23	10.2694
Maximum deviation				0.2			

Table 8.23 Comparison of  $K_2 \times 10^{10}$  values prediction by NN2\_K2 and experiment data from Millero et al. (2006) Range: T=<1.1-50.4 °C >, S=<3.47-36 wt % >

Temp	Salinity	K2exp	NN2_K2	Temp	Salinity	K2exp	NN2_K2
1.1	3.47	1.14	1.1336	35	2.91	7.94	3.6246
1.2	3.47	1.16	1.1366	35	4.40	8.79	3.8154
1	4.35	1.19	1.1533	35	5.48	8.97	3.9657
1.2	4.70	1.32	1.1689	35	8.41	8.89	4.4491
1.2	4.93	1.39	1.1751	35	11.93	10.00	5.2175
1	5.56	1.38	1.1858	35	14.50	9.84	5.8321
1	6.28	1.49	1.2059	35	14.50	11.46	5.8321
1.2	8.15	1.90	1.2691	35	14.50	11.43	5.8321
1.2	8.15	1.90	1.2691	35	17.88	11.97	6.5528
1.2	9.97	2.09	1.3283	35	17.88	11.89	6.5528
1.1	10.35	2.07	1.3374	40	1.76	10.26	4.2371
5	22.17	3.67	2.4962	40	2.91	10.02	4.4068
5	22.17	3.79	2.4962	40	3.93	11.43	4.5682
5	23.47	4.06	2.6983	40	9.58	11.32	5.7434
6	24.00	3.99	2.8953	40	9.58	11.51	5.7434
5	25.47	3.99	2.9968	40	12.63	11.53	6.5217
5	25.47	3.99	2.9968	40	13.78	12.53	6.8009
5	25.47	4.30	2.9968	40	13.78	12.74	6.8009
5	26.35	4.27	3.1131	40	16.46	12.94	7.3997
5	26.35	4.34	3.1131	40	16.46	13.09	7.3997
5	26.35	4.30	3.1131	45	43.29	16.60	14.7069
25	31.85	10.84	6.9636	50	9.53	16.71	8.2738
25	31.85	10.89	6.9636	50	9.53	17.42	8.2738
25	31.85	10.84	6.9636	50.4	12.40	17.30	9.1168
25	31.85	10.89	6.9636	49.7	14.98	17.58	9.5365
25	34.00	11.51	7.3622	50.2	14.98	20.61	9.6714
25	34.00	11.46	7.3622	50.2	17.73	21.33	10.3063
25	34.00	11.38	7.3622	50.2	19.72	21.18	10.7639
25	34.00	11.51	7.3622	50	21.16	24.10	11.0426
25	36.06	11.43	7.7586	50.1	21.16	24.10	11.0703
25	36.06	11.40	7.7586	50	21.25	27.48	11.0627
25	36.06	11.25	7.7586	50.3	24.00	27.48	11.7837
25	36.06	11.86	7.7586	49.7	28.02	27.61	12.5490
Maximum deviation				0.0012			

Table 8.24 Comparison of  $K1 \times 10^7$  values prediction by NN3\_K1 and experiment data from Millero et al. (1997) Range: T=<1-40 °C >, S=<5-35 wt %>

Temp	Salinity	K1exp	NN3_K1	Temp	Salinity	K1exp	NN3_K1
1.00	5	4.8796	5.4554	16.00	25	10.8329	10.51634
1.50	5	4.9508	5.4865	16.50	25	10.9689	10.64813
2.00	5	5.0221	5.5182	17.00	25	11.1049	10.78124
2.50	5	5.0934	5.5504	17.50	25	11.2409	10.91562
3.00	5	5.1647	5.5833	18.00	25	11.3769	11.05121
3.50	5	5.2360	5.6167	18.50	25	11.5129	11.18798
4.00	5	5.3072	5.6508	19.00	25	11.6446	11.32587
4.50	5	5.3785	5.6854	19.50	25	11.7684	11.46482
5.00	5	5.4498	5.7207	20.00	25	11.8923	11.60478
5.50	5	5.5211	5.7566	20.50	25	12.0161	11.74569
1.00	15	6.2363	6.6420	21.00	25	12.1399	11.8875
1.50	15	6.3397	6.7082	21.50	25	12.2638	12.03014
2.00	15	6.4431	6.7757	22.00	25	12.3876	12.17354
2.50	15	6.5466	6.8446	22.50	25	12.5114	12.31765
3.00	15	6.6500	6.9150	23.00	25	12.6369	12.46239
3.50	15	6.7535	6.9868	23.50	25	12.7672	12.6077
4.00	15	6.8569	7.0601	24.00	25	12.8976	12.75351
4.50	15	6.9603	7.1348	24.50	25	13.028	12.89975
5.00	15	7.0638	7.2110	25.00	25	13.1583	13.04634
5.50	15	7.1672	7.2887	33.50	35	17.2121	16.75422
6.00	15	7.2707	7.3678	34.00	35	17.3726	16.89407
6.50	15	7.3741	7.4484	34.50	35	17.5331	17.03268
7.00	15	7.4769	7.5305	35.00	35	17.6918	17.16999
7.50	15	7.5796	7.6141	35.50	35	17.8436	17.30596
8.00	15	7.6824	7.6991	36.00	35	17.9952	17.44053
8.50	15	7.7851	7.7857	36.50	35	18.1467	17.57368
12.50	25	9.9003	9.633818	37.00	35	18.2983	17.70534
13.00	25	10.0321	9.755358	37.50	35	18.4499	17.83549
13.50	25	10.164	9.878461	38.00	35	18.6015	17.96408
14.00	25	10.2958	10.0031	38.50	35	18.7531	18.09108
14.50	25	10.4277	10.12924	39.00	35	18.904	18.21645
15.00	25	10.5609	10.25685	39.50	35	19.0503	18.34017
15.50	25	10.6969	10.3859	40.00	35	19.1677	18.46219
Maximum deviation				0.11			



Table 8.25 Comparison of  $K_2 \times 10^{10}$  values prediction by NN3\_K2 and experiment data from Millero et al. (1997) Range: T=<1-40 °C >, S=<5-35 wt. %>

Temp	Salinity	K1exp	NN3_K2	Temp	Salinity	K1exp	NN3_K2
1.00	5	1.3793	1.6777	16.00	25	6.435	6.121299
1.50	5	1.4106	1.7007	16.50	25	6.565	6.23595
2.00	5	1.4419	1.7242	17.00	25	6.695	6.352719
2.50	5	1.4732	1.7481	17.50	25	6.8249	6.471638
3.00	5	1.5044	1.7723	18.00	25	6.9549	6.592737
3.50	5	1.5357	1.7969	18.50	25	7.0849	6.716048
4.00	5	1.5670	1.8220	19.00	25	7.2148	6.841604
4.50	5	1.5983	1.8474	19.50	25	7.3448	6.969435
5.00	5	1.6296	1.8733	20.00	25	7.4748	7.099573
5.50	5	1.6608	1.8995	20.50	25	7.6047	7.232051
1.00	15	2.4808	2.6591	21.00	25	7.7526	7.366901
1.50	15	2.5463	2.7050	21.50	25	7.9033	7.504153
2.00	15	2.6119	2.7517	22.00	25	8.0541	7.64384
2.50	15	2.6775	2.7994	22.50	25	8.2049	7.785995
3.00	15	2.7430	2.8481	23.00	25	8.3556	7.930648
3.50	15	2.8086	2.8976	23.50	25	8.5064	8.077831
4.00	15	2.8742	2.9482	24.00	25	8.6571	8.227577
4.50	15	2.9398	2.9997	24.50	25	8.8079	8.379916
5.00	15	3.0053	3.0522	25.00	25	8.9587	8.53488
5.50	15	3.0709	3.1057	33.50	35	15.148	14.76752
6.00	15	3.1365	3.1603	34.00	35	15.4166	15.02786
6.50	15	3.2021	3.2159	34.50	35	15.6853	15.29194
7.00	15	3.2676	3.2726	35.00	35	15.9539	15.55978
7.50	15	3.3332	3.3304	35.50	35	16.2225	15.83139
8.00	15	3.3988	3.3893	36.00	35	16.4912	16.10679
8.50	15	3.4643	3.4493	36.50	35	16.7598	16.38598
12.50	25	5.5729	5.37545	37.00	35	17.0284	16.66899
13.00	25	5.6877	5.476138	37.50	35	17.3198	16.95582
13.50	25	5.8025	5.578729	38.00	35	17.6153	17.24648
14.00	25	5.9172	5.683254	38.50	35	17.9108	17.54098
14.50	25	6.0451	5.789743	39.00	35	18.2063	17.83931
15.00	25	6.1751	5.898226	39.50	35	18.5018	18.14149
15.50	25	6.3051	6.008735	40.00	35	18.7207	18.44752
Maximum deviation				0.21			

Table 8.26 Comparison of  $K1 \times 10^7$  values prediction by NN3\_K1 and experiment data from Mehrbach et al. (1973) Range: T=<0-35 °C>, S=<19-43wt %>

Temp	Salinity	K1exp	NN1_K1	Temp	Salinity	K1exp	NN1_K1
0	19	0.498	0.67805	22	37	0.987	1.355724
1	19	0.512	0.692283	23	37	0.999	1.38609
2	19	0.525	0.707133	24	37	1.01	1.416496
3	19	0.539	0.72261	25	37	1.021	1.446887
4	19	0.552	0.738726	26	37	1.032	1.477204
5	19	0.565	0.755487	27	37	1.042	1.507392
6	19	0.579	0.772901	28	37	1.052	1.537395
7	19	0.592	0.790971	29	37	1.061	1.567159
8	19	0.605	0.809698	30	37	1.069	1.596631
9	19	0.618	0.829082	31	37	1.077	1.625761
10	19	0.631	0.849119	32	37	1.085	1.6545
11	27	0.733	0.946317	25	40	1.053	1.480342
12	27	0.747	0.970407	26	40	1.064	1.510562
13	27	0.761	0.995138	27	40	1.074	1.540596
14	27	0.775	1.020487	28	40	1.084	1.57039
15	27	0.788	1.046428	29	40	1.093	1.599892
16	27	0.801	1.072931	30	40	1.102	1.629052
17	27	0.814	1.099964	31	40	1.11	1.657822
18	27	0.827	1.127488	32	40	1.118	1.686157
19	27	0.839	1.155466	33	40	1.125	1.714014
20	27	0.851	1.183852	34	40	1.132	1.741355
21	27	0.862	1.2126	35	40	1.138	1.768142
0	33	0.617	0.764327	25	43	1.084	1.513433
1	33	0.634	0.782392	26	43	1.095	1.543474
2	33	0.65	0.80116	27	43	1.105	1.573272
3	33	0.667	0.820638	28	43	1.115	1.602777
4	33	0.683	0.840826	29	43	1.125	1.631937
5	33	0.699	0.861726	30	43	1.134	1.660706
6	33	0.716	0.883335	31	43	1.142	1.689039
7	33	0.732	0.905647	32	43	1.15	1.716894
8	33	0.747	0.928654	33	43	1.157	1.744232
9	33	0.763	0.952344	34	43	1.164	1.771017
10	33	0.779	0.976702	35	43	1.17	1.797218
Maximum deviation				0.36			

Table 8. 27 Comparison of  $K_2 \times 10^{10}$  values prediction by NN3\_K2 and experiment data from Mehrbach et al. (1973) Range: T=<0-35 °C>, S=<19-43 wt%>

Temp	Salinity	K2exp	NN3_K2	Temp	Salinity	K2exp	NN3_K2
0	19	1.67	2.900551	22	37	7.36	10.20646
1	19	1.73	3.004457	23	37	7.6	10.58843
2	19	1.81	3.112544	24	37	7.83	10.9833
3	19	1.88	3.224964	25	37	8.07	11.39132
4	19	1.96	3.341876	26	37	8.3	11.81278
5	19	2.05	3.463438	27	37	8.54	12.24791
6	19	2.14	3.589818	28	37	8.77	12.69699
7	19	2.23	3.721183	29	37	9	13.16023
8	19	2.34	3.857709	30	37	9.22	13.63787
9	19	2.44	3.999571	31	37	9.44	14.13011
10	19	2.55	4.146952	32	37	9.65	14.63716
11	27	3.85	5.350089	25	40	8.66	12.16584
12	27	3.99	5.553113	26	40	8.92	12.61334
13	27	4.14	5.763918	27	40	9.18	13.07507
14	27	4.29	5.982753	28	40	9.44	13.55128
15	27	4.45	6.209869	29	40	9.69	14.04219
16	27	4.61	6.445522	30	40	9.94	14.54801
17	27	4.78	6.68997	31	40	10.19	15.06892
18	27	4.95	6.943474	32	40	10.43	15.6051
19	27	5.12	7.206296	33	40	10.66	16.1567
20	27	5.3	7.478701	34	40	10.88	16.72385
21	27	5.48	7.760954	35	40	11.09	17.30667
0	33	3.34	4.097399	25	43	9.27	12.97372
1	33	3.43	4.252189	26	43	9.56	13.44759
2	33	3.52	4.413191	27	43	9.85	13.9362
3	33	3.61	4.580628	28	43	10.15	14.43977
4	33	3.72	4.754727	29	43	10.43	14.95849
5	33	3.83	4.935722	30	43	10.72	15.49255
6	33	3.95	5.12385	31	43	11	16.04212
7	33	4.07	5.319358	32	43	11.27	16.60735
8	33	4.2	5.522493	33	43	11.54	17.18835
9	33	4.34	5.73351	34	43	11.79	17.78523
10	33	4.49	5.952667	35	43	12.04	18.39805
Maximum deviation				0.736			

## Chapter 9

### Conclusions and Future Work

#### 9.1 Conclusions

Desalination technology is one of the main sources of fresh water from sea, estuary or brackish water. As presented in Chapter 1, the gap between the demand for freshwater and available is increasingly widening around the world. Therefore, there is a need to accelerate the development of new and reliable water desalination technologies as well as to increase the efficiency of already installed plants. MSF desalination process is one of the main thermal desalination technologies nowadays. Modelling, simulation and optimisation help achieving better design and operation of MSF processes leading to low-cost production of fresh water. This study presented a steady state mathematical model with the effect of  $\text{CaCO}_3$  fouling and non-condensable gases. gPROMS modeling tool was used in modelling, simulation and optimisation of MSF process in this work. The following conclusion can be drawn from this work.

#### *Chapter Four*

In this chapter, detailed steady state mathematical model are developed for MSF brine recycle (BR) process. The developed model is based on mass balance, energy balance, and heat transfer equations coupled with the correlations for physical properties for all the streams of brine and distillate. The physical properties in the developed model were function of temperature and salinity. In addition the developed model included the geometry of the stages, the different non-idealities involved in the process, the temperature loss across the demister and condenser tubes.

## *Chapter Five*

The steady state  $\text{CaCO}_3$  fouling resistance model as function of surface temperature has been developed and implemented in full MSF process model using gPROMS in this chapter. First, the  $\text{CaCO}_3$  fouling resistance ( $R_f$ ) in the brine heater, recovery stages and rejection stages were investigated at different seawater temperature ( $T_{\text{seawater}}$ ) and top brine temperature (TBT). The results show increasing in the  $\text{CaCO}_3$  fouling resistance with increased seawater temperature and top brine temperature by 8 % and 50 % respectively. This increasing was due to the decrease of the solubility of calcium carbonate with increase the temperature.

For fixed water demand and fixed design (number of stages), the MSF operating parameters such as steam temperature, recycle brine and seawater rejected flowrate are optimized while minimizing the total operating cost of the process with increasing and decreasing in the  $\text{CaCO}_3$  fouling resistance ( $R_f$ ). For any seawater temperature, the total annual operating cost increases as fouling resistance increases due to build in scale formation. On the other hand, as the fouling resistance decrease by any scale control techniques during maintenance, the total operating cost decrease. Furthermore, the steam cost show increasing as the fouling resistance increase due to the increase in steam consumption. Also the optimization results show increasing in the brine recycle flow rate ranged from (24-39%) while the steam temperature and rejected seawater flow rate remains constant for different seawater temperature.

## *Chapter Six*

Correlations for different freshwater demand/consumption profile at different time of the day are developed based on actual data from the literature. Furthermore, a simple polynomial dynamic seawater temperature profile is developed to predict seawater

temperature at different time of the day. An intermediate storage tank is considered between the MSF process and the client to add flexibility in meeting the customer demand. A dynamic model for the storage tank level has been implemented in the steady state MSF process model using gPROMS. For a given design, an optimal operation scheme for MSF desalination process dependent on variable seawater temperature is considered to cope with flexible and irregular freshwater demand. Two cases of dynamic fresh water demand have been included in this study. Case 1 considers the fresh water demand during weekend days while the freshwater demand during week days has been considered in case 2.

For several process configuration (the design), some of the operation parameters of the MSF process such as seawater recycle flow rate and brine recycle flow rate at discrete time interval are optimised, while minimised the total operating costs with fixed steam temperature, variable freshwater demand/consumption and seawater temperature throughout the day. The total operating cost decreases as the number of stages of MSF desalination plant increase for both case studies. The plant production flowrate and the operation parameters such as brine recycle flowrate and rejected seawater flowrate show flexible operation with the tank level to meet the variation in the freshwater during the day. The results clearly also show that the advantage of using the intermediate storage tank adds flexible scheduling in the MSF plant design and operation parameters to meet the variation in freshwater demand with varying seawater temperatures without interrupting or fully shutting down the plant at any time during the day.

### *Chapter Seven*

Non-condensable gases are a serious problem in MSF plants. They reduce the performance, efficiency of MSF and increase the cost. Also, the releases of CO<sub>2</sub> from the evaporating brine in seawater distillers play an important role in alkaline scale

formation in MSF distiller. In this chapter, gPROMS modelling tool has been used to model the effect of NCG on the MSF process. The simulation results showed clearly the effect of NCG on the overall heat transfer coefficient in heat recovery and rejection sections. The model was then used to study the sensitivity of two important parameters in the presence of 0.015% of NCG: the seawater temperature which is subject to seasonal variation, and the steam temperature in the brine heater which controls TBT of the process (indirectly controlling the design of the process). The results showed that the steam temperature played an important role to maintain the production rate of freshwater at different seasons.

The interaction of design (number of flash chambers) and operation (steam flowrate, steam temperature, recycle brine flowrate, bottom brine temperature) in the context of fixed fresh water demand and seasonal variation of seawater temperature was then studied via repetitive simulation. For a given design, the results showed that some of the operating parameters had to be adjusted by 70% for seawater temperature rise of 15%.

### *Chapter Eight*

Accurate estimation of first dissociation constant ( $K_1$ ) and second dissociation constant ( $K_2$ ) in seawater due to temperature and salinity is important in studying the role of NCGs and scale formation in MSF distiller. Several empirical correlations exist in the literature to predict  $K_1$  and  $K_2$ . However, in this work, three NN based correlations for predicting  $K_1$  and  $K_2$  as function in temperature and salinity were developed. The NN based correlations predicted the experimental  $K_1$  and  $K_2$  very closely. Predictions by different NN based correlations (for different temperature and salinity) within the training range followed the expected trends and it was within the engineering accuracy.

## 9.2 Future Work

Following suggestions can be made for future work:

- The results of calcium carbonate fouling deposition factor model with the steady state MSF process model should be validated with experimental or real plant data.
- A dynamic model of calcium carbonate fouling deposition factor coupled with a dynamic model for the MSF process can be developed in the future work.
- The developed model of calcium carbonate fouling deposition factor can be updated to include the effect of many variables such as velocity, foulant concentration and for other scale deposition type like calcium sulfate and magnesium hydroxide.
- Variable demands of freshwater with changing seawater temperature (during the day) could be build up in optimisation framework considering hybrid desalination ( Mixed MSF, RO) process with intermediate storage.
- A steady state MSF process model coupled with a dynamic model for the storage tank can be validated with real plant or experimental data by using gPROMS validation tool (experimental design tools).
- The dynamic model of MSF process coupled with dynamic model of storage tank should be developed to study the controller design in the future work.
- The results of the steady state MSF process model coupled with the effect of non-condensable gases should be validated with real plant data.



- The results of the steady state MSF process model with the effect of non-condensable gases can be used in the design of the venting system in the future work.
- The effect of non-condensable gases (NCGs) with varying seawater properties such as temperature, CO<sub>2</sub> concentrations, and salinity can be applied to the other thermal desalination process such as multiple effect evaporator (MEE).
- In order to use NN correlations in further calculations in MSF plant, updating the NN developed correlations with experimental data of the dissociation constant of carbonic acid in seawater at similar conditions of MSF desalination process should be done in the future work.
- Apply a (K<sub>1</sub>) and (K<sub>2</sub>) NN based correlations in hybrid model with a steady state MSF process model to study scaling tendency of calcium carbonate and the CO<sub>2</sub> release process in MSF distiller.
- Similar NN based correlations can be developed for other seawater properties such as density, viscosity, corrosion, scaling.

## References

- Abdel-Jabbar, N.M., Qiblawey, H.M., Mjalli, F.S. and Ettouney, H. (2007). Simulation of large capacity MSF brine circulation plants, *Desalination*, **204**, 501-514.
- Abduljawad, M. and Ezzeghni, U. (2010). Optimization of Tajoura MSF desalination plant, *Desalination*, **254**, 23-28
- Abu-Eid, Z.M., and Fakhoury, A.G. (1974). Some special design features of Kuwait MSF Plants, *Desalination*, **23**, 263-284.
- Al-Ahmad, M. (2008). Factors Affecting Scale Formation in Sea Water Enviroments- An Experimental Approach, *Chem. Eng. Technol.*, **31**(1), 149-156.
- Al-Ahmad, M. and Abdul Aleem, F. (1993). Scale Formation and Fouling Problems Effect on The Performance of MSF and RO Desalination Plants in Saudi Arabia, *Desalination*, **93**, 287-310.
- Al-Ahmad, M. and Aleem, F.A. (1994). Scale formation and fouling problems and their predicted reflection on the performance of desalination plants in Saudi Arabia, *Desalination*, **96**, 409-419.
- Al-Anezi, k. and Hilal, N. (2007). Scale formation in desalination plants: effect of carbon dioxide solubility, *Desalination*, **204**, 385-402.
- Alasfour, F.N. and Abdulrahim, H.K. (2009). Rigorous steady state modeling of MSF–BR desalination system, *Desalination and Water Treatment*, **1**, 259-276.

Al-Anezi, K. and Johnson, D.J.(2008). An atomic force microscope study of calcium carbonate adhesion to desalination process equipment: effect of anti-scale agent, *Desalination*,**220**, 359-370.

AlBahou, M., Al-Rakkaf, Z., Zaki, H., and Ettouney, H. (2007). Desalination experience in Kuwait, *Desalination*, **204**, 403-415.

Al-Enezi, G. and Fawzi, N. (2002). Design consideration of RO units: case studies, *Desalination*, **153**, 281-286.

Al-Fulaij, H. (2011). Dynamic Modeling of Multi Stage Flash (MSF) Desalination Plant. PhD thesis. University of College London.

Al-Fulaij, H., Cipollina, A., Bogle, D., and Ettouney, H. (2010). Once through Multistage Flash Desalination: gPROMS Dynamic and Steady State Modeling, *Desalination and Water Treatment*, **18**, 46-60.

Al-Rawajfeh, A.E. (2004). Modeling and simulation of CO<sub>2</sub> release in multiple effect distiller for seawater desalination, Ph.D. Thesis, Martin-Luther University of Halle-Wittenberg, Shaker Verlag, Aachen.

Al-Rawajeh, A.E. (2008). Simultaneous desorption-crystallization of CO<sub>2</sub>-CaCO<sub>3</sub> in multi-stage flash (MSF) distillers, *Chem. Eng. And Process*, **47**, 2262-2269.

Al-Rawajfeh, A.E., Glade, H., Qiblawey, H.M., Ulrich, J. (2004).Simulation of CO<sub>2</sub> release in multiple-effect distillers, *Desalination*, **166**, 41-52.

Al-Rawajfeh, A.E., Glade, H., Ulrich, J. (2003). CO<sub>2</sub> release in multiple-effect distillers controlled by mass transfer with chemical reaction, *Desalination*, **156**, 109-123.

Al-Rawajfeh, A.E., Glade, H., Ulrich, J. (2005). Scaling in multiple-effect distillers: the role of CO<sub>2</sub> release, *Desalination*, **182**, 209-219.

Al-Shayji, K.A. (1998). Modelling, simulation, and optimisation of large-scale commercial desalination plants, Ph.D. Dissertation, Virginia Polytechnic Institute and State University, USA.

Al-Sofi, M.A., Khalaf S. and Al-Omran A. (1989). Practical experience in scale control in MSF evaporators, *Desalination*, **73**, 313-325.

Al-Sofi, M.A. (1999). Fouling phenomena in multi stage flash (MSF) distillers, *Desalination*, **126**, 61-76.

Al Sum, E.A., Al-Radif, A. and Aziz, S. (1993). Performance of materials used for the venting system in WED's desalination plants (MSF), *Desalination*, **93**, 517-527

Al-Sum, E.A. and Hodgkiess, T. (1997). Investigation of the chemistry of alkaline scale formation: Influence of vacuum, heat flux and some antiscalants on the thermal decomposition of bicarbonate, Proc. IDA and World congress on Desalination and Water Reuse, Madrid, vol.3, 519-530.

Alvisi, M.A., Franchini, M. and Marinelli, A. (2007). A short-term pattern-based model for water-demand forecasting, *Journal of Hydroinformatics*, **91**, 39-50.

Aly, N.H. and El-Fiqi, A. (2003). Thermal performance of seawater desalination system. *Desalination*, **158**, 127-142.

Aly, S.E. and Fathalah, K. (1995). MSF - a mathematical model, Proc. IDA World Congress, Abu Dhabi, 203-226.

Assiry, A.M., Gaily, M. H., Alsamee, M., Sarifudin, A. (2010). Electrical conductivity of seawater during ohmic heating, *Desalination*, **260**, 7-19.

Azaroual, M., Kerveven, Ch., Durance, M.-V. and Durst, P. (2004). SCALE2000: reaction-transport software dedicate to thermokinetic prediction and quantification of scales Applicability to desalination problem, *Desalination*, **165**, 409-419.

Aziz, N., Mujtaba, I.M. and Hussain, M.A. (2001). Set point tracking in batch reactor: Use of PID and Generic Model Control with Neural Network Techniques. Application of Neural Network and other Learning Technologies in process Engineering (Eds I. M. Mujtaba and M.A. Hussain Imperial College Press, London, pp 217-2424.

Baig, H., Antar, M.A. and Zubair, S.M. (2011). Performance evaluation of a once-through multi-stage flash distillation system: Impact of brine heater fouling, *Energy Conversion and Management* , **52**, 1414-1425.

Bott, T.R. (1995). Fouling of heat exchangers , Elsevier Science & Technology Books.

Bowen, W.R., Hilal, N. and Lovitt, R.W. (1998). A new technique for membrane characteristic: direct measurement of the force of adhesion of a single particle using on atomic force microscope, *J. Membrane Science*, **139**, (2), 269-274.

Casini, G.F. (1983). The application of a high temperature scale control additive in a Middle East MSF plant. *Desalination*, **47**, 19-24.

Clelland, D.W. and Stewart J.M. (1966). The optimisation and design of large scale multi-stage flash distillation plants, *Desalination*, **1**, 61-76.

Coleman, A. K. (1971). Optimisation of a single effect, multi-stage flash distillation desalination system, *Desalination*, **9**, 315-331.

Cooper, K.G., Hanlon, L.G., Smart G.M. and Talbot, R.E. (1983). A Model for The Fouling of M.S.F. Plants Bases on Data from Operating Units, *Desalination*, **47**, 37-47.

Darwish, M.A. (1991). Thermal analysis of multi-stage flash desalting system, *Desalination*, **85**, 59-79.

Delyannis, E. and Belessiotis, V. (2010). Desalination: The recent development path, *Desalination*, **264**, 206-213.

Dickson, A.G. and Riley, J.P. (1979). The estimation of acid dissociation constants in seawater media from potentiometric titration with strong base, *Mar. Chem.*, **7**, 89-99.

Donner, J., Fokken, J., Boeck, K., Glade, H. and Will, S. (2008) .CO<sub>2</sub> release in vertical tube falling film evaporators, *Desalination*, **222**, 626-638.

Ekpo, E.E. and Mujtaba, I.M. (2008). Evaluation of neural networks-based controllers in batch polymerization of methyl methacrylate, *Neurocomputing*, **71**, 1401-1412.

El-Dahshan, M.E. (2001). Corrosion and scaling problems present in some desalination plants in Abu Dhabi, *Desalination*, **138**, 371-377.

El-Dessouky, H.T., Alatiqi, I. and Ettouney, H.M. (1998). Process synthesis: The multi-stage flash desalination system. *Desalination*, **115**, 155-179.

El-Dessouky, H.T. and Ettouney, H.M. (2002). Fundamentals of salt water desalination. Amsterdam; Elsevier Science Ltd.

- El-Dessouky, H.T., Alatiqi, I.M., Ettouney, H.M. and Al-Deffeeri, N.S. (2000). Performance of wire mesh mist eliminator, *Chemical Engineering and Processing*, **39**, 129-139.
- El-Dessouky, H.T., Shaban, H. and Al-Ramadan, H. (1995). Steady state analysis of multi-stage flash desalination process, *Desalination*, **103**, 271.
- El-Dessouky, H. and Bingulac, S. (1996). Solving equations simulating the steady state behavior of the multi stage flash desalination process. *Desalination* , **107**, 171-193.
- El-Dessouky, H.T. and Khalifa, T.A. (1985). Scale formation and its effect on the performance of once through MSF plant, *Desalination*, **55**, 199-217.
- Elliot, M.N, Hodgson, T.D. and Harris, A. (1974). Additives for alkaline scale control at temperatures above 93°C (200°F), *Desalination*, **14**, 43-55.
- Ellis, R.D., Glater, J. and Mc Cutchan, J.W. (1971). Alkaline scale abatement by carbon dioxide injection, *Environ Sci. Tech.*, **5**, 350-356.
- El-Nashar, A.M. (1998). Optimization of operating parameters of MSF plants through automatic set point control, *Desalination*, **116**, 89-107.
- El-Sadek, A. (2010). Water desalination: An imperative measure for water security in Egypt, *Desalination*, **250**, 876-884.
- Ettouney, H.M., El-Dessouky, H.T. and Alatiqi, I. (1999). Understand thermal desalination. *Chemical Eng. Prog.* , **95**, 43-54.

Ettouney, H.M., El-Dessouky, H.T., and Al-Juwayhel, F. (2002). Performance of the once through multistage flash desalination. *Proc. Instn. Mech. Engrs. Part A, Power and Energy* , **216**, 229-242 .

Fritzmann, C., Lowenberg, J., Wintegens, T. and Melin, T. (2007). State-of-the-art of reverse osmosis desalination, *Desalination*, **216**, 1-76.

Gao, P., Zhang, L., Cheng, K. and Zhang, H. (2007). A new approach to performance analysis of a seawater desalination system by an artificial neural network, *Desalination*, **205**, 147-155.

Geigy, C. (1978) Noncondensable Gases and the Venting of Seawater Evaporators, Bulletin DB 2.2.

Genther, K., Gregorzewski, A., and Seifert, A. (1993). The effects and limitations issued by non-condensable gases in sea water distillers, *Desalination*, **93**, 207-234.

Glade, H. and Genthner, K. (1995). The problem of predicting CO<sub>2</sub> releases in MSF distillers, Proc. IDA World Congress on Desalination and Water Sciences, Abu Dhabi, UAE, 2, 365–386.

Glade, H. (1999). Chemical reaction kinetics and mass transfer phenomena controlling the release of CO<sub>2</sub> in MSF distillers. Proc. IDA World Congress on Desalination and Water Reuse, San Diego, U.S.A., 1999, Vol. 1; 375-388.

Glade, H., Meyer, J. and Will, S. (2005). The release of CO<sub>2</sub> in MSF and ME distillers and its use for the recarbonation of the distillate: a comparison, *Desalination*, **182**, 99-110.

Gosling, I. (2005). Process simulation and modeling for industrial bioprocessing tools and techniques, *Ind. Biotechnology*, **1**, (2), 106-109.



Goyet, C. and Poisson, A. (1989). New determination of carbonic acid dissociation constant in seawater as function of temperature and salinity, *Deep Sea Res.* , **36**,1635-1654.

gPROMS (2005). gPROMS User Guide 2005: Process System Enterprise Ltd (PSE).

Greaves, M.A., Mujtaba, I.M., Barolo, M., Trotta, A. and Hussain, M.A. (2003). Neural–Network Approach to Dynamic Optimisation of Batch Distillation Application to a Middle-vessel Column, *Chemical Engineering Research and Design*, **81**, 393-401.

Hagan, M.T., Demuth, H.B., Beal, M.H. (1996).Neural Network Design. Boston: PWS.

Hamed, O.A., Al-Sofi, M.K., Mustafa, G. M. and Dalvi, A. (1999). The performance of different anti-scalants in multi-stage flash distillers, *Desalination*, **123**, 185-194.

Hawaidi, E.A and Mujtaba, I.M. (2010). Sensitivity of Brine Heater Fouling on Optimization of Operation Parameters of MSF Desalination Process using gPROMS, in Proceedings of 20<sup>th</sup> European Symposium on *Computer Aided Chemical Engineering*, pp 1787-1792, Eds.S. Pierucci and G. Buzzi Ferraris, Naples, Italy, 6-10 June, 2010.

Hawaidi, E.A and Mujtaba, I.M. (2011). Freshwater production by MSF desalination process: Coping with variable demand by flexible design and operation, *Computer Aided Chemical Engineering*, **29**, 1180-1184.

Hawaidi, E.A and Mujtaba, I.M. (2011) Meeting variable freshwater demand by flexible design and operation of the Multistage flash Desalination process, *Industrial and Engineering Chemistry Research*, **50**, 10604-10614.

Helal, A. Medani, M., Soliman, M. and Flower, J. (1986). Tridiagonal matrix model for multistage flash desalination plants, *Computer & chemical engineering*, **10**(4), 327-342.

Helal, A.M., El-Nashar, A.M., Al-Kahtheeri, E. and Al-Malek, S. (2003). Optimal design of hybrid RO/MSF desalination plants Part I: Modeling and algorithms, *Desalination*, **154**, 43-66.

Herrera, M., Torgo, L., Izquierdo, J. and Perez-Garcia, R. (2010) Predictive models for forecasting hourly urban water demand, *Journal of Hydrology*, **387**, 141-150.

Hillier,H. (1952). Scale formation in sea-water distilling plants and its prevention, *proc. Inst. Mech. Eng.*, London, 1B, 295-322.

Hussain,A.(Ed.) (2003) Integrated power and desalination plants. Oxford.

Hussain, A., Hassan, A., Al-Gobaisi, D., Al-Radif, A., Woldai, A. and Sommariva, C. (1993). Modeling, simulation, optimization and control of multistage flash (MSF) desalination plants Part2: modeling and simulation, *Desalination*, **92**, 21-41.

Khalfallah, H.A. (2009). Modelling and optimization of Oxidative Desulfurization Process for Model Sulfur Compounds and *Heavy Gas Oil*. PhD Thesis. University of Bradford.

Khan, A.H., *Desalination Process and Multi-Stage Flash Distillation Practice*, Elsevier, Amsterdam, 1986.

Khan, R.A. (1972). Effect of non-condensable in seawater evaporators. *Chem. Eng. Prog.* **68**, 79-80.

Khawaji, A.D., Kutubkhanah, I.K. and Wie, J.M. (2007). A 13.3 MGD seawater RO desalination plant for Yanbu Industrial City. *Desalination*, **203**, 176-188 .

Khawaji, A.D., Kutubkhanah, I.K. and Wie, J. (2008). Advances in seawater desalination technologies, *Desalination*, 221, 47-69.

Langelier, W.F. (1954). Mechanism and control of scale formation in seawater distillation, *Journal AWWA*, **46**, 461.

Langelier, W.F. (1936). The analytical control of anticorrosion water treatment, *Journal AWWA*, **36**, 472.

Lee, H., Hong, M., Han, S., Cho, S. and Moon, S. (2009). Fouling of an anion exchange membrane in the electro dialysis desalination process in the presence of organic foulants, *Desalination* , **238** ,60–69

Lukin, G.Y. (1982). Calculation for decarbonation of seawater with adiabatic evaporation. *Thermal Engineering*, **29**, 687-688.

Lukin, G.Y. and Kalashnik, V.V. (1982) Calculation for decarbonation of sea water with adiabatic evaporation, *Chemical Engineering*, **29**, 687-688.

Malayeri, M.R. and Muller-Steinhagen, H. (2007). An overview of Fouling Mechanisms, Prediction and Mitigation Strategies for Thermal Desalination Plants, Eleventh International Water Technology Conference, IWTC11, Sharm El-Sheikh, Egypt, 299313.

Malayeri, M.R. and Muller-Steinhagen, H. (2007). An overview of Fouling Mechanisms, Prediction and Mitigation Strategies for Thermal Desalination Plants, Eleventh International Water Technology Conference, IWTC11,299-313, Sharm El-Sheikh, Egypt.

Mandil M.A. and Ghafour, E.E. (1970). Optimization of multi-stage flash evaporation plants, *Chemical Engineering Science*, **3**, 611-621.

Mehrbach, C., Culberson, C.H. and Hawley, J.E. (1973). Measurements of the apparent dissociation constant of carbonic acid in seawater at atmospheric pressure, *Limnol. Oceanogr.* **18**, 897-907.

Millero, F.J. (1995). Thermodynamics of the carbon dioxide system in the ocean, *Geochim. Et Cosmochim. Acta*, **59**, 661-677.

Millero, F.J. (1996). Chemical oceanography, 2<sup>nd</sup> edition, CRC press, Boca Raton.

Millero, F.J. (1997). A chemical equilibrium model for the carbonate system in natural water. *Croat. Chem. Acta.* **70**, 1-38.

Millero, F.J., Feistel, R., Wright, D.G. and McDougall, T.J. (2008). The composition of standard seawater and the reference-composition salinity, *Deep-Sea Research*, **55**, 50-72.

Millero F.J., Graham, T.B., Huang, F., Bustos-Serrano, H., and Pierrot, D. (2006). Dissociation constants of carbonic acid in seawater as a function of salinity and temperature. *Marine Chemistry*, **100**, 80-94.

Mojica, F.J. and Millero, F.J. (2002). The values of  $pK_1 + pK_2$  for the dissociation of carbonic acid in seawater, *Geochim. Cosmochim. Acta*, **66**, 2529-2540.

- Morris, A.J., Montague, G.A., and Willis, M.J. (1994). Artificial neural networks: studies in process modelling and control. Trans. *ICHEME*, **723**-19.
- Mubarak, A. (1998) A kinetic model for scale formation in MSF desalination plants. Effect of antiscalants, *Desalination*, **120**, 33-39.
- Mujtaba, I.M. and Hussain, M.A. (Eds.) (2001). Application of neural networks and other learning technologies in process engineering, London: Imperial College Press.
- Mujtaba, I.M., Aziz, N. and Hussain, M.A. (2006). Neural Network based Modelling and Control in batch reactor, *Chemical Engineering Research and Design*, **84**, 635-644.
- Mussati, S., Aguirre, P. and Scenna, N. J. (2001). Optimal MSF plant design, *Desalination*, **138**, 341-347.
- Mussati, S.F., Marcovecchio, M.G., Aguirre, P.A. and Scenna, N.J.(2004a).A new global optimization algorithm for process design: its application to thermal desalination processes, *Desalination*,**166**,129-140.
- Mussati, S.F., Marcovecchio, M.G., Aguirre, P.A. and Scenna, N.J. (2004b). A rigorous, mixed-integer, nonlinear programming model (MINLP) for synthesis and optimal operation of cogeneration seawater desalination plants, *Desalination*, **166**, 339-345.
- Mussati, S.F., Aguirre, P.A. and Scenna, N.J. (2005). Optimisation of alternative structures of integrated power and desalination plants, *Desalination*, **182**, 123-129.
- Mussati, S.F., Barttfeld, M., Aguirre, P.A. and Scenna, N.J. (2008). A disjunctive programming model for superstructure optimization of power and desalting plants, *Desalination*, **222**, 457-465.

Oldfield, J.W. (1987). Vapour side corrosion in MSF plants, *Desalination*, **66**,171-187.

Omar, A.M. (1983). Simulation of M.S.F. desalination plants. *Desalination*,**45**, 65-76 (45).

Patel S. and Finan M.A. (1999). New antifoulants for deposit control in MSF and MED plants. *Desalination*, **124**, 63-74.

Ror, R.N., Roy, L.N. ,Vogel, K.M., Poter-Moore, C., Peason, T., Good, C.E., Millero, F.J and Campbell, D.M., (1993), the dissociation constants of carbonic acid in seawater at salinities 5 to 45 and temperature 0 to 45°C, *Mar. Chem.*,**44**, 249-267.

Rosso, M., Beltramini, A., Mazzotti, M., Morbidelli, M. (1996). Modelling of multistage flash desalination plants, *Desalination*, **108**, 365-374.

Ryznar, J.W. (1944). A new index for determining amount of calcium carbonate scale formed by water, *Journal AWWA*, **36**, 472.

Said S., Mujtaba I.M. and Emtir M. (2010). Modelling and simulation of the effect of non-condensable gases on heat transfer in the MSF desalination plants using gPROMS software, *computer Aided Process Engineering*, **28**, 25-30.

Said S., Emtir M and Mujtaba I.M. (2011). Neural Network based correlations for estimating the first and second dissociation constant of carbonic acid in seawater, *Chemical Engineering Transactions*, **24**, 523-528.

Sassi K. , M. and Mujtaba, I.M. (2011). Optimal design and operation of reverse osmosis desalination process with membrane fouling , *Chemical Engineering Journal*, **171** , 582– 593

Shams El-Din A.M. and Mohammed R.A. (1989). The problem of alkaline scale formation from a study on Arabian Gulf water. *Desalination*, **71**, 313-324.

Shams El din, A.M. and Mohammed, R.A. (1994). Brine and scale chemistry in MSF distillers. *Desalination*, **99**, 73-111.

Shams El-Din A.M., EL-Dahshan, M.E., Mohammed R.A. (2002). Inhibition of the thermal decomposition of  $\text{HCO}_3^-$  A novel approach to the problem of alkaline scale formation in seawater desalination plants. *Desalination*, **142**, 151-159.

Shams El-Din A.M., EL-Dahshan, M.E., Mohammed R.A. (2005). Scale formation in flashing chambers of high-temperature MSF distillers. *Desalination*, **177**, 241-258.

Soliman, M.A., (1981). A mathematical model for MSF multi-stage flash desalination plants, *Journal of Engineering Science University of Riyadh*, **7(2)**, 143–150.

Sourirajan, S. and J.P. Agrawal (1996). Reverse Osmosis, *Industrial and Engineering Chemistry*, **61**, 62-89.

Stumm, W. and Morgan, J.J. (1981). An introduction emphasizing chemical equilibria in natural waters, 2<sup>nd</sup> edition, J. Wiley, New York.

Tanvir, M.S. (2007). Neural network based hybrid modeling and MINLP based optimization of MSF desalination process using gPROMS. PhD thesis. University of Bradford.

Tanvir, M. S. and Mujtaba, I.M. (2006a). Modelling and Simulation of MSF Desalination Process using gPROMS and Neural Network based Physical Property Correlation, *Computer Aided Process Engineering*, **21**, 315-320.

Tanvir, M. and Mujtaba, I.M (2006b). Simulation of MSF Desalination Process for Fixed Water Demand using gPROMS and Neural Network based Temperature Elevation Correlation, In Proceeding of IWC2006 Conference, 300, 12-14 June, Portugal.

Tanvir, M.S. and Mujtaba, I.M. (2006). Neural network based correlations for estimating temperature elevation for seawater in MSF desalination process, *Desalination*, **195**, 251-272.

Tanvir, M.S. and Mujtaba, I.M (2007). Optimisation of MSF Desalination Process for Fixed Water Demand using gPROMS, *Computer Aided Chemical Engineering*, **24**, 763

Tanvir, M.S. and Mujtaba, I.M (2008). Optimisation of Design and Operation of MSF Desalination Process using MINLP Technique in gPROMS, *Desalination*, **222**, 419-430.

Temperley, T.G. (1997) The coming of age of desalination, *IDA World Congress on Desalination and Water Sciences*, Madrid, Spain.

Thomas, P.J., Bhattacharyya, S., Patra, A. and Rao, G.P. (1998). Steady state and dynamic simulation of multi-stage flash desalination plants: A case study, *Computers Chem. Eng.*, **22** 1515–1529.

Tijl, P. (2005). Capabilities of gPROMS and Aspen Custom Modeler, Using the Sec-Butyl-Alcohol Stripper Kinetics Case Study, Eindhoven Technical University.

UN. (2011). United Nations, Department of Economic and Social Affairs, Population Division, Population Estimates and Projections Sections. Retrieved 2011, from <http://www.un.org/en/development/desa/index.html>



Wade, N., Willis, J. and Mcorley, J. (1999). The Taweelah A2 independent water and power project, *Desalination*, **125**, 191-202.

Wangnick, K. (1995) How incorrectly determined physical and constructional properties the seawater and brine regimes influence the design and size of an MSF desalination plant-simulus for further thought, Proceeding of the IDA world Congress on Desalination and Water science, Abu Dhabi, Vol.2, 201-218.

Watson Desalination Consultants. Technology Review. (1979), Technology review and handbook: High temperature scale inhibitors for seawater desalination. A multi-client steady, Barentt St. Manassas, U.S.A.

Watzdorf, R. and Marquardt, W. (1997) Application of rigorous electrolyte thermodynamics to the modeling of MSF-desalination plants, *IDA World Congress on Desalination and Water Reuse*, Proceedings of the IDA World Congress, Madrid-Spain, **5**, 287-304.

Yasunaga, K., Fujita, M., Ushiyama, T., Yoneyama, K., Takayabu, Y.N. and Yoshizaki, M. (2008). Diurnal Variations in Precipitable Water Observed by Shipborne GPS over the Tropical Indian Ocean, *SOLA*, **4**, 97-100.

Zupan, J. and Gasteiger, J. (1999). Neural Networks in chemistry and drug design, Weinheim, Germany: Wiley-VCH.

## List of Publications

### *Journal papers*

1. Said S., Mujtaba I.M. and Emtir M. (2011). Neural Network Based Correlations for Estimating the First and Second Dissociation Constant of Carbonic Acid in Seawater, *Chemical Engineering Transactions*, **24**, 523-528.
2. Said S., Mujtaba I.M. and Emtir M. (2012). Modelling and Optimisation of MSF Desalination Process: impact of Calcium Carbonate Scale Depositon, (under preparation).
3. Said S., Mujtaba I.M. and Emtir M. (2012). Flexible Design and Operation of MSF Desalination Process: Coping with different Freshwater Demand, (under preparation).
4. Said S., Mujtaba I.M. and Emtir M. (2012). Developing a Carbonic Acid Dissociation Constants Correlations using Neural networks, (under preparation).

### *Conference papers*

1. Said S., Mujtaba I.M. and Emtir M. (2009). Modelling and simulation of the effect of non-condensable gases on heat transfer of the MSF desalination plants, *Proceeding of International conference on energy, environment and water desalination*, 8-9 December 2009, Tripoli-Libya.
2. Said S., Mujtaba I.M. and Emtir M. (2010). Modelling and simulation of the effect of non-condensable gases on heat transfer in the MSF desalination plants using gPROMS software, *Computer Aided Process Engineering*, **28**, 25-30, Elsevier.

3. Said S., Mujtaba I.M. and Emtir M. (2011). Neural Network Based Correlations for Estimating the First and Second Dissociation Constant of Carbonic Acid in Seawater, *Proceeding of the 10<sup>th</sup> International conference on Chemical and Process Engineering*, 8-11 May 2011, Florence-Italy.
4. Said S., Mujtaba I.M. and Emtir M. (2012). Effect of Fouling Factors on the Optimisation of MSF Desalination Process for Fixed Water Demand Using gPROMS, *Proceeding of the 9th International conference on Computational Management*; 18-20 April 2012, London-UK.
5. Said S., Mujtaba I.M. and Emtir M. (2012). Flexible Design and Operation of MSF Desalination Process: Coping with Uniform and Irregular Freshwater Demand, *Proceeding of the 9th International conference on Computational Management*; 18-20 April 2012, London-UK.